SIEMENS

MAGNETOM Flash

The Magazine of MRI

Issue Number 3/2015 | Simultaneous Multi-Slice Supplement

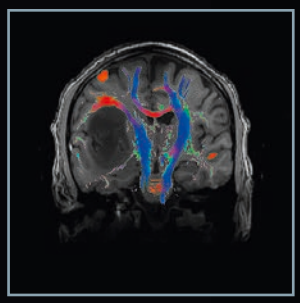

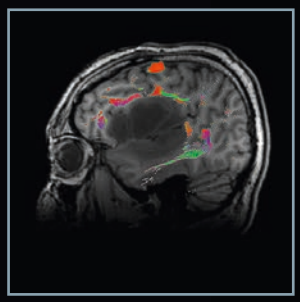

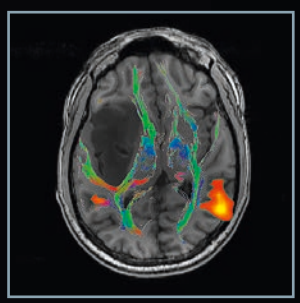

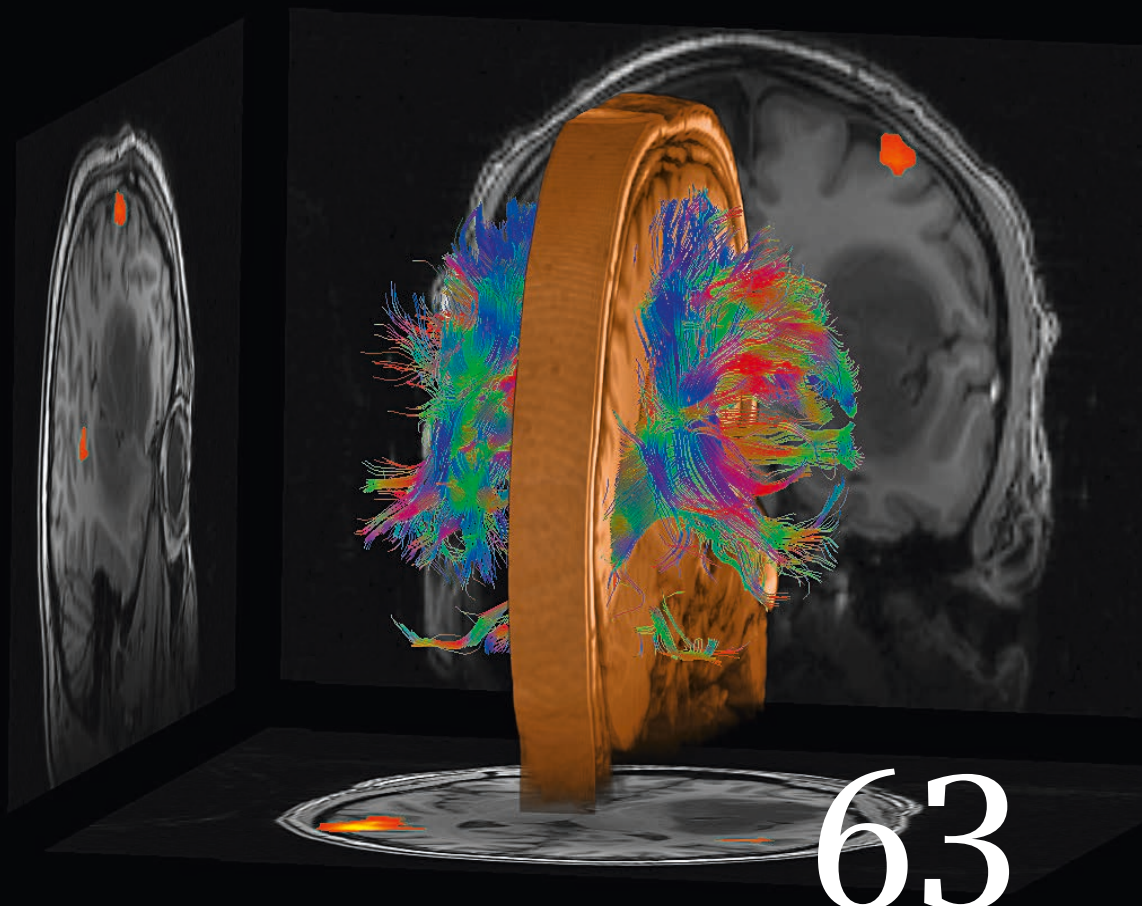

63

SIEMENS

Expert Talks

Don’t miss the talks of experienced and renowned experts on all aspects of MR imaging

siemens.com/magnetom-world

MRI Technology and Methodology: A Look into the Future

Peter Jezzard

Oxford University
(Oxford, UK)

New Application Opportunities Using MR Fingerprinting

Mark A. Griswold

Case Western Reserve University
(Cleveland, OH, USA)

A 5 Minute Clinical Brain Protocol

Lawrence Wald

Massachusetts General Hospital (Boston, MA, USA)

A Chairman’s Perspective on Radiology

Stefan Schoenberg

Mannheim University Medical Center (Mannheim, Germany)

Visit us at

www.siemens.com/magnetom-world

Go to

Clinical Corner > Clinical Talks

Peter Jezzard trained as an undergraduate in physics at the University of Manchester, before commencing a PhD in non-medical MR physics at the University of Cambridge. In 1991 he switched to biomedical MR, having moved to the National Institutes of Health, USA, to take up a post-doctoral, and later Unit Chief, position. He remained there for seven years, working in the NHLBI and NIMH, mostly on projects related to the development of functional measurements in the brain. In 1998 he moved back to the UK where he became a founding member of the Oxford Centre for Functional Magnetic Resonance Imaging of the Brain (FMRIB). Initially a member of the MRC External Staff embedded in Oxford University, he was appointed to a tenured university professorship in neuroimaging in 2003, and to a fellowship at University College. His current scientific interests lie in the development of non-invasive measures of brain physiology, and their application to cerebrovascular and neuropsychiatric disorders. He also directs the Oxford-Nottingham EPSRC-MRC Centre for Doctoral Training in Biomedical Imaging, and is a past President of the International Society for Magnetic Resonance in Medicine.

Dear MAGNETOM Flash reader,

It is my pleasure to introduce this special MAGNETOM Flash issue on the topic of simultaneous multi-slice (SMS) imaging [1, 2]. It is quite a technical topic, but it is my firm belief that this is a huge advance for the modality of magnetic resonance imaging, and soon you will all be using this technology. So here is your opportunity to understand this revolutionary technique from the pioneers themselves, and to prepare yourself for using SMS in your daily practice.

To understand the SMS revolution it is first necessary to understand another recent innovation in the field, namely parallel imaging. In parallel imaging (whether SENSE image-based [3], or GRAPPA raw-data-based [4]) the amount of data acquired in the phase-encode direction is reduced (under-sampled) and the missing information is provided by the differing spatial sensitivity profiles of the array elements in the receive RF coil. Thus, the process of spatial encoding has moved in recent years from being something that is entirely achieved by manipulating the field gradients (once slice selection has occurred) to something that is shared between field gradient encoding and the sensitivity profiles of the RF coil array elements.

Simultaneous multi-slice imaging takes this a stage further by exciting multiple slices at the same time, and then spatially encoding their signals in a simultaneous manner. Historically this would have led to the images from each slice sitting on top of one another, resulting in a rather horrible mess. But with the advent of array receive coils, and with image reconstruction principles that are closely related to parallel imaging, it is possible to separate the signals from the various slices. This can be accomplished since the different array elements of the receive coil 'see' each slice with a different sensitivity (due to their greater or lesser proximity to a given slice). The image reconstruction algorithm can then unpick the signal contributions and restore them to their separate slice locations, especially if the aliasing from the different images is arranged in a controlled pattern (see the discussion on CAIPIRINHA in the article by Breuer et al. [5]).

So what is the advantage of simultaneous multi-slice? The main advantage is that it offers yet another means by which the scan time can be reduced. In principle the imaging speed can be increased by a factor equal to the number of slices that are excited simultaneously. Typically this is a factor of 2 to 4. It is also possible to combine SMS and conventional parallel imaging, although there are limits to what can be achieved since the tricks used to restore under-sampled data in conventional SENSE/GRAPPA are the same ones that separate signals from the different slices in SMS. Nevertheless, and as this special issue shows, there are plenty of applications where SMS principles can be deployed to great benefit, and where a new chapter in the story of MRI is being ushered in.

"There are plenty of applications where SMS principles can be deployed to great benefit, and where a new chapter in the story of MRI is being ushered in."

Dr. Peter Jezzard

Applications of SMS

SMS approaches will have impact in many areas where imaging speed is key. In diffusion tractography imaging, for example as described by Setsompop et al. [6] and Shepherd [7] in this issue, SMS allows a greater number of diffusion directions to be sampled per unit time. This should lead to improved data quality and more feasible clinical applicability. Other articles in this issue show how clinical diffusion imaging in the musculoskeletal system, spine, body, and even the heart, is benefitted by the application of SMS. In the realm of functional imaging SMS can greatly improve the temporal sampling efficiency of fMRI, leading to better resting-state fMRI connectivity maps. Indeed, technique enhancements of SMS have constituted a major part of, and have had a major impact on, the NIH-funded Human Connectome Project [8].

SMS also offers the opportunity to bring clinically unfeasible scan times back into the realm of reality. A good example of this is the readout-segmented EPI (RESOLVE)[1] method, that allows higher resolution diffusion data to be acquired, with dramatically reduced geometric distortion and spatial blurring than is the case for snapshot EPI. However, as originally conceived the RESOLVE sequence led to unreasonable scan times for anything other than very basic diffusion-weighted imaging. With the inclusion of SMS[1] (see the articles by Frost et al. [9] and Runge et al. [10]) the scan times can be brought back down to tolerable durations.

But surely, I hear you remark, there must be a catch to this. Nothing in MRI ever comes for free. There is always a trade off. The answer is that SMS does come reasonably close to offering increased speed without much of a penalty, at least in the regime of well-behaved parallel imaging reconstruction. But clearly there are some limitations that must be acknowledged. One is that the specific absorption rate (SAR) of the pulse sequence is increased by having RF pulses that selectively excite multiple slices (to first approximation this is quadratic with the additional number of slices that are excited). The related PINS (power independent of number of slices) method [10] suggests a solution to the SAR problem, albeit with compromises in the off-resonance performance of the PINS excitation profiles. Indeed, hybrid combinations of PINS and 'conventional' SMS RF pulses can also be considered [11]. Another source of potential artifact that has had to be overcome is the possibility of signal 'bleed' between slices. A clean separation of signal is needed to avoid misinterpretation, particularly for measurements of subtle signal changes such as in fMRI. As shown in the paper by Setsompop et al. [6] LeakBlock algorithms can be used to minimize this cross-slice contamination.

In summary, this special issue describes the latest exciting developments in fast scanning that represent another technological revolution in magnetic resonance imaging. I am quite sure that if you are not already using SMS techniques to improve your scan times, and improve your image quality, then you soon will be!

[1] The product is still under development and not commercially available yet. Its future availability cannot be ensured.

References

1 Larkman DJ, Hajnal JV, Herlihy AH, Coutts GA, Young IR, Ehnholm G. Use of multicoil arrays for separation of signal from multiple slices simultaneously excited. J Magn Reson Imaging. 2001 Feb; 13(2):313-7.
2 Barth M, Breuer F, Koopmans PJ, Norris DG, Poser BA. Simultaneous multislice (SMS) imaging techniques. Magn Reson Med in press.
3 Pruessmann KP, Weiger M, Scheidegger B, Boesiger P. SENSE: sensitivity encoding for fast MRI. Magn Reson Med 1999; 42:952-962.
4 Griswold MA, Jakob PM, Heidemann RM, Nittka M, Jellus V, Wang J, Kiefer B, Haase A. GeneRalized Autocalibrating Partially Parallel Acqusitions (GRAPPA). Magn Reson Med 2002; 47:1202-1210.
5 Breuer FA, Blaimer M, Griswold M, Jakob P. CAIPIRINHA – Revisited. [this issue].
6 Setsompop K, Cauley SF, Wald LL. Advancing diffusion MRI using simultaneous multi-slice echo planar imaging. [this issue].
7 Shepherd T. Perspective – high potential impact of simultaneous multi-slice diffusion acquisition strategies on future clinical neuroradiology practice. [this issue].
8 Uğurbil K, Auerbach EJ, Moeller S, Xu J, Vu A, Glasser MF, Lenglet C, Sotiropoulos SN, Smith SM, Behrens TJ, van Essen D, Yacoub E. Slice acceleration in the 3 Tesla component of the Human Connectome Project. [this issue].
9 Frost R, Koopmans PJ, Harston GW, Kennedy J, Jezzard P, Miller K, Porter DA. High-resolution diffusion-weighted neuroimaging at 3T and 7T with simultaneous multi-slice RESOLVE. [this issue].
10 Runge VM, Richter JK, Klarhöfer M, Beck T, Heverhagen JT. Simultaneous multi-slice (slice accelerated) diffusion EPI: early experience for brain ischemia and cervical lymphadenopathy. [this issue]
11 Norris DG, Koopmans PJ, Boyacioğlu R, Barth M. Power independent of number of slices radiofrequency pulses for low-power simultaneous multislice excitation. Magn Reson Med. 2011 Nov;66(5):1234-40.
12 Eichner C, Heidemann RM. Rapid high spatial resolution diffusion MRI at 7 Tesla using simultaneous multi-slice acquisition. [this issue].

Content

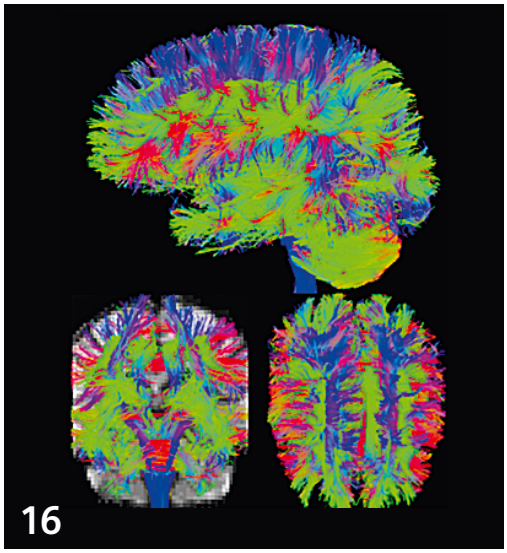

16

Advancing Diffusion MRI Using SMS EPI

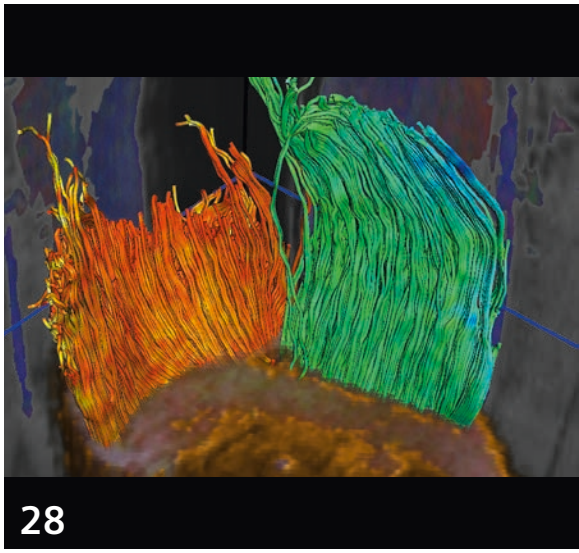

28

Accelerated DTI of Skeletal Muscle Using SMS Acquisition

Editorial Comment

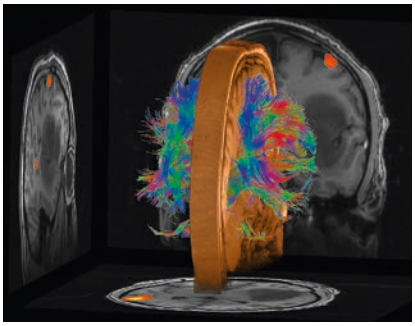

Cover image courtesy of
Andreas J. Bartsch
(Radiologie Bamberg, Germany; Departments of Neuroradiology, Universities of Heidelberg and Wuerzburg, Germany; Oxford Centre for Functional MRI of the Brain (FMRIB), University of Oxford, UK)

SMS Diffusion

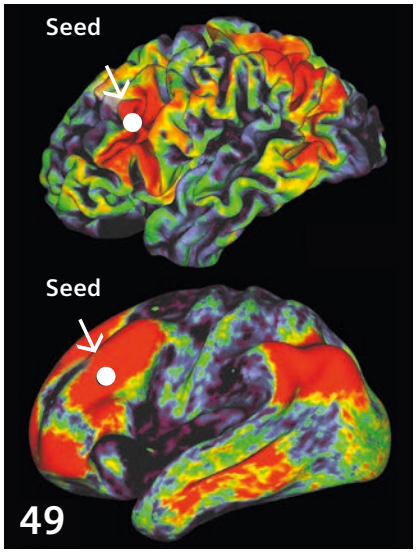

Slice Acceleration in the 3T Component of the Human Connectome Project

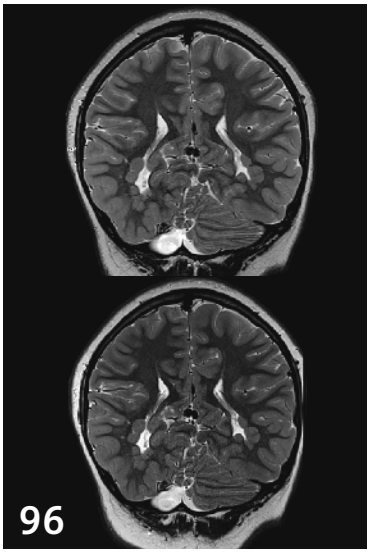

Epilepsy Imaging with SMS TSE

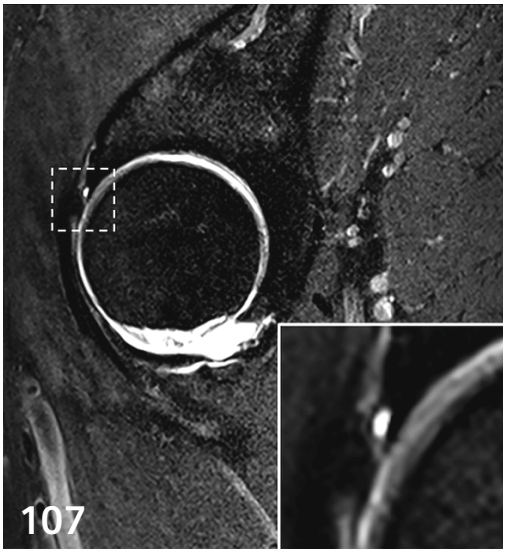

Improved Visualization of Femoroacetabular Impingement Cartilage Damage with Multiband SMS Acceleration

SMS BOLD

SMS RESOLVE

SMS TSE

[1] The product is still under development and not commercially available yet. Its future availability cannot be ensured.

CAIPIRINHA – Revisited

Felix Breuer[1], Martin Blaimer[1], Mark Griswold[2], Peter Jakob[3]

[1] Research Center, Magnetic Resonance Bavaria e.V. (MRB), Würzburg, Germany
[2] Case Center for Imaging Research, Case Western Reserve University, Cleveland, OH, USA
[3] Würzburg University, Department of Experimental Physics 5 and Research Center, Magnetic Resonance Bavaria e.V. (MRB), Würzburg, Germany

Introduction

Image acquisition time is one of the most important considerations for clinical magnetic resonance imaging (MRI). The development of multi-coil receiver hardware as well as dedicated parallel acquisition techniques (PAT) and respective reconstruction methods allowed for significant decrease of acquisition times in almost all clinical applications. This, for example, enables much shorter breath-holds in abdominal MRI and improves the temporal resolution of dynamic scans but can also be applied to improve image quality while keeping the acquisition time constant. Thus, today, parallel imaging techniques play a substantial role in everyday clinical routine.

Every parallel imaging technique combines (1) a specific acquisition scheme of *k*-space data with a (2) respective reconstruction method.

(1) **Parallel acquisition** operates by reducing the amount of data necessary to form an image. In the Cartesian case, this is usually accomplished by uniformly undersampling the *k*-space (e.g. skipping every other phase-encoding line) resulting in so-called 'aliasing artifacts' in the image domain.

(2) **Parallel reconstruction** methods seek to compensate the lack of spatial encoding by taking into account the spatial sensitivity information, provided by a multi-coil receiver array and can be divided into 2 main groups (Fig. 1): algorithms that combine undersampled images from the individual coil elements in the image domain to a global image, e.g. SENSE [1]. And algorithms that combine the frequency information of each coil

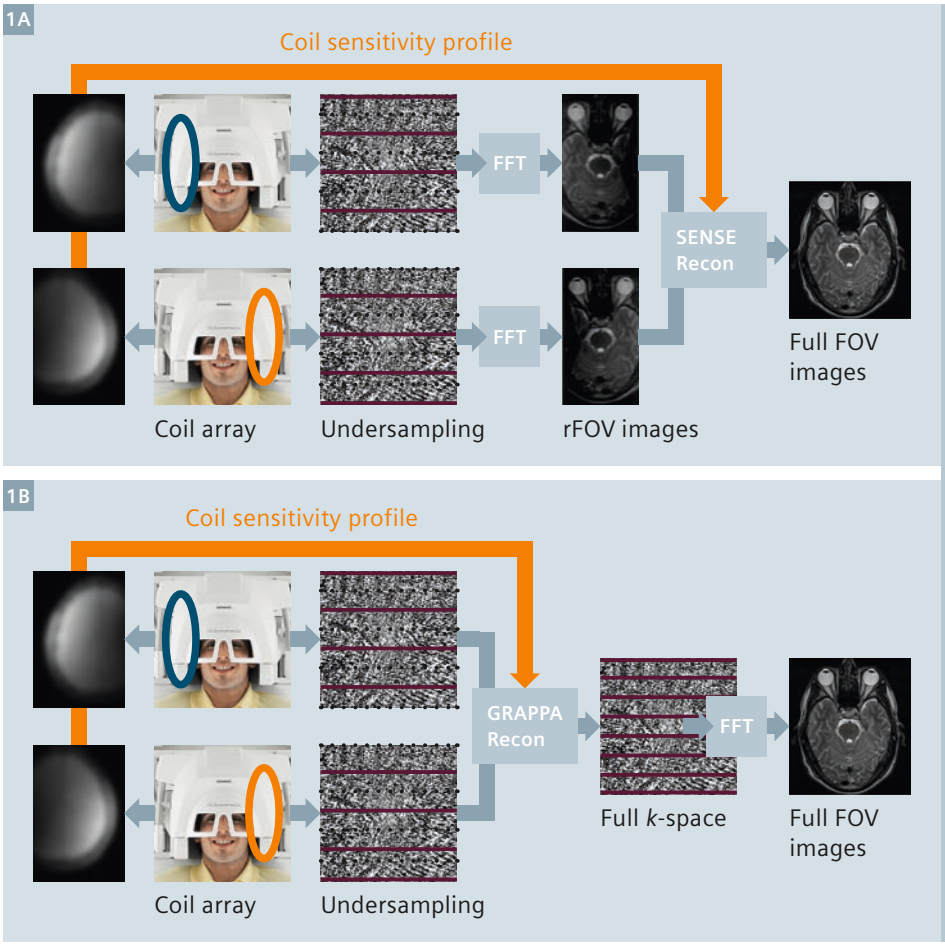

1 Procedure of reconstructing the image information from undersampled datasets with SENSE (**1A**, image based) and GRAPPA (**1B**, *k*-space based). Coil sensitivity profiles and frequency information is received with individual coil elements. With SENSE, reduced FOV images are reconstructed first and unaliased afterwards using the sensitivity information. With GRAPPA the sensitivity information from each coil element is used right at the beginning to calculate missing echos followed by Fourier transformation.

element in the *k*-space domain before Fourier transformation, e.g. GRAPPA [2].

Unfortunately, the PAT concept is intrinsically associated with a signal-to-noise (SNR) loss compared to a fully encoded image. The SNR is reduced

a) by the square root of the acceleration factor, simply due to the fact that less data is acquired, and

b) by the so-called *g*-factor, depending strongly on the encoding capabilities of the underlying receiver array.

Thus, PAT is often limited to applications with sufficiently high base SNR, such as volumetric imaging methods. With the newest generation of MR systems providing up to 128 independent receiver channels, further scan time reductions are potentially achievable. However, in conventional 2D clinical imaging, parallel imaging today is still restricted to relatively moderate scan time reductions (PAT factors of 2-3) due to intrinsic limitations in the coil sensitivity variations along one phase-encoding direction (1D parallel imaging). In 3D and simultaneous multi-slice imaging, parallel encoding can be carried out in two encoding directions (PAT^2 or 2D parallel imaging), thereby employing the sensitivity variations in both phase-encoding directions, as has been demonstrated in, for example, 2D SENSE [3] and MS SENSE [4]. This concept has been shown to significantly improve the reconstruction conditions, allowing for higher accelerations of the acquisition (>3). However, both techniques require sufficient sensitivity variations in two encoding directions for successful image reconstruction and therefore strongly depend on the underlying coil geometry, which is described by the *g*-factor. As mentioned above, spatial encoding with a receiver array is associated with a certain noise amplification known as '*g*-factor noise'. Quantitative *g*-factor estimation methods have been derived for SENSE [1] and GRAPPA reconstructions [5] and serve as a quality metric for PAT reconstructions. One important approach to reduce this *g*-factor noise for a given application is the optimization of the receiver array geometry (e.g. number of coils, coil arrangement) towards the application at hand. However, hardware limitations, the diversity of patient weight and size, the need for flexibility regarding a wider range of applications, as well as sequence or protocol specific considerations, hamper the viability.

The CAIPRINHA concept (Controlled Aliasing In Parallel Imaging Results IN Higher Acceleration) is a specific data acquisition technique that allows to partially overcome these requirements and limitations by modifying the aliasing conditions in a well defined manner. This leads to an improved *g*-factor when compared to standard acquisition with the same acceleration factor. CAIPIRINHA takes effect already during the data acquisition by modifying the RF excitation or gradient encoding scheme in order to use the coil encoding power of the underlying receiver array to full capacity. The concept has been successfully applied so far to 3D imaging where data reduction can be carried out in two phase-encoding directions (2D-CAIPIRINHA) [7] and simultaneous multi-slice imaging (MS-CAIPIRINHA) [6]. In addition, both strategies can be extended to the third remaining direction, namely the read-out direction, by utilizing e.g. zig-zag-shaped read-out trajectories [8] or wave-CAIPI [9, 10]. The following provides a brief overview of 2D-CAIPIRINHA and S-CAIPIRINHA.

Improving parallel imaging performance with CAIPIRINHA

2D-CAIPIRINHA

In contrast to conventional 2D imaging where only one phase-encoding direction is available for scan-time reduction (1D PAT), 3D volumetric imaging with a second phase-encoding direction offers the potential to choose the direction in which undersampling is performed, or even to accelerate in both phase-encoding directions at the same time (2D PAT / PAT^2), where the total PAT factor is the product of the acceleration factors in the individual phase-encoding directions, e.g. 2 x 3 = 6. Given a receiver array geometry providing sensitivity variations in

2

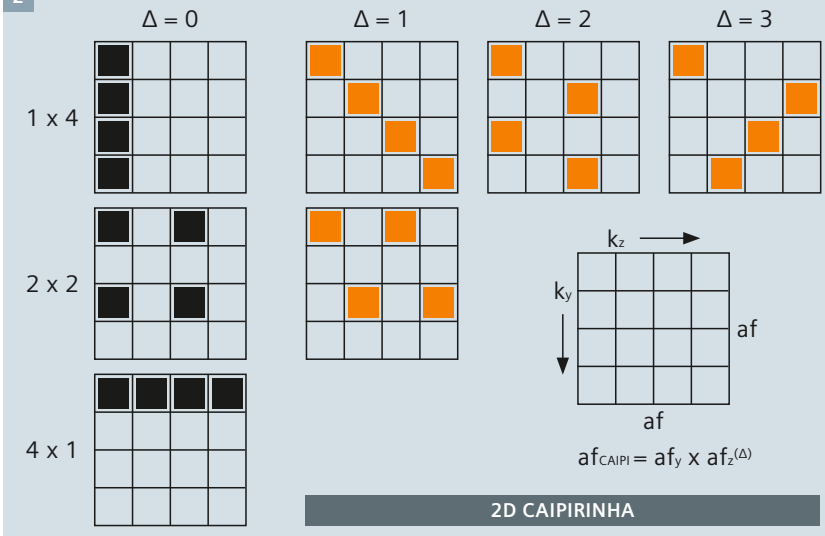

2 Procedure of generating 2D-CAIPIRINHA sampling patterns for a given total acceleration factor, here PAT = 4. All possible sampling schemes can be represented by a PAT x PAT elementary cell with PAT sampling positions to fill. For each undersampling rate in the k_y direction (PAT_y), multiple patterns can be created by shifting sampling positions at row k_y in the k_z direction by a different amount Δ, whereas Δ runs from 0 to PAT_{z-1}, and PAT_z = PAT/PAT_y. Sampling patterns without shift (Δ = 0) are 2D PAT standard acquisitions, while all the other patterns are represented by 2D-CAIPIRINHA-type acquisitions (PAT = PAT_y x PAT_z (Δ)) indicated by the red sampling positions.

both phase-encoding directions, this strategy has shown the potential to allow for higher total image accelerations compared to undersampling schemes restricted to only one direction [4, 5]. However, since the sensitivity variations available for the PAT reconstruction depend not only on the coil geometry but also on the image position and orientation, the FOVs and encoding directions as well as the object position, size and shape, the right choice of the undersampling rate for the individual phase-encoding directions is not easily predictable and remains a challenging task. Thus, in many applications the reconstructed images suffer from severe residual artifacts or strong noise amplifications, depending on the choices made by the operator.

Again, the CAIPIRINHA concept has shown to partially overcome these limitations. It has been realized that, besides the standard rectangular sampling patterns with undersampling using simple integer reductions, many other patterns are conceivable where the sampling positions are shifted from their original positions in the 2D phase-encoding scheme. Here, we restrict ourselves to sampling positions on so-called 'sheared grids' which form periodic lattices [16] resulting in exactly PAT superimposed image pixels at an acceleration factor of PAT as it is the case in all standard rectangular patterns. The procedure of generating the available **2D-CAIPIRINHA** patterns is schematically displayed in Figure 2 for a total image acceleration of PAT = 4. The sampling schemes can be represented by a PAT x PAT elementary cell with PAT sampling positions to fill. For each undersampling rate in the ky direction (PAT_y), multiple patterns can be created by shifting sampling positions at row ky in the kz direction by a different amount d, whereas d runs from 0 to PAT_{z-1}, and PAT_z = PAT /PAT_y. Sampling patterns without shift (d = 0) are 2D standard acquisitions, while all the other patterns are represented by 2D-CAIPIRINHA-type acquisitions. This concept can also be used for prime number accelerations (PAT = 2, 3, 5 ...) where standard accelerations only allow undersampling in one of the phase-encoding directions. The required shifts in *k*-space can simply be realized by applying additional gradient offsets to the phase-encoding gradient tables. These 2D-CAIPIRINHA sampling patterns, analogous to the phase-cycles in simultaneous multi-slice imaging, modify the appearance of aliasing in 2D parallel imaging compared to conventional rectangular reduction schemes and have the potential to relax the requirements of integer reductions to great extent. This is demonstrated in more detail in the original publication [7]. By shifting the sampling positions in a well-directed manner, aliasing can be shifted in such a way that sensitivity variations provided by the underlying receiver array are employed more efficiently. In some cases, the amount

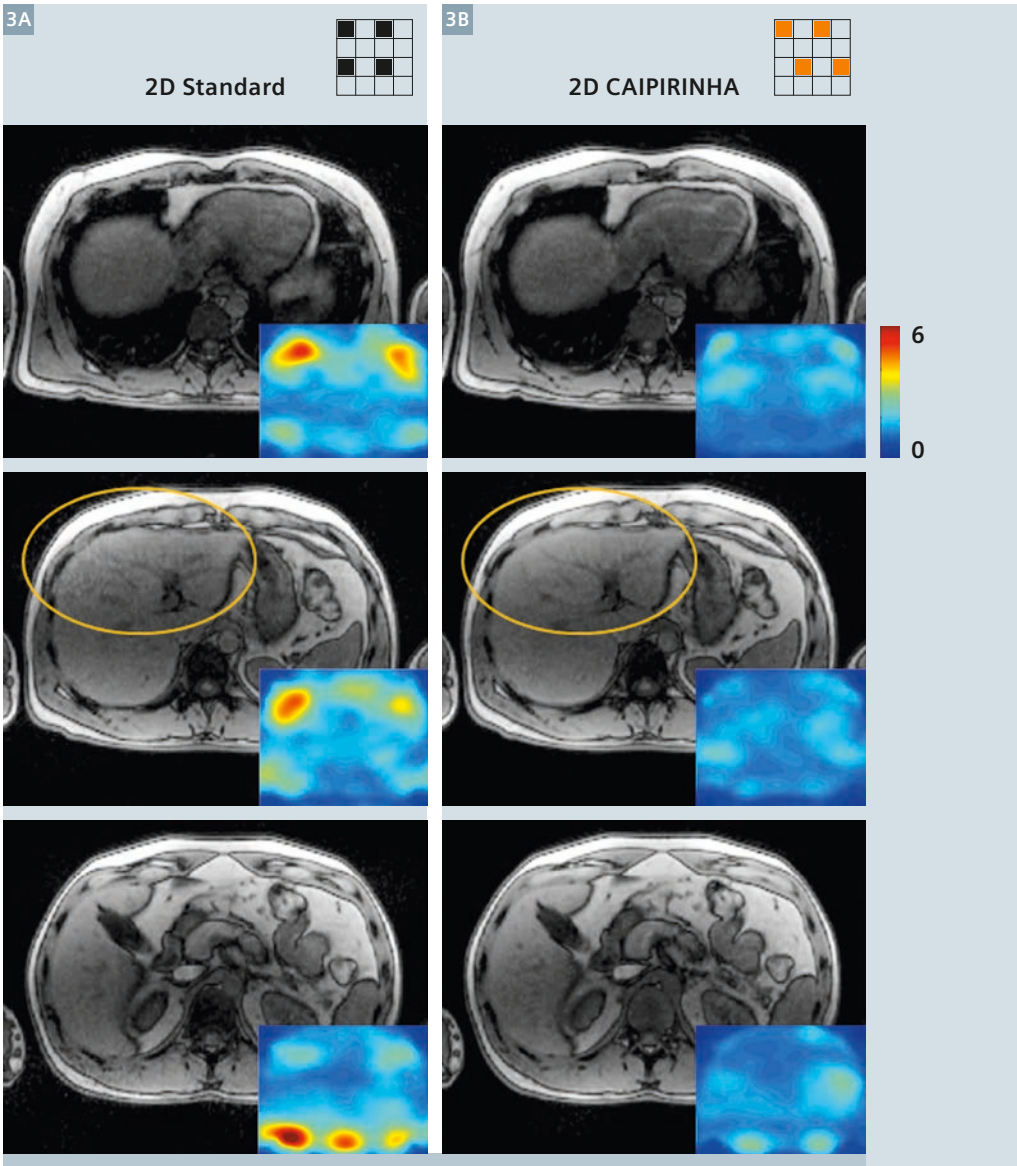

3 *In vivo* liver example; volunteer: Compared are GRAPPA reconstructions (3 example slices) derived from two different reduction schemes **(3A)** Standard 2 x 2 and **(3B)** 2D-CAIPIRINHA 2 x $2^{(1)}$. In addition, the corresponding GRAPPA *g*-factor maps are displayed. In the indicated region the SNR benefit of 2D-CAIPIRINHA can be appreciated.

Imaging details: 1.5T MAGNETOM Avanto, 6-channel body matrix coil combined with 6 channels from the spine matrix coil; VIBE PAT = 4, extra reference scan matrix 32 x 24 x 24. FOV 400 x 312.5 mm^2, matrix 320 x 170 x 50, total acquisition time 9 s breath-hold.

of aliasing can even be reduced. These modified aliasing conditions may then result in a further improvement in parallel imaging reconstruction conditions and therefore in better image quality. Recently, this concept has also been extended to more generalized sampling schemes which are not restricted to sheared grids [17].

In order to demonstrate the benefit of 2D-CAIPIRINHA in vivo, two subsequent accelerated (PAT = 4) abdominal 9 s breath-hold VIBE experiments were carried out on a volunteer. In Figure 3, GRAPPA reconstructions from three out of 50 slices from

a) a standard 2D-PAT 2 x 2 and

b) a 2D-CAIPIRINHA 2 x 2[1]

acquisitions are displayed. In addition, the corresponding *g*-factor maps of the GRAPPA reconstructions are displayed as a quantitative measure of image quality. As indicated by the lower *g*-factor values in the 2D-CAIPIRINHA reconstructions, the improvement of image quality can clearly be observed, even on a visual scale (see region indicated by the orange circle).

Furthermore, the improvements in image quality associated with 2D-CAIPIRINHA are demonstrated taking four different T1-weighted 3D FLASH experiments of a volunteer's brain with different acceleration factors and acquisition schemes (Fig. 4). The acquisitions compared are

a) a standard 2D-PAT 2 x 2,

b) a 2D-CAIPIRINHA 2 x 2[1],

c) a 2D-CAIPIRINHA 1 x 5[2] and

d) a standard 1D-PAT 5 x 1 scheme.

Displayed are the central sections of the reconstructed 3D image data in the sagittal, coronal and axial view in addition to the corresponding quantitative *g*-factor maps. Comparing reconstruction results from PAT = 4 (a) and (b), the improvement of 2D-CAIPIRINHA can clearly be appreciated. Comparing results from PAT = 5 (c) and (d), the gain in SNR is even more obvious. In this case, the parallel imaging performance of 2D-CAIPIRINHA 1 x 5[2] (c) compares pretty well with the standard PAT = 4 (2 x 2) acquisition employed in (a).

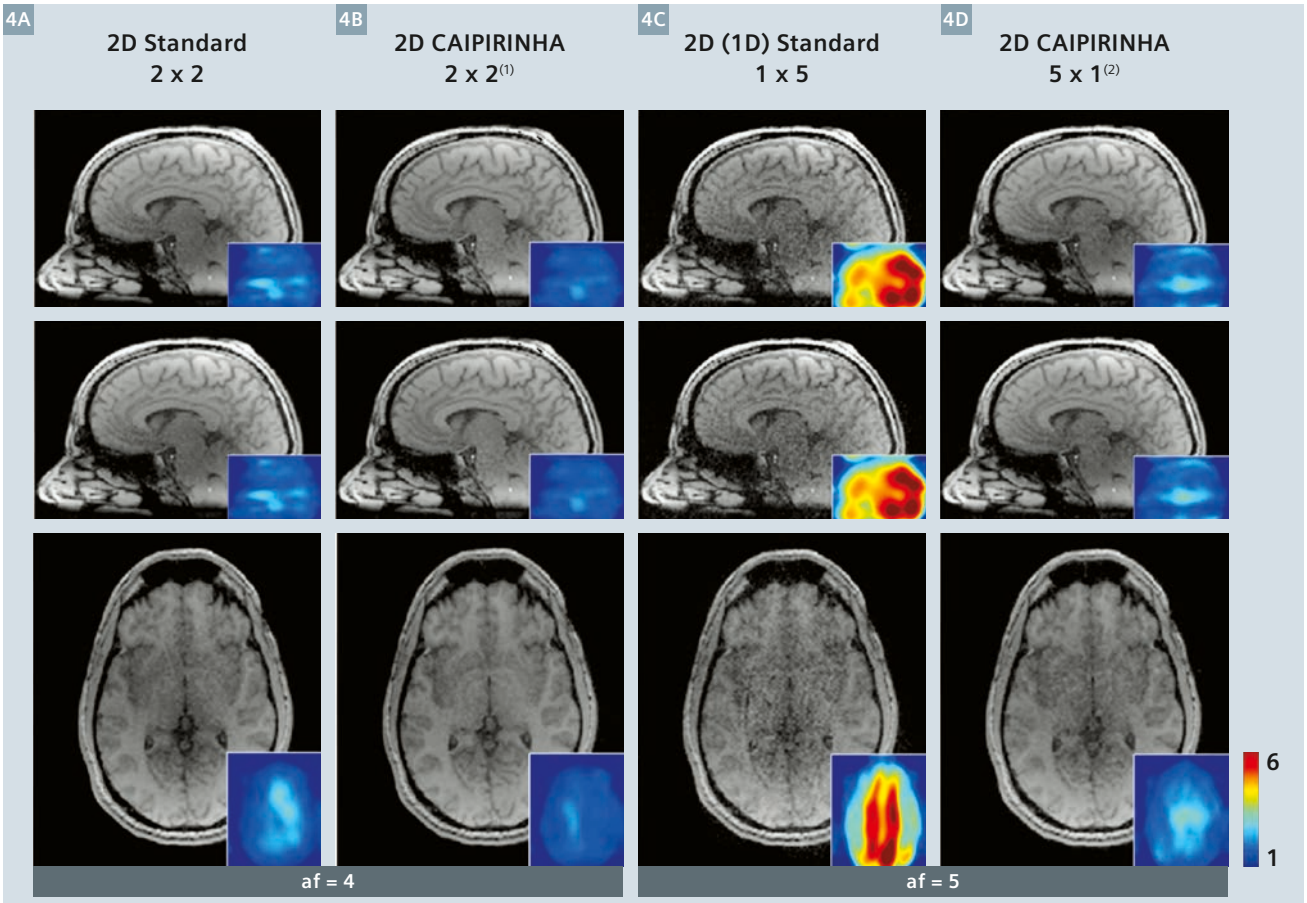

3 *In vivo* 3D FLASH brain imaging using different acceleration schemes: **(4A)** Standard 2D-PAT 2 x 2 **(4B)** 2D-CAIPIRINHA 2 x 2[1] **(4C)** Standard 1D-PAT 5 x 1 **(4D)** 2D-CAIPIRINHA 1 x 5[2]. Displayed are central slices in the sagittal, coronal and axial views. In addition, the corresponding GRAPPA *g*-factor maps are shown.

Imaging details: 3T MAGNETOM Skyra, 20-channel head-neck matrix coil, 3D FLASH, GRAPPA with extra reference scan, matrix 32 x 32 x 32, TE / TR 4.3 ms / 16 ms, FA 35°, FOV 256 x 208 x 204 mm³, matrix 256 x 168 x 144; partial Fourier factor 7/8, total scan time 1 min 40 s (PAT = 4) and 1 min 16 s (PAT = 5).

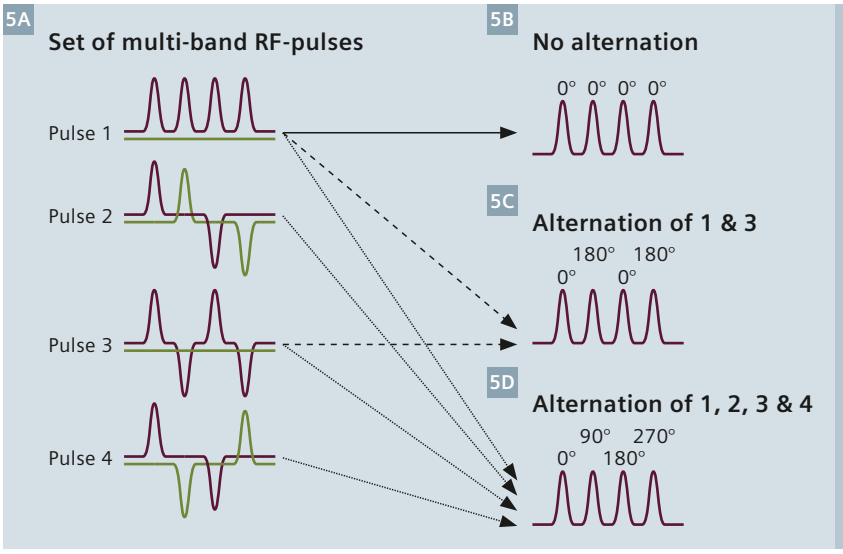

5 Multi-slice excitation with alternating RF pulses taken from **(5A)** a set of 4 RF pulses with different phase modulations (pulse 1 to 4) allows one to provide the individual slices with well defined phase-cycles along the phase-encoding direction. The real part (red) and imaginary part (green) of the pulses are plotted. **(5B)** Using only one pulse (e.g. pulse 1), no phase-cycle is provided (0°, 0°, 0°, 0°). **(5C)** Alternation between pulses 1 and 3 yield no phase-cycle for slice 1 and 3 and an 180° phase cycle for slices 2 and 4 (0, 180°, 0, 180°). **(5D)** Alternation of all 4 pulses allows one to provide all the individual slices with an individual phase-cycle (0, 90°, 180°, 270°).

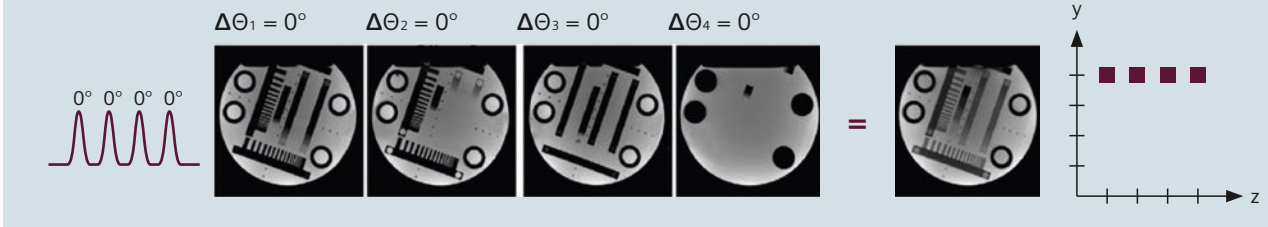

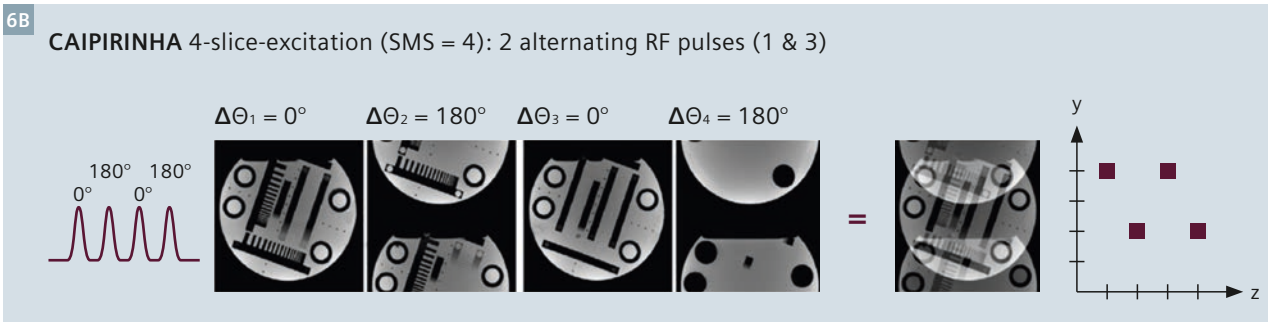

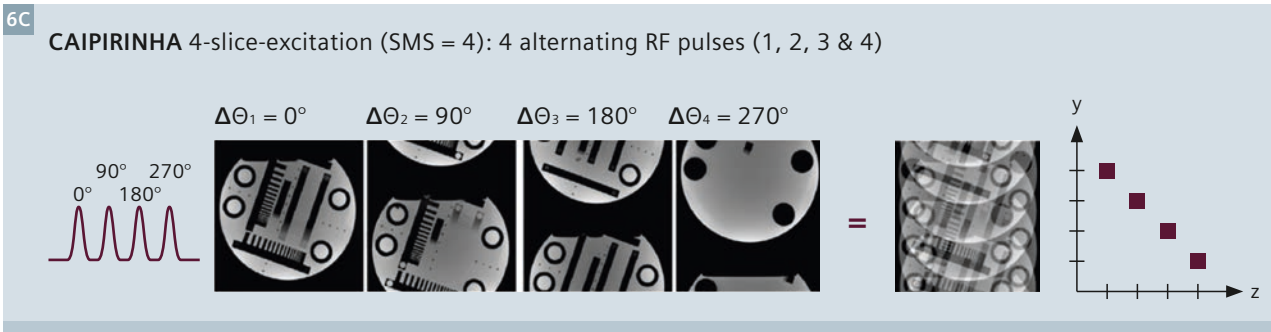

6 **(6A)** Standard 4-times-accelerated simultaneous 4-slice experiment. The same pulse is applied for subsequent excitations (phase-encoding lines), resulting in all 4 slices projected onto each other. **(6B)** CAIPIRINHA 4-times accelerated simultaneous 4-slice-experiment alternating between e.g. pulses 1 and 3 for subsequent excitations, thereby providing slice 2 and slice 4 with a 180° phase cycle. According to the Fourier Shift Theorem, slices 2 and 4 appear shifted by half of the FOV with respect to slices 1 and 3 in the resulting folded image. **(6C)** CAIPIRINHA 4-times-accelerated simultaneous 4-slice experiment alternating between pulse 1, 2, 3 and 4 for subsequent excitations, thereby providing each slice with a different phase-cycle (0°, 90°,180°, 270°). Each slice appears shifted by FOV/4 with respect to their adjacent slice in the folded image.

While the 2D-CAIPIRINHA patterns in general appear to be more tolerant against user influence and suboptimal patient positioning, the automated extraction of the optimal pattern for the given imaging setup remains a challenging task and has not been sufficiently answered.

MS-CAIPIRINHA

Simultaneous multi-slice (SMS) imaging offers an SNR benefit over standard single-slice imaging which may be either translated into shorter acquisition times or higher spatial resolution. SMS comprises RF excitations with specialized multi-band pulses as displayed in Figure 5. After multi-band excitation, the received signals will accrue from all the slices (bands) and thus are subject to the subsequent gradient-encoding sequence. Simply replacing the standard single-slice excitation pulse with a multi-slice pulse in an MR imaging sequence will therefore result in an image with all the simultaneously excited slices projected onto each other (Figure 6A). As mentioned above, the parallel imaging concept provides an elegant way to separate multiple image signals which are aliased into one image pixel. Thus, sufficient sensitivity variations of the underlying receiver array along the slice direction will then allow for separation of the slices using adapted standard PAT reconstruction algorithms [4, 11]. However, in cases where the sensitivity variations along the slice direction are not sufficient, e.g. as a result of small slice distances or suboptimal coil geometry, the PAT reconstruction will fail and result in large noise amplification. Sensitivity variations, potentially available along the other spatial directions, here the phase-encoding direction, are not employed.

It has been demonstrated that increasing the field-of-view (FOV) by the number of simultaneously excited slices allows the individual slices to be shifted with respect to each other in an extended FOV (along the phase-encoding) [12, 13] such that the slices show no superposition. A similar concept is Hadamard-aided RF encoding [14]. The required shifts mentioned above can be accomplished by employing dedicated alternating multi-band RF pulses providing the individual bands with well-defined phase-cycles along the phase-encoding direction (e.g using the set of RF pulses displayed in Figure 5). Due to the volumetric excitation, this approach offers a benefit in SNR efficiency of square root of the number of simultaneously excited slices compared to single-slice acquisitions, however at the cost of increased pulse energy deposition.

Using this concept in combination with image acceleration (fewer phase-encoding steps), superimposed slices with individual shifts along the phase-encoding direction can be realized by employing alternation of RF pulses taken, e.g. from the set of pulses given in Figure 5. A four-slice excitation at an acceleration of PAT = 4 using only RF pulse 1 yields a superimposition of 4 image pixels originating from all the 4 slices at the same location in the phase-encoding direction (Fig. 6A). Employing an alternation of RF pulses (e.g. pulse 1 and pulse 3, or pulses 1, 2, 3 and 4), the individual slices can be shifted with respect to each other in the FOV (Figs. 6B, C). In this way, as demonstrated in the corresponding *zy*-plots, aliased pixels may now originate from both different slices and different locations in the phase-encoding direction in a well defined manner (MS-CAIPIRINHA), thereby allowing the PAT reconstruction to take advantage of sensitivity variations in the slice and the phase-encoding direction, resulting in lower *g*-factors and consequently a higher SNR.

The benefit of MS-CAIPIRINHA is demonstrated *in vivo* employing a 4-times-accelerated simultaneous 4-slice experiment: Figure 7 shows 4 slices in a volunteer's brain (slice positions are indicated in the sagittal brain image), which are excited simultaneously using specialized multi-band RF pulses taken from the set of pulses given in Figure 5A. In the case of non-alternating RF pulses [4] (MS-Standard), each slice is subject to the same phase cycle along the phase-encoding direction (LR). The slices appear projected directly on top of each other, thereby allowing the PAT reconstruction (here GRAPPA-SENSE hybrid [11]) only to use sensitivity variations available in the slice direction. Due to the relatively small slice distances, the relatively high acceleration factor (PAT = 4) and the limited sensitivity variations provided by the coil array in the slice direction, the reconstruction results in large noise amplifications and thus unacceptable image quality. However, using a MS-CAIPIRINHA acquisition in combination with an adapted GRAPPA reconstruction, the folded image pixels can now be separated almost without any noise amplification. In this example, an MS-CAIPIRINHA scheme as depicted in Figure 6B has been employed. Alternation of pulses 1 and 3 provides slices 2 and 4 with a 180° phase-cycle along the phase-encoding direction, causing these slices to appear shifted by FOV/2 with respect to the slices 1 and 3 which had no phase modulation. Thus, in this case, MS-CAIPIRINHA allowed the acquisition of 4 slices in the same time normally required for a single slice without losing SNR.

In addition, the applicability of MS-CAIPIRINHA to cardiac perfusion imaging is demonstrated in Figure 8. A two-slice CAIPIRINHA saturation recovery TrueFISP sequence has been employed using a total acceleration of PAT = 3. This allows for the acquisition of 12 slices (8 slices in the short-axis view and 4 in the long axis) in only two cardiac cycles. A repetition of the sequence during contrast agent uptake has the potential for cardiac perfusion imaging with significantly increased spatial coverage in high temporal resolution [15].

Conclusion

In all current parallel acquisition techniques, aliasing artifacts resulting from an undersampled acquisition are removed by a specialized PAT image reconstruction algorithm. The CAIPIRINHA concept aims on modifying the appearance of the aliasing artifacts already during the acquisition to improve the following parallel image reconstruction procedure. Specifically, this concept has been successfully applied to 3D imag-

7

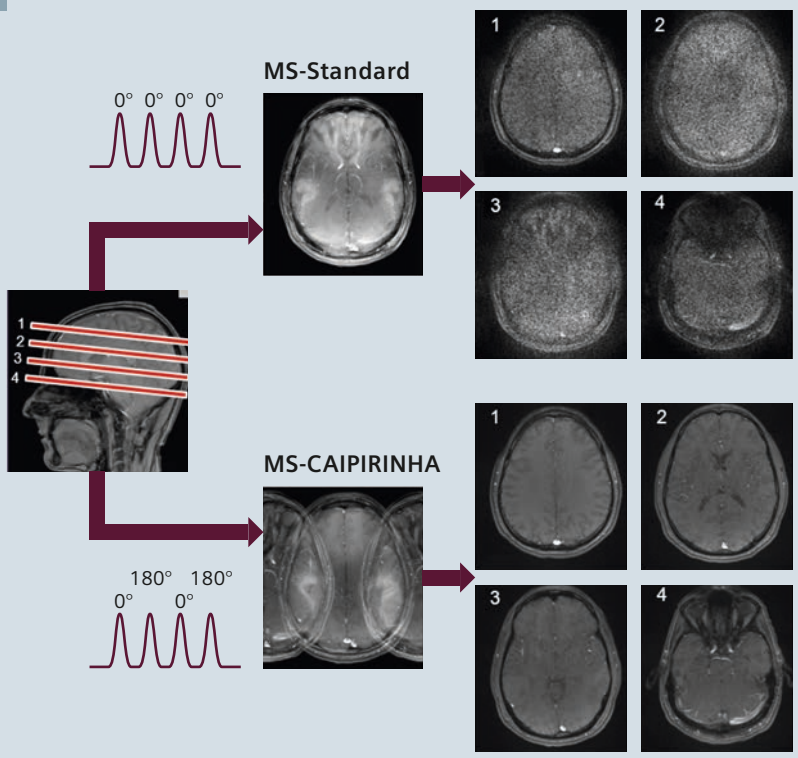

7 *In vivo* brain example:
4 x accelerated simultaneous 4-slice experiment using no phase cycling (MS-Standard) results in superimposition of all the slices directly on top of each other. Due to the lack of sufficient sensitivity variations along the slice direction, strong noise amplifications can be observed after GRAPPA reconstruction. Using MS-CAIPIRINHA, employing 2 alternating multi-band RF pulses, slices 2 and 4 appear shifted with respect to slices 1 and 3 in the folded image. In this way, sensitivity variations in the phase-encoding direction (LR) can be used in addition to the sensitivity variations available in the slice direction. The concept results in significantly improved image quality after GRAPPA reconstruction.

Imaging parameters: 3T MAGNETOM Skyra, TE 3.4 ms, TR 100 ms, FA 50°, FOV 178 x 220 mm², matrix 208 x 320, slice thickness 4 mm, distance factor 300%.

8

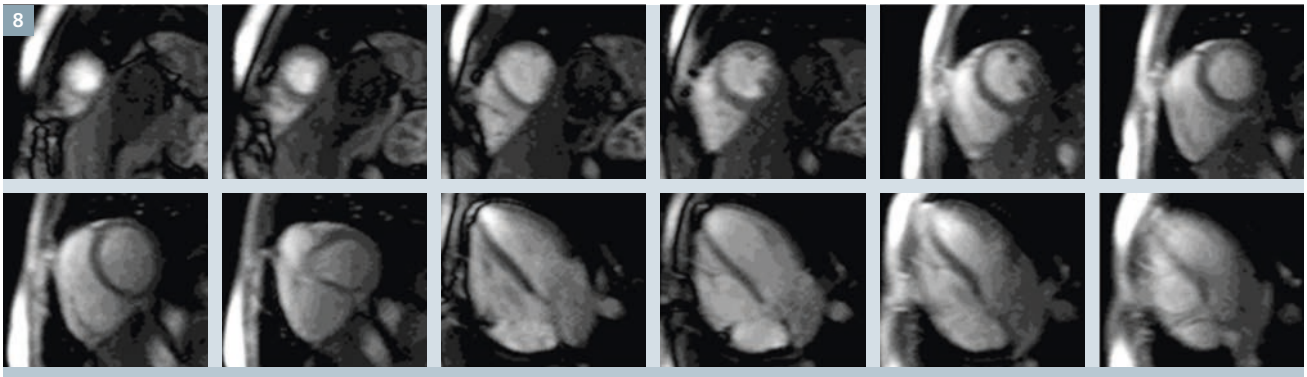

8 *In vivo* cardiac example: The MS-CAIPIRINHA approach enables the acquisition of up to 6 slices per cardiac cycle. Here, 12 slices are acquired within 2 cardiac cycles (8 slices in short-axis view and 4 in the long axis).

Imaging parameters: 1.5 T MAGNETOM Avanto, 32-channel cardiac array (Rapid Biomedical, Würzburg, Germany); Sequence: SR-TrueFISP, CAIPIRINHA phase cycle +90°/-90°; FOV 320 x 260 mm², matrix: 128 x 77, resolution 2.5 x 3.4 mm², slice thickness 10 mm, distance factor (two-slice pulse) of short/long axis: 200%/100%; partial Fourier 6/8, measurements: 20, TR 2.8 ms, TI 120 ms, TE 1.4 ms, FA 50°, reconstruction algorithm GRAPPA (R=3). *Images courtesy of Daniel Stäb.*

ing (2D-CAIPIRINHA) and clinically even to the often more routinely used 2D sequences (TSE; ss-EPI) with simultaneous multi-slice imaging (MS-CAIPIRINHA).

2D-CAIPIRINHA

In conventional PAT-accelerated 3D imaging, data reduction is performed in two spatial dimensions simultaneously by integer-valued undersampling in each phase-encoding direction. Though sensitivity variations can be exploited in two spatial dimensions, this sampling strategy provides suboptimal encoding performance. The 2D-CAIPIRINHA strategy modifies aliasing in a controlled manner already during the data acquisition. This is accomplished by shifting sampling positions in the two-dimensional phase-encoding scheme with respect to each other. In this way, at certain image acceleration values, an optimal sampling pattern can be found which minimizes signal overlap and at the same time allows one to efficiently take advantage of all the sensitivity variations provided by the coil array in the 2D phase-encoding plane. Thus, 2D-CAIPIRINHA provides optimal reconstruction performance given a certain coil configuration and object shape, and therefore results in optimal image reconstruction quality.

MS-CAIPIRINHA

Similar to 2D-CAIPIRINHA, aliasing in simultaneous multi-slice acquisitions can be modified already during the acquisition by employing alternating RF pulses for subsequent phase-encoding lines, thereby allowing the imprint of the individual slices with individual phase-cycles causing the slices to appear shifted with respect to each other thereby improving the reconstruction process minimizing *g*-factor-related noise enhancements. Thus, a CAIPIRINHA-type 4-slice excitation with low *g*-factor values (close to 1) allows the acquisition of 4 slices in the same time usually required for 1 slice without loss of SNR. The initial approach of alternating RF pulses introduced here, however, is not applicable for single-shot sequences such as EPI where only a single RF pulse is used to acquire all lines of *k*-space. Innovative concepts like blipped-CAIPINHA (see also the Article by Kawin Setsompop) where additional gradient magnetic fields are used during the readout to generate the required phase modulations allow to apply SMS to more advanced acquisition schemes such as SSFP [15] EPI [18] and radial [19] simultaneous multi-slice imaging.

However, it is important to note that multi-slice excitations are associated with significantly increased energy deposition, currently limiting the method to a moderate number of simultaneously excited slices, and/or to low flip angles. However, recently, a promising concept for reducing the RF power of multi-band pulses has been introduced [20]. Thus, MS-CAIPIRINHA is expected to become a powerful strategy in the near future allowing for significantly acceleration of many clinical protocols while almost preserving image quality.

Acknowledgments

The authors would like to thank Daniel Neumann from the *Research Center Magnetic Resonance Bavaria (MRB), Würzburg, Germany* and Daniel Stäb from the *Institute for Diagnostic Radiology, University Hospital Würzburg, Germany* for providing material.

In addition, the authors are extremely grateful for receiving continuing support from the colleagues from *Siemens Healthcare*, especially Stephan Kannengiesser, Dominik Nickel, Berthold Kiefer, Mathias Nittka, Vladimir Jellus and Randall Kroeker.

References

1 Pruessmann KP, Weiger M, Scheidegger B, Boesiger P. SENSE: sensitivity encoding for fast MRI. Magn Reson Med 1999; 42:952-962.

2 Griswold MA, Jakob PM, Heidemann RM, Nittka M, Jellus V, Wang J, Kiefer B, Haase A. GeneRalized Autocalibrating Partially Parallel Acqusitions (GRAPPA). Magn Reson Med 2002; 47:1202-1210.

3 Weiger M, Pruessmann KP, Boesiger P. 2D SENSE for faster 3D MRI. MAGMA. 2002 Mar; 14(1):10-9.

4 Larkman DJ, Hajnal JV, Herlihy AH, Coutts GA, Young IR, Ehnholm G. Use of multicoil arrays for separation of signal from multiple slices simultaneously excited. J Magn Reson Imaging. 2001 Feb; 13(2):313-7.

5 Breuer FA, Kannengiesser SA, Blaimer M, Seiberlich N, Jakob PM, Griswold MA. General formulation for quantitative G-factor calculation in GRAPPA reconstructions. Magn Reson Med. 2009 Sep;62(3):739-46.

6 Breuer FA, Blaimer M, Heidemann RM, Mueller MF, Griswold MA, Jakob PM. Controlled Aliasing in Parallel Imaging Results in Higher Acceleration (CAIPIRINHA) for Multislice Imaging. Magn Reson Med 2005; 53:684-691.

7 Breuer FA, Blaimer M, Mueller MF, Seiberlich N, Heidemann RM, Griswold MA, Jakob PM. Controlled aliasing in volumetric parallel imaging (2D CAIPIRINHA). Magn Reson Med. 2006 Mar;55(3):549-56.

8 Breuer FA, Moriguchi H, Seiberlich N, Blaimer M, Jakob PM, Duerk JL, Griswold MA. Zigzag sampling for improved parallel imaging. Magn Reson Med. 2008 Aug;60(2):474-8.

9 Bilgic B, Gagoski BA, Cauley SF, Fan AP, Polimeni JR, Grant PE, Wald LL, Setsompop K. Wave-CAIPI for highly accelerated 3D imaging. Magn Reson Med. 2015 Jun;73(6):2152-62.

10 Gagoski BA, Bilgic B, Eichner C, Bhat H, Grant PE, Wald LL, Setsompop K. RARE/turbo spin echo imaging with Simultaneous Multislice Wave-CAIPI. Magn Reson Med. 2015 Mar;73(3):929-38.

11 Blaimer M, Breuer FA, Seiberlich N, Mueller MF, Heidemann RM, Jellus V, Wiggins G, Wald LL, Griswold MA, Jakob PM. Accelerated volumetric MRI with a SENSE/GRAPPA combination. J Magn Reson Imaging. 2006 Aug;24(2):444-50.

12 Muller S. Simultaneous multislice imaging (SIMUSIM) for improved cardiac imaging. Magn Reson Med. 1989 Apr;10(1):145-55.

13 Glover GH. Phase-offset multiplanar (POMP) volume imaging: a new technique. J Magn Reson Imaging. 1991 Jul-Aug; 1(4):457-61.

14 Souza SP, Szumowski J, Dumoulin CL, Plewes DP, Glover G. SIMA: simultaneous multislice acquisition of MR images by Hadamard-encoded excitation. J Comput Assist Tomogr. 1988 Nov-Dec;12(6):1026-30.

15 Stäb D, Ritter CO, Breuer FA, Weng AM, Hahn D, Köstler H. CAIPIRINHA accelerated SSFP imaging. Magn Reson Med. 2011 Jan;65(1):157-64

16 Willis NP and Bresler Y. Optimal scan design for time varying tomographic imaging {II}: Efficient design and experimental validation. IEEE Trans. Image Processing, 1995 May; 4: 654-666.

17 Wu B, Millane RP, Watts R, Bones PJ. Improved matrix inversion in image plane parallel MRI. Magn Reson Imaging. 2009 Sep;27(7):942-53.

18 Setsompop K, Gagoski BA, Polimeni JR, Witzel T, Wedeen VJ, Wald LL. Blipped-controlled aliasing in parallel imaging for simultaneous multislice Echo Planar Imaging with reduced g-factor penalty. Magn Reson Med. 2011 Aug 19.

19 Yutzy SR, Seiberlich N, Duerk JL, Griswold MA. Improvements in multislice parallel imaging using radial CAIPIRINHA. Magn Reson Med. 2011 Jun;65(6):1630-7.

20 Norris DG, Koopmans PJ, Boyacioğlu R, Barth M. Power independent of number of slices radiofrequency pulses for low-power simultaneous multislice excitation. Magn Reson Med. 2011 Nov;66(5):1234-40.

Contact

Dr. Felix Breuer
Research Center
Magnetic Resonance Bavaria e.V. (MRB)
Am Hubland
97074 Würzburg, Germany
Phone: +49 (0) 931 318 3060
Fax: +49 (0) 931 318 4680
breuer@mr-bavaria.de

Advancing Diffusion MRI Using Simultaneous Multi-Slice Echo Planar Imaging

Kawin Setsompop[1, 2]; Stephen F. Cauley[1, 2]; Lawrence L. Wald[1, 2]

[1] Martinos Center for Biomedical Imaging, Department of Radiology, Massachusetts General Hospital, Charlestown, MA, USA
[2] Department of Radiology, Harvard Medical School, Boston, MA, USA

Introduction

There has been a recent significant interest in the use of parallel imaging based Simultaneous Multi-Slice (SMS) acquisition [1] to increase the temporal efficiency of many imaging sequences in MRI. In particular, the use of SMS for diffusion MRI (dMRI) and functional MRI (fMRI) has fundamentally changed the scope of studies that clinicians and researchers are able to perform with these imaging sequences. For dMRI, SMS has opened up the possibility of obtaining information from many more diffusion encoding directions in a limited timeframe, to enable more complex/advanced diffusion acquisitions to be performed in clinical and neuroscientific settings.

Due to the use of diffusion encoding gradients in dMRI, large temporally and spatially varying phase contamination exists, which hampers the utility of multi-shot acquisitions. As such, dMRI acquisitions are often based on rapid single-shot 2D spin-echo EPI sequence. This sequence provides high quality imaging but at a cost of being highly inefficient. Figure 1 shows the sequence diagram for such acquisition, where a single 2D imaging slice is excited, after which diffusion encoding is performed and the data for that particular slice is then readout/received using EPI encoding. This process is repeated multiple times, once for each imaging slice, until whole-brain coverage is achieved. As depicted, the diffusion encoding period can represent a significant portion of the acquisition time. This diffusion encoding is performed using magnetic field gradient pulses which provide encoding to the whole imaging volume. However, for each acquisition period, only a single slice is excited and acquired, and the lengthy diffusion encoding has to be repeated for all imaging slices, leading to large inefficiency.

1

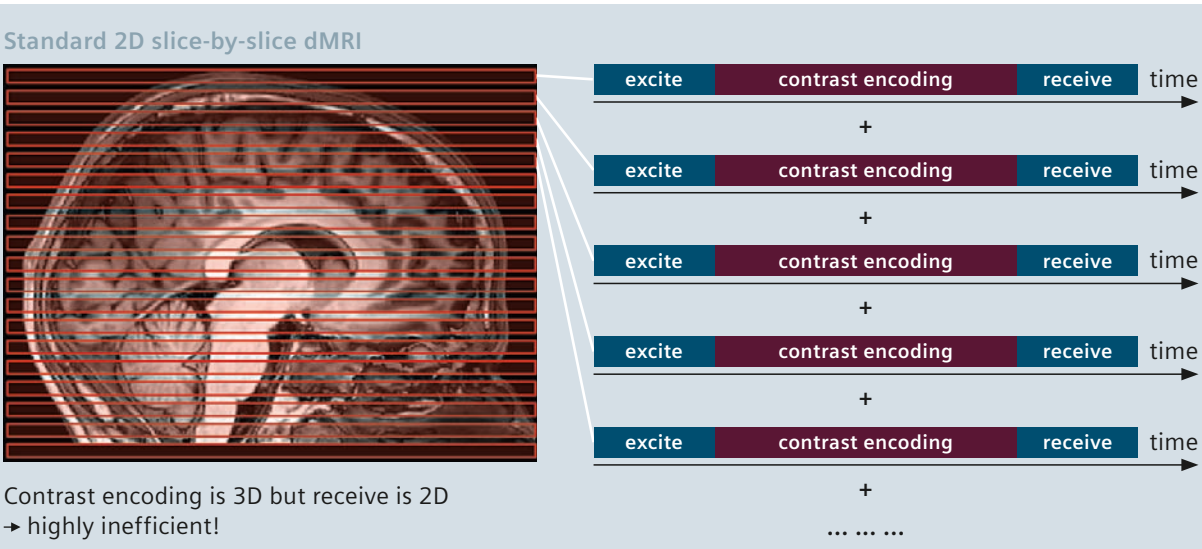

1 The inefficiency of standard 2D DWI techniques is illustrated. Although the lengthy diffusion contrast-encoding encompasses the entire volume, only a single slice is acquired. Simultaneous multi-slice enables the concurrent acquisition of several imaging slices during a single diffusion encoding. Unlike typical in-plane acceleration techniques, which only shorten the receive portion of the acquisition, SMS allows for proportional reductions in total scan time as the multiband factor is increased.

The use of conventional 2D parallel imaging acceleration [2-4] in dMRI can reduce the number of phase encoding steps of EPI which reduces image distortion and blurring artifacts. However, such technique does not provide significant acceleration to dMRI, since they only shorten the EPI encoding period and not the other components of the data acquisition, in particular the lengthy diffusion encoding. The use of simultaneous multi-slice (SMS) acceleration [1], on the other hand, allows for the concurrent acquisition of several imaging slices (the slices will appear collapsed before reconstruction) during each acquisition period, thereby reducing the number of acquisition periods needed to perform volumetric acquisition. Thus, SMS is much more effective at providing scan time reduction in dMRI, where the total scan time is now reduced by a factor equal to the number of simultaneously excited slices (multiband (MB) factor). Additionally, unlike conventional parallel imaging, SMS does not shorten the EPI encoding period and is not affected by the undesirable $\sqrt{R}$ SNR penalty of conventional parallel imaging.

Several SMS methods have been applied to single shot SMS-EPI, including Wideband imaging [5, 6], Simultaneous Image Refocusing (SIR) [7, 8] and parallel image reconstruction based multi-slice imaging [9, 10]. However, the presence of significant artifact and/or signal-to-noise (SNR) loss from these methods have prevented their wide scale adoption in dMRI. In particular, parallel imaging based multi-slice imaging suffers from high *g*-factor noise amplification in brain MRI. This is due to the fact that the imaging field-of-view (FOV) along the slice direction is typically small for brain acquisitions, causing the aliased voxels of the simultaneously acquired slices to be spatially close which makes it hard to tease them apart. An improved parallel imaging strategy termed CAIPIRINHA [11], which creates an inter-slice image shift between simultaneously acquired slices to increase the distance between the aliased voxels has been proposed as a way to reduce the *g*-factor penalty associated with SMS. The CAIPIRINHA method creates an inter-slice shift by utilizing a different RF pulse for the data acquisition of each *k*-space line, where each RF pulse is designed to induce a different phase modulation to each of the slices that are being acquired simultaneously. This is feasible for multi-shot acquisitions but not for single-shot EPI where only a single RF pulse is used to acquire all lines of *k*-space. An initial attempt to adopt CAIPIRINHA for single-shot EPI acquisitions was performed by Nunes *et al*. [9]. Here, a Wideband-like approach was used in the phase encoding and readout directions to increase the distance between aliased voxels. However, this resulted in voxel tilting (blurring) artifacts and heavily restricted the distance that could be imposed between aliased voxels. In this article, we describe the blipped-CAIPIRINHA method [12] which is a modification of Nunes' approach, to generate the desired voxel shifts in the phase encoding direction without tilting artifacts. This approach has provided us with the ability to perform high quality parallel imaging based SMS-EPI acquisition that can be used to significantly shorten dMRI acquisition time.

Blipped-CAIPIRINHA

The blipped-CAIPIRINHA method utilizes additional G_z magnetic field gradient blips during the EPI readout. Figure 2 shows the standard G_x and G_y gradients of the EPI encoding, along with these additional G_z gradient blips. These G_z blips are applied concurrently with the G_y phase encoding blips to create a different phase modulation between the simultaneously excited slices for the data acquisition of each *k*-space line. For this example, the G_z blips are being applied to create a FOV/2 shift along the phase encoding (PE) direction between two simultaneously acquired slices (collapsed image shown in top-right of Figure 2). In order to create the desired inter-slice shift, an appropriate gradient blip area must be used for these G_z blips. Specifically, in the example in

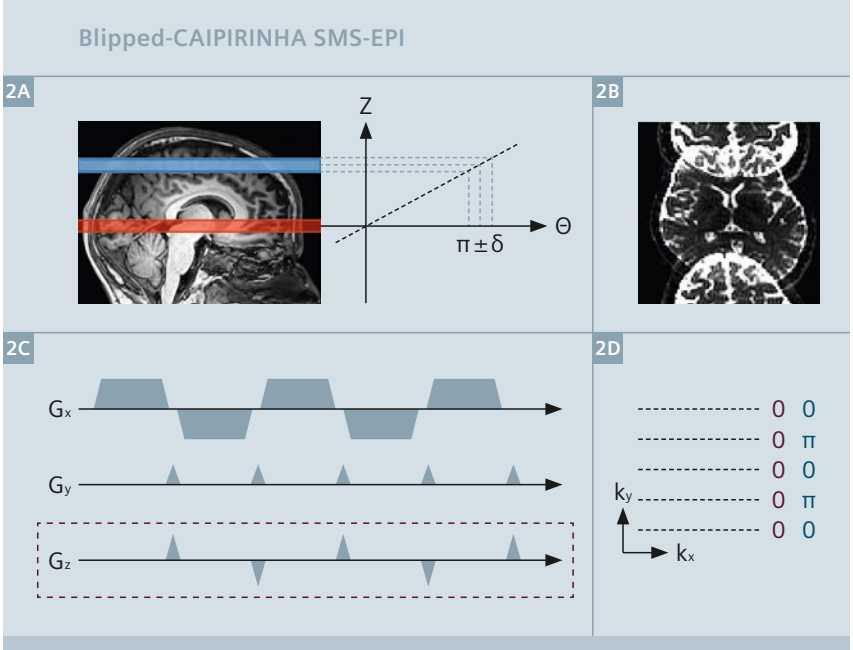

2 A blipped-CAIPIRINHA SMS-EPI gradient scheme applied across the X, Y and Z (Readout, Phase-Encode, and Slice) axes is illustrated. The G_z gradient blips required to create a FOV/2 shift between two simultaneously acquired slices are shown (collapsed image in **2B**). The blipped-CAIPIRINHA method varies the sign of the G_z gradient blips in order to avoid accumulation of through-slice phase variation, which would result in voxel titling artifacts. The accumulated phase applied to each of the k_y lines are shown for the two slices **(2D).**

Figure 2, each G_z blip will have to create a π phase increment to the spins located at the upper slice (blue) and no increment to the lower slice (red). The phase modulations along k_y caused by the G_z blip train are shown on the lower-right of Figure 2, for the upper (blue) and lower (red) imaging slices. With no phase modulation to the lower slice, this slice remains unaffected. On the other hand, the linear phase moduation along k_y at π phase increment for the top slice causes this slice to shift by FOV/2 along the PE direction. As such, a desired FOV/2 inter-slice shift is achieved.

It is important to note that each G_z blip will also introduce a small phase variation 2δ across the finitely thick slices being acquired as shown in Figure 2. This through-slice phase variation created by each blip will result in a very minor signal attenuation (typically less than 1%).
The important concept in blipped-CAIPIRINHA is the utilization of alternating positive and negative gradient blips to limit ability of the gradient moment and this through-slice phase variation to accumulate during the EPI encode and cause significant signal attenuation. This solves the issue of the Wideband approach where only positive G_z blips are employed which results in accumulation of through-slice dephasing and voxel tilting artifacts. Thus, the blipped-CAIPIRINHA method facilitates efficient CAIPIRINHA controlled aliasing schemes for simultaneously acquired slices in EPI. This can be seen clearly when examining the 3× slice-accelerated (SMS 3) example acquired using a 32-channel head coil at 3T shown in Figure 3. Here, the *g*-factor associated with FOV/2 shift and no-shift parallel imaging reconstructions are compared (both with slice-GRAPPA reconstruction). When no-shift was applied between the simultaneously acquired slices, the average retained SNR (1 / *g*-factor) dropped significantly to 68%. The blipped-CAIPIRINHA method with FOV/2 shift retained over 99% of the SNR, while removing the 3.5 voxel tilt that would have been present with the standard wideband approach. Thereby, blipped-CAIPIRINHA enables three times faster acquisitions in dMRI without incurring significant SNR penalty. (Note that in some regions the retained SNR is slightly greater than unity indicating some noise cancellation in the reconstruction process as previously demonstrated in low acceleration in-plane GRAPPA acquisitions [13]).

3 SMS-3 Blipped-CAIPIRINHA with 32-channel head coil

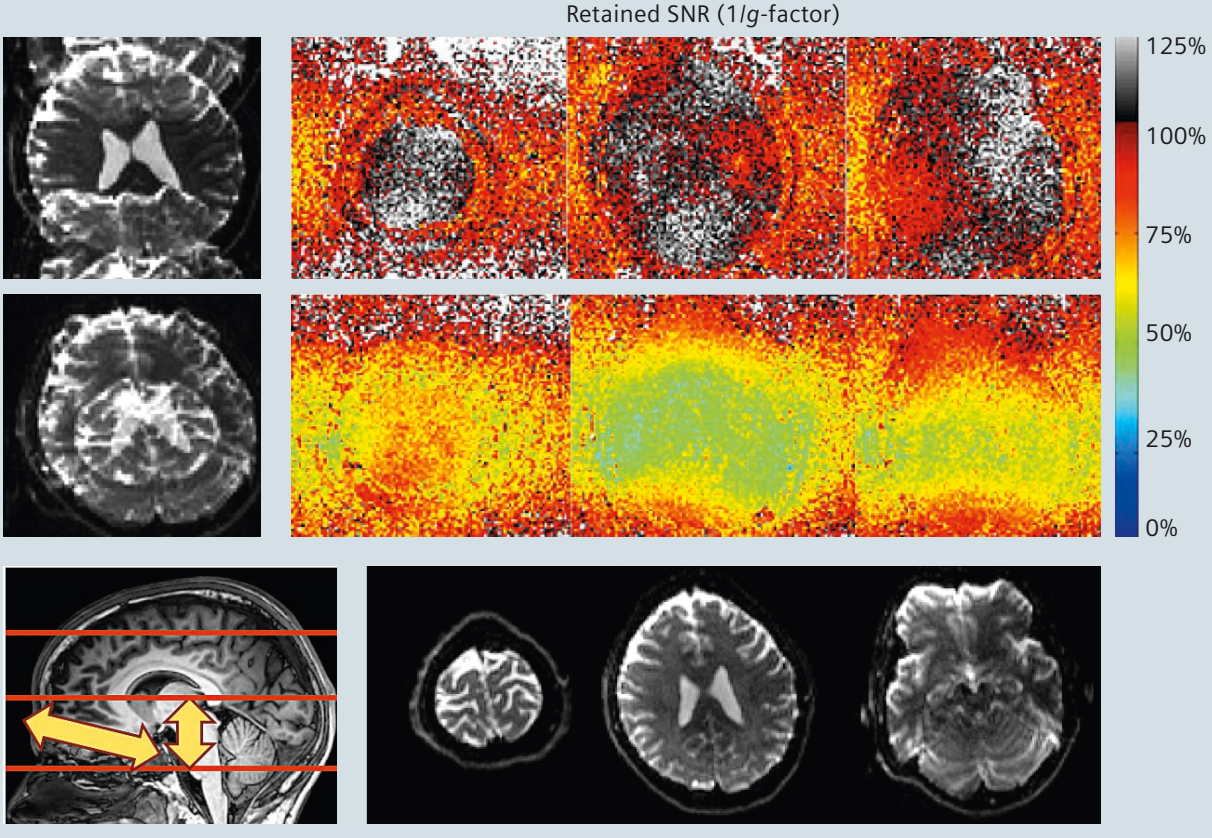

3 SMS-EPI at SMS-3 acceleration acquired at 3T using Siemens' 32-channel coil. The *g*-factor associated with FOV/2 shift and no-shift parallel imaging reconstructions are compared. The retained SNR (1 / *g*-factor), when no-shift was applied dropped significantly to 68%. The blipped-CAIPIRINHA method with FOV/2 shift retained over 99% of the SNR, while avoiding the 3.5 voxel tilt associated with standard wideband approaches.

RF pulse design and image reconstruction

When considering the use of blipped-CAIPIRINHA for high slice acceleration factors, there are several sequence design and image reconstruction aspects that need to be carefully developed. Of particular importance to diffusion-weighted imaging (DWI) is the design of the multiband RF pulse that allows for multiple slices to be simultaneously excited in SMS acquisitions. Multiband RF pulses cause an increase in SAR, which is especially problematic for DWI since it relies on high SAR spin-echo 90-180 pulses. At SMS-3 acceleration, the use of the VERSE algorithm [14] has been shown to provide adequate SAR reduction for *in vivo* DWI at 3T [15]. However, the benefit of SAR reduction from VERSE comes at a cost of slice profile distortion at off-resonance frequencies. This can be mitigated by the use of the SLR algorithm for RF pulse design along with a high time-bandwidth product that improves the slice-profile quality prior to the application of VERSE. Figure 4 (A, B) shows multiband 90-180 pulses with slice acceleration factor 3 designed using both the SLR and VERSE algorithms. Figure 4A shows the VERSE 90 and 180 RF pulses along with corresponding gradient pulses. Figure 4B shows the comparison of slice-profiles obtained from a standard single-slice 90-180 RF pulse pair and those obtained from the slice acceleration factor 3 RF pulse pair. Here, the high-quality slice profiles are achieved at both on resonance and 50 Hz off-resonance.

In addition to the combined design of VERSE and SLR, a number of other approaches have been developed to reduce both SAR and peak-power of MB pulses. These techniques are particularly beneficial at higher slice accelerations and/or for ultra-high field imaging. In order to reduce peak-power, a phase optimization scheme [16], a pulse time-shift method [17] and a combined approach [18, 19] of phase optimization with the use of 90° and 180° pulses with spatially-varying phases that combine to provide a flat spin-echo excitation phase have been

Multiband RF pulse: SLR & VERSE algorithm
high quality slice profile and low SAR

4A

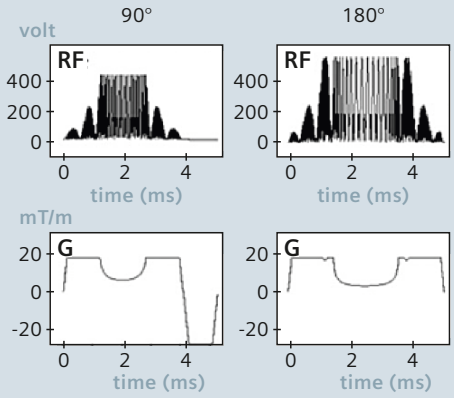

4B

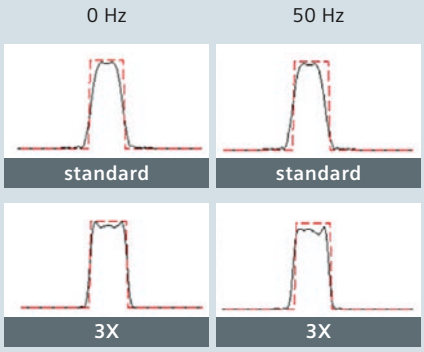

Slice-GRAPPA recon: leak-block and dual kernel

4C

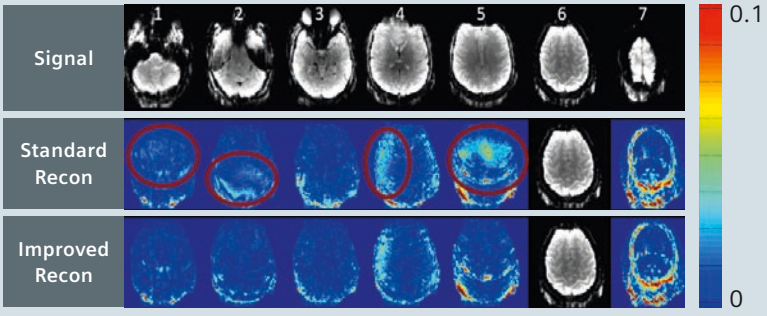

4D

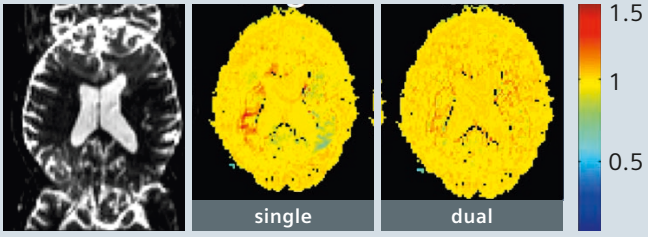

4 Critical implementation aspects for the blipped-CAIPIRINHA method are highlighted. The multiband 90-180 pulses with slice acceleration factor-3 designed using both the SLR and VERSE algorithms are shown. **(4A)** The VERSE 90 and 180 RF pulses along with corresponding Gradient pulses. **(4B)** A comparison of slice-profiles from a standard single-slice 90-180 RF pulse pair and those obtained from the slice acceleration factor 3 RF pulse pair. These pulses are necessary to ensure image quality while limiting peak-power and SAR. The benefits of the 'LeakBlock' Slice-GRAPPA reconstruction technique in reducing leakage signal contamination between simultaneously acquired slices is shown **(4C)**.The individual leakage signal contaminations onto the 6th imaging slice (for a SMS 7 acquisition) are greatly reduced when compared with standard slice-GRAPPA reconstruction. The use of 'dual kernel' slice-GRAPPA to separate SMS 3 blipped-CAIPIRINHA EPI with FOV/2 shift data is shown **(4D)**. The dual kernels operate specifically to the even and the odd lines of the slice-collapsed *k*-space data, and enable clean separation of both of the slice data and associated ghost (prior to the application of typical ghost correction).

proposed. In addition, the Power Independent of Number of Slices (PINS) [20] and MultiPINS [21] RF pulse designs have been proposed as a strategy to excite/refocus a large number of imaging slices simultaneously without increasing peak power or SAR.

A number of techniques have been developed in order to improve the quality of SMS-EPI image reconstruction. The original SENSE/GRAPPA approach for SMS reconstruction [22] has been modified to facilitate CAIPIRINHA acquisitions with inter-slice FOV shifts [23-25]. Slice-GRAPPA [12], which has been widely-used for blipped-CAIPIRINHA SMS-EPI reconstruction, has been redesigned to provide robust reconstruction through a 'LeakBlock' technique [26]. This technique reduces the leakage signal contamination between simultaneously acquired slices and has been shown to improve temporal stability at high accelerations. Figure 4C shows a comparison of signal leakage contamination in the standard and the improved LeakBlock slice-GRAPPA reconstructions for blipped-CAIPIRINHA acquisition at SMS-7 using a 32-channel head coil. It can be clearly seen that the individual leakage signal contaminations onto the 6th imaging slice are greatly reduced using the LeakBlock reconstruction.

Another important consideration for SMS-EPI reconstruction is in the minimization of N/2 image ghosting artifacts. For SMS-EPI, this is a particular concern since a different slice-specific ghost correction could be required for each of the simultaneously acquired imaging slices (due to differences in phase error of the N/2 ghost for different slice locations). Thus, the N/2 ghost cannot be cleanly removed from the slice-collapsed dataset prior to the parallel imaging (slice-unaliasing) reconstruction. The use of a 'dual kernel' slice-GRAPPA, where separate GRAPPA kernels are applied to the even and the odd lines of the slice-collapsed *k*-space data has been shown to overcome this issue [15]. This method enables a clean separation of both of the slice data and associated ghost, prior to the application of typical ghost correction.

Figure 4D shows a comparison of the N/2 ghost artifact level for an SMS-3 blipped-CAIPIRINHA SMS-EPI with FOV/2 shift reconstructed using i) single kernel slice-GRAPPA and ii) dual kernel slice-GRAPPA approaches. Note that the ghost artifact of the top imaging slice in the SMS acquisition lands directly in the center of the imaging FOV of the middle imaging slice (due to the FOV/2 inter-slice shift). This prevents the single kernel slice-GRAPPA approach from accurately unaliasing the ghosting artifact. Figure 4 shows the corresponding large reconstruction artifact in the center of the middle imaging slice. With the use of dual kernel slice-GRAPPA, this artifact has been mitigated. The dual kernel approach has been successfully applied to SENSE/GRAPPA reconstruction [27] and an extension of the method has been used to overcome artifacts associated with phase-encode line bunching [28]. Finally, for SENSE based reconstruction of SMS data, a slice-specific phase error of the ghost artifact has been successfully incorporated into the parallel imaging reconstruction [29].

Diffusion-weighted imaging applications

With the careful design of RF pulses and the image reconstruction framework, blipped-CAIPIRINHA allows for the efficient acquisition of high quality SMS-EPI data for DWI. In clinical settings, where time is limited, DWI is often restricted to only a small number of diffusion encoding directions. This constrains studies to only examine the most basic diffusion information, such as the apparent diffusion coefficient (ADC). With the use of blipped-CAIPIRINHA SMS-EPI, diffusion-weighted acquisitions can be accelerated robustly by 3-fold to provide high quality data with negligible SNR loss and artifact levels. This has allowed for more diffusion directions to be obtained in a clinically relevant time-frame, enabling more complex diffusion models/metrics (e.g. Fractional Anisotropy (FA), Diffusion Kurtosis, and fiber tracking) to be considered. Figure 5 demonstrates the use of blipped-CAIPIRINHA to achieve 3-fold acceleration for typical neuroimaging acquisitions based upon Diffusion Tensor Imaging (DTI), Q-ball, and Diffusion Spectrum Imaging (DSI). Here, the color FA, Orientation Distribution Function (ODF), and the fiber tracking results from these diffusion models are compared using standard SMS-1 and blipped-CAIPIRINHA SMS-3 acquisitions. In all cases, the high quality of the results is maintained at a 3-fold speed up with the blipped-CAIPIRINHA technique.

There is a growing interest in the application of DWI to areas outside the brain, where it has also proven to be highly sensitive to tissue abnormalities. Similar to the neuroimaging applications described above, blipped-CAIPIRINHA SMS-EPI can play a role in speeding up acquisitions in the body. Here, a large in-plane FOV has to be encoded and in-plane acceleration (typically a factor of 2) is used to reduce image distortion. While accelerations in the slice and in-plane directions are compatible, the use of both can lead to a high total acceleration factor (the product of the two acceleration factors) and result in higher *g*-factor noise amplifications. For the DWI applications where SNR is inherently low, it is desirable to keep the noise penalty to a minimum. Thus, a combined SMS-2 and in-plane-2 acceleration strategy is typically employed for blipped-CAIPIRINHA SMS-EPI in the body.

Figure 6 shows DWI results for liver, whole-body, and breast imaging from a standard in-plane-2 acceleration with and without the inclusion of blipped-CAIPIRINHA SMS factor 2. The imaging results are near identical, with the blipped-CAIPIRINHA acquisition providing a 2-fold speed up in imaging time. This is particularly useful for whole-body DWI, where a large number of imaging slices are acquired. Reducing these lengthy scans (often ~20 minutes is required for standard diffusion scans focusing on the basic ADC metric) will have a significant impact on the wide-spread adoption of whole-body DWI in clinical settings.

5

3x Faster brain dMRI

Q-ball: 12 min → 4 min

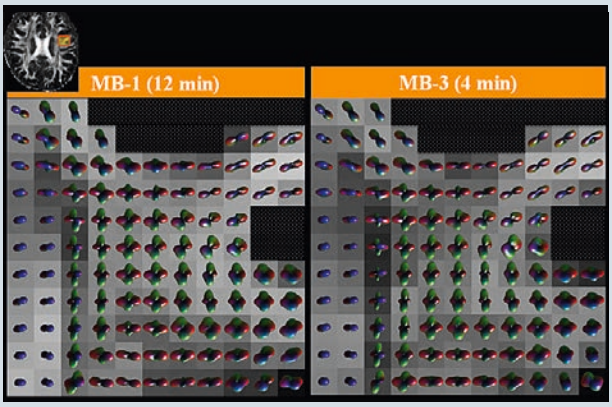

DTI: 10 min → 3 min

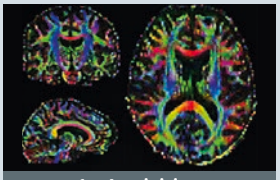

1x Aquisition

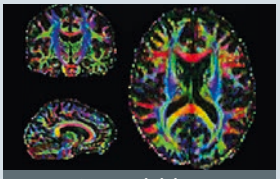

3x Aquisition

DSI: 45 min → 15 min

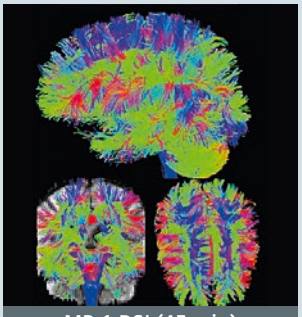

MB-1 DSI (45 min)

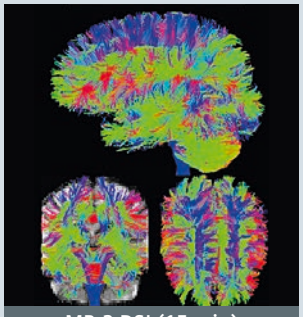

MB-3 DSI (15 min)

5 Diffusion Tensor Imaging, Q-ball, and Diffusion Spectrum Imaging are compared using standard SMS 1 and blipped-CAIPIRINHA SMS 3 acquisitions at 3T using Siemens' 32-channel head coil. The high level of similarities in color FA, Orientation Distribution Function, and the fiber tracking results can be clearly seen.

6

Applications outside of the brain

Liver diffusion

b = 50

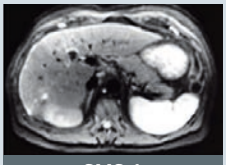

SMS-1

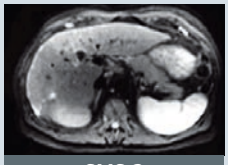

SMS-2

b = 400

SMS-1

SMS-2

b = 800

SMS-1

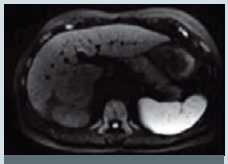

SMS-2

ADC

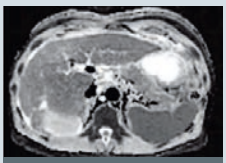

SMS-1

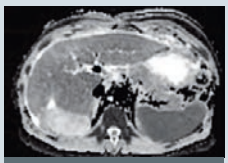

SMS-2

Whole-body diffusion

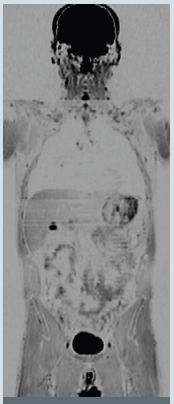

SMS-1

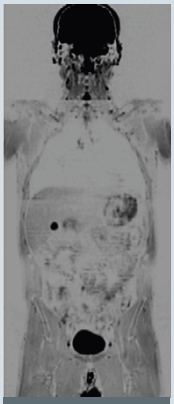

SMS-2

Breast diffusion

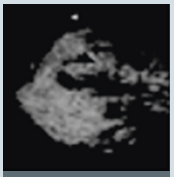

SMS-1

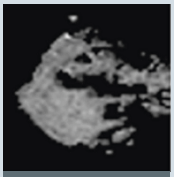

SMS-2

6 Emerging applications of DWI in the body are demonstrated. Blipped-CAIPIRINHA with SMS 2 and in-plane GRAPPA 2 was used in large FOV body diffusion. Relative to conventional DWI with in-plane GRAPPA 2, similar image quality can be seen. Blipped-CAIPIRINHA SMS enables effective combination of in-plane GRAPPA acceleration which is critical for the reduction of distortions especially in large FOV DWI of the body. With blipped-CAIPIRINHA SMS-EPI, scan time reductions to a factor of 2 with similar image quality can be obtained for the liver, breast, and whole-body DWI.

References

1 Larkman DJ, Hajnal J V, Herlihy AH, Coutts GA, Young IR, Ehnholm G. Use of multicoil arrays for separation of signal from multiple slices simultaneously excited. J Magn Reson imaging. 2001;13:313–7.

2 Pruessmann KP, Weiger M, Scheidegger MB, Boesiger P. SENSE: sensitivity encoding for fast MRI. Magn Reson Med [Internet]. 1999 Nov;42(5):952–62. Available from: 10.1002/(SICI)1522-2594(199911)42:5<952::AID-MRM16>3.0.CO;2-S.

3 Griswold MA, Jakob PM, Heidemann RM, Nittka M, Jellus V, Wang J, et al. Generalized autocalibrating partially parallel acquisitions (GRAPPA). Magn Reson Med [Internet]. 2002 Jun [cited 2014 Jan 21];47(6):1202–10. Available from: http://www.ncbi.nlm.nih.gov/pubmed/12111967.

4 Sodickson DK, Manning WJ. Simultaneous acquisition of spatial harmonics (SMASH): fast imaging with radiofrequency coil arrays. Magn Reson Med [Internet]. 1997 Oct;38(4):591–603. Available from: http://www.ncbi.nlm.nih.gov/pubmed/9324327.

5 Paley MNJ, Lee KJ, Wild JM, Griffiths PD, Whitby EH. Simultaneous parallel inclined readout image technique. Magn Reson Imaging [Internet]. 2006 Jun [cited 2014 Sep 9];24(5):557–62. Available from: http://www.ncbi.nlm.nih.gov/pubmed/16735176.

6 Weaver JB. Simultaneous Multislice Acquisition of MR Images. 1988;284:275–84.

7 Feinberg D a., Reese TG, Wedeen VJ. Simultaneous echo refocusing in EPI. Magn Reson Med. 2002;48(1):1–5.

8 Reese TG, Benner T, Wang R, Feinberg D a., Van Wedeen J. Halving imaging time of whole brain diffusion spectrum imaging and diffusion tractography using simultaneous image refocusing in EPI. J Magn Reson Imaging. 2009;29(3):517–22.

9 Nunes RG, Hajnal J V, Golay X, Larkman DJ. Simultaneous slice excitation and reconstruction for single shot EPI . Proc Intl Soc Mag Reson Med. 2006. p. 293.

10 Moeller S, Yacoub E, Olman C a, Auerbach EJ, Strupp J, Harel N, et al. Multiband multislice GE-EPI at 7 tesla, with 16-fold acceleration using partial parallel imaging with application to high spatial and temporal whole-brain fMRI. Magn Reson Med [Internet]. 2010 May [cited 2014 Jan 21];63(5):1144–53. Available from: http://www.pubmedcentral.nih.gov/articlerender.fcgi?artid=2906244&tool=pmcentrez&rendertype=abstract.

11 Breuer FA, Blaimer M, Heidemann RM, Mueller MF, Griswold MA, Jakob PM. Controlled aliasing in parallel imaging results in higher acceleration (CAIPIRINHA) for multi-slice imaging. Magn Reson Med. 2005;53:684–91.

12 Setsompop K, Gagoski BA, Polimeni JR, Witzel T, Wedeen VJ, Wald LL. Blipped-controlled aliasing in parallel imaging for simultaneous multislice echo planar imaging with reduced g-factor penalty. Magn Reson Med [Internet]. 2012 May [cited 2014 Jan 21];67(5):1210–24. Available from: http://www.pubmedcentral.nih.gov/articlerender.fcgi?artid=3323676&tool=pmcentrez&rendertype=abstract.

13 Polimeni JR, Wiggins GC, Wald LL. Characterization of artifacts and noise enhancement introduced by GRAPPA reconstructions. Proc Intl Soc Mag Reson Med. 2008. p. 1286.

14 Conolly SM, Nishimura DG, Macovski A, Glover GH. Variable-rate selective excitation. J Magn Reson [Internet]. 1988 Jul [cited 2012 Jul 4];78(3):440–58. Available from: http://linkinghub.elsevier.com/retrieve/pii/002223648890131X.

15 Setsompop K, Cohen-Adad J, Gagoski BA, Raij T, Yendiki A, Keil B, et al. Improving diffusion MRI using simultaneous multi-slice echo planar imaging. Neuroimage [Internet]. Elsevier Inc.; 2012 Oct 15 [cited 2014 Jan 30];63(1):569–80. Available from: http://www.pubmedcentral.nih.gov/articlerender.fcgi?artid=3429710&tool=pmcentrez&rendertype=abstract.

16 Wong E. Optimized phase schedules for minimizing peak RF power in simultaneous multi-slice RF excitation pulses. Proc Intl Soc Mag Reson Med [Internet]. 2012 [cited 2014 Jan 21]. p. 2209. Available from: http://scholar.google.com/scholar?hl=en&btnG=Search&q=intitle:Optimized+phase+schedules+for+minimizing+peak+RF+power+in+simultaneous+multi-slice+RF+excitation+pulses#0.

17 Auerbach EJ, Xu J, Yacoub E, Moeller S, Uğurbil K. Multiband accelerated spin-echo echo planar imaging with reduced peak RF power using time-shifted RF pulses. Magn Reson Med. 2013 May;69(5):1261–7.

18 Zhu K, Kerr AB, Pauly JM. Nonlinear-Phase Multiband 90°-180° RF Pair With Reduced Peak Power. Proc Intl Soc Mag Reson Med. 2014. p. 1440.

19 Sharma A, Bammer R, Stenger VA, Grissom W a. Low peak power multiband spokes pulses for B 1 + inhomogeneity-compensated simultaneous multislice excitation in high field MRI. Magn Reson Med [Internet]. 2015;doi: 10.1002/mrm.25455. Available from: http://doi.wiley.com/10.1002/mrm.25455.

20 Norris DG, Koopmans PJ, Boyacioğlu R, Barth M. Power Independent of Number of Slices (PINS) radiofrequency pulses for low-power simultaneous multislice excitation. Magn Reson Med [Internet]. 2011 Nov [cited 2014 Jan 10];66(5):1234–40. Available from: http://www.ncbi.nlm.nih.gov/pubmed/22009706.

21 Eichner C, Wald LL, Setsompop K. A low power radiofrequency pulse for simultaneous multislice excitation and refocusing. Magn Reson Med [Internet]. 2014 Oct [cited 2014 Sep 25];72:949–58. Available from: http://www.ncbi.nlm.nih.gov/pubmed/25103999.

22 Blaimer M, Breuer F a, Seiberlich N, Mueller MF, Heidemann RM, Jellus V, et al. Accelerated volumetric MRI with a SENSE/GRAPPA combination. J Magn Reson imaging [Internet]. 2006 Aug [cited 2014 Oct 13];24(2):444–50. Available from: http://www.ncbi.nlm.nih.gov/pubmed/16786571.

23 Stäb D, Ritter CO, Breuer F a, Weng AM, Hahn D, Köstler H. CAIPIRINHA accelerated SSFP imaging. Magn Reson Med. 2011;65:157–64.

24 Blaimer M, Choli M, Jakob PM, Griswold M a, Breuer F a. Multiband phase-constrained parallel MRI. Magn Reson Med [Internet]. 2013 Apr [cited 2014 Jul 21];69(4):974–80. Available from: http://www.pubmedcentral.nih.gov/articlerender.fcgi?artid=3606646&tool=pmcentrez&rendertype=abstract.

25 Moeller S, Vu AT, Auerbach E, Ugurbil K, Yacoub E. RO extended FOV SENSE/GRAPPA for multiband imaging with FOV shift. Proc Intl Soc Mag Reson Med. 2014. p. 4396.

26 Cauley SF, Polimeni JR, Bhat H, Wald LL, Setsompop K. Interslice leakage artifact reduction technique for simultaneous multislice acquisitions. Magn Reson Med [Internet]. 2014 [cited 2014 Jan 28];72:93–102. Available from: http://www.ncbi.nlm.nih.gov/pubmed/23963964.

27 Koopmans PJ, Poser BA, Breuer FA. 2D-SENSE-GRAPPA For Fast, Ghosting-Robust Reconstruction of In-Plane and Slice Accelerated Blipped-CAIPI-EPI. Proc Intl Soc Mag Reson Med. 2015. p. 2410.

28 Moeller S, Auerbach EJ, Vu AT, Lenglet C, Sotiropoulos SN, Ugurbil K, et al. EPI 2D ghost correction and integration with multiband : application to diffusion imaging at 7T. Proc Intl Soc Mag Reson Med. 2015. p. 248.

29 Zhu K, Dougherty RF, Takahashi A, Pauly J, Kerr AB. Nyquist Ghosting Correction For Simultaneous Multislice Echo Planar Imaging. 2014. p. 647.

Contact

Kawin Setsompop
Massachusetts General Hospital
Martinos Center for Biomedical Imaging
Building 75, Room 2.102, 13th Street
Charlestown, MA, 02129, USA
Phone: +1 617-669-6640
kawin@nmr.mgh.harvard.edu

SIEMENS

The MAGNETOM World

Your portal to talks, articles and case studies

siemens.com/magnetom-world

Siemens' global MRI community offers peer-to-peer support and information. Radiologists, physicists, cardiologists, and technologists, have all contributed with publications, presentations, training documents, case studies, and more – all freely available to you via this unique network.

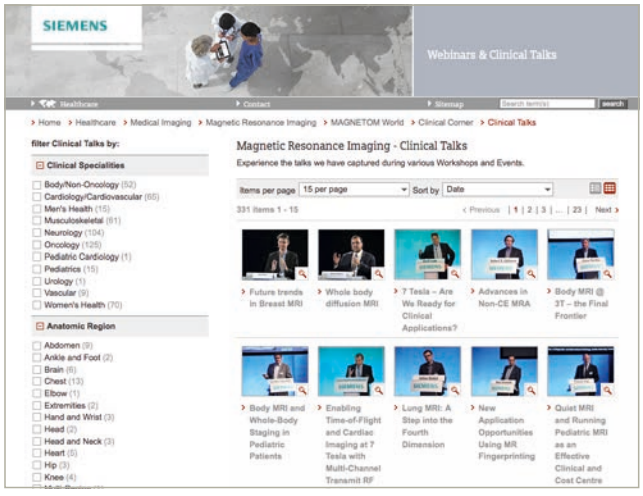

Don't miss the >300 lectures and presentations by international and renowned experts on all aspects of MRI that will allow you to be exposed to new ideas an alternative approaches.

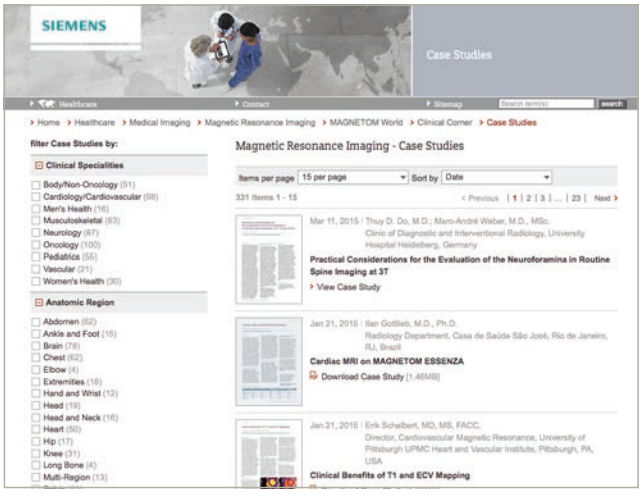

The centerpiece of the MAGNETOM World Internet platform consists of MAGNETOM users' results. Here you will find case reports, articles and application tips allowing you to optimize your daily work.

Put the advantages of the MAGNETOM World to work for you!

siemens.com/magnetom-world

Perspective – High Potential Impact of Simultaneous Multi-Slice Diffusion Acquisition Strategies on Future Clinical Neuroradiology Practice

Timothy Shepherd, M.D., Ph.D.

Assistant Professor, Neuroradiology Section, Department of Radiology, New York University, New York, NY, USA

Diffusion has become a critical component of almost all neuroradiology protocols for the head [1] with potential important roles in spine and neck now being better defined [2, 3]. The most impactful application over the past 25 years has been that diffusion is essential for the diagnosis of acute stroke, a frequent indication for MRI in hospitals throughout the world. Diffusion MRI also helps determine subsequent clinical management decisions in this stroke population [1]. Tissue diffusion properties can be informative for characterizing a variety of other neurological conditions such as perioperative or drug-related cytotoxic edema, specific tumor diagnoses (e.g. epidermoid) and tumor grading (e.g. lymphoma) [4]. Early mathematical models of diffusion anisotropy that are widely available for clinical use, such as diffusion tensor imaging (DTI), can be used to indirectly assess white matter integrity. DTI can characterize white matter pathology not evident or readily detected with other conventional MRI sequences (e.g. normal-appearing white matter in multiple sclerosis) [5]. DTI data can be used to create tractography estimations for localizing eloquent white matter pathways, such as the arcuate fasciculus, for preoperative surgical planning of anatomic corridors and extent of resection [6].

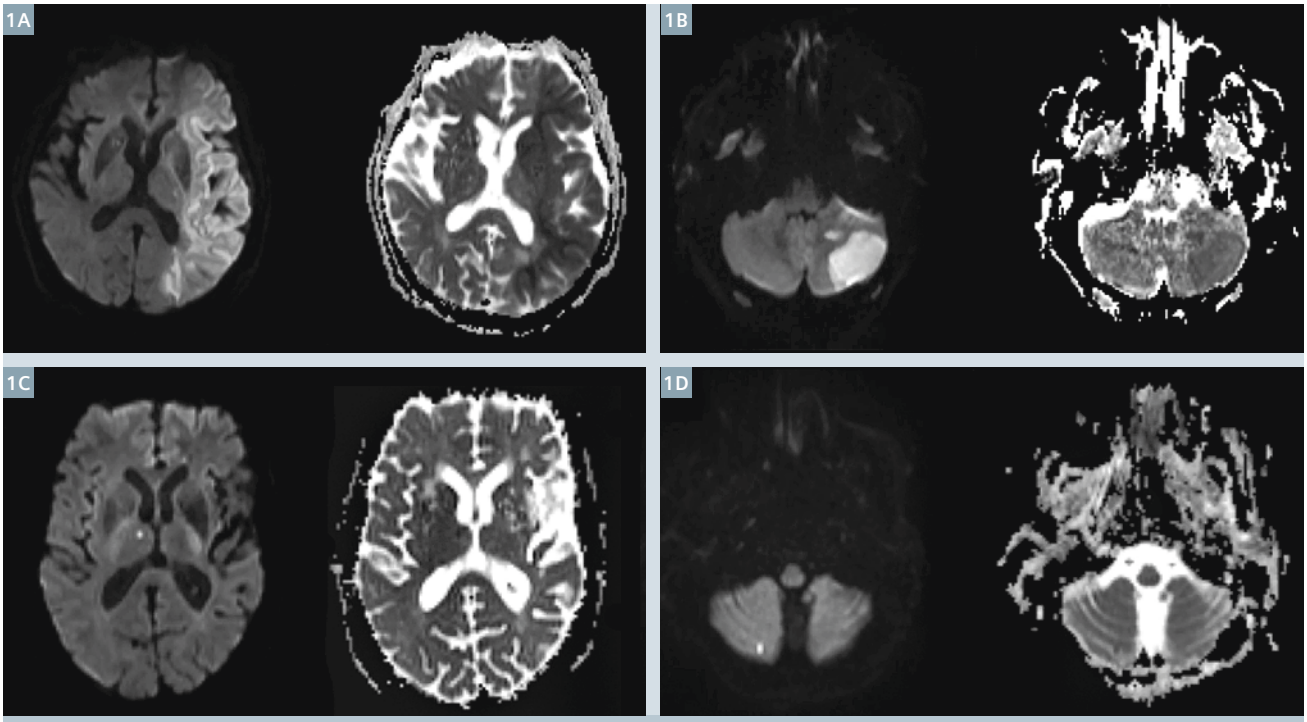

1 Simultaneous multi-slice axial diffusion trace and apparent diffusion coefficient maps in 4 different clinical patients with ischemic infarcts – large left middle cerebral artery territory **(1A)**, left anterior inferior cerebellar territory **(1B)**, right thalamus **(1C)** and right peripheral cerebellar hemisphere **(1D)**. Note while there was a small drop in apparent signal-to-noise in the posterior fossa using SMS diffusion with a 20-channel head & neck coil, large and small, focal posterior fossa infarcts remain well-delineated (panels 1B, D respectively).

For current routine clinical imaging, diffusion trace and apparent diffusion coefficient (ADC) maps have proven most efficient and practical – these generally only require 3 or 6 diffusion encoding directions for sufficient accuracy during qualitative clinical interpretation. Such scans can be acquired in 2-3 minutes on most modern MRI scanners, whereas DTI for tractography purposes can require 10+ minute acquisitions. More recent acquisition strategies and their companion advanced data analysis techniques developed over the past 15 years provide more information about the tissue environment than diffusion trace or DTI-derived parameters, yet remain relatively limited to application in volunteers and/or selected patient populations under carefully controlled conditions. Such sophisticated techniques require longer acquisitions to increase the number of gradient directions, increase spatial resolution, and/or to acquire images at multiple diffusion-weightings (e.g., b-values of 1500-4000 s/mm^2). These acquisitions result in lower signal-to-noise ratio (SNR) that also can require more signal averages. Scan time for such acquisitions is largely affected by image geometry (number of slices and resolution/matrix size), number of averages and diffusion encoding directions [7], but quickly approaches 15-30 minutes, making it impractical for use in most sick patients. Thus, higher angular resolution diffusion acquisition strategies [8, 9], measures of non-Gaussian diffusion [10], advanced biophysical modeling [11, 12, 13] and high spatial resolution diffusion studies of cortical and hippocampal layers [14, 15] have shown exciting potential utility for studying nervous tissue in disease that is thus far unrealized in daily clinical practice.

Recently, simultaneous multi-slice (SMS) acquisition with a blipped-CAIPIRINHA readout has demonstrated the potential to reduce scan times for 2D multislice diffusion EPI [16, 17]. This technique relies on exciting multiple slices simultaneously and reconstructing them individually using the slice GRAPPA method. Since multiple slices are excited simultaneously, the overall repetition time (TR) for a desired spatial coverage can be reduced. The SMS acceleration method is SNR preserving with no intrinsic reduction in signal due to reduced sampling. The only SNR penalty is due to *g*-factor related losses during slice GRAPPA reconstruction. In simple terms for practicing radiologists like myself, this new SMS technology allows us to acquire the same diffusion data for a variety of clinical and translational research applications using a much shorter TR and shortened overall scan time. Alternatively SMS can be used to increase slice resolution and/or increase the overall volume of coverage in the same scan time.

At our institution, we were quick to recognize the potential practical workflow advantages for SMS diffusion to reduce scan time requirements in our patient population. In our initial explorations of the SMS diffusion application in healthy volunteers, we learned that one must pay particular attention to correct fat saturation. With single-shot EPI, an unsaturdated fat signal affects only a single slice. With SMS, there is potential for aliasing into all simultaneously acquired slices. With TR reduction below 2.5 seconds, factors such as increased acoustic noise may make patients less comfortable. We also noted that SMS trace images have more T1-weighting than we were used to seeing – this 'T1-shine through' is most evident in the limbic cortical regions and in the central portions of the cortical spinal tract as it descends through the hemispheric white matter away from the hand knob region. We directly compared the axial diffusion sequence for our routine MRI head protocol to an SMS version with acceleration factor of 2 and a TR reduced by 50%. Scans were performed on a MAGNETOM Skyra 3T (Siemens Healthcare, Erlangen, Germany) with a Head/Neck 20 coil. With the calibration scan required for the SMS reconstructions, scan time was reduced approximately 40%, thereby saving 1 minute per scan. Given that a diffusion-weighted sequence is present in almost all neuroradiology protocols, this 1 minute time savings would translate into sufficient time for an additional 2-3 patient scans per day per magnet at a busy outpatient practice. Similar results are expected for coronal diffusion acquisitions although this is not a part of our institution's routine protocols. Further time savings might be realized with 3 or 4-fold slice acceleration using array coils with more receive elements (such as a Siemens 64-channel head and neck coil). In a blinded side-by-side comparison, 3 neuroradiologists universally agreed that image quality was equivalent between the routine and SMS-accelerated axial diffusion trace sequence and calculated ADC images such that the latter was acceptable for routine clinical work (see examples in Fig. 1).

Next we compared diffusion tensor imaging and deterministic tractography for presurgical planning cases – again, side-by-side comparison of data obtained with SMS acceleration factor of 2 appeared equivalent and appropriate for use in clinical care. Tractography results for the corticospinal tract and arcuate fasciculus in close proximity to various ipsilateral intra-axial neoplasms were equivalent for routine and SMS-based high angular resolution diffusion acquisitions (see example in Fig. 2). Our referring neurosurgeons have been very happy with the resulting data and have used SMS-derived tractography as part of their routine workflow on a weekly basis for surgical planning over the past 9 months. Thus far, we have scanned over 1000 patients with MRI head protocols using SMS diffusion without problems or patient recalls for diffusion image quality. The initial results of these comparisons were reported at RSNA last year [18] and a more detailed report has been submitted for publication.

Completing routine clinical scans faster has many practical advantages for patients and radiology administrators, but what I personally am most excited about is the potential for SMS-accelerated diffusion to enable more translational research in patient populations with advanced diffusion acquisition and postpro-

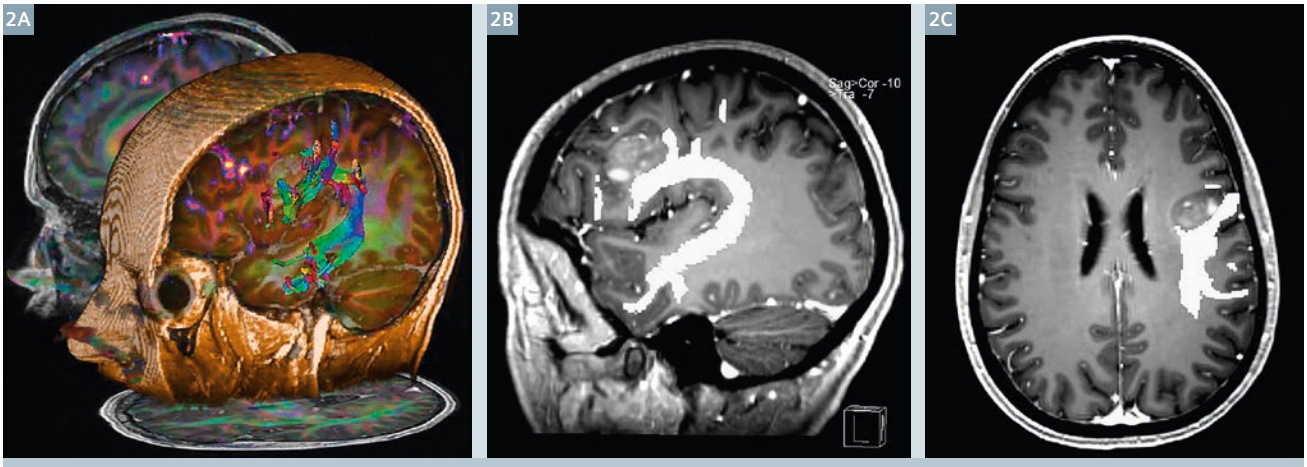

2 Deterministic diffusion tensor tractography of the arcuate fasciculus based on a simultaneous multi-slice diffusion dataset from a left-language dominant patient with a left frontal operculum high-grade glioma (**2A**: 3D lateral projection of tracts on MPRAGE with overlay from fMRI word generation task). Oblique sagittal and axial 2D reformats (**2B, C** respectively) demonstrate that the tumor margin abuts the inferior and medial margins of the tractography-visualized frontal projections of the arcuate fasciculus. Over the past year we have consistently obtained excellent tractography results for presurgical planning patients using SMS diffusion acquisition strategies – the accelerated acquisition quickly provides a diffusion dataset with high angular resolution, reduces patient motion problems and leaves more available scan time for detailed functional MRI assessment of eloquent cortex.

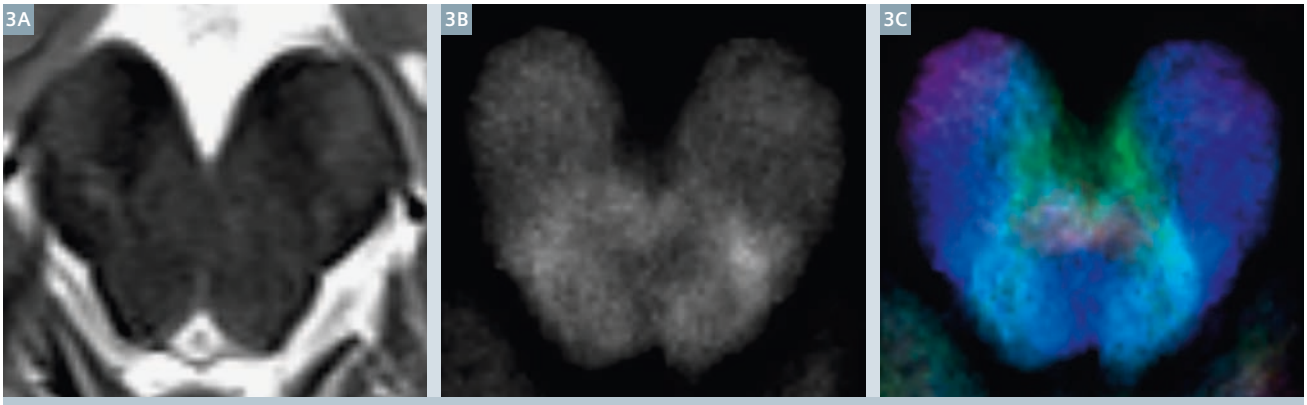

3 Short scan times enabled by simultaneous multi-slice diffusion should facilitate more frequent clinical use or implementation of advanced diffusion acquisitions and postprocessing. Here an example of caudal midbrain anatomy depicted with conventional axial T2 **(3A)**, track density images **(3B)** and direction-encoded track density **(3C)**. This advanced diffusion technique requires high angular resolution diffusion acquisitions (64 directions, b = 2500 s/mm^2), but can be acquired with SMS approaches in under 10 minutes. Exquisite anatomical detail is obtained and may be exploited in the future for new biomarkers of brainstem pathology and functional neurosurgery planning [for details see 19-21].

cessing strategies. Frankly, most patients, particularly elderly sick patients, will not tolerate individual scan sequence scan times beyond 8-10 minutes well. SMS acquisition strategies finally may allow us to apply advanced diffusion strategies reported at research meetings to *real* patients. As an example, over the past 6 months, we have been using SMS-diffusion acquisition strategies to acquire high angular resolution multiple *b*-shell scans for diffusion kurtosis imaging and advanced models of mesoscopic tissue structure in over 500 patients as part of an NIH-funded study – it would not be practical to include this acquisition using conventional diffusion acquisitions because of scan time and workflow limitations on our busy clinical scanners. We also use SMS to obtain diffusion data sufficient for super-resolution tract density imaging (TDI) [19] to define thalamic substructures for functional neurosurgery planning in patients with essential tremor and Parkinson's disease [20]. Recent results indicate SMS diffusion acquisitions combined with TDI can reveal internal brainstem anatomy not previously seen in living patients using 3T MRI [21] (see examples in Fig. 3). These latter two results from our group suggest neuroradiologists may need to relearn detailed anatomy

for deep gray nuclei and brainstem structures that were previously considered difficult or impossible to visualize outside autopsy. Such studies also could lead to direct targeting opportunities in the future for functional neurosurgery applications.

Finally, it should be emphasized that the best models of human pathology are living human patients! The present difficulty studying real patients with long diffusion scan times has so far limited application of advanced biophysical models of tissue mesoscopic structure derived from diffusion data to cooperative, motivated outpatients with chronic conditions, animal models of human disease, and *ex vivo*, formaldehyde-fixed samples, where many water diffusion and relaxation properties are altered [22, 23]. I personally anticipate that SMS diffusion techniques will provide a substantial new window of opportunity to study many new patient populations with both acute and chronic pathologies directly – this should result in improved understanding of human neurologic diseases, such as the nervous tissue changes associated with acute stroke. SMS appears to represent a transformative technology for translating advanced diffusion MRI applications into clinical practice.

References

1 Schaefer PW, Grant PE, Gonzalez RG. Diffusion-weighted MR imaging of the brain. Radiology 2000; 217(2): 331-345.

2 Andre JB, Zaharchuk G, Saritas E, et al. Clinical evaluation of reduced field-of-view diffusion-weighted imaging of the cervical and thoracic spine and spinal cord. Am J Neuroradiol 2012; 33(10): 1860-1866.

3 Thoeny HC. Diffusion-weighted MRI in head and neck radiology: applications in oncology. Cancer Imaging 2011; 10: 209-214.

4 Barajas RF Jr, Rubenstein JL, Chang JS, Hwang J, Cha S. Diffusion-weighted MR imaging derived apparent diffusion coefficient is predictive of clinical outcome in primary central nervous system lymphoma. Am J Neuroradiol 2010; 31(1): 60-66.

5 Mesaros S, Rocca MA, Kacar K, et al. Diffusion tensor MRI tractography and cognitive impairment in multiple sclerosis. Neurology 2012; 78(13): 969-975.

6 Wu JS, Zhou LF, Tang WJ, et al. Clinical evaluation and follow-up outcome of diffusion tensor imaging-based functional neuronavigation: a prospective, controlled study in patients with gliomas involving pyramidal tracts. Neurosurgery 2007; 61(5): 935-948.

7 Mukherjee P, Chung SW, Berman JI, Hess CP, Henry RG. Diffusion tensor MR imaging and fiber tractography: technical considerations. Am J Neuroradiol 2008; 29(5): 843-852.

8 Tuch, DS. Q-ball imaging. Magn Reson Med 2004; 52(6): 1358-1372.

9 Wedeen VJ, Hagmann P, Tseng WY, Reese TG, Weisskoff RM. Mapping complex tissue architecture with diffusion spectrum magnetic resonance imaging. Magn Reson Med 2005; 54(6): 1377-1386.

10 Jensen JH, Helpern JA. MRI quantification of non-Gaussian water diffusion by kurtosis analysis. NMR Biomed 2010; 23(7): 698-710.

11 Assaf Y, Freidlin RZ, Rohde GK, Basser PJ. New modeling and experimental framework to characterize hindered and restricted water diffusion in brain white matter. Mag Reson Med 2004; 52(5): 965-978.

12 Zhang H, Schneider T, Wheeler-Kingshott CA, Alexander DC. NODDI: Practical in vivo neurite orientation dispersion and density imaging of the human brain. Neuroimage 2012; 61(4): 1000-1016.

13 Fieremans EJ, Jensen JH, Tabesh A, Hu C, Helpern J.A. White matter model for diffusional kurtosis imaging. Paper presented at: ISMRM 2010. Proceedings of the 18th Annual Meeting of the International Society for Magnetic Resonance in Medicine: 2010 May 1-7; Stockholm, Sweden.

14 McNab JA, Polimeni JR, Wang R, et al. Surface based analysis of diffusion orientation for identifying architectonic domains in the in vivo human cortex. Neuroimage 2013; 69: 87-100.

15 Shepherd T, Ozarslan E, Yachnis AT, King MA, Blackband SJ. Diffusion tensor microscopy indicates the cytoarchitectural basis for diffusion anisotropy in the human hippocampus. Am J Neuroradiol; 28(5): 958-964.

16 Setsompop K, Gagoski BA, Polimeni JR, Witzel T, Wedeen VJ, Wald LL. Blipped-controlled aliasing in parallel imaging for simultaneous multislice echo planar imaging with reduced g-factor penalty. Magn Reson Med 2012; 67(5): 1210-1024.

17 Xu J, Moeller S, Auerbach EJ, et al. Evaluation of slice accelerations using multiband echo planar imaging at 3T. Neuroimage 2013; 83: 991-1001.

18 Young MG, Cohen BA, Glielmi C, et al. Multiband sequence reduces scan time for diffusion MRI and tractography in clinical patients. Paper presented at: RSNA 2014. Proceedings of the 100th Scientific Assembly and Annual Meeting of the Radiological Society of North America; 2014 Nov 30 – Dec 5; Chicago, USA.

19 Calamante F, Tournier JD, Jackson GD, Connelly A. Tract density imaging (TDI) : super-resolution white matter imaging using whole-brain track density mapping. Neuroimage 2010; 53(4): 1233-1243.

20 Shepherd TM, Chung S, Glielmi C, Mogilner AY, Boada F, Kondziolka D. 3-Tesla magnetic resonance imaging track density imaging to identify thalamic nuclei for functional neurosurgery. Paper presented at: CNS 2014. Proceedings of the 63rd Annual Congress of Neurological Surgeons; 2014 Oct 18-22; Boston, USA.

21 Hoch M, Chung S, Yoshimoto A, Ben-Eliezer N, Fatterpekar G, Shepherd TM. Advanced multiparametric MRI reveals detailed in vivo brainstem anatomy at 3-T. Paper presented at: ASNR 2015. Proceedings of the 53rd Annual Meeting of the American Society of Neuroradiology; 2015 Apr 25-30; Chicago, USA.

22 Shepherd TM, Flint JJ, Thelwall PE., et al. Postmortem interval alters the water relaxation and diffusion properties of rat nervous tissue – implications for MRI studies of human autopsy samples. Neuroimage 2009; 44(3): 820-826.

23 Shepherd TM, Thelwall PE, Stanisz GJ, Blackband SJ. Aldehyde fixative solutions alter the water relaxation and diffusion properties of nervous tissue. Magn Reson Med 2009; 62(1): 26-34.

Contact

Timothy Shepherd
NYU School of Medicine
NYU Langone Medical Center
Department of Radiology
660 First Avenue
New York, NY 10016
USA
Phone: +1 212/263-8487
Timothy.Shepherd@nyumc.org

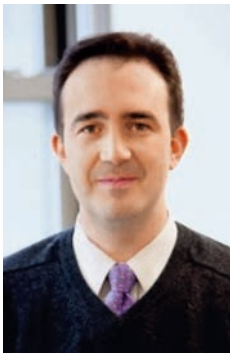

Accelerated Diffusion Tensor Imaging of Skeletal Muscle Using Simultaneous Multi-Slice Acquisition

Lukas Filli, M.D.[1]; Marco Piccirelli, Ph.D.[2]; David Kenkel, M.D.[1]; Roman Guggenberger, M.D.[1]; Gustav Andreisek, M.D., MBA[1]; Thomas Beck, Ph.D.[3]; Val M. Runge, M.D.[4]; Andreas Boss, M.D., Ph.D.[1]

[1] Institute of Diagnostic and Interventional Radiology, University Hospital Zurich, University of Zurich, Switzerland
[2] Department of Neuroradiology, University Hospital Zurich, University of Zurich, Switzerland
[3] MR Application Development, Siemens Healthcare, Erlangen, Germany
[4] Department of Diagnostic, Interventional and Pediatric Radiology, University Hospital of Bern, Inselspital, Bern, Switzerland

Abstract

Simultaneous multi-slice acquisition with CAIPIRINHA reduces the scan time in diffusion-weighted magnetic resonance imaging. In this article, we resume our early experience with this technique for accelerated diffusion tensor imaging of skeletal muscle [1].

Introduction

Diffusion tensor imaging (DTI) is based on measuring the diffusion of water molecules along six or more gradient directions. In contrast to conventional diffusion-weighted imaging, DTI provides voxel-wise information not only on the amount (mean diffusivity, MD) but also on the anisotropy (fractional anisotropy, FA) and direction of diffusion.

In previous studies, DTI was used for characterizing the fiber course and physiological muscle behavior as well as pathological changes such as muscle tears or edema [2-7]. Theoretically, skeletal muscle has an ideal tissue structure for DTI applications given its long, parallel fibers. However, the relatively short T2 relaxation time in muscle leads to an inherently unfavorable signal-to-noise ratio (SNR), which needs to be compensated by the acquisition of multiple signal averages. Thus, the clinical applicability of muscle DTI is currently limited by its long scan time.

A promising new approach to overcome this limitation is simultaneous multi-slice acquisition with blipped-CAIPIRINHA [8-10]. In brief, this technique excites multiple slices at once and applies phase shifts during readout. The reconstruction uses the spatial sensitivity of coil elements to separate the signal contributions from the different slices. We used this technique for accelerated DTI of the calf muscles and hypothesized that similar image quality could be achieved compared to standard DTI.

Methods

We scanned the calf of eight healthy subjects (age, 29.4 ± 2.9 years) in a 3T scanner (MAGNETOM Skyra, Siemens Healthcare, Erlangen, Germany) with a dedicated 15-channel knee coil. DTI was performed by applying 20 different diffusion encoding directions at a b-value of 500 s/mm^2. In addition to a conventional DTI sequence, simultaneous multi-slice acquisition was performed with a dedicated work-in-

1

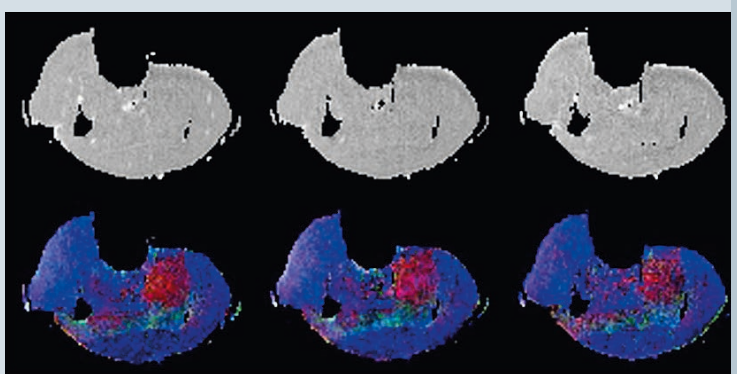

1 Example axial MD and color-coded FA maps at the level of the maximum calf diameter. The signal-free areas anteriorly and laterally correspond to the tibia and fibula, respectively. SA = slice acceleration. *Used with permission from [1].*

2

2 Examples of fiber tracking in the medial (orange) and lateral (cyan) gastrocnemius muscles. Fiber tracking was performed by placing a seed region of interest at the level of the maximum calf diameter. SA = slice acceleration. *Used with permission from [1].*

Table 1:

	Conventional DTI		Slice acceleration factor 2		Slice acceleration factor 3	
	MD (10^{-3} mm²/s)	FA	MD (10^{-3} mm²/s)	FA	MD (10^{-3} mm²/s)	FA
Medial gastrocnemius	1.62 ± 0.09	0.22 ± 0.01	1.60 ± 0.04	0.23 ± 0.02	1.61 ± 0.12	0.24 ± 0.02
Lateral gastrocnemius	1.68 ± 0.06	0.22 ± 0.02	1.64 ± 0.10	0.23 ± 0.02	1.68 ± 0.10	0.24 ± 0.02
Soleus	1.67 ± 0.10	0.24 ± 0.03	1.64 ± 0.08	0.23 ± 0.02	1.65 ± 0.09	0.27 ± 0.04
Tibialis anterior	1.74 ± 0.10	0.35 ± 0.05	1.71 ± 0.14	0.36 ± 0.05	1.83 ± 0.10	0.38 ± 0.06

Fractional anisotropy (FA) and mean diffusivity (MD) measured in the calf muscles. *Used with permission from [1].*

progress package[1] running on the *syngo* MR D13C platform. Two different protocols were acquired with a slice acceleration factor of two and three slices, respectively.

In all sequences, we measured MD and FA values in the medial and lateral gastrocnemius, soleus, and tibialis anterior muscles. In addition, DTI fiber tracking was performed with dedicated post-processing software ('Neuro 3D' application, *syngo* MMWP, Siemens Healthcare, Erlangen, Germany). The success of fiber tracking was compared between the standard and slice-accelerated DTI sequences both quantitatively (number of tracks, average track length) and qualitatively (anatomical precision score, ranging from 1 = poor to 5 = excellent). Last, the SNR was estimated for all sequences by using the subtraction method [11, 12].

Results

Compared to the conventional DTI sequence (7:24 min), significantly shorter acquisition times could be achieved with slice acceleration factor 2 (3:53 min) and 3 (2:38 min).

MD values were similar in all sequences ($p \geq 0.20$). FA values were similar in conventional DTI and two-fold slice acceleration but higher with three-fold slice acceleration ($p = 0.006$) (Table 1).

Fiber tracking worked equally well with conventional DTI and two-fold slice acceleration. However, with three-fold slice acceleration, a significant decrease in the number of tracks ($p < 0.001$) and the anatomical precision score ($p \leq 0.005$) was observed in the soleus and tibialis anterior muscles.

The overall SNR was 57.3 ± 6.6 in conventional DTI, 45.3 ± 11.2 with two-fold slice acceleration, and 35.1 ± 8.2 with three-fold slice acceleration. However, the SNR per minute increased with higher slice acceleration (conventional DTI: 7.7 ± 1.1; slice acceleration factor 2: 11.7 ± 3.0; slice acceleration factor 3: 13.3 ± 3.1).

Discussion

Simultaneous multi-slice acquisition with blipped-CAIPIRINHA proved feasible for accelerated DTI of skele-

[1] The product is still under development and not commercially available yet. Its future availability cannot be ensured.

3

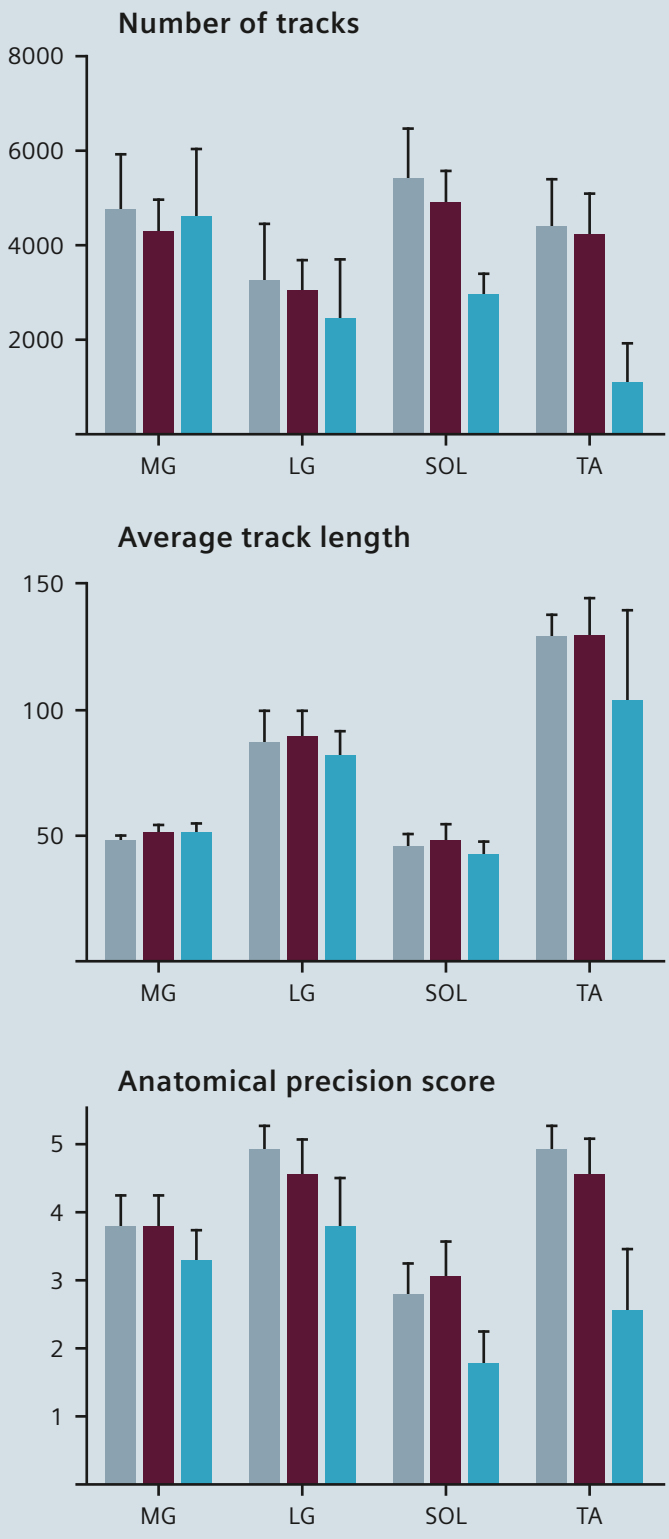

3 Performance of fiber tracking regarding the number of tracks, average track length [mm] and anatomical precision score. SA = slice acceleration. *Used with permission from [1].*

Conventinal DTI
2x SA
3x SA

tal muscle. With the parameters used in our study, a slice acceleration factor of 2 turned out to be the optimal compromise between reduction of acquisition time, quantification accuracy and image quality. Threefold slice acceleration was limited by two factors: First, FA values were significantly higher compared to conventional DTI, which may be attributed to the reduced SNR [13, 14]; second, fiber tracking was impaired regarding number of tracks and anatomical precision, likely due to the lower SNR.

Whereas previous studies used only 6–10 diffusion encoding directions [15-18], we used 20 because recent

works proposed at least 12 or even 20 directions for accurate estimation of anisotropy [19, 20]. In contrast, we only acquired two signal averages (compared to 6-10 in the above-mentioned studies). Additional signal averages would elevate the SNR but do not influence the minimum sampling requirement of the diffusion tensor [21]. With our DTI parameters, all sequences yielded an SNR above the critical threshold of 25 for accurate muscle DTI [19].

The scan time reduction by almost 50% notably increases the clinical applicability of muscle DTI. It can be assumed that simultaneous multi-slice acquisition with blipped-CAIPIRINHA also qualifies for the assessment of tears or hematoma [2-4], where muscle DTI has its greatest potential for clinical application.

References

1 Filli L, Piccirelli M, Kenkel D, et al. Simultaneous Multislice Echo Planar Imaging With Blipped Controlled Aliasing in Parallel Imaging Results in Higher Acceleration: A Promising Technique for Accelerated Diffusion Tensor Imaging of Skeletal Muscle. Investigative radiology. 2015;50:456-63. doi:10.1097/RLI.0000000000000151.

2 Fan RH, Does MD. Compartmental relaxation and diffusion tensor imaging measurements in vivo in lambda-carrageenan-induced edema in rat skeletal muscle. NMR in biomedicine. 2008;21:566-73. doi:10.1002/nbm.1226.

3 Zeng H, Zheng JH, Zhang JE, et al. Grading of rabbit skeletal muscle trauma by diffusion tensor imaging and tractography on magnetic resonance imaging. Chinese medical sciences journal = Chung-kuo i hsueh k'o hsueh tsa chih / Chinese Academy of Medical Sciences. 2006;21:276-80.

4 Zaraiskaya T, Kumbhare D, Noseworthy MD. Diffusion tensor imaging in evaluation of human skeletal muscle injury. Journal of magnetic resonance imaging : JMRI. 2006;24:402-8. doi:10.1002/jmri.20651.

5 Froeling M, Oudeman J, Strijkers GJ, et al. Muscle Changes Detected by Diffusion-Tensor Imaging after Long-Distance Running. Radiology. 2014:140702. doi:10.1148/radiol.14140702.

6 Okamoto Y, Kemp GJ, Isobe T, et al. Changes in diffusion tensor imaging (DTI) eigenvalues of skeletal muscle due to hybrid exercise training. Magnetic resonance imaging. 2014. doi:10.1016/j.mri.2014.07.002.

7 Noehren B, Andersen A, Feiweier T, et al. Comparison of twice refocused spin echo versus stimulated echo diffusion tensor imaging for tracking muscle fibers. Journal of magnetic resonance imaging : JMRI. 2014. doi:10.1002/jmri.24585.

8 Setsompop K, Gagoski BA, Polimeni JR, et al. Blipped-controlled aliasing in parallel imaging for simultaneous multislice echo planar imaging with reduced g-factor penalty. Magnetic resonance in medicine : official journal of the Society of Magnetic Resonance in Medicine / Society of Magnetic Resonance in Medicine. 2012;67:1210-24. doi:10.1002/mrm.23097.

9 Chang WT, Setsompop K, Ahveninen J, et al. Improving the spatial resolution of magnetic resonance inverse imaging via the blipped-CAIPI acquisition scheme. NeuroImage. 2014;91:401-11. doi:10.1016/j.neuroimage.2013.12.037.

10 Eichner C, Jafari-Khouzani K, Cauley S, et al. Slice accelerated gradient-echo spin-echo dynamic susceptibility contrast imaging with blipped CAIPI for increased slice coverage. Magnetic resonance in medicine : official journal of the Society of Magnetic Resonance in Medicine / Society of Magnetic Resonance in Medicine. 2014;72:770-8. doi:10.1002/mrm.24960.

11 Price RR, Axel L, Morgan T, et al. Quality assurance methods and phantoms for magnetic resonance imaging: report of AAPM nuclear magnetic resonance Task Group No. 1. Medical physics. 1990;17:287-95.

12 Khalil C, Hancart C, Le Thuc V, et al. Diffusion tensor imaging and tractography of the median nerve in carpal tunnel syndrome: preliminary results. European radiology. 2008;18:2283-91. doi:10.1007/s00330-008-0971-4.

13 Jones DK, Cercignani M. Twenty-five pitfalls in the analysis of diffusion MRI data. NMR in biomedicine. 2010;23:803-20. doi:10.1002/nbm.1543.

14 Lau AZ, Tunnicliffe EM, Frost R, et al. Accelerated human cardiac diffusion tensor imaging using simultaneous multislice imaging. Magnetic resonance in medicine : official journal of the Society of Magnetic Resonance in Medicine / Society of Magnetic Resonance in Medicine. 2014. doi:10.1002/mrm.25200.

15 Galban CJ, Maderwald S, Uffmann K, et al. A diffusion tensor imaging analysis of gender differences in water diffusivity within human skeletal muscle. NMR in biomedicine. 2005;18:489-98. doi:10.1002/nbm.975.

16 Sinha S, Sinha U, Edgerton VR. In vivo diffusion tensor imaging of the human calf muscle. Journal of magnetic resonance imaging : JMRI. 2006;24:182-90. doi:10.1002/jmri.20593.

17 Lansdown DA, Ding Z, Wadington M, et al. Quantitative diffusion tensor MRI-based fiber tracking of human skeletal muscle. J Appl Physiol (1985). 2007;103:673-81. doi:10.1152/japplphysiol.00290.2007.

18 Heemskerk AM, Sinha TK, Wilson KJ, et al. Repeatability of DTI-based skeletal muscle fiber tracking. NMR in biomedicine. 2010;23:294-303. doi:10.1002/nbm.1463.

19 Froeling M, Nederveen AJ, Nicolay K, et al. DTI of human skeletal muscle: the effects of diffusion encoding parameters, signal-to-noise ratio and T2 on tensor indices and fiber tracts. NMR in biomedicine. 2013;26:1339-52. doi:10.1002/nbm.2959.

20 Jones DK. The effect of gradient sampling schemes on measures derived from diffusion tensor MRI: a Monte Carlo study. Magnetic resonance in medicine : official journal of the Society of Magnetic Resonance in Medicine / Society of Magnetic Resonance in Medicine. 2004;51:807-15. doi:10.1002/mrm.20033.

21 Papadakis NG, Murrills CD, Hall LD, et al. Minimal gradient encoding for robust estimation of diffusion anisotropy. Magnetic resonance imaging. 2000;18:671-9.

Contact

Lukas Filli, M.D.
Institute of Diagnostic and Interventional Radiology
University Hospital Zurich
University of Zurich
Raemistrasse 100
CH-8091 Zurich
Switzerland
Phone +41 44 225 11 11
lukas.filli@usz.ch

Simultaneous Multi-Slice Accelerated Free-Breathing Diffusion-Weighted Imaging in Abdomen and Pelvis

Chika Obele, M.D.[1]; Himanshu Bhat, Ph.D.[2]; Hersh Chandarana, M.D.[1]

[1] Department of Radiology, NYU School of Medicine, New York, NY, USA
[2] Siemens Healthcare, MR R&D Collaborations, Charlestown, MA, USA

Abstract

Accelerated free-breathing diffusion-weighted imaging of the abdomen and pelvis is feasible with simultaneous multi-slice acquisition with maintained integrity of the diagnostic image quality. In this article we show clinical examples where the accelerated SMS technique was noted to decrease acquisition time by approximately 40%.

Introduction

Diffusion-weighted imaging (DWI) offers many benefits in abdomen and pelvis imaging particularly for evaluation of several abdominopelvic diseases such as focal and diffuse liver disease, prostate cancer, focal renal disease, and uterine cancer [1, 2]. There are also several investigational applications showing the importance of DWI in assessment of tumor response [3, 4] and predicting the aggressiveness of some tumors such as bladder cancer [5, 6]. Given the many benefits and potential applications of DWI in the abdomen and pelvis, in addition to the ease in which it can be integrated into existing clinical protocols, DWI has become a commonly used MRI sequence and an integral part of our abdominopelvic MR imaging protocols.

Conventional DWI using single-shot spin-echo echo-planar (SS EPI) technique can be acquired in multiple ways including a free-breathing (FB) technique with or without navigator and with multiple breath-hold (BH) technique [1]. The BH technique is constrained by the breath-hold capacity of the patient and thus is limited in the number of b-values that can be acquired, the resolution that can be achieved, and has low signal-to-noise ratio (SNR) due to inability to acquire multiple averages given the time constraints. The FB techniques are limited due to long acquisition time and inefficiency of the navigated scheme. FB acquisition with multiple averages (instead of navigator) is a preferred compromise at our institution as this is faster than the navigated acquisition scheme and is shown to have better image quality and higher resolution compared to the breath-hold acquisition. Despite the use of parallel imaging techniques like GRAPPA for in-plane acceleration, there is a need to further accelerate FB DWI acquisition. Recent introduction of the simultaneous multi-slice (SMS) DWI technique has the potential to further speed-up DWI acquisition [7]. We will briefly discuss the SMS technique below and share our clinical experience for abdominal and pelvic DWI imaging with SMS acquisition scheme.

SMS: basics and principle

SMS relies on exciting multiple slices simultaneously and reconstructing them individually using the slice

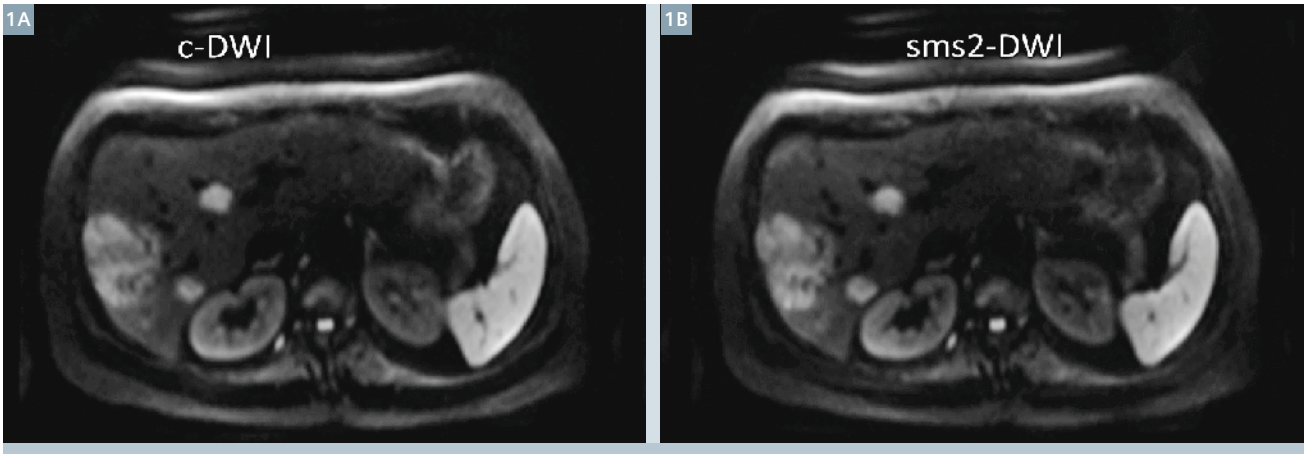

1 55-year-old female with weight loss. Multiple hyperintense liver lesions are demonstrated on both the DWI acquisition schemes. The acquisition time for SMS2-DWI **(1B)** was approximately 40% shorter than the conventional acquisition scheme **(1A).**

GRAPPA method. Since multiple slices are excited simultaneously the overall TR for a desired spatial coverage is reduced, leading to scan time reduction by the same factor. In order to minimize the g-factor SNR penalty during slice GRAPPA reconstruction, the blipped-CAIPIRINHA scheme is used to impart a relative FOV shift in the phase encoding direction between the simultaneously excited slices [7]. One key aspect of SMS compared with other acceleration techniques is that it does not suffer from the typical square-root of acceleration factor SNR penalty due to data under-sampling. Further technical details about SMS acquisition and reconstruction can be found elsewhere in this publication.

Abdominal SMS diffusion-weighted imaging

Liver MRIs were conducted on a clinical 3T system with peak gradient amplitude of 45 mT/m and slew rate of 200 T/m/s (MAGNETOM Skyra, Siemens Healthcare, Erlangen, Germany). The scan was performed using an 18-channel body matrix receive coil. A routine liver protocol was utilized including pre-contrast DWI. DWI was performed with transverse free-breathing single-shot echo-planar (EP) acquisitions with monopolar tri-directional trace weighting diffusion gradients (Fig. 1). Two different acquisition schemes were used as below.

Conventional DWI (c-DWI): TR 4500 ms, TE 66 ms, matrix 164 x 123, voxel size (interpolated) 2.3 x 2.3 x 5 mm, 34 axial 5 mm slices with inter-slice gap of 0.5 mm, bandwidth 1386 Hz/pix, parallel imaging acceleration factor of 2, 3 b-values (0, 400, and 800 s/mm^2), and 4 averages; and acquisition time of 2:29 minutes.

SMS DWI with twofold acceleration (SMS2-DWI): TR 2400 ms, TE 66 ms, matrix 164 x 123, voxel size (interpolated) 2.3 x 2.3 x 5 mm, 34 axial 5 mm slices with inter-slice gap of 0.5 mm, bandwidth 1386 Hz/pix, parallel imaging acceleration factor of 2, 3 b-values (0, 400, and 800 s/mm^2), and 4 averages. Two slices were acquired simultaneously using blipped-CAIPIRINHA (slice shift = $FOV_{phase}/3$) and individual slices are reconstructed using slice GRAPPA reconstruction. With SMS2-DWI TR was reduced to 2400 msec (from 4500 msec with conventional DWI), resulting in decrease in acquisition time of approximately 40% to 1:28 minutes.

Clinical scenario 1: A 55-year-old female with weight loss was found to have multiple inconclusive lesions on liver ultrasound. Multiple hyperintense liver lesions are demonstrated on both DWI acquisition schemes. The acquisition time for SMS2-DWI was approximately 40% shorter than the conventional acquisition scheme (Fig. 1).

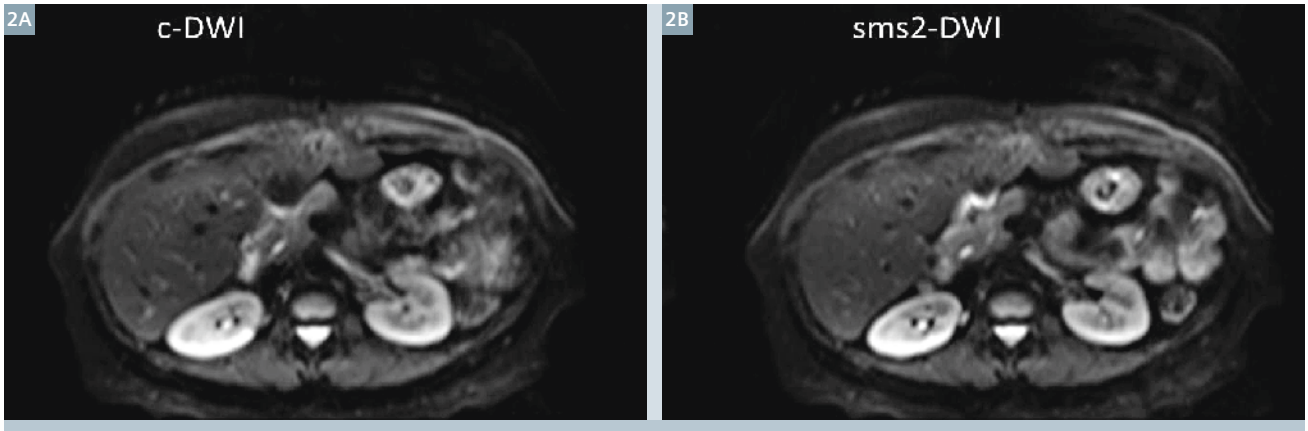

2 50-year-old Asian woman post liver transplantation for HBV cirrhosis and hepatocellular carcinoma. MRI of transplanted liver demonstrates comparable image quality between the two acquisition schemes but with 45% shorter scan time with accelerated SMS acquisition **(2B)**.

Clinical scenario 2: 50-year-old Asian woman post liver transplantation for Hepatitis B virus-related (HBV) cirrhosis and hepatocellular carcinoma. MRI of transplanted liver demonstrates comparable image quality between the two acquisition schemes but with 40% shorter scan time with accelerated SMS.

Pelvic SMS diffusion-weighted imaging

Patients underwent pelvis MRI on a clinical 3T system with peak gradient amplitude of 45 mT/m and a slew rate of 200 T/m/s (MAGNETOM Skyra, Siemens Healthcare, Erlangen, Germany). A routine pelvis protocol was utilized including pre-contrast DWI. DWI was performed with transverse free-breathing single-shot echo-planar (EP) acquisitions with monopolar tri-directional trace weighting diffusion gradients (Fig. 3). Two different acquisition schemes were used as below.

Conventional DWI (c-DWI): TR 5600 ms, TE 54 ms, matrix 164 x 164, voxel size (interpolated) 2.3 x 2.3 x 6 mm, 25 axial 6 mm slices with inter-slice gap of 0.6 mm, bandwidth 2032 Hz/pix, parallel imaging factor of 2, 5 b-values (0, 50, 100, 400, and 800 s/mm^2), and 4 averages for acquisition time of 5:08 minutes.

SMS DWI with twofold acceleration (SMS2-DWI): TR 2700 ms, TE 54 ms, matrix 164 x 164, voxel size (interpolated) 2.3 x 2.3 x 6 mm, 25 axial 6 mm slices with inter-slice gap of 0.6 mm, bandwidth 1681 Hz/pix, parallel imaging factor of 2, 5 b-values (0, 50, 100, 400, and 800 s/mm^2), and 4 averages, for acquisition time of 2:42 minutes. Two slices were acquired simultaneously using blipped-CAIPIRINHA (slice shift = $FOV_{phase}/3$) and individual slices are reconstructed using slice GRAPPA reconstruction. With accelerated SMS acquisition TR was reduced to 2700 msec from 5600 msec for conventional acquisition. This resulted in ~ 45% decrease in acquisition time.

Clinical scenario 3: A 42-year-old female with history of endometriosis presented with abdominal pain. The DWI images were similar, with approximately 45% reduction in imaging time with SMS2-DWI (Fig. 3).

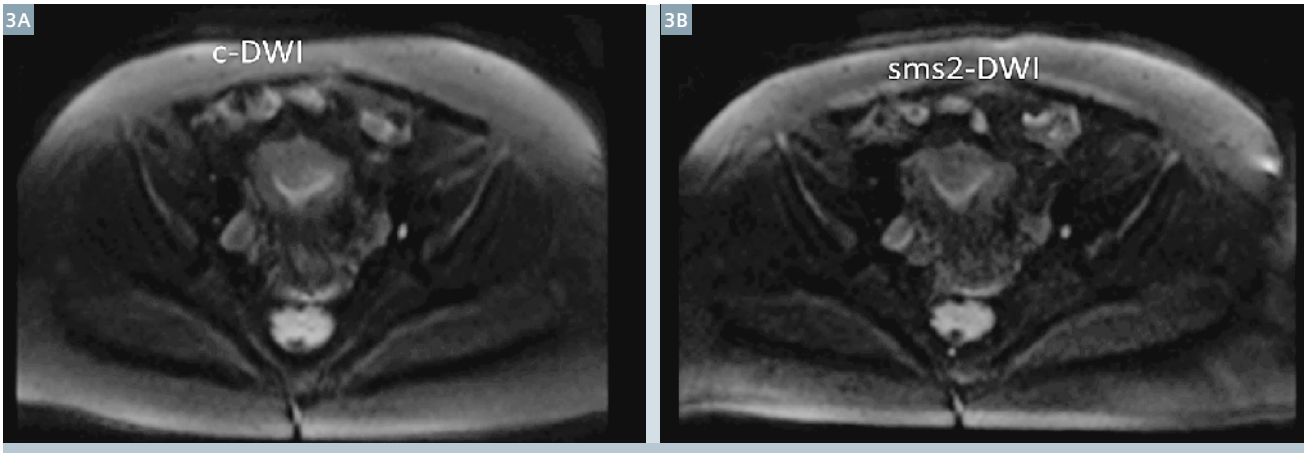

3 42-year-old female with history of endometriosis presented with abdominal pain. The image quality of c-DWI **(3A)** and SMS2-DWI **(3B)** is similar but with approximately 45% decrease in acquisition time with SMS2-DWI.

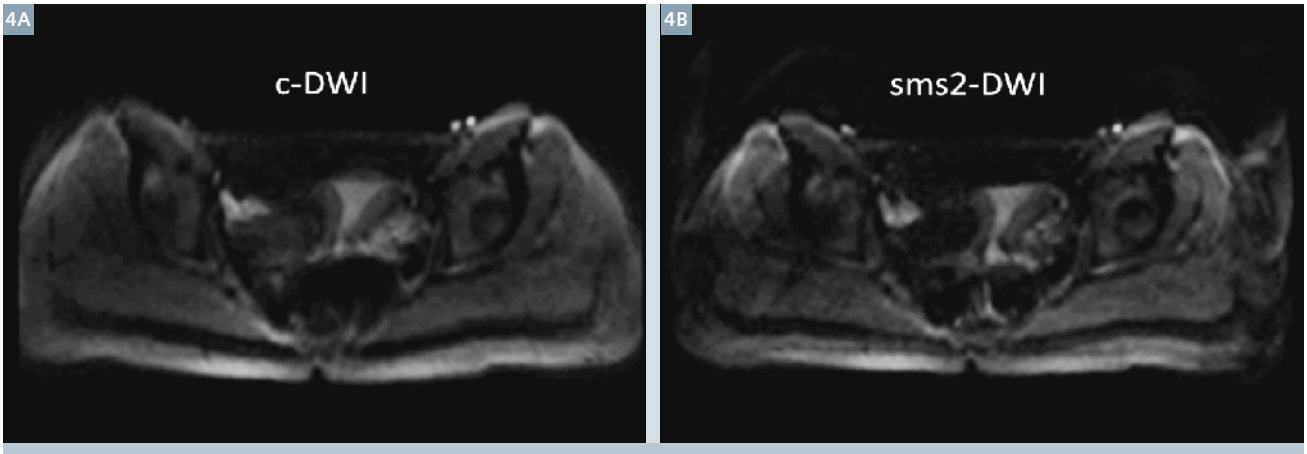

4 22-year-old female patient with increasing dysmenorrhea and enlarging left ovary cyst. MRI demonstrates comparable image quality between the conventional DWI **(4A)** and SMS DWI **(4B)** technique with near 45% reduction in acquisition time with SMS2-DWI.

Case scenario 4: 22-year-old female patient with increasing dysmenorrhea and enlarging left ovary cyst. MRI demonstrates comparable image quality between the conventional DWI and SMS DWI technique with approximately 45% reduction in acquisition time with SMS-DWI (Fig. 4).

Conclusion

We have incorporated SMS DWI with 2-fold acceleration in our clinical protocol for abdominopelvic imaging which has allowed us to achieve near two-fold acceleration in free-breathing DWI acquistion with multiple averages. These time-savings can be used to either improve volumetric coverage or resolution of the DWI or shorten the overall exam time.

References

1 Taouli, B. and D.M. Koh, Diffusion-weighted MR imaging of the liver. Radiology, 2010. 254(1): p. 47-66.
2 Qayyum, A., Diffusion-weighted imaging in the abdomen and pelvis: concepts and applications. Radiographics, 2009. 29(6): p. 1797-810.
3 Koh, D.M., et al., Predicting response of colorectal hepatic metastasis: value of pretreatment apparent diffusion coefficients. AJR Am J Roentgenol, 2007. 188(4): p. 1001-8.
4 Kamel, I.R., et al., Unresectable hepatocellular carcinoma: serial early vascular and cellular changes after transarterial chemoembolization as detected with MR imaging. Radiology, 2009. 250(2): p. 466-73.
5 Rosenkrantz, A.B., et al., Whole-lesion diffusion metrics for assessment of bladder cancer aggressiveness. Abdom Imaging, 2015. 40(2): p. 327-32.
6 Kobayashi, S., et al., Diagnostic performance of diffusion-weighted magnetic resonance imaging in bladder cancer: potential utility of apparent diffusion coefficient values as a biomarker to predict clinical aggressiveness. Eur Radiol, 2011. 21(10): p. 2178-86.
7 Setsompop K., et. al. Blipped-controlled aliasing in parallel imaging for simultaneous multislice echo planar imaging with reduced g-factor penalty. Magn Reson Med. 2012 May;67(5):1210-24.
8 Obele, C.C., et al., Simultaneous Multislice Accelerated Free-Breathing Diffusion-Weighted Imaging of the Liver at 3T. Abdom Imaging, 2015.

Contact

Hersh Chandarana, M.D.
Department of Radiology
NYU School of Medicine
660 First Avenue
New York, NY 10016
USA
hersh.chandararna@nyumc.org

Did you know that ...

"With DotGO it's going to be so much easier and quicker to build protocols on the fly and not interfere with taking table time away from the patients. Previously, to build a protocol from scratch would take 20 minutes. With DotGO, I was able to create a protocol in 45 seconds. Having consistency in our MRI protocols and examinations is extremely important. Our reputation is to provide the highest quality MRI examinations for our patients and referring physicians. DotGO will help us to do that."

Anthony Pavone

Zwanger-Pesiri Radiology
(New York, USA)

More clinical articles, tips & tricks, talks on Siemens unique Dot engines at

www.siemens.com/magnetom-world-dot

Rapid High Spatial Resolution Diffusion MRI at 7 Tesla Using Simultaneous Multi-Slice Acquisition

Cornelius Eichner[1,2]; Robin M. Heidemann[3]

[1] Max Planck Institute for Human Cognitive and Brain Sciences, Leipzig, Germany
[2] A. A. Martinos Center for Biomedical Imaging, MGH, Harvard Medical School, Boston, MA, USA
[3] Siemens Healthcare, Erlangen, Germany

Abstract

High quality diffusion-weighted MRI (dMRI) data can be obtained with very high isotropic spatial resolution at ultra-high magnetic field strength such as 7 Tesla (T). Due to the high resolution it is necessary to acquire a large number of imaging slices for whole brain coverage, which results in long acquisition times (TA) of more than an hour. Obviously, Simultaneous multi-slice (SMS) acquisition technology is a prerequisite to significantly reduce the extensive acquisition times of these studies. However, the large energy deposition into the subject caused by the employed Multiband (MB) RF-pulses limit the efficiency of SMS methods. This can be addressed by replacing the MB pulses by Power Independent of Number of Slices (PINS) pulses[1]. However, this comes at the expense of a reduced bandwidth and increased off-resonance dependency, which degrades the image quality. With a new RF pulse design, given the name MultiPINS[1], the RF energy is further reduced and/or the pulse length is shortened. This is achieved by combining MB with PINS RF pulses. *In vivo* dMRI results were recorded with the MultiPINS approach at high spatial resolutions at 7T showing a 3-fold scan time reduction.

[1] The product is still under development and not commercially available yet. Its future availability cannot be ensured.

Introduction

Diffusion MRI (dMRI) is an essential tool in neuroscience to study the structural connectivity of the human brain *in vivo*. Due to the complex structure of the brain, it is necessary to acquire data with high isotropic spatial resolution. Sub-millimeter isotropic resolution dMRI of the human brain *in vivo* is feasible at 7T [1]. However, due to the high isotropic resolution it is necessary to acquire a large number of imaging slices, which results in long acquisition times (TA) of about an hour and more – a major limitation of this technique.

1

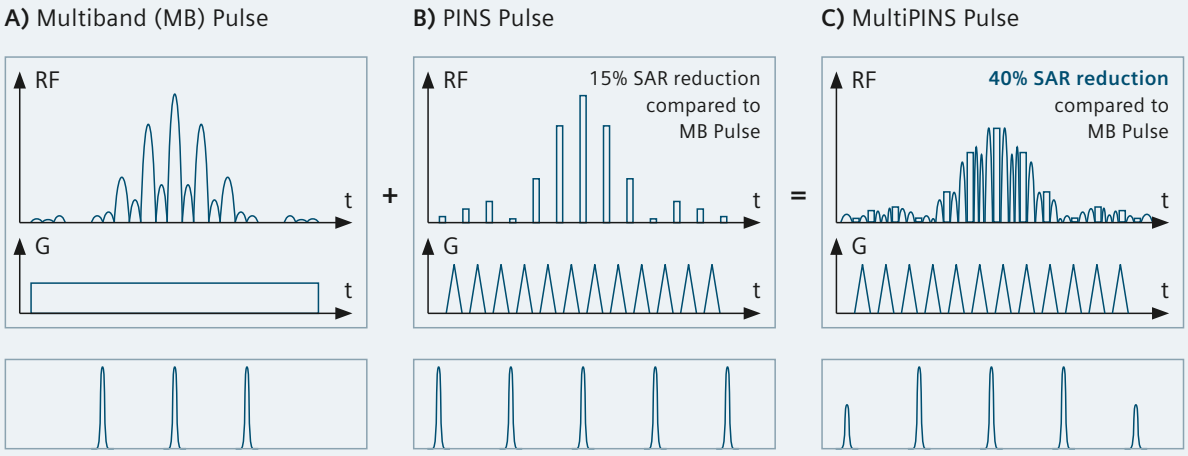

1 Example SMS RF pulses with resulting slice profiles; energy reductions that resulted from pulse settings used in this work.

Acquiring multiple slices simultaneously, and unfolding them using information from multi-channel coil arrays [2], can address this speed problem and shorten TA. The CAIPIRINHA approach [3] was developed to reduce the g-factor noise for SMS imaging and has been recently adapted to EPI acquisitions [4] (blipped-CAIPIRINHA). However, the high-energy deposition of Multiband (MB) pulses (Fig. 1A) that are typically used for SMS imaging limit the acquisition speed of SMS methods at 7T, due to SAR/power constraints – especially if high flip angles are employed [5]. For moderate slice acceleration factors (e.g. MB = 2), SMS dMRI data can be acquired also at 7T [6]. In the case of higher slice acceleration factors, the RF power will limit the acquisition speed at 7T.

Recently Norris et al. showed that a periodic slice excitation pattern, suitable for SMS acquisition, can be created without significant increase in power deposition by multiplying a single-slice RF pulse with a Dirac comb function, to end up in a Power Independent of Number of Slices (PINS) pulse [7] (Fig. 1B). This approach has been successfully applied to 7T for structural and functional spin-echo experiments [8] as well as RF power consuming sequences such as Turbo Spin-Echo [9]. In this study, we combine ZOOPPA[1], an outer volume suppression (OVS) technique [1], for diffusion MRI at 7T with blipped-CAIPIRINHA [4] and PINS pulses [7] to obtain high spatial and angular resolution dMRI with significantly reduced TA. Furthermore, by combining MB and PINS RF excitation, we created a new 'Multi-PINS' RF pulse type[1] to further reduce power deposition for SMS excitation (Fig. 1C). For this new MultiPINS pulse, a MB RF pulse is first reshaped to follow the excitation *k*-space traversal of the blipped gradient waveform of the PINS pulse. The reshaped MB pulse can then be mixed directly with the PINS pulse to create a MultiPINS pulse with suitable excitation characteristic for SMS imaging (Fig. 1C). To minimize SAR, an optimal mixing ratio between MB and PINS (0% being pure PINS and 100% being pure MB pulse along PINS gradient trajectory) can be easily determined empirically prior to acquisition.

Methods

The high-resolution diffusion MRI data were acquired on a 7T whole-body MR scanner[2] (Siemens Healthcare, Erlangen, Germany) equipped with a 32-element head coil and a gradient system achieving a maximum amplitude of 70 mT/m with a slew-rate of 200 T/m/s. A Stejskal-Tanner diffusion-weighted EPI sequence [10] was modified to employ ZOOPPA OVS and SMS blipped-CAIPIRINHA. SMS is used to accelerate the acquisition by 3 folds, while ZOOPPA is used to reduce the imaging volume-of-interest and associated image distortion artifact. To reduce SAR/power deposition of the SMS method, a PINS/MultiPINS pulse was utilized for RF refocusing. Energy calculations were performed for the MultiPINS SMS pulses, to find out optimal energy settings with short pulse durations. *In vivo* diffusion-weighted images with 99 slices of 1 mm and 75 slices of 1.4 mm isotropic resolutions were acquired at 60 diffusion directions with a b-value of 1000 s/mm^2 and 7 interspersed b0 non-diffusion-weighted images (for motion correction). To increase the signal-to-noise ratio of the 1 mm isotropic resolution dataset, 4 averages were recorded. In the case of the 1 mm isotropic dataset, multiple fiber orientations were modeled with constrained spherical deconvolution followed by streamline fiber tracking with MRtrix (http://www.brain.org.au/software/mrtrix/). The 1.4 mm isotropic data set was acquired as a single average, resulting in a total acquisition time of about 3 minutes. Data were corrected for motion and eddy currents distortion artifacts with FSL and registered to a structural scan using Freesurfer. A color-coded FA map was calculated using the diffusion toolkit (http://www.trackvis.org/).

Results and discussion

We have shown that dMRI data at 7T can be acquired in a significantly shortened acquisition time. We recorded a 1 mm isotropic resolution with 60 diffusion directions in just 6 minutes, by applying blipped-CAIPIRINHA and ZOOPPA OVS

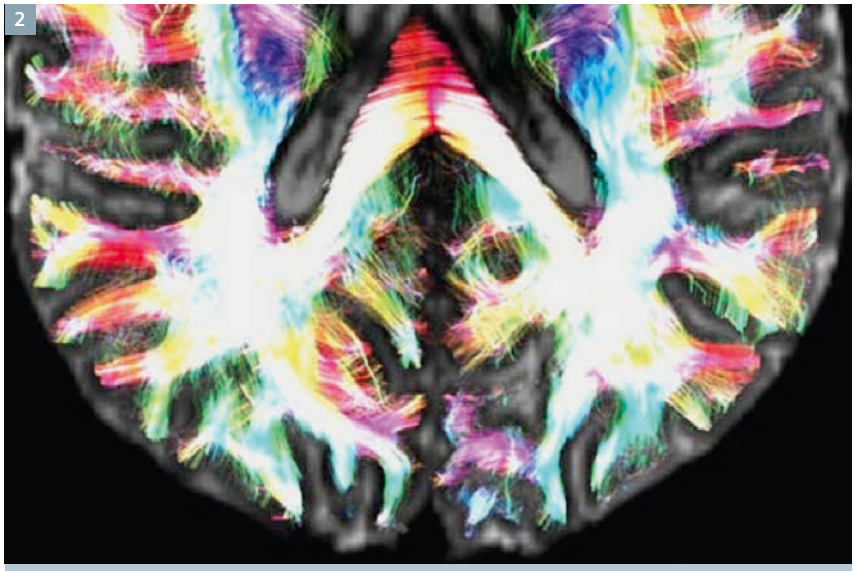

2 Streamline fiber tracking of 100 000 fibers (5 mm slab) of coronal and axial brain slices. Four times averaged 7T dMRI data with 1 mm isotropic resolution.

[1] The product is still under development and not commercially available yet. Its future availability cannot be ensured.

[2] MAGNETOM 7T is ongoing research. All data shown are acquired using a non-commercial system under institutional review board permission. MAGNETOM 7T is still under development and not commercially available yet. Its future availability cannot be ensured.

(see Table 1) (Fig. 2). Furthermore, a whole brain dataset with 1.4 mm isotropic resolution and 60 diffusion directions was recorded in only 3:30 minutes (Fig. 3). We used PINS/MultiPINS pulses for refocusing to reduce SAR, and thus to gain the full benefit of SMS imaging at 7T.

Conclusion

For ultra-high-resolution dMRI (1 mm isotropic or better) at 7T, the acquisition time becomes the major hindrance for a broad use of this application. We employed the blipped-CAIPIRINHA SMS technique in conjunction with PINS refocusing pulses as well as with a newly developed hybrid MB/PINS RF pulse to record dMRI data at 7T. The application of low power RF pulses in this SMS sequence enables the acquisition of high-resolution dMRI data at 7T in a significantly reduced scan time of 6:15 min for a 1 mm resolution dMRI scan and 3:30 min for a 1.4 mm isotropic resolution dMRI scan. The slice acceleration enables high-resolution dMRI acquisition at 7T within a timeframe short enough for clinical use, as well as combined *in vivo* anatomical, functional and diffusion studies at the same ultra-high-resolution level within a single scan session.

Table 1

Resolution	1 mm w/o SMS	1 mm MB=3	1.4 mm MB=3
TR (ms)	13600	5000	3000
TE (ms)	68	64	69
Slices	99	99	75
FOV (mm²)	180 x 125	180 x 120	180 x 180
TA (min)	4 x 15:52	4 x 6:15	1x 3:30

Comparable diffusion-weighted protocols for slice accelerated and non-accelerated with SMS blipped-CAIPIRINHA. 60 diffusion directions, b = 1000 s/mm² with different slice acceleration factors (SMS).

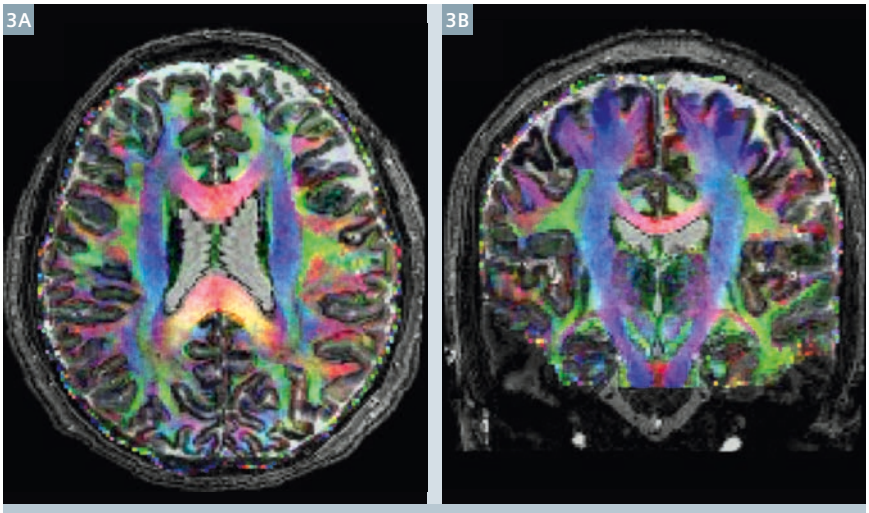

3 Axial **(3A)** and coronal **(3B)** views of color coded FA diffusion data recorded at 1.4 mm isotropic resolution in 3:30 min.

References

1 R.M. Heidemann, A. Anwander, T. Feiweier, T. R. Knösche, R. Turner, "K-space and q-space: Combining ultra-high spatial and angular resolution in diffusion imaging using ZOOPPA at 7T," NeuroImage, 60(2), 967–978, 2012.

2 D.J. Larkman, J.V. Hajnal, A.H. Herlihy, G.A. Coutts, I.R. Young, G. Ehnholm, "Use of multicoil arrays for separation of signal from multiple slices simultaneously excited," JMRI, 13(2), 313–7, 2001.

3 F.A. Breuer, M. Blaimer, R.M. Heidemann, M.F. Müller, M.A. Griswold, P.M. Jakob, "Controlled aliasing in parallel imaging results in higher acceleration (CAIPIRINHA) for multi-slice imaging," Magn Reson Med, 53(3), 684–91, 2005.

4 K. Setsompop, B.A. Gagoski, J.R. Polimeni, T. Witzel, V.J. Wedeen, L.L. Wald, "Blipped-controlled aliasing in parallel imaging for simultaneous multislice echo planar imaging with reduced g-factor penalty," Magn Reson Med, 67(5), 1210–24, 2012.

5 C. Eichner, "Combining ZOOPPA and blipped CAIPIRINHA for diffusion weighted imaging at 7T" In Proceedings of the 29th Annual Meeting ESMRMB, Lisbon, Vol. 4, p. 45111, 2012.

6 A.T. Vu, "High resolution whole brain diffusion imaging at 7 T for the Human Connectome Project", NeuroImage (2015), http://dx.doi.org/10.1016/j.neuroimage.2015.08.004.

7 D.G. Norris, P.J. Koopmans, R. Boyacioglu, M. Barth, "Power independent of number of slices (PINS) radiofrequency pulses for low-power simultaneous multislice excitation" Magn Reson Med, 66(5), 1234–40, 2011.

8 P.J. Koopmans, R. Boyacioglu, M. Barth, D.G. Norris, "Whole brain, high resolution spin-echo resting state fMRI using PINS multiplexing at 7 T," NeuroImage, 62(3), 1939–46, 2012.

9 D.G. Norris, R. Boyacioglu, J. Schulz, M. Barth, P.J. Koopmans. "Application of PINS radiofrequency pulses to reduce power deposition in RARE/turbo spin echo imaging of the human head," Magn Reson Med, 00(July), 2013.

10 E.O. Stejskal, J.E. Tanner, "Spin diffusion measurements: spin echoes in the presence of a time-dependent field gradient," The Journal of Chemical Physics, 42, 288, 1965.

Contact

Cornelius Eichner
Max Planck Institute for Human Cognitive and Brain Sciences
Stephanstraße 1A
04103 Leipzig
Germany
Phone: +49 341 9940-2428
ceichner@cbs.mpg.de

Myocardial First-Pass Perfusion Imaging with High Resolution and Extended Coverage Using Multi-Slice CAIPIRINHA

Daniel Stäb, Dipl. Phys.[1,2]; Felix A. Breuer, Ph.D.[3]; Christian O. Ritter, M.D.[1]; Andreas Greiser, Ph.D.[4]; Dietbert Hahn, M.D.[1]; Herbert Köstler, Ph.D.[1,2]

[1] Institute of Radiology, University of Würzburg, Würzburg, Germany
[2] Comprehensive Heart Failure Center (CHFC), Würzburg, Germany
[3] Research Center Magnetic Resonance Bavaria (MRB), Würzburg, Germany
[4] Siemens Healthcare, Erlangen, Germany

Background

Contrast-enhanced myocardial first-pass perfusion MR imaging (MRI) is a powerful clinical tool for the detection of coronary artery disease [1–4]. Fast gradient echo sequences are employed to visualize the contrast uptake in the myocardium with a series of saturation prepared images. However, the technique is strictly limited by physiological constraints. Within every RR-interval, only a few slices can be acquired with low spatial resolution, while both high resolution and high coverage are required for distinguishing subendocardial and transmural infarcted areas [5] and facilitating their localization, respectively.

Acceleration techniques like parallel imaging (pMRI) have recently shown their suitability for improving the spatial resolution in myocardial first-pass perfusion MRI [5–7]. Within clinical settings, 3 to 4 slices can be acquired every heartbeat with a spatial resolution of about 2.0 × 2.0 mm² in-plane [6]. However, for increasing anatomic coverage [8], standard parallel imaging is rather ineffective, as it entails significant reductions of the signal-to-noise ratio (SNR):

a) In order to sample more slices every RR-interval, each single-slice measurement has to be shortened by a certain acceleration factor R, which inevitably comes along with an √R-fold SNR reduction.

1A

Conventional MS-CAIPIRINHA for coverage extension
Multi-slice excitation and RF phase cycling

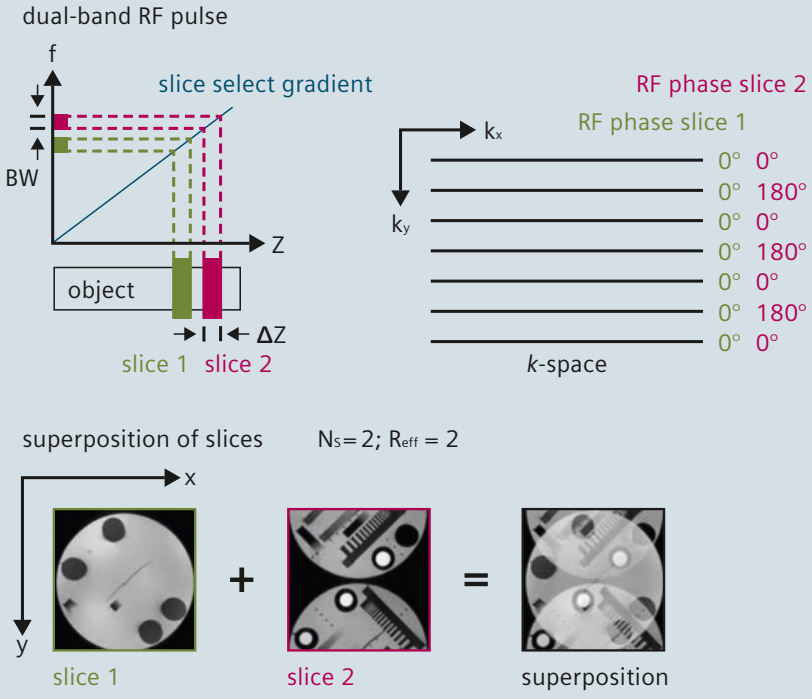

1A MS-CAIPIRINHA with two slices simultaneously excited ($N_s = 2$). A dual-band RF pulse is utilized to excite two slices at the same time (BW = excitation bandwidth). During data acquisition, each slice is provided with an individual RF phase cycle. A slice specific constant RF phase increment is employed (0° in slice 1, 180° in slice 2) between succeeding excitations. Consequently, the two slices appear shifted by ½ FOV with respect to each other. In this way, the overlapping pixels originate not only from different slices, but also from different locations along the phase encoding direction (y), facilitating a robust slice separation using pMRI reconstruction techniques. Using the two-slice excitation, effectively a two-fold acceleration is achieved ($R_{eff} = 2$).

b) During image reconstruction, the SNR is further reduced by the so-called geometry (g)-factor [9], an inhomogeneous noise-amplification depending on the encoding capabilities of the receiver array.

In addition, unless segmented acquisition techniques are utilized [10], the saturation recovery (SR) magnetization preparation has to be taken into account:

c) The preparation cannot be accelerated itself. Hence, the acceleration factor R has to be higher than the factor by which the coverage is extended. This leads to an increase of the SNR-reduction discussed in (a).

d) Subsequent to the preparation, the signal increases almost linearly with time. Thus, shortening the acquisition by a factor of R is linked to an additional R-fold SNR-loss.

As demonstrated recently [11], most of these limitations can be overcome by employing the MS-CAIPIRINHA (Multi-Slice Controlled Aliasing In Parallel Imaging Results IN Higher Acceleration) concept[1] [12, 13] for simultaneous 2D multi-slice imaging. By simultaneously scanning multiple slices in the time conventionally required for the acquisition of one single slice, this technique enables a significant increase in anatomic coverage. Since image acquisition time is preserved with respect to the single-slice measurement, the technique does not experience any SNR reductions despite the *g*-factor noise amplification of the required pMRI reconstruction [11, 12]. The MS-CAIPIRINHA concept can also be employed with acceleration factors that are higher than the number of slices excited at the same time. By utilizing this acceleration for increasing spatial resolution, the technique facilitates myocardial first-pass perfusion examinations with extended anatomic coverage and high spatial resolution. A short overview of the concept is set out below, followed by a presentation of *in-vivo* studies that demonstrate the capabilities of MS-CAIPIRINHA in contrast-enhanced myocardial first-pass perfusion MRI.

1B

MS-CAIPIRINHA with $R_{eff} > N_s$ for improving coverage and resolution
Multi-slice excitation, *k*-space undersampling and RF phase cycling

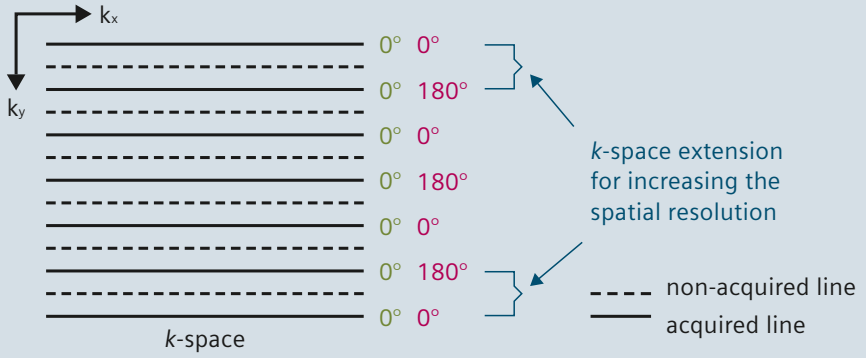

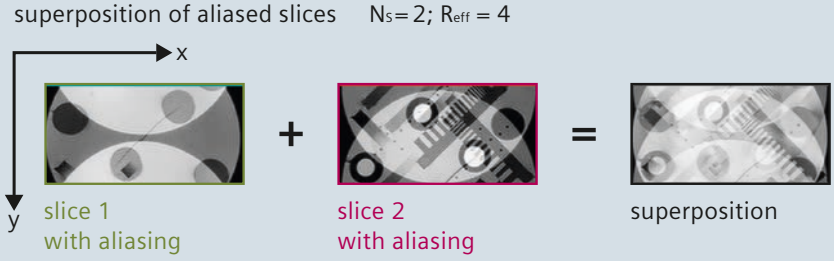

1B MS-CAIPIRINHA with an effective acceleration factor higher than the number of slices excited simultaneously. Again, two slices are excited at the same time employing the same RF phase cycles as in (1A), but *k*-space is undersampled by a factor of two. The slices and their undersampling-induced aliasing artifacts appear shifted with respect to each other by ½ FOV and can be separated using pMRI reconstruction techniques. Effectively, a four-fold acceleration is achieved ($R_{eff} = 4$). The additional acceleration can be employed to extend *k*-space and to improve the spatial resolution.

Improving anatomic coverage and spatial resolution with MS-CAIPIRINHA

MS-CAIPIRINHA

The MS-CAIPIRINHA concept [12, 13] is based on a coinstantaneous excitation of multiple slices, which is accomplished by means of multi-band radiofrequency (RF) pulses (Fig. 1A). Being subject to the identical gradient encoding procedure, the simultaneously excited slices appear superimposed on each other, unless the individual slices are provided with different rf phase cycles. In MS-CAIPIRINHA, the latter is done in a well-defined manner in order to control the aliasing of the simultaneously excited slices. Making use of the Fourier shift theorem, dedicated slice specific RF phase cycles are employed to shift the slices with respect to each other in the field-of-view (FOV) (Fig. 1A). The slice separation is performed using pMRI reconstruction techniques. However, the shift of the slices causes superimposed pixels to originate from not only different slices, but also different locations along the phase encoding direction. Thus, the MS-CAIPIRINHA concept allows the pMRI reconstruction to take advantage of coil sensitivity variations along

[1] The product is still under development and not commercially available yet. Its future availability cannot be ensured.

Reprinted from MAGNETOM Flash (51) 1/2013

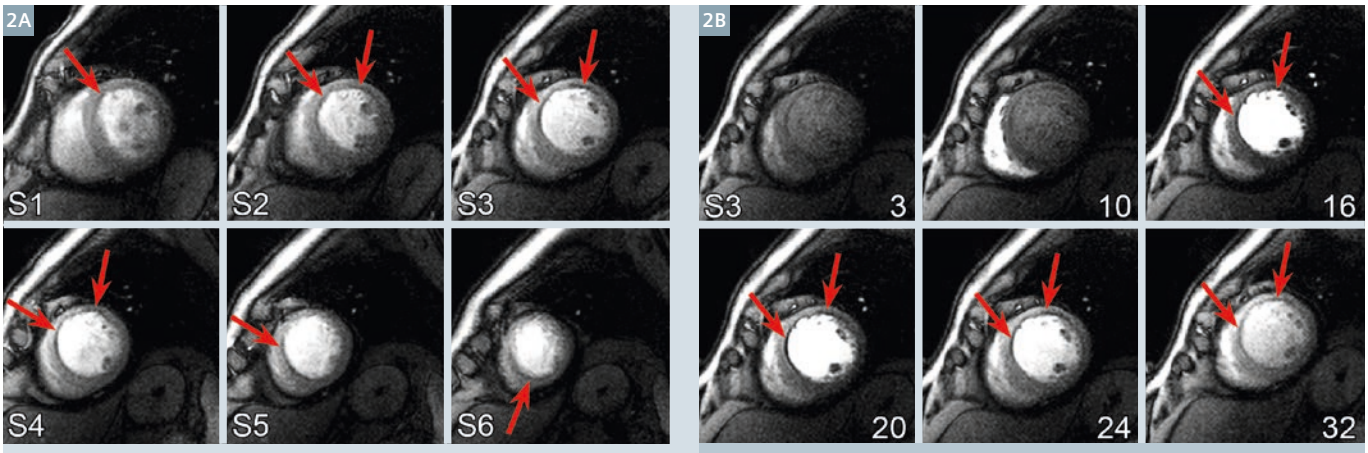

2 Myocardial first-pass perfusion study on a 52-year-old male patient after ST-elevating myocardial infarction and acute revascularization. Myocardial perfusion was examined in 6 adjacent slices by performing 3 consecutive MS-CAIPIRINHA acquisitions every RR-interval (FOV 320 × 360 mm²; matrix 160 × 180; TI 125 ms; T_{Acq} 223 ms; distance between simultaneously excited slices: 24 mm). **(2A)** Sections of the reconstructed images of all 6 slices showing the pass of the contrast agent through the myocardium. The hypoperfused area is depicted by arrows. **(2B)** Image series showing the contrast uptake in the myocardium of slice 3. The acquisition time point (RR-interval) is given for each image and the perfusion defect is indicated by arrows. **(2C)** *g*-factor maps for the reconstruction shown in (2A).

two dimensions and to perform the slice separation with low *g*-factor noise amplification [12].

By conserving image acquisition time with respect to an equivalent single-slice measurement, the technique is not subject to any further SNR penalties. MS-CAIPIRINHA hence allows extending the coverage in 2D multi-slice imaging in a very efficient manner. Applied to myocardial first-pass perfusion imaging, the concept facilitates the acquisition of 6 slices every heartbeat with an image quality that is comparable to that of conventional 3-slice examinations [11].

Additional acceleration

While extending the coverage can be accomplished by simultaneous multi-slice excitation, improving the spatial resolution requires additional *k*-space data to be sampled during image acquisition. Of course, as the FOV and the image acquisition time are to be conserved, this can only be achieved by means of additional acceleration.

However, the effective acceleration factor of MS-CAIPIRINHA is not restricted to the number of slices excited simultaneously. By applying simultaneous multi-slice excitation to an imaging protocol with reduced phase FOV, i.e. equidistant *k*-space undersampling, supplementary in-plane acceleration can be incorporated (Fig. 1B). The RF phase modulation forces the two simultaneously excited slices and their in-plane aliasing artifacts to be shifted with respect to each other in the FOV. As before, image reconstruction and slice separation is performed utilizing pMRI methods. Employed like this, the MS-CAIPIRINHA concept facilitates an increase of both, anatomic coverage and spatial resolution with high SNR efficiency. Since image acquisition time does not have to be shortened, SNR is only affected by the voxel size and the noise amplification of the pMRI reconstruction.

Imaging

Perfusion datasets were obtained from several volunteers and patients. The study was approved by the local Ethics Committee and written informed consent was obtained from all subjects. All examinations were performed on a clinical 3T MAGNETOM Trio, a Tim system (Siemens Healthcare, Erlangen, Germany), using a dedicated 32-channel cardiac array coil (Siemens Healthcare, Erlangen, Germany) for signal reception. Myocardial perfusion was assessed using a SR FLASH sequence (FOV 320 × 300-360 mm²; matrix 160 × 150-180; TI 110-125 ms; TR 2.8 ms; TE 1.44 ms; T_{Acq} 191-223 ms; slice thickness 8 mm; flip angle 12°). Two slices were excited at the same time (distance between simultaneously excited slices: 24-32 mm) and shifted by ½ FOV with respect to each other by respectively providing the first and second slice with a 0° and 180° RF phase cycle. In order to realize a spatial resolution of 2.0 × 2.0 mm² within the imaging plane, *k*-space was undersampled by a factor of 2.5, resulting in an overall effective acceleration factor of 5.

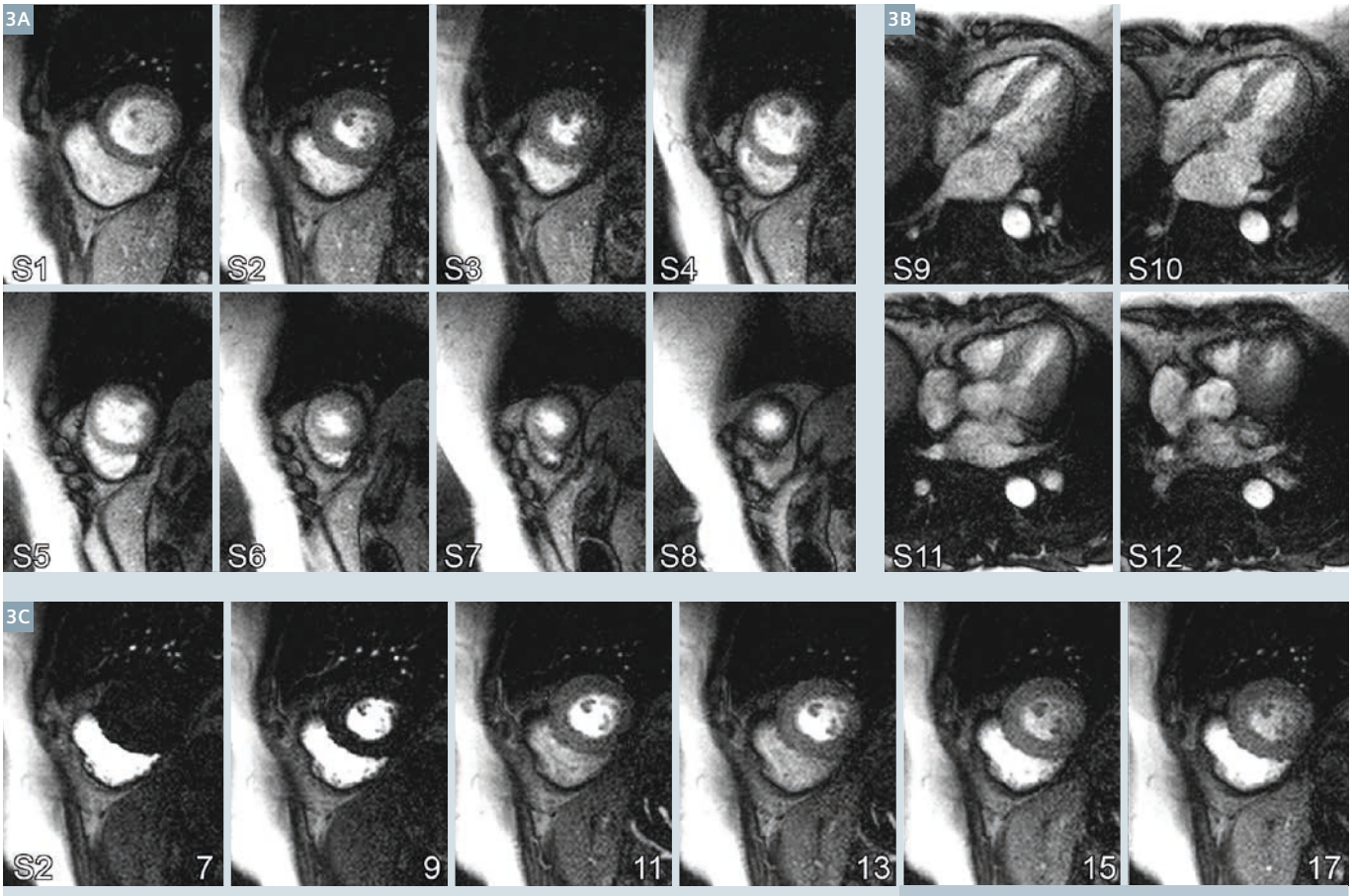

3 Myocardial first-pass perfusion study on a 51-year-old female volunteer with whole-heart coverage. 6 consecutive MS-CAIPIRINHA acquisitions were performed every two RR-intervals (FOV 320 × 300 mm²; matrix 160 x 150; TI 110 ms; T_{Acq} 191 ms; distance between simultaneously excited short/long axis slices: 32/16 mm). **(3A)** Sections of the reconstructed short axis images. **(3B)** Sections of the reconstructed long axis images. **(3C)** Series of image sections showing the contrast uptake in the myocardium of slice 2. The acquisition time point (RR-interval) is given for each image. **(3D)** *g*-factor maps for the reconstructions shown in (3A). **(3E)** *g*-factor maps for the reconstructions shown in (3B). **(3F)** Measurement scheme. The acquisition was performed with a temporal resolution of 1 measurement every 2 RR-intervals.

All first-pass perfusion measurements were conducted in rest over a total of 40 heartbeats. All subjects were asked to hold their breaths during the acquisition as long as possible. Every RR-interval, 3 to 4 consecutive MS-CAIPIRINHA acquisitions were performed in order to sample the contrast uptake of the myocardium. For contrast-enhancement, a contrast agent bolus (4 ml, Gadobutrol, Bayer HealthCare, Berlin, Germany) followed by a 20 ml saline flush was administered at the beginning of each perfusion scan. Image reconstruction was performed using an offline GRAPPA [14] reconstruction. The according weights were determined from a separate full FOV calibration scan. To evaluate the GRAPPA reconstruction, an additional noise scan was obtained and the *g*-factor noise enhancement was quantified [15]. All calculations were performed on a standalone PC using Matlab (The MathWorks, Natick, MA, USA).

Results

Figure 2 shows the results of a myocardial first-pass perfusion examination with 6-slices on a 52-year-old male patient (91 kg, 185 cm) on the fourth day after STEMI (ST-elevating myocardial infarction) and acute revascularization. Sections of the reconstructed images of all examined slices are depicted, showing the first pass of contrast agent through the myocardium (Fig. 2A). Also displayed is a series of image sections demonstrating contrast uptake in slice 3 (Fig. 2B). The GRAPPA reconstruction separated the simultaneously excited slices without visible artifacts. The *g*-factor maps (Fig. 2C) indicate generally low noise amplification. Thus, in comparison to the high effective acceleration factor of 5, the images provide excellent image quality. Both contrast and SNR allow for a clear delineation of the subendocardial hypoperfused area within the anterior and septal wall of the myocardium (arrows).

The results of a first-pass perfusion study with whole-heart coverage are displayed in Fig. 3. In a 51-year-old female volunteer, first-pass perfusion was examined in eight short (Fig. 3A) and four long axis slices (Fig. 3B). In order to accomplish the 12-slice examination and to achieve whole-heart coverage, temporal resolution was reduced by a factor of two with respect to the examination displayed in Fig. 2. The contrast uptake of the myocardium was sampled with 1 measurement every two RR-intervals by performing 3 out of 6 consecutive double-slice MS-CAIPIRINHA acquisitions every heartbeat (Fig. 3F). Image reconstruction could be performed without visible artifacts and generally low noise amplification (Figs. 3D and E). Only in a few regions, the *g*-factor maps show moderate noise enhancement. In the images, the myocardium is homogeneously contrasted and the contrast agent uptake is clearly visible (Fig. 3C).

The findings of a first-pass perfusion study in a 48-year-old male patient (80 kg, 183 cm) on the eighth day after STEMI and acute revascularization are presented in Fig. 4. An overall of 8 slices were acquired with a temporal resolution of 1 measurement every RR-interval by performing 4 consecutive MS-CAIPIRINHA acquisitions after each ECG trigger pulse. Sections of the reconstructed images, showing the first pass of contrast agent through the myocardium in all 8 slices (Fig. 4A) are depicted together with sections demonstrating the process of contrast uptake in slice 5 (Fig. 4B). Despite the breathing motion (Fig. 4D), the GRAPPA reconstruction performed robustly and separated the slices without significant artifacts. The *g*-factor noise amplification is generally low and moderate within a few areas (Fig. 4C).

In the images, the hypoperfused subendocardial region in the anterior wall can be clearly identified (arrows). As can be seen from the enlarged section of slice 5 (Fig. 4F), the technique provides sufficient spatial resolution to distinguish between subendocardial and transmural perfusion defects. These findings correspond well to the results of a subsequently performed Late Enhancement study (Fig. 4E) delineating a transmural infarction zone of the anterior wall (midventricular to apical).

Discussion

Contrast-enhanced myocardial first-pass perfusion MRI with significantly extended anatomic coverage and high spatial resolution can be successfully performed by employing the MS-CAIPIRINHA concept for simultaneous multi-slice imaging. Basically, two different acceleration approaches are combined: the simultaneous excitation of two slices on the one hand and *k*-space undersampling on the other. While the first directly doubles the number of slices acquired, the second provides sufficient acceleration for improving the spatial resolution. The proposed imaging protocols provide an effective acceleration factor of 5, which is sufficient for the acquisition of 6 to 8 slices every RR-interval with a high spatial resolution of $2.0 \times 2.0 \times 8\,mm^3$. Correspondingly, whole-heart coverage can be achieved by sampling 12 slices with a temporal resolution of 1 measurement every 2 RR-intervals. Since the slices can be planned with individual thickness and pairwise specific orientation, the concept thereby provides high flexibility. With image acquisition times of 191 ms, it also supports stress examinations in 6 slices up to a peak heart rate of 104 bpm.

Employing a dedicated 32-channel cardiac array coil, the image reconstructions could be performed without significant reconstruction artifacts and only low to moderate *g*-factor noise amplification. Also in presence of breathing motion, the GRAPPA reconstruction performed robustly. The images provided sufficient SNR and contrast between blood, myocardium and lung tissue to delineate small perfusion defects and to differentiate between subendocardial and transmural hypoperfused areas.

Compared to conventional parallel MRI, the MS-CAIPIRINHA concept benefits from the high SNR efficiency discussed earlier. Simultaneous multi-slice excitation allows increasing the coverage without supplementary *k*-space undersampling. At the same time the *g*-factor noise amplifi-

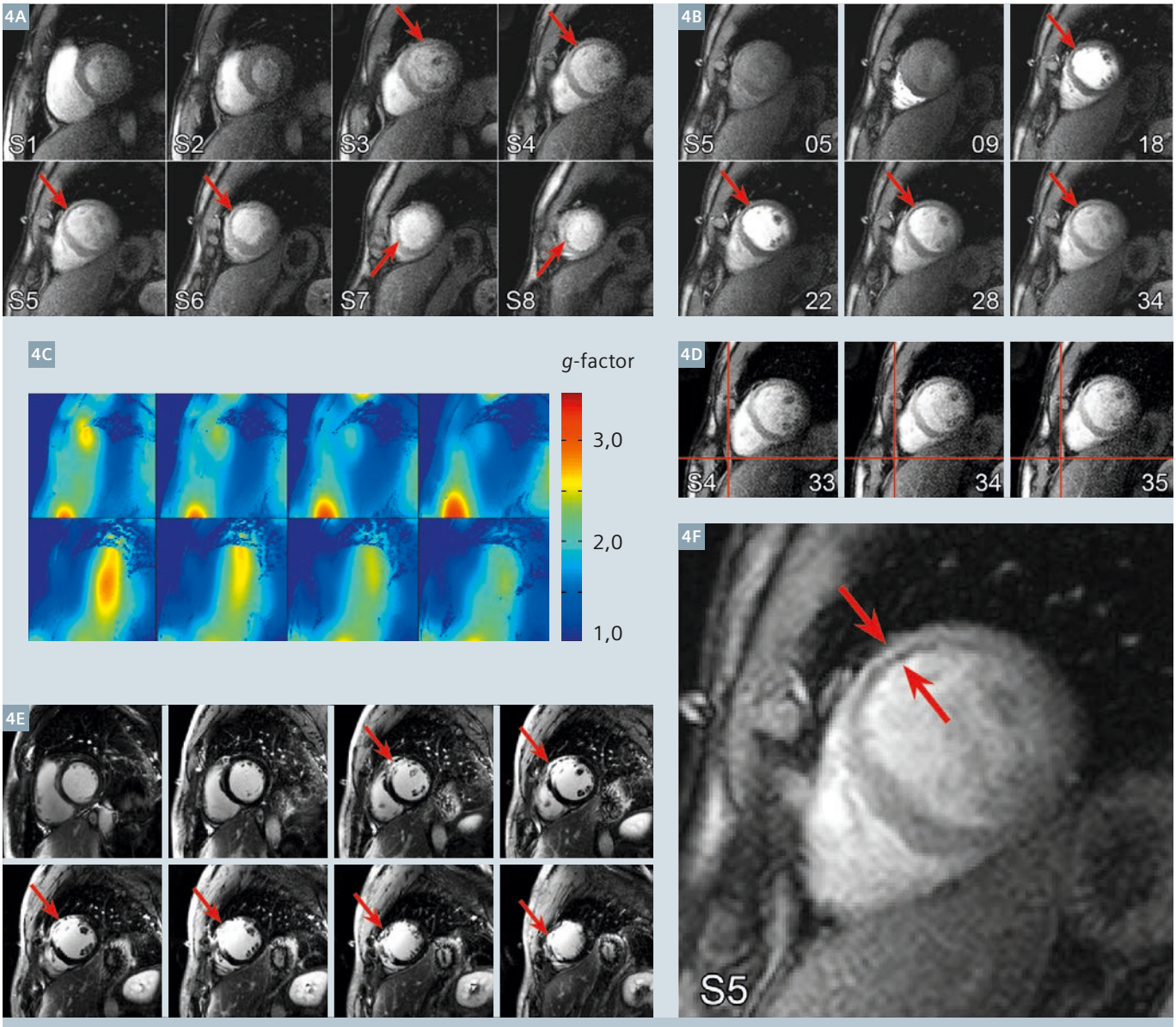

4 Myocardial first-pass perfusion study on a 48-year-old male patient after ST-elevating myocardial infarction and acute revascularization. 8 slices were acquired every RR-interval by performing 4 consecutive MS-CAIPIRINHA acquisitions (FOV 320 × 300 mm²; matrix 160 × 150; TI 110 ms; T_{Acq} 191 ms; flip angle 10°; distance between simultaneously excited slices: 32 mm). **(4A)** Sections of the reconstructed images of all 8 slices showing the first pass of the contrast agent through the myocardium. The hypoperfused area is depicted by arrows. **(4B)** Image series showing the contrast uptake in the myocardium of slice 5. The acquisition time point (RR-interval) is given for each image and the perfusion defect is indicated by arrows. **(4C)** *g*-factor maps for the reconstruction shown in (4A). **(4D)** Displacement of the heart due to breathing motion, example for slice 4. **(4E)** Late gadolinium enhancement. **(4F)** Enlarged section of slice 5. The technique allows distinguishing between subendocardial and transmural perfusion defects.

cation is minimized by exploiting coil sensitivity variations in both, slice and phase-encoding direction. Thus, despite the doubled anatomic coverage, the image quality obtained is comparable to that of an accelerated measurement with standard coverage and high spatial resolution [5]. An important feature of the MS-CAIPIRINHA concept in myocardial first-pass perfusion MRI is the frame-by-frame reconstruction, which prevents the reconstructed images to be affected by temporal blurring. Moreover, arrhythmia and breathing motion only impact the underlying time frame and not the whole image series, as it is likely for reconstruction techniques incorporating the temporal domain [16–19].

Simultaneous multi-slice excitation is, of course, linked to an increase in the amount of energy that is deployed to the subject under investigation. Thus, limitations have to be expected at higher field strengths or when using sequences with larger flip angles, such as TrueFISP. At 1.5 Tesla, the application of the MS-CAIPIRINHA concept to TrueFISP has been successfully demonstrated utilizing advanced RF phase cycling [11].

In all *in-vivo* examinations, the distance between the two slices excited simultaneously was maximized in order to make use of the highest possible coil sensitivity variations in slice direction and to minimize the *g*-factor penalty. Thus, the spatial distance between consecutively acquired cardiac phases is large which might be a possible drawback for correlating hypoperfused regions of the myocardium. While the latter was feasible for all *in-vivo* studies, slice distance naturally can be reduced at the expense of slightly more noise enhancement.

Conclusion

Utilizing the MS-CAIPIRINHA concept for simultaneous multi-slice imaging, contrast-enhanced myocardial first-pass perfusion MRI can be performed with an anatomic coverage of 6 to 8 slices every heart beat and a high spatial resolution of $2.0 \times 2.0 \times 8\,mm^3$. Based on the simultaneous excitation of multiple slices, the concept provides significantly higher SNR than conventional in-plane acceleration techniques with identical acceleration factor and facilitates an accurate image reconstruction with only low to moderate *g*-factor noise amplification. Taking into account the high flexibility, simple applicability and short reconstruction times in addition to the high robustness in presence of breathing motion or arrhythmia, the concept can be considered a promising candidate for clinical perfusion studies.

Acknowledgements

The authors would like to thank the Deutsche Forschungsgemeinschaft (DFG) and the Federal Ministry of Education and Research (BMBF), Germany for grant support.

References

1 Atkinson DJ, Burnstein D, Edelman RR. First-pass cardiac perfusion: evaluation with ultrafast MR imaging. Radiology 1990; 174:757–762.
2 Wilke N, Jerosch-Herold M, Wang Y, Yimei H, Christensen BV, Stillman E, Ugurbil K, McDonald K, Wilson RF. Myocardial Perfusion Reserve: Assessment with Multisection, Quantitative, First-Pass MR Imaging. Radiology 1997; 204:373–384.
3 Rieber J, Huber A, Erhard I, Mueller S, Schweyer M, Koenig A, Schiele TM, Theisen K, Siebert U, Schoenberg SO, Reiser M, Klauss V. Cardiac magnetic resonance perfusion imaging for the functional assessment of coronary artery disease: a comparison with coronary angiography and fractional flow reserve. Eur Heart J 2006; 27:1465–1471.
4 Schwitter J, Nanz D, Kneifel S, Bertschinger K, Büchi M, Knüsel PR, Marincek B, Lüscher TF, Schulthess GK. Assessment of Myocardial Perfusion in Coronary Artery Disease by Magnetic Resonance. Circulation 2001; 103:2230–2235.
5 Ritter CO, del Savio K, Brackertz A, Beer M, Hahn D, Köstler H. High-resolution MRI for the quantitative evaluation of subendocardial and subepicardial perfusion under pharmacological stress and at rest. RoFo 2007; 179:945–952.
6 Strach K, Meyer C, Thomas D, Naehle CP, Schmitz C, Litt H, Bernstein A, Cheng B, Schild H, Sommer T. High-resolution myocardial perfusion imaging at 3 T: comparison to 1.5 T in healthy volunteers. Eur Radiol 2007; 17:1829–1835.
7 Jung B, Honal M, Hennig J, Markl M. k-t-Space accelerated myocardial perfusion. J Magn Reson Imag 2008; 28:1080–1085.
8 Köstler H, Sandstede JJW, Lipke C, Landschütz W, Beer M, Hahn D. Auto-SENSE perfusion imaging of the whole human heart. J Magn Reson Imag 2003; 18:702–708.
9 Pruessmann KP, Weiger M, Scheidegger MB, Boesiger P. SENSE: sensitivity encoding for fast MRI. Magn Reson Med 1999; 42:952–962.
10 Kellman P, Derbyshire JA, Agyeman KO, McVeigh ER, Arai AE. Extended coverage first-pass perfusion imaging using slice-interleaved TSENSE. Magn Reson Med 2004; 51:200–204.
11 Stäb D, Ritter CO, Breuer FA, Weng AM, Hahn D, Köstler H. CAIPIRINHA accelerated SSFP imaging. Magn Reson Med 2011; 65:157–164.
12 Breuer FA, Blaimer M, Heidemann RM, Mueller MF, Griswold MA, Jakob PM. Controlled aliasing in parallel imaging results in higher acceleration (CAIPIRINHA) for multi-slice imaging. Magn Reson Med 2005; 53:684–691.
13 Breuer F, Blaimer M, Griswold M, Jakob P. Controlled Aliasing in Parallel Imaging Results in Higher Acceleration (CAIPIRINHA). Magnetom Flash 2012; 49:135–142.
14 Griswold MA, Jakob PM, Heidemann RM, Nittka M, Jellus V, Wang J, Kiefer B, Haase A. Generalized autocalibrating partially parallel acquisitions (GRAPPA). Magn Reson Med 2002; 47:1202–1210.
15 Breuer FA, Kannengiesser SAR, Blaimer M, Seiberlich N, Jakob PM, Griswold MA. General formulation for quantitative G-factor calculation in GRAPPA reconstructions. Magn Reson Med 2009; 62:739–746.
16 Adluru G, Awate SP, Tasdizen T, Whitaker RT, Dibella EVR. Temporally constrained reconstruction of dynamic cardiac perfusion MRI. Magn Reson Med 2007; 57: 1027–1036.
17 Otazo R, Kim D, Axel L, Sodickson DK. Combination of compressed sensing and parallel imaging for highly accelerated first-pass cardiac perfusion MRI. Magn Reson Med 2010; 64:767–776.
18 Ge L, Kino A, Griswold M, Mistretta C, Carr JC, Li D. Myocardial perfusion MRI with sliding-window conjugate-gradient HYPR. Magn Reson Med 2009; 62:835–839.
19 Plein S, Kozerke S, Suerder D, Luescher TF, Greenwood JP, Boesiger P, Schwitter J. High spatial resolution myocardial perfusion cardiac magnetic resonance for the detection of coronary artery disease. Eur Heart J 2008; 29:2148–2155.

Contact

Daniel Stäb
Institute of Radiology
University of Würzburg
Oberdürrbacher Str. 6
97080 Würzburg
Germany
staeb@roentgen.uni-wuerzburg.de

Cardiac Diffusion Tensor MRI Using Simultaneous Multi-Slice Acquisition with a Blipped-CAIPIRINHA Readout

Choukri Mekkaoui[1]; Timothy G. Reese[1]; Marcel P. Jackowski[2]; Himanshu Bhat[3]; David E. Sosnovik[1,4]

[1] Athinoula A. Martinos Center for Biomedical Imaging, Department of Radiology, Massachusetts General Hospital, Harvard Medical School, Boston, MA, USA
[2] Department of Computer Science, Institute of Mathematics and Statistics, University of São Paulo, São Paulo, Brazil
[3] Siemens Healthcare, Charlestown, MA, USA
[4] Cardiovascular Research Center, Cardiology Division, Massachusetts General Hospital, Harvard Medical School, Boston, MA, USA

Background

Heart muscle is highly anisotropic with an intricate microstructure, well suited to characterization with diffusion tensor imaging (DTI) [1]. The most widely used measure of fiber organization in the myocardium is the helix angle (HA), simply defined as the inclination of the myofiber out of the local short-axis plane. Myofibers in the subendocardium have a positive HA, while those in the subepicardium have a negative HA [1, 2]. These myofibers are further arranged into laminar sheets, which slide against each other allowing the myocardium to thicken during systole [3, 4]. Alterations of this microstructure due to heart disease affect its mechanical efficiency and also could contribute to arrhythmias [5, 6]. These microstructural changes can precede symptoms and thus a non-invasive evaluation could be of significant clinical value.

The motion of the heart is five orders of magnitude greater than the self-diffusion of water. Therefore, approaches that are sensitive to the microscopic diffusion of water, but not to cardiac motion and strain, are needed for successful *in vivo* imaging [7-9]. One approach to enable *in vivo* DTI uses a diffusion-encoded stimulated echo (STE) sequence (Fig. 1), which can be implemented on most clinical scanners [10, 11]. The diffusion-encoded STE sequence is played out over two successive heartbeats. The first and second 90° excitation pulses are applied in the first heartbeat, and the third excitation pulse in the second heartbeat. The diffusion-encoding gradients are monopolar and placed immediately after the first and third excitation pulses. The main appeal of the STE approach is its conceptual immunity to cardiac motion. Ideally, each monopolar diffusion gradient occurs at exactly the same time in two sequential R-R intervals. Hence, not only is the phase due to the diffusion-encoding gradient unwound, but the influence of cardiac motion on the phase of the magnetization also is unwound.

The use of a STE sequence, however, introduces a high degree of inefficiency into the acquisition due to the dual-gated acquisition. Additionally, the STE is half the amplitude of a spin-echo. Consequently most investigators have used ~8 averages per slice in order to achieve sufficient signal-to-noise (SNR) during diffusion-encoded STE acquisitions, taking 5-7 minutes per slice [12]. The inefficiency of the STE approach frequently requires the anatomical coverage of the acquisition to be compromised. For instance, only 3 short-axis slices can be imaged in ~15 minutes, which covers only 25% of the myocardium [12]. New approaches to improve anatomical coverage and reduce scan time are thus sorely needed. The development of simultaneous multi-slice (SMS) acquisition using a blipped Controlled Aliasing in Parallel Imaging (blipped-CAIPIRINHA) readout holds great promise [13, 14], and could play a key role in facilitating the more widespread use of cardiac DTI.

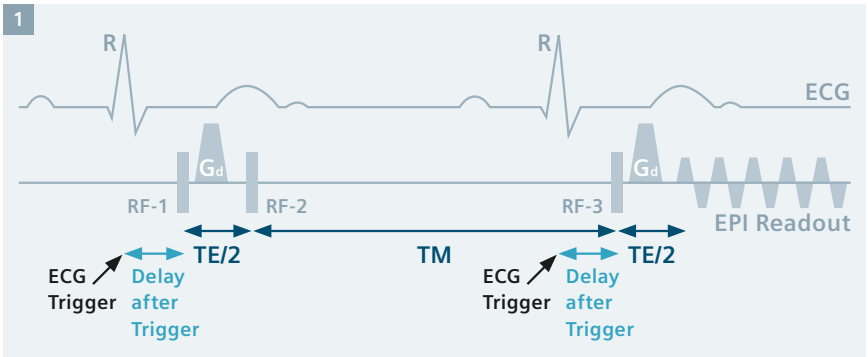

1 Dual gated stimulated echo (STE) sequence. Three 90° excitation pulses (RF) are applied over two successive heartbeats. The excitation (RF-1), refocusing (RF-3), and diffusion dephase and rephrase occur at the same time in the R-R intervals, thereby exploiting periodicity of heart motion to rewind motion related dephasing. Additionally, the long diffusion time (including TM), allows a sufficient b-value to be produced on clinical scanners without the need for an excessively long TE.

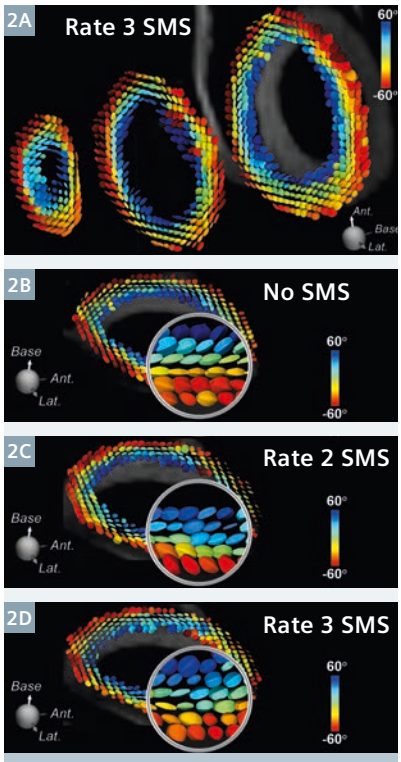

2 **(2A)** Simultaneous acquisition of 3 slices with rate 3 SMS. The gap between the slices is 500% of slice thickness. The tensor field is represented by supertoroids color-coded by HA. Supertoroid fields resulting from no SMS **(2B)**, rate 2 **(2C)**, and rate 3 **(2D)** SMS acquisitions of the same mid-ventricular slice are consistent with the transmural change in HA from positive in the subendocardium to negative in the subepicardium.

Implementation

The technical details of SMS excitation using blipped-CAIPIRINHA have been described in detail elsewhere in this volume. The technique has been used extensively in the brain [13, 14], and preliminary experience with it in the heart appears promising [15]. In the current article, we describe our experience with this technique for cardiac DTI in healthy volunteers.

Breath-hold DTI was performed on a clinical 3T scanner (MAGNETOM Skyra, Siemens Healthcare, Erlangen, Germany) with a 34-element receive coil[1] (18 anterior and 16 posterior elements). Images were acquired with a diffusion-encoded STE sequence, which was volume-selected in the phase-encode axis using a slab selective radiofrequency (RF) pulse. Acquisition parameters included: FOV 360 x 180 mm, resolution 2.5 x 2.5 x 8 mm^3, in-plane GRAPPA rate 2, TE 34 ms, b-value 500 s/mm^2, 10 diffusion-encoding directions, and 8 averages. Twelve short-axis slices were acquired in the systolic sweet spot of the cardiac cycle to mitigate strain effects [11, 16]. Imaging was performed with no SMS, and rates 2 and 3 SMS. HA was derived from the diffusion tensor, which was estimated from the diffusion-weighted images. Fiber tracts were constructed by integrating the primary eigenvector field into streamlines using an adaptive 5^{th} order Runge-Kutta approach [5].

Results and impact

With no SMS, 96 breath-holds were required to cover the entire LV. Using rate 2 SMS, this was reduced to 48 breath-holds, and with rate 3 SMS to 32. With rate 3 SMS, the acquisition time was approximately 20 minutes for whole-heart coverage. Image quality was well preserved using both rates 2 and 3 SMS. This is demonstrated in Figure 2, where the diffusion tensor in each voxel is represented by the supertoroidal model [17]. The glyphs are parameterized by the magnitude and orientation derived from the diffusion tensor and color-coded by HA. The transmural evolution in HA from positive in the subendocardium to negative in the subepicardium is well resolved in all 3 slices with rate 3 SMS. Glyph fields using rates 2 and 3 SMS of a mid-ventricular slice compare favorably with those acquired with no SMS, and are consistent with expected transmural evolution in HA.

Tractography of the heart has previously been performed over a small anatomical range (3-5 slices) or with very large slice gaps. Meaningful tractography requires the entire heart to be imaged without any slice gaps.

[1] The product is still under development and not commercially available yet. Its future availability cannot be ensured.

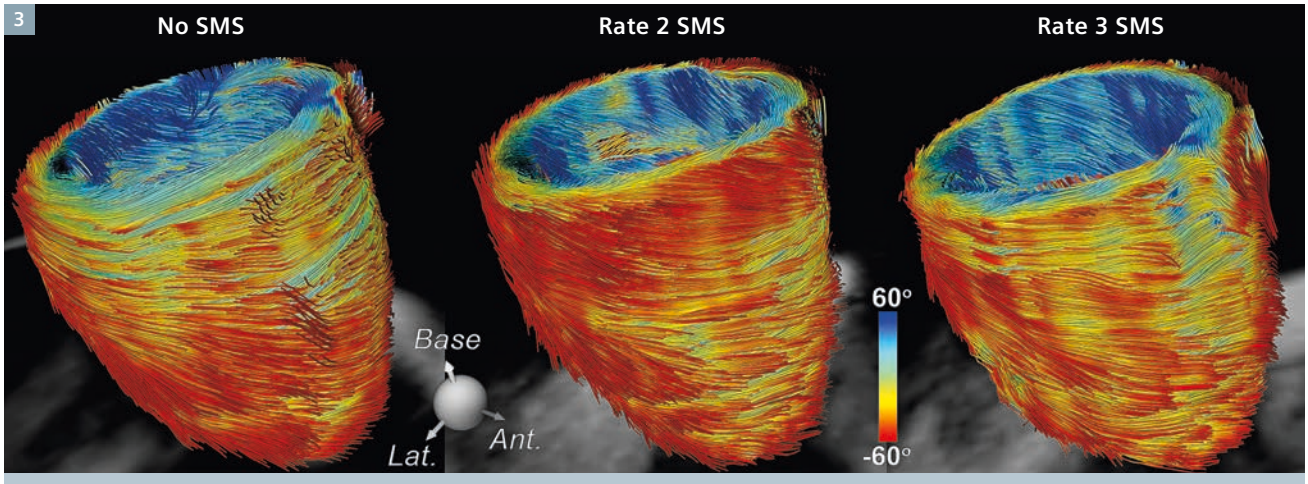

3 Tractography of the entire LV, color-coded by HA, of the same subject imaged with no SMS, and rates 2 and 3 SMS. Tracts obtained using rates 2 and 3 SMS compare favorably and are in agreement with those obtained with no SMS.

With no SMS, this takes over 60 minutes to acquire. However, as shown in Figure 3, fiber tracts of the entire LV were successfully obtained with rates 2 and 3 SMS, and are qualitatively comparable with those obtained with no SMS.

Discussion

DTI of the heart has the potential to improve the understanding, diagnosis and management of a range of cardiovascular diseases. However, the main limitation is long scan times. With current techniques, the acquisition of 3 short-axis slices takes ~20 minutes. We demonstrated that using SMS, scan time was reduced by 3-fold. The simultaneous acquisition of 3 slices (basal, medial, and apical), as shown in Figure 2, takes ~5 minutes. While imaging only 3 slices yields limited coverage of the LV, the utility of this approach has been demonstrated in first-pass perfusion studies of the heart [18]. The additional acquisition of DTI images in the same 3 short-axis slices would add little time to a clinical study and could be of substantial value.

DTI of the entire heart, while more demanding, could provide a unique way to evaluate myocardial microstructure. SMS combined with further technical advances may facilitate the clinical translation of whole-heart DTI, enabling the reliable characterization of myocardial structure in a wide range of patients with cardiac diseases.

References

1 Streeter DD, Jr., Spotnitz HM, Patel DP, Ross J, Jr., Sonnenblick EH. Fiber orientation in the canine left ventricle during diastole and systole. Circ Res. 1969;24(3):339-47.

2 Scollan DF, Holmes A, Winslow R, Forder J. Histological validation of myocardial microstructure obtained from diffusion tensor magnetic resonance imaging. Am J Physiol. 1998;275(6 Pt 2):H2308-18.

3 LeGrice IJ, Smaill BH, Chai LZ, Edgar SG, Gavin JB, Hunter PJ. Laminar structure of the heart: ventricular myocyte arrangement and connective tissue architecture in the dog. Am J Physiol. 1995;269(2 Pt 2):H571-82.

4 Dou J, Tseng WY, Reese TG, Wedeen VJ. Combined diffusion and strain MRI reveals structure and function of human myocardial laminar sheets in vivo. Magn Reson Med. 2003;50(1):107-13.

5 Mekkaoui C, Huang S, Chen HH, Dai G, Reese TG, Kostis WJ et al. Fiber architecture in remodeled myocardium revealed with a quantitative diffusion CMR tractography framework and histological validation. J Cardiovasc Magn Reson. 2012;14:70.

6 Trayanova NA. Whole-heart modeling: applications to cardiac electrophysiology and electromechanics. Circ Res. 2011;108(1):113-28.

7 Sosnovik DE, Wang R, Dai G, Reese TG, Wedeen VJ. Diffusion MR tractography of the heart. J Cardiovasc Magn Reson. 2009;11:47.

8 Nguyen C, Fan Z, Sharif B, He Y, Dharmakumar R, Berman DS et al. In vivo three-dimensional high resolution cardiac diffusion-weighted MRI: a motion compensated diffusion-prepared balanced steady-state free precession approach. Magn Reson Med. 2014;72(5):1257-67. doi:10.1002/mrm.25038.

9 Gamper U, Boesiger P, Kozerke S. Diffusion imaging of the in vivo heart using spin echoes--considerations on bulk motion sensitivity. Magn Reson Med. 2007;57(2):331-7. doi:10.1002/mrm.21127.

10 Reese TG, Weisskoff RM, Smith RN, Rosen BR, Dinsmore RE, Wedeen VJ. Imaging myocardial fiber architecture in vivo with magnetic resonance. Magn Reson Med. 1995;34(6):786-91.

11 Tseng WY, Reese TG, Weisskoff RM, Wedeen VJ. Cardiac diffusion tensor MRI in vivo without strain correction. Magn Reson Med. 1999;42(2):393-403.

12 Nielles-Vallespin S, Mekkaoui C, Gatehouse P, Reese TG, Keegan J, Ferreira PF et al. In vivo diffusion tensor MRI of the human heart: reproducibility of breath-hold and navigator-based approaches. Magn Reson Med. 2013;70(2):454-65.

13 Setsompop K, Cohen-Adad J, Gagoski BA, Raij T, Yendiki A, Keil B et al. Improving diffusion MRI using simultaneous multi-slice echo planar imaging. NeuroImage. 2012;63(1):569-80. doi:10.1016/j.neuroimage.2012.06.033.

14 Setsompop K, Gagoski BA, Polimeni JR, Witzel T, Wedeen VJ, Wald LL. Blipped-controlled aliasing in parallel imaging for simultaneous multislice echo planar imaging with reduced g-factor penalty. Magn Reson Med. 2012;67(5):1210-24. doi:10.1002/mrm.23097.

15 Lau AZ, Tunnicliffe EM, Frost R, Koopmans PJ, Tyler DJ, Robson MD. Accelerated human cardiac diffusion tensor imaging using simultaneous multislice imaging. Magn Reson Med. 2015;73(3):995-1004. doi:10.1002/mrm.25200.

16 Stoeck CT, Kalinowska A, von Deuster C, Harmer J, Chan RW, Niemann M et al. Dual-phase cardiac diffusion tensor imaging with strain correction. PLoS One. 2014;9(9):e107159. doi:10.1371/journal.pone.0107159.

17 Mekkaoui C, Chen IY, Chen HH, Kostis WJ, Pereira F, Jackowski MP et al. Differential response of the left and right ventricles to pressure overload revealed with diffusion tensor MRI tractography of the heart in vivo. Journal of Cardiovascular Magnetic Resonance. 2015;17(Suppl 1):O3-O. doi:10.1186/1532-429X-17-S1-O3.

18 Stab D, Wech T, Breuer FA, Weng AM, Ritter CO, Hahn D et al. High resolution myocardial first-pass perfusion imaging with extended anatomic coverage. J Magn Reson Imaging. 2014;39(6):1575-87. doi:10.1002/jmri.24303.

Timothy G. Reese

Choukri Mekkaoui

Contact

Choukri Mekkaoui
Athinoula A. Martinos Center for Biomedical Imaging
149 13th Street
Charlestown, MA 02129, USA
Phone: +1 617 724-3407
Fax: 617 726-7422
mekkaoui@nmr.mgh.harvard.edu

Slice Acceleration in the 3 Tesla Component of the Human Connectome Project

Kâmil Uğurbil[1]; Edward J. Auerbach[1]; Steen Moeller[1]; Junqian Xu[4]; An Vu[1]; Matthew F. Glasser[3]; Christophe Lenglet[1]; Stamatios N. Sotiropoulos[2]; Stephen M. Smith[2]; Timothy EJ Behrens[2]; David Van Essen[3]; Essa Yacoub[1]

[1] Center for Magnetic Resonance Research (CMRR), University of Minnesota, Minneapolis, MN, USA
[2] Oxford Centre for Functional MRI of the Brain (FMRIB), University of Oxford, UK
[3] Department of Anatomy & Neurobiology, Washington University School of Medicine, St. Louis, MO, USA
[4] Translational and Molecular Imaging Institute, Icahn School of Medicine at Mount Sinai, New York, NY, USA

Introduction

The Human Connectome Project (HCP) was launched on the principle of undertaking significant new advances in magnetic resonance (MR) based imaging of the human brain and using these advanced technologies to generate to-date the most complete and accurate description of the connections among gray matter locations in the human brain at the millimeter scale.

At the time HCP was initiated, a growing number of studies had revealed important insights through systematic studies of whole-brain connectivity (e.g. [1-6]) using resting-state functional magnetic resonance imaging (rfMRI) and diffusion imaging (dMRI). rfMRI uses correlations in the spontaneous temporal fluctuations in an fMRI time series to deduce '*functional connectivity*' (e.g. [7-11]) and, dMRI provides the input for tractography algorithms used for the reconstruction of the complex axonal fiber architecture so as to infer '*structural connectivity*' (e.g. reviews [12, 13]). Despite their promise, however, each of these MR methods faces serious technical *limitations*. These include a high incidence of false positives and false negatives [13, 14] that arise from the indirect nature of functional imaging signals [15], dependence on neurovascular coupling [16], the presence of confounding long-range correlations of vascular origin [17], and the complexity of water diffusion in the microenvironment of the brain (e.g. [18, 19]). Given these neurobiological and neurophysiological challenges, undertaking significant new methodological developments to overcome or ameliorate these limitations was considered imperative for the success of the HCP.

A primary challenge in the fMRI component of the HCP is the ability

1

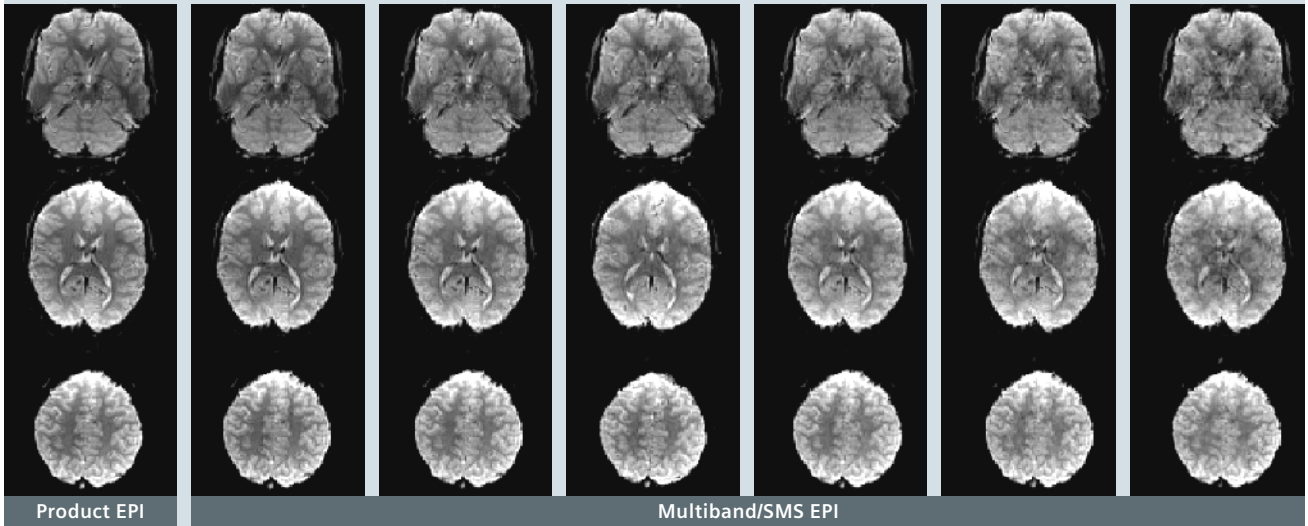

1 Slice accelerated Multiband/SMS images from the HCP obtained at 3T at different acceleration factors. Three slices from a 2 mm isotropic resolution, 64 slice whole brain data set obtained with slice acceleration up to MB factor of 12. For comparison, images were acquired with the same TR (4.8 s) based on the minimum TR attainable with standard EPI (i.e. MB = 1). The example axial slices shown were not from the same MB slice group. Achievable TR at a given MB factor is listed below the MB factors given to show the acceleration potential. *Adapted from Uğurbil et al. 2013 [24], and Xu et al., 2013 [36].*

to capture functional mapping signals with the highest possible fidelity to the underlying gray/white matter neuronal architecture. Therefore, improving spatial resolution for the HCP data was one of the targets set out by the HCP investigators from the inception of the project. However, there is always a compromise between spatial resolution and the total volume acquisition time. Higher spatial resolution requires larger number of slices to cover the volume-of-interest (in the HCP, the whole human brain) and hence leads to a longer TR. Longer TRs are not desirable in fMRI; if they become significantly longer than the T1, image signal-to-noise ratio (SNR) per unit time suffers. In addition, slower acquisitions undermine the accurate sampling of the basal fluctuations in an fMRI time series, potentially degrading efforts to clean up the time series of undesirable sources of fluctuations (such as those induced by respiration and cardiac pulsation), and lead to fewer samples within a given total acquisition time, reducing the statistical power in the analysis of the time series. Thus, it was critical to accelerate the data acquisition rate without significantly impacting image SNR.

Accelerating image acquisition is also critical for dMRI. Improvements in SNR per unit time enable higher spatial resolution without commensurately longer data acquisition times, and/or allow for more extensive sampling of the diffusion encoding space (i.e. q-space, defined by the magnitude and orientations of the diffusion-weighting gradients) so as to more accurately estimate the orientation of white matter fiber bundles, especially in regions where multiple fiber bundles intersect one another at various angles or where fiber bundles bend or fan out and split into multiple trajectories.

In this article, we briefly review the technical developments undertaken for data acquisition at 3 Tesla within the Washington University-University of Minnesota (WU-Minn) Consortium of the HCP (http://humanconnectome.org), composed primarily of three institutions, Washington University, University of Minnesota, Center for Magnetic Resonance Research (CMRR), and Oxford University. An accompanying article by Yacoub et al. in this issue of MAGNETOM Flash describes a parallel effort at 7 Tesla within this consortium. An overview of the overall HCP project is discussed in [20] and more comprehensive and detailed accounts of improvements and optimizations are given in references [21-25].

Pushing image acquisition speed

Improving fMRI data acquisition speed, while critical for the HCP, is relevant to human neuroimaging in general and was already recognized in work prior to the HCP for very high-resolution fMRI applications at ultrahigh magnetic fields [26, 27]. Motivated by the prospect of whole-brain, very high resolution functional mapping at 7T, Moeller et al. [26, 27] used multi-slice GRE EPI[1] at 7T with concurrent accelerations along both the slice and in-plane phase-encode directions, achieving 16-fold two-dimensional acceleration. Multiple slices were simultaneously excited using multiband RF pulses; the signals generated by these multiple slices were acquired simultaneously in a single EPI echo train, with *k*-space undersampling in the phase-encode direction. These simultaneously acquired slices were unaliased using parallel imaging principles and the coil sensitivity profiles of the multichannel receive array employed for data collection. Excellent functional maps at 7T with 1.5 mm isotropic resolution and 88 slices in 1.25 s, or 1 x 1 x 2 mm^3 resolution with 90 slices in 1.5 s were achieved [26, 27].

The use of multiband excitation pulses to simultaneously excite and collect multiple slices (referred to as Multiband (MB) or Simultaneous Multi-Slice (SMS) technique interchangeably) dates back to 2001, when it was demonstrated using gradient recalled echoes, collecting a single *k*-space line at a time (i.e. FLASH), imaging a leg with a spine coil [28]. This approach was further advanced with the introduction of the CAIPIRINHA (Controlled Aliasing In Parallel Imaging Results IN Higher Acceleration) [29, 30] concept where unaliasing of slices was improved significantly by manipulating the phase of the RF excitation pulses progressively for each *k*-space line, so as to effectively shift the simultaneously acquired slices relative to each other in the phase-encoding direction. These earlier initiatives did not catch the attention of the neuroimaging community. However, Moeller at al. [26, 27] demonstrated an application where such rapid volume coverage using Multiband/SMS EPI is critical, thus catalyzing a major interest in this approach. Subsequently, a modified 'blip' strategy in Multiband/SMS EPI, termed 'blipped-CAIPIRINHA', that balances the blips so as to minimize the voxel tilting of the earlier blipping implementation [31] was introduced [32, 33], providing major improvements in *g*-factor noise and achievable slice accelerations, adding to the attractiveness of the approach in EPI based techniques such as fMRI and dMRI.

Initial efforts in the WU-Minn consortium also tried to accelerate beyond what was feasible with Multiband/SMS EPI by combining it with the SIR approach [34], a technique we referred to as Multiplexed-EPI (M-EPI) [35]. A similar combination was also described in an abstract the same year [32]. Multiplexed EPI essentially takes the SIR sequence, where ***s*** RF pulses are applied sequentially in time leading to temporally resolved echoes from the ***s*** different slices, and makes each RF pulse a multiband pulse with ***m*** bands (where ***m*** and ***s*** are positive integers); the result is simultaneous acquisition of ***m*** times ***s*** (i.e. ***m*** x ***s***) slices in a single echo train that contains both simultaneously acquired as well as temporally shifted echoes. Using this method to accelerate whole-brain coverage, the WU-Minn HCP consortium demonstrated [35] that the statistical significance of the Resting-State Networks (RSNs) detected by high dimensional ICA analysis from rfMRI time series significantly improved, and the normally long acquisition time of dMRI was reduced

[1] The product is still under development and not commercially available yet. Its future availability cannot be ensured.

2-4 fold. However, because of the longer echo trains inherent in SIR, the combined technique is not universally advantageous, and the realizable gains depend on several factors, including spatial resolution, MB acceleration capabilities, desired temporal resolution, and the need for in-plane accelerations. As such, in the HCP, Multiplexed EPI was not employed; rather Multiband/SMS EPI with control aliasing ('blipped-CAIPIRINHA') and *without* the use of in-plane phase-encode acceleration was adapted in the WU-Minn consortium as the sequence for the 3T HCP data acquisition.

An example of the type of Multiband/SMS images with 2 mm isotropic nominal resolution obtained in the initial evaluation phase on the WU-Minn 3T HCP scanner (Connectom-Skyra[2], Siemens Healthcare, Erlangen, Germany) is illustrated in Figure 1 for different MB factors (i.e. the number of simultaneously excited slices, or the slice acceleration factor). For comparison, images from the standard EPI sequence (corresponding to MB = 1) available on the scanner are also provided. Although the TR was kept constant at the value attainable for the MB1 so as to maintain identical contrast in these images, the minimum achievable volume TR to cover the whole brain is also indicated for each MB factor. The data were acquired using a 32-channel standard Siemens head coil. Careful scrutiny of the images indicates that MB = 12 data still show much detailed structure although they clearly display greater artifact level. Figure 2 illustrates 18 slices from a whole-head acquisition comparing standard EPI (MB1) images and MB6 Multiband acquisition at 3T at the same TR; excellent EPI image quality is evident in MB = 6 as well as the standard MB = 1 case.

A quantitative analysis of these data is possible using *g*-factors [36] that reflect noise amplification due to the use of parallel imaging using the formulation developed for in-plane parallel imaging along the phase-encode dimension [37]. However, *g*-factors themselves do not inform about residual aliasing among the simultaneously acquired slices. To address this, we introduced a metric named the *L*-factor (leakage factor) [36, 38] that quantifies residual aliasing.

L-factor maps of residual aliasing are illustrated in Figure 3 for Multiband/SMS EPI imaging with MB = 3, 4, 8 and 12 from data acquisition sequences employed for the HCP. Such maps illustrated that there is no perceptible 'leakage' from the center slice to the two adjacent slices for MB = 3 or 4 and the calculated *L*-factor was 0.03 with or without PE_{SHIFT}. With MB = 8 and 12, there is small leakage (Fig. 3), but not sufficient to impact fMRI data.

The objectives of the WU-Minn HCP consortium entailed not only improved pulse sequences but also implementation on the HCP scanners for efficient, stable and robust performance. Therefore, significant efforts were invested in evaluating the performance of the sequences and the associated image reconstruc-

2

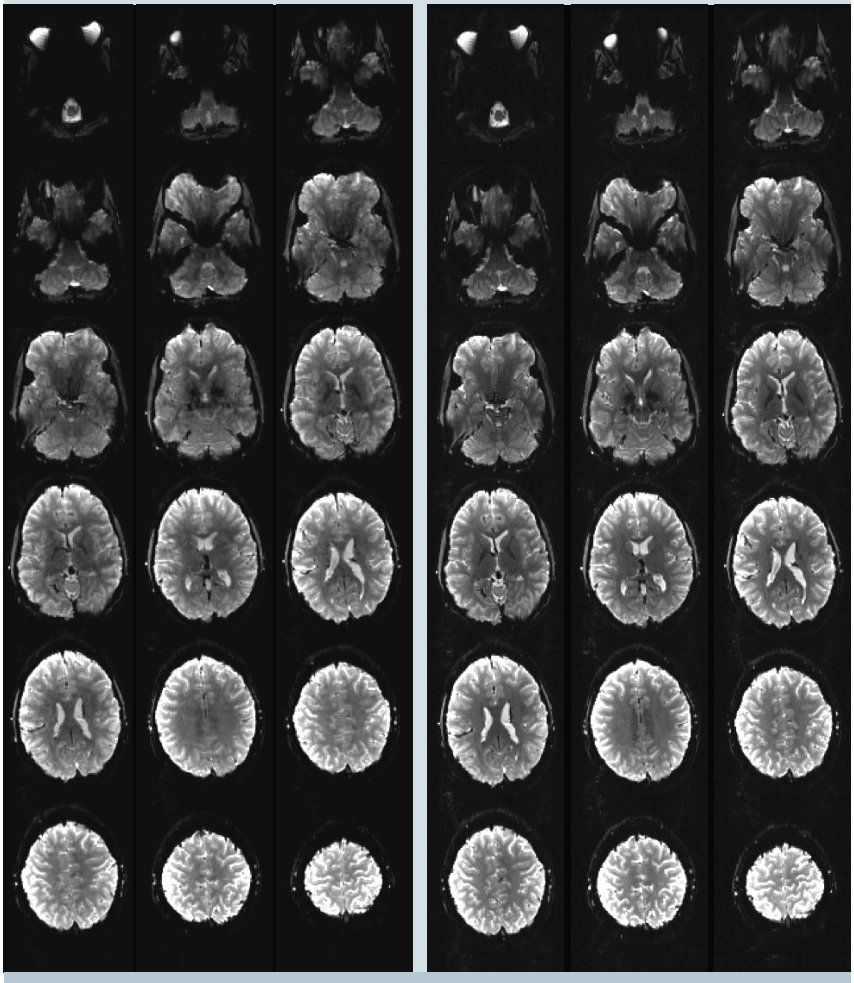

2 Comparing 6-fold slice accelerated Multiband/SMS images at 3T with unaccelerated standard acquisition. Selected slices from a 1.6 mm isotropic, 80 slice whole-brain data set obtained with PE_{SHIFT} = FOV/3, MB factor 6 and standard EPI (MB = 1). TE = 30 ms; 6/8 Partial Fourier along phase-encode direction. TR = 6.7 s for both, set by the minimum TR attainable with MB = 1. Minimum TR that would be possible with MB = 6 acquisition with these parameters would be 1.1 s. Data was obtained with a 32-channel coil on the 3T WU-Minn HCP scanner. *Adapted from Uğurbil et al., 2013 [24] and Xu et al., 2013 [36].*

[2] Product is ongoing research. All data shown are acquired using a non-commercial system under institutional review board permission.

3

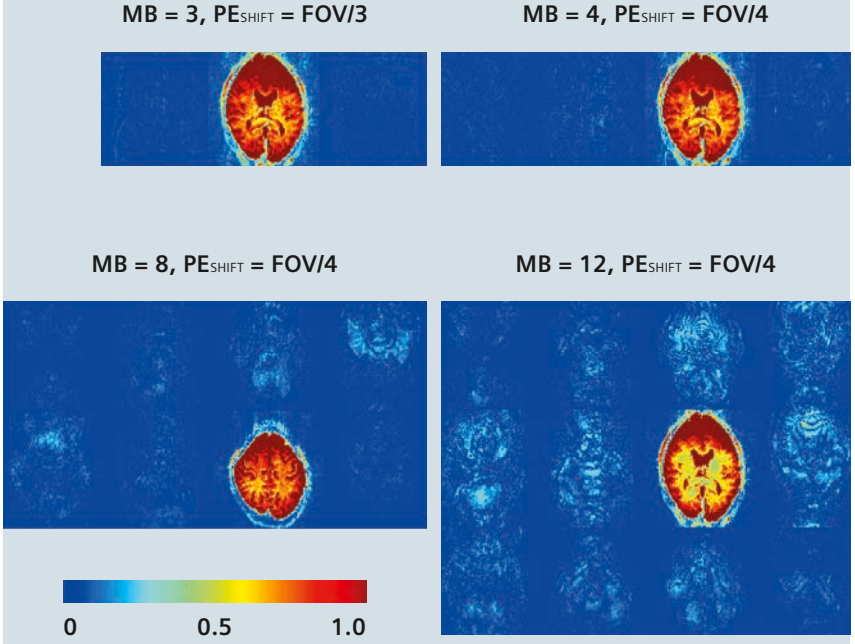

3 Quantifying residual aliasing among simultaneously acquired slices. Signal leakage (*L*-factor) maps showing residual aliasing among simultaneously acquired slices at 3T for MB3, MB4, MB8 and MB12 with PE$_{SHIFT}$. The oscillation imposed on slice (appears in red/yellow color) 'leaks' into other simultaneously acquired slices due to resdiual aliasing. *Adapted from Xu et al. 2013*. We describe the shift induced in the phase-encode direction by controlled aliasing as a fraction of the field-of-view (FOV) and refer to it using the label PE$_{SHIFT}$; thus a PE$_{SHIFT}$ of FOV/4 has a maximal shift of ¼ of the FOV in the phase-encode direction between the simultaneously excited slices. *Adapted from Xu et al. 2013 [36], Moeller et al. 2012 [38].*

Table 1

	rfMRI and tfMRI	dMRI
Multiband Factor (i.e. slice acceleration factor)	8	3
In-plane phase-encode acceleration	None	None
Spatial resolution	2 mm isotropic	1.25 mm isotropic
TE	33 ms	89 ms
TR (whole volume)	0.72 s	5.5 s
Δ	Not applicable	43.1 ms
δ	Not applicable	10.6 ms
q-space sampling	Not applicable	3 shell HARDI b = 1000, 2000, 3000 s/mm^2 270 non-collinear directions

HCP acquisition parameters employed at 3T for fMRI and dMRI.

tion algorithms. The evaluation took place in two stages. The first stage involved evaluation of image quality, temporal stability, noise increase due to parallel imaging, and residual aliasing among the simultaneously excited slices [24]. The second stage examined the performance of the sequences, and the different acquisition parameters for detection of resting-state networks and task activation for fMRI, robustness to subject motion (described in greater detail in [22]), and various metrics for diffusion imaging (also described in greater detail in [21]). Both stages were critical and ultimately led to the final protocol selection [24]. The parameters decided upon for the 3T protocol in the HCP are summarized in Table 1.

The fMRI (both resting-state and task) were run with MB factor of 8 (i.e. 8 fold slice acceleration) at 3T using the 32-channel coil from Siemens Healthcare. Such high slice accelerations are not feasible in dMRI because of peak power limitations and ultimately power deposition (SAR) since dMRI uses spin-echo sequences with nominally 90° and 180° excitation and refocusing pulses, respectively. We qualify the flip angles as 'nominal' because even at 3T and even with a body coil transmission, the flip angle is not uniform in the human head [24]. In fMRI, only an excitation pulse is employed and this pulse is adjusted to lower flip angles (i.e. the Ernst angle) to optimize SNR for the reduced TR made possible with slice acceleration, hence lowering power deposition per pulse. Although methods were developed in the WU-Minn HCP consortium to alleviate the peak power [39] and SAR limitations [40, 41] for Multiband/SMS imaging within the HCP, they were not ready in time to be exhaustively tested for the 3T data collection phase of the WU-Minn HCP. Some of these techniques were, however, adopted in the 7T phase of the project [42].

The HCP 3T protocol does not use in-plane phase encoding acceleration; if possible, we decided to avoid this in order to maximally accelerate the fMRI time series along the slice direction and to avoid the SNR penalty that comes with reduced *k*-space coverage when accelerating along the phase

encode direction. EPI image quality (with the distortion corrections realized by obtaining images with phase-encode running in opposite directions, and also corrected for eddy current effects for dMRI [43, 44]) were considered excellent both for fMRI and dMRI acquisitions [21, 22]. Furthermore, when the performance of 3T dMRI acquisitions with in-plane acceleration was evaluated in terms of fibre crossing sensitivity and uncertainty, they did not perform as well as just using slice acceleration alone. This was likely because of the SNR loss that comes with in-plane phase-encode acceleration.

Rigid body motion of the subject's head is a major problem in the analysis of data from an fMRI time series. As a result, methods for correcting rigid body motion in an fMRI time series by 'realigning' volumetric data is routinely performed in fMRI data analysis. When parallel imaging is employed, the problem of motion becomes more complex because 'reference' or 'calibration' scans that are obtained typically at the beginning of the data collection period and the subsequently acquired accelerated data in the fMRI time series are no longer fully consistent. This problem was evaluated in the HCP fMRI data. The 'conventional' volumetric realignment, which ignores the potential additional problem of a mismatch between the calibration scan and the subsequent images, was found to be surprisingly successful with the Multiband/SMS EPI fMRI data (MB = 8) when motion occurred during the acquisition of the fMRI time series [22]. This likely reflects the fact that coil sensitivity profiles are spatially slowly varying functions. However, motion during the acquisition of the calibration scan when parallel imaging along the phase encoding was employed was a major problem. This confound was not present in the 3T HCP data because phase-encode parallel imaging was not employed; but it was an issue for the 7T HCP data.

Since the 3T component of HCP *does not* use phase encoding acceleration, the calibrations scans are based on single slice versions of the *single-shot* slice selective EPI employed subsequently in the Multiband/SMS acquisition. However, if acceleration along the phase encoding direction is employed, one cannot just use images of each slice obtained individually in a single-shot using acceleration along phase encoding direction. Calibration scans are also needed for the phase-encode undersampling and this is typically done using *segmented multi-shot (as opposed to single-shot)* EPI. Segmented EPI sampling of *k*-space is prone to degradation induced by subject motion as well as physiological processes related to respiration and cardiac pulsation [27]; this degradation typically appears in the form of 'ghosting' artifacts, i.e. displacement of signal intensities to regions where they should not be. Respiration can be a source of small rigid body motion of the head but it also affects MR images, especially EPI through perturbations of the B_0 field over the brain caused by alterations of air-filled lung volume during the respiration cycle [45, 46] because air has significantly different magnetic susceptibility than tissue. Cardiac pulsation induces *non*-rigid body motion in the brain, most prominent in ventral parts, particularly in the brainstem.

Thus, a *segmented* EPI acquisition is not necessarily optimal as a calibration scan for unaliasing images obtained with simultaneous acceleration along the slice and phase-encode directions. Instead, we examined the use of standard GRE images, acquiring one *k*-space line after an RF pulse (i.e. FLASH) as a calibration scan, acquired with a lower resolution than the final resolution of the subsequently accelerated data. This approach provided significant improvements and is employed in the 7 Tesla component of the HCP [24, 42] as well as in the 3T Lifespan piloting efforts undertaken within the HCP.

Examples from HCP data

rfMRI came to existence with the observation that functionally related areas that are co-activated in a task (and detected by task fMRI) show correlated spontaneous fluctuations in the absence of any task when the subjects are simply 'resting' in the magnet [7]. This led to the concept that functionally linked areas (though not necessarily all directly connected) exhibit distinct spontaneous oscillations and thus can be extracted from the rfMRI data [47]. Hence it is possible to identify from rfMRI data so called resting-state networks (RSNs) that are classified, for example as 'visual' or 'sensory-motor', or 'language' etc. networks. The identifications are based on the observation that the spatial patterns that are depicted in these RSNs (which resemble activation maps but are actually regions that display temporally-correlated spontaneous fluctuations) have similarities to collection of regions activated by task based fMRI. This is an important observation since it supports the concept that RSNs reflect neuronal processes and not necessarily temporally correlated fluctuations that can be observed in the brain but are not linked to neuronal activity (e.g. [17]).

The HCP fMRI data obtained with slice acceleration and subsequently cleaned by independent component analysis (ICA) based methods [48] provide excellent and convincing demonstration of the correspondence between areas seen in task fMRI and RSNs extracted from ICA analysis of rfMRI time series. They strengthen the argument that regions that are intimately linked functionally do have correlated spontaneous fluctuations even when they are not actively involved in the execution of a task.

Of course, rfMRI data yield many RSNs (in this regard, HCP data are unique in being able to identify a very large number of such RSNs that are much more fine grained than what was previously available [22, 49]). It is not immediately possible to identify an association between all of these RSNs and activation patterns elicited with specific tasks. This is expected. For example, a visuo-motor task, such as moving a joy stick in the direction of a target presented to the subject, will yield a very large number of activated areas in the brain. A single RSN that corresponds to those areas likely is not identified.

4

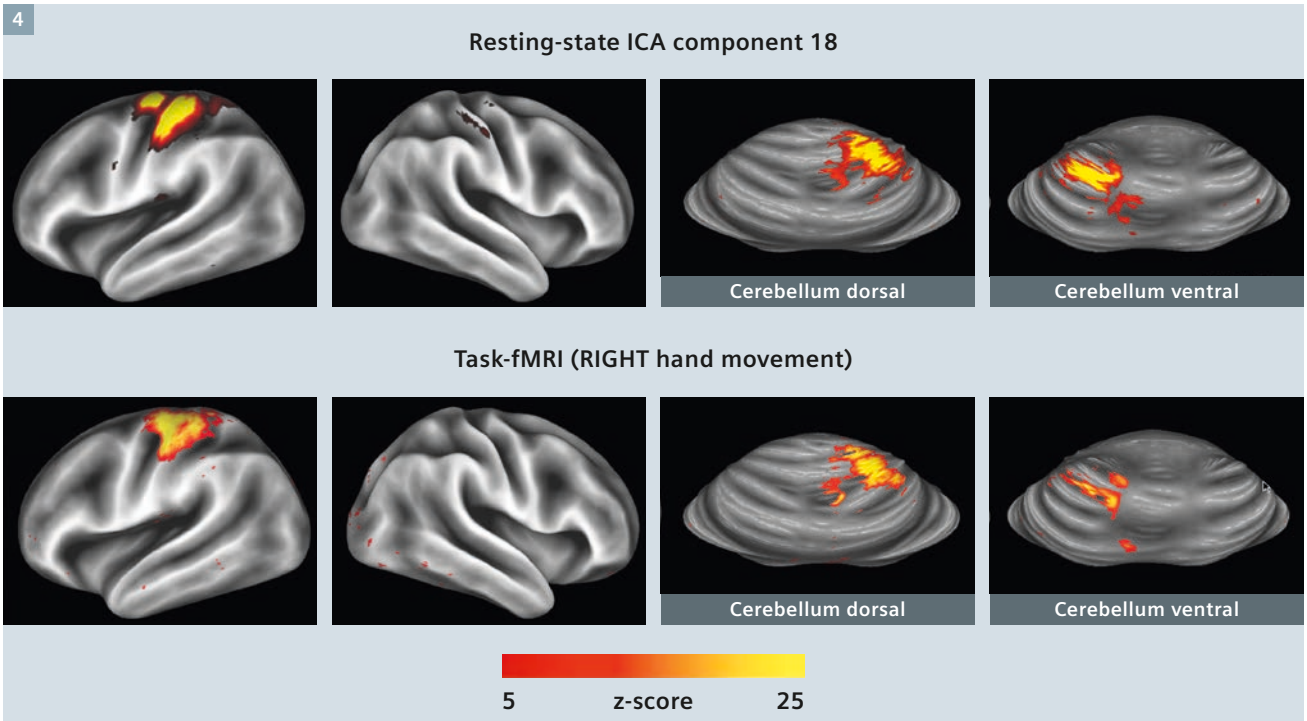

4 Comparison between activation patterns observed with task-fMRI when subjects are performing a simple 'hand task' with the right hand and an ICA component extracted from the resting-state fMRI data from the HCP database. Patterns mapped onto the group-average cerebral surfaces (first two panels) and onto the inflated cerebellar atlas surface that has been mapped to the MNI atlas stereotaxic space [Van Essen, 2009]. Resting-state fMRI component 13 from a 100-dimensional ICA decomposition (with 82 components judged to be signal), applied to the 66 subjects in the HCP Q1 data release having four rfMRI runs. *Adapted from Van Essen et al. 2013 [50].*

5

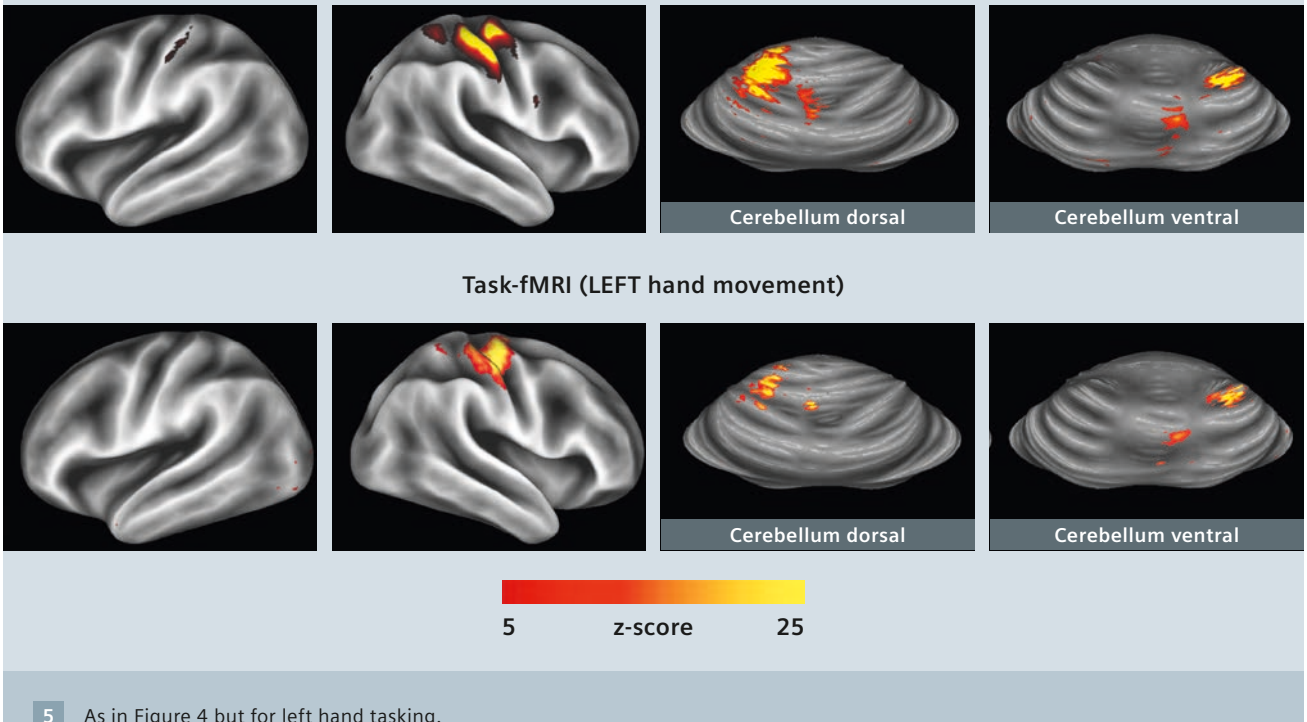

5 As in Figure 4 but for left hand tasking.

Instead, RSNs that represent motor networks, visual networks and others (likely involving parietal areas) together will represent the task induced activation pattern. The collections of RSNs that can explain the activation pattern induced by such a task would yield important information about networks engaged in that task.

However, for simple tasks, it is in fact possible to find correspondence between task based fMRI and an RSN which is an ICA component obtained from the rfMRI. An example from the HCP 3T data is shown in Figure 4, which illustrates this cross-modal comparison with data mapped to a cortical and cerebellar surface map [50]. The bottom row shows the group-average task activation from the right-hand 'hand movement' task, analyzed for a group of 20 unrelated subjects scanned for the HCP database. It includes activation in the expected location in the left motor cortex (left panel), and also at two distinct locations in dorsal and ventral cerebellum, matching published reports [4]. The top row shows a spatially corresponding ICA component from a 100-component group-level ICA-based network decomposition (with 82 'signal' components), carried out on 66 HCP subjects scanned at 3T from the first quarter data release. The correspondence in spatial patterns between the rfMRI ICA component and the task-fMRI activation is striking [50].

Figure 5 illustrates the same for the left hand tasking. Now the cortical and cerebellar hemispheres are expected to be flipped for both the ICA component and task activation pattern; indeed, this is what is observed and again similarities are striking.

Anatomical and functional connectivity data can be probed using a seed based approach, where connectivity derived from rfMRI is represented as a correlation of signal fluctuations of each voxel with the seed voxel, and anatomical connections are represented as a probabilistic connectivity derived from dMRI data of each voxel to the seed voxel. For any given voxel or seed locations, one expects to find similarities between such functional and anatomical connectivity maps. Figure 6 (top row) shows probabilistic streamlines that can be created in the Connectome workbench (Fig. 6A) and probabilistic connectivity represented on the brain surface (Fig. 6B) in a single subject from a seed location placed in the orbitofrontal cortex (location indicated by arrows in Figs. 6A, B). The lower row in Figure 6 compares functional versus structural connectivity on the flattened cortical surface from a group of 9 subjects from the same seed location. Given that the two methods have different limitations and errors, the fact that similar data are obtained in the functional versus the structural connectivity maps is reassuring.

It should be noted, however, that such structural vs. functional connectivity maps (Figs. 6C and D, respectively) need not be identical even if they suffered no errors. In a network,

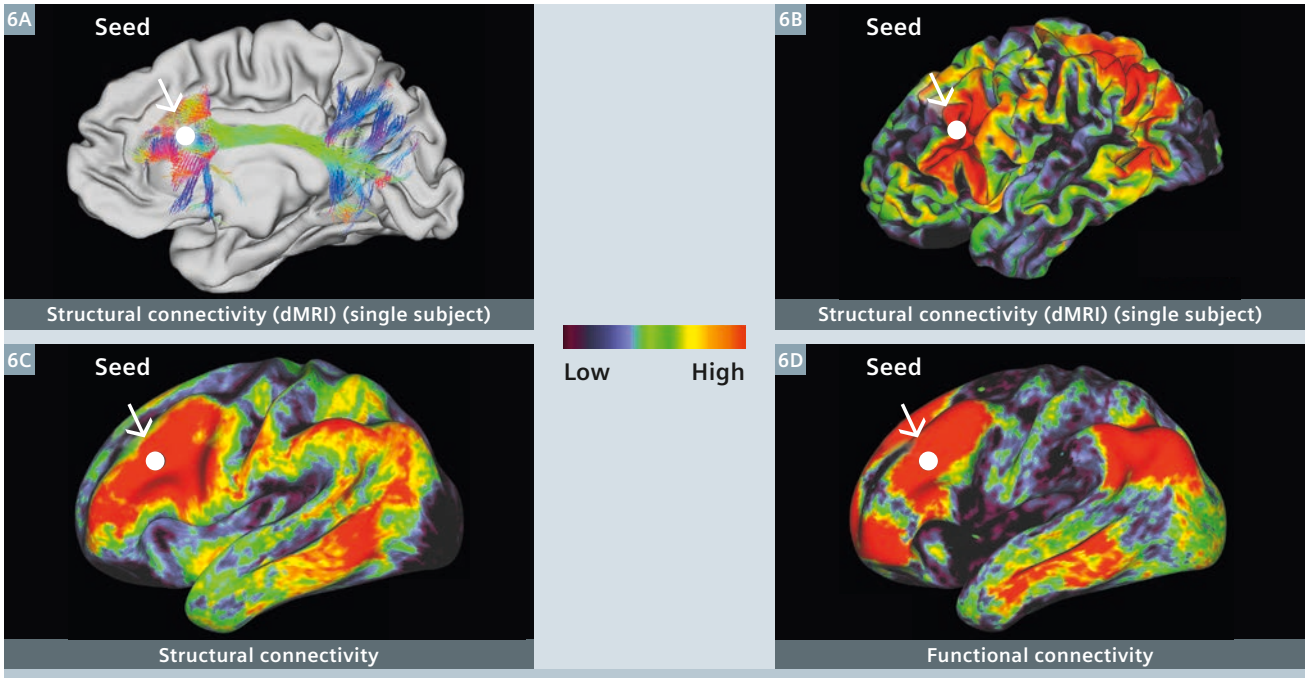

6 Structural connectivity obtained from dMRI versus functional connectivity derived from resting-state fMRI data, in an individual and in group averages. Connectivity trajectory visualization for a single HCP subject (100307). Probabilistic trajectories seeded from a single gray ordinate in left frontal cortex (white dot identified also by an arrow) and intersecting the white/gray matter boundary surface in at least one more location **(6A)**. Probabilistic structural connectivity of the same subject as viewed on the cortical surface **(6B)**. Structural connectivity values in a group average (9 HCP subjects) for the same seed location (white dot), viewed on the inflated cortical surface. The values are displayed using a logarithmic scale **(6C)**. Functional connectivity values for the same seed location, displayed on the inflated surface **(6D)**. The values correspond to the average functional connectivity of a group of 20 HCP subjects. (Note: seed in Panel 6A is not the same as in 6B, C, and D). *Adapted from Van Essen et al., 2013 [50].*

each region does not have to have a direct (anatomical) connection to every other region. For example in a network of 3 nodes, identified as 1,2, and 3, node 1 can be directly connected to node 2 and node 3 but no direct connection exists between nodes 2 and 3. This situation may lead to interesting patterns if we compare the probabilistic 'anatomical connectivity' map derived from the dMRI and the 'functional connectivity' map obtained from rfMRI. In this case, nodes 1, 2, and 3 can still show correlated spontaneous fluctuations. Putting a 'seed' in node 1 to generate such maps should yield identical anatomical and functional connectivity maps; but putting a 'seed' in node 2 or 3 will yield partially overlapping anatomical and functional connectivity maps, reflecting the fact that node 2 and 3 have no direct anatomical connectivity but still display correlated spontaneous fluctuations that have 'functional connectivity', in this case indirectly through another node.

Conclusion

The 3T protocols in the WU-Minn HCP Consortium are now 'frozen' and produce data that are significantly higher quality than what has been possible using conventional methods and instrumentation to date. Nevertheless, intense efforts were still devoted to further methodological developments within the WU-Minn consortium, largely targeting optimization of the 7T HCP data collection and are detailed in [42]. However, the impact of these developments is also anticipated to go well beyond the current HCP and is expected to spread to future efforts at any field strength. Accelerated volume coverage, whether with Multiband/SMS as currently employed in the HCP, or new approaches to be developed, may soon become the default acquisition scheme in fMRI and dMRI studies. The utility of these MR techniques are relevant to potential new initiatives investigating connectomics, for example, in relation to development, life-span, and/or brain diseases. Such initiatives will be able to take full advantage of on-going methodological improvements that would be available at the time of their start.

Acknowledgements

The work reported in this article was supported by the Human Connectome Project (1U54MH091657) from the 16 Institutes and Centers of the National Institutes of Health that support the NIH Blueprint for Neuroscience Research and by Biotechnology Research Center (BTRC) grant P41 EB015894 from NIBIB, and NINDS Institutional Center Core Grant P30 NS076408. The authors would like to thank Siemens Healthcare for collaboration and support during the Human Connectome Project.

References

1 Hagmann P, Cammoun L, Gigandet X, Meuli R, Honey CJ, Wedeen VJ, Sporns O. Mapping the structural core of human cerebral cortex. PLoS Biol 2008;6(7):e159.
2 van den Heuvel MP, Stam CJ, Kahn RS, Hulshoff Pol HE. Efficiency of functional brain networks and intellectual performance. J Neurosci 2009;29(23):7619-7624.
3 Nelson SM, Cohen AL, Power JD, Wig GS, Miezin FM, Wheeler ME, Velanova K, Donaldson DI, Phillips JS, Schlaggar BL, Petersen SE. A parcellation scheme for human left lateral parietal cortex. Neuron 2010;67(1):156-170.
4 Yeo BT, Krienen FM, Sepulcre J, Sabuncu MR, Lashkari D, Hollinshead M, Roffman JL, Smoller JW, Zollei L, Polimeni JR, Fischl B, Liu H, Buckner RL. The organization of the human cerebral cortex estimated by intrinsic functional connectivity. J Neurophysiol 2011;106(3):1125-1165.
5 Mars RB, Jbabdi S, Sallet J, O'Reilly JX, Croxson PL, Olivier E, Noonan MP, Bergmann C, Mitchell AS, Baxter MG, Behrens TE, Johansen-Berg H, Tomassini V, Miller KL, Rushworth MF. Diffusion-weighted imaging tractography-based parcellation of the human parietal cortex and comparison with human and macaque resting-state functional connectivity. J Neurosci 2011;31(11):4087-4100.
6 Power JD, Cohen AL, Nelson SM, Wig GS, Barnes KA, Church JA, Vogel AC, Laumann TO, Miezin FM, Schlaggar BL, Petersen SE. Functional network organization of the human brain. Neuron 2011;72(4):665-678.
7 Biswal B, Yetkin FZ, Haughton VM, Hyde JS. Functional Connectivity in the Motor Cortex of Resting Human Brain Using Echo-Planar Mri. Magnetic Resonance in Medicine 1995;34(4):537-541.
8 Fox MD, Raichle ME. Spontaneous fluctuations in brain activity observed with functional magnetic resonance imaging. Nat Rev Neurosci 2007;8(9):700-711.
9 Vincent JL, Patel GH, Fox MD, Snyder AZ, Baker JT, Van Essen DC, Zempel JM, Snyder LH, Corbetta M, Raichle ME. Intrinsic functional architecture in the anaesthetized monkey brain. Nature 2007;447(7140):83-86.
10 Beckmann CF, DeLuca M, Devlin JT, Smith SM. Investigations into resting-state connectivity using independent component analysis. Philos Trans R Soc Lond B Biol Sci 2005;360(1457):1001-1013.
11 Smith SM, Miller KL, Salimi-Khorshidi G, Webster M, Beckmann CF, Nichols TE, Ramsey JD, Woolrich MW. Network modelling methods for FMRI. Neuroimage 2011;54(2):875-891.
12 Mori S, Zhang J. Principles of diffusion tensor imaging and its applications to basic neuroscience research. Neuron 2006;51(5):527-539.
13 Jbabdi S, Johansen-Berg H. Tractography: where do we go from here? Brain connectivity 2011;1(3):169-183.
14 Iturria-Medina Y, Sotero RC, Canales-Rodriguez EJ, Aleman-Gomez Y, Melie-Garcia L. Studying the human brain anatomical network via diffusion-weighted MRI and Graph Theory. Neuroimage 2008;40(3):1064-1076.
15 Uludag K, Muller-Bierl B, Ugurbil K. An integrative model for neuronal activity-induced signal changes for gradient and spin echo functional imaging. Neuroimage 2009;48(1):150-165.
16 Iadecola C. Neurovascular regulation in the normal brain and in Alzheimer's disease. Nat Rev Neurosci 2004;5(5):347-360.
17 Mitra PP, Ogawa S, Hu X, Ugurbil K. The nature of spatiotemporal changes in cerebral hemodynamics as manifested in functional magnetic resonance imaging. Magn Reson Med 1997;37(4):511-518.
18 Panagiotaki E, Schneider T, Siow B, Hall MG, Lythgoe MF, Alexander DC. Compartment models of the diffusion MR signal in brain white matter: a taxonomy and comparison. NeuroImage 2012;59(3):2241-2254.
19 Van Essen DC, Jbabdi S, Sotiropoulos SN, Chen C, Dikranian K, Coalson T, John Harwell J, Behrens TEJ, Glasser MF. Mapping Connections in Humans and Nonhuman Primates: Aspirations and Challenges for Diffusion Imaging. Diffusion MRI (2nd Edition); 2013.
20 Van Essen DC, Smith SM, Barch DM, Behrens TE, Yacoub E, Ugurbil K, for the WU-Minn HCP Consortium. The WU-Minn Human Connectome Project: An overview. Neuroimage 2013;80:62-79.
21 Sotiropoulos SN, Jbabdi S, Xu J, Andersson JL, Moeller S, Auerbach EJ, Glasser MF, Hernandez M, Sapiro G, Jenkinson M, Feinberg DA, Yacoub E, Lenglet C, Van Essen DC, Ugurbil K, Behrens TE, for the

WU-Minn HCP Consortium. Advances in diffusion MRI acquisition and processing in the Human Connectome Project. Neuroimage 2013;80:125-143.
22 Smith SM, Beckmann CF, Andersson J, Auerbach EJ, Bijsterbosch J, Douaud G, Duff E, Feinberg DA, Griffanti L, Harms MP, Kelly M, Laumann T, Miller KL, Moeller S, Petersen S, Power J, Salimi-Khorshidi G, Snyder AZ, Vu AT, Woolrich MW, Xu J, Yacoub E, Ugurbil K, Van Essen DC, Glasser MF, for the WU-Minn HCP Consortium. Resting-state fMRI in the Human Connectome Project. Neuroimage 2013;80:144-168.
23 Glasser MF, Sotiropoulos SN, Wilson JA, Coalson TS, Fischl B, Andersson JL, Xu J, Jbabdi S, Webster M, Polimeni JR, Van Essen DC, Jenkinson M, Consortium WU-MH. The minimal preprocessing pipelines for the Human Connectome Project. Neuroimage 2013;80:105-124.
24 Ugurbil K, Xu J, Auerbach EJ, Moeller S, Vu AT, Duarte-Carvajalino JM, Lenglet C, Wu X, Schmitter S, Van de Moortele PF, Strupp J, Sapiro G, De Martino F, Wang D, Harel N, Garwood M, Chen L, Feinberg DA, Smith SM, Miller KL, Sotiropoulos SN, Jbabdi S, Andersson JL, Behrens TE, Glasser MF, Van Essen DC, Yacoub E, for the WU-Minn HCP Consortium. Pushing spatial and temporal resolution for functional and diffusion MRI in the Human Connectome Project. Neuroimage 2013;80:80-104.
25 Barch DM, Burgess GC, Harms MP, Petersen SE, Schlaggar BL, Corbetta M, Glasser MF, Curtiss S, Dixit S, Feldt C, Nolan D, Bryant E, Hartley T, Footer O, Bjork JM, Poldrack R, Smith S, Johansen-Berg H, Snyder AZ, Van Essen DC, Consortium WU-MH. Function in the human connectome: Task-fMRI and individual differences in behavior. Neuroimage 2013;80:169-189.
26 Moeller S, Yacoub E, Olman CA, Auerbach E, Strupp J, Harel N, Ugurbil K. Multiband multislice GE-EPI at 7 tesla, with 16-fold acceleration using partial parallel imaging with application to high spatial and temporal whole-brain fMRI. Magn Reson Med 2010;63(5):1144-1153.
27 Moeller S, Auerbach E, van de Moortele P-F, Adriany G, Ugurbil K. fMRI with 16 fold reduction using multibanded multislice sampling. Proc Int Soc Mag Reson Med 2008;16:2366.
28 Larkman DJ, Hajnal JV, Herlihy AH, Coutts GA, Young IR, Ehnholm G. Use of multicoil arrays for separation of signal from multiple slices simultaneously excited. J Magn Reson Imaging 2001;13(2):313-317.
29 Breuer FA, Blaimer M, Heidemann RM, Mueller MF, Griswold MA, Jakob PM. Controlled aliasing in parallel imaging results in higher acceleration (CAIPIRINHA) for multi-slice imaging. Magn Reson Med 2005;53(3):684-691.
30 Breuer FA, Blaimer M, Mueller MF, Seiberlich N, Heidemann RM, Griswold MA, Jakob PM. Controlled aliasing in volumetric parallel imaging (2D CAIPIRINHA). Magn Reson Med 2006;55(3):549-556.
31 Nunes RG, Hajnal JV, Golay X, Larkman DJ. Simultaneous slice excitation and reconstruction for single shot EPI. Proc Int Soc Mag Reson Med 2006;14:293.
32 Setsompop K, Gagoski BA, Polimeni J, Witzel T, Wedeen VJ, Wald LL. Blipped CAIPIRINHA for simultaneous multi-slice EPI with reduced g-factor penalty. Proc Int Soc Mag Reson Med 2010;18:551.
33 Setsompop K, Gagoski BA, Polimeni JR, Witzel T, Wedeen VJ, Wald LL. Blipped-controlled aliasing in parallel imaging for simultaneous multislice echo planar imaging with reduced g-factor penalty. Magn Reson Med 2012;67(5):1210-1224.
34 Feinberg DA, Reese TG, Wedeen VJ. Simultaneous echo refocusing in EPI. Magn Reson Med 2002;48(1):1-5.
35 Feinberg DA, Moeller S, Smith SM, Auerbach E, Ramanna S, Gunther M, Glasser MF, Miller KL, Ugurbil K, Yacoub E. Multiplexed echo planar imaging for sub-second whole brain FMRI and fast diffusion imaging. PLoS ONE 2010;5(12):e15710.
36 Xu J, Moeller S, Auerbach EJ, Strupp J, Smith SM, Feinberg DA, Yacoub E, Ugurbil K. Evaluation of slice accelerations using multiband echo planar imaging at 3 T. Neuroimage 2013;83:991-1001.
37 Pruessmann KP, Weiger M, Scheidegger MB, Boesiger P. SENSE: sensitivity encoding for fast MRI. Magn Reson Med 1999;42(5):952-962.
38 Moeller S, Xu J, Auerbach EJ, Yacoub E, Ugurbil K. Signal Leakage(L-factor) as a measure for parallel imaging performance among simultaneously multi-Slice (SMS) excited and acquired signals. Proc Int Soc Mag Reson Med 2012;20:519.
39 Auerbach EJ, Xu J, Yacoub E, Moeller S, Ugurbil K. Multiband accelerated spin-echo echo planar imaging with reduced peak RF power using time-shifted RF pulses. Magn Reson Med 2013;69(5):1261-1267.
40 Wu X, Schmitter S, Auerbach EJ, Ugurbil K, Van de Moortele PF. A generalized slab-wise framework for parallel transmit multiband RF pulse design. Magn Reson Med 2015.
41 Wu X, Schmitter S, Auerbach EJ, Moeller S, Ugurbil K, Van de Moortele PF. Simultaneous multislice multiband parallel radio-frequency excitation with independent slice-specific transmit B1 homogenization. Magn Reson Med 2013;70(3):630-638.
42 Vu AT, Auerbach E, Lenglet C, Moeller S, Sotiropoulos SN, Jbabdi S, Andersson J, Yacoub E, Ugurbil K. High resolution whole brain diffusion imaging at 7T for the Human Connectome Project. Neuroimage 2015;122:318-331.
43 Andersson JL, Sotiropoulos SN. Non-parametric representation and prediction of single- and multi-shell diffusion-weighted MRI data using Gaussian processes. Neuroimage 2015;122:166-176.
44 Andersson JL, Skare S, Ashburner J. How to correct susceptibility distortions in spin-echo echo-planar images: application to diffusion tensor imaging. Neuroimage 2003;20(2):870-888.
45 Pfeuffer J, Van De Moortele PF, Ugurbil K, Hu X, Glover GH. Correction of physiologically induced global off-resonance effects in dynamic echo-planar and spiral functional imaging. Magn Reson Med 2002;47(2):344-353.
46 Van De Moortele PF, Pfeuffer J, Glover GH, Ugurbil K, Hu X. Respiration-induced B0 fluctuations and their spatial distribution in the human brain at 7 Tesla. Magn Reson Med 2002;47(5):888-895.
47 Smith SM, Fox PT, Miller KL, Glahn DC, Fox PM, Mackay CE, Filippini N, Watkins KE, Toro R, Laird AR, Beckmann CF. Correspondence of the brain's functional architecture during activation and rest. Proc Natl Acad Sci U S A 2009; 106(31):13040-13045.
48 Griffanti L, Salimi-Khorshidi G, Beckmann CF, Auerbach EJ, Douaud G, Sexton CE, Zsoldos E, Ebmeier KP, Filippini N, Mackay CE, Moeller S, Xu J, Yacoub E, Baselli G, Ugurbil K, Miller KL, Smith SM. ICA-based artefact removal and accelerated fMRI acquisition for improved resting state network imaging. Neuroimage 2014;95:232-247.
49 Smith SM, Vidaurre D, Beckmann CF, Glasser MF, Jenkinson M, Miller KL, Nichols TE, Robinson EC, Salimi-Khorshidi G, Woolrich MW, Barch DM, Ugurbil K, Van Essen DC. Functional connectomics from resting-state fMRI. Trends Cogn Sci 2013;17(12):666-682.

Contact

Kâmil Uğurbil, Ph.D.
Director Center for Magnetic Resonance Research
Department of Radiology 1-211C CMRR
University of Minnesota
2021 Sixth Street SE
Minneapolis, MN 55455, USA
Phone: +1 612-626-9591
kamil@cmrr.umn.edu

Simultaneous Multi-Slice (SMS) Imaging for Pre-Surgical BOLD fMRI and Diffusion Tractography: Case Illustrations

Andreas J. Bartsch[1,2,3]

[1] Radiologie Bamberg, Germany
[2] Departments of Neuroradiology, Universities of Heidelberg and Wuerzburg, Germany
[3] Oxford Centre for Functional MRI of the Brain (FMRIB), University of Oxford, UK

Introduction

Simultaneous multi-slice (SMS) imaging accelerates the temporal sampling of MRI and enables unprecedented increases in temporal resolution. This is of interest not just for research, but for various clinical applications that are currently emerging.

Dense temporal sampling by SMS offers new insights into temporal dynamics when time-series are studied and has been shown to improve the sensitivity of resting-state fMRI, for example (cf. the corresponding article by Miller et al. in this issue; [15, 19]). At the same time, it can be used to encode more information in diffusion MRI (e.g., by recording more diffusion directions; Fig. 1), to shorten acquisition times, or to increase spatial image resolution and / or coverage [8, 10, 18].

1

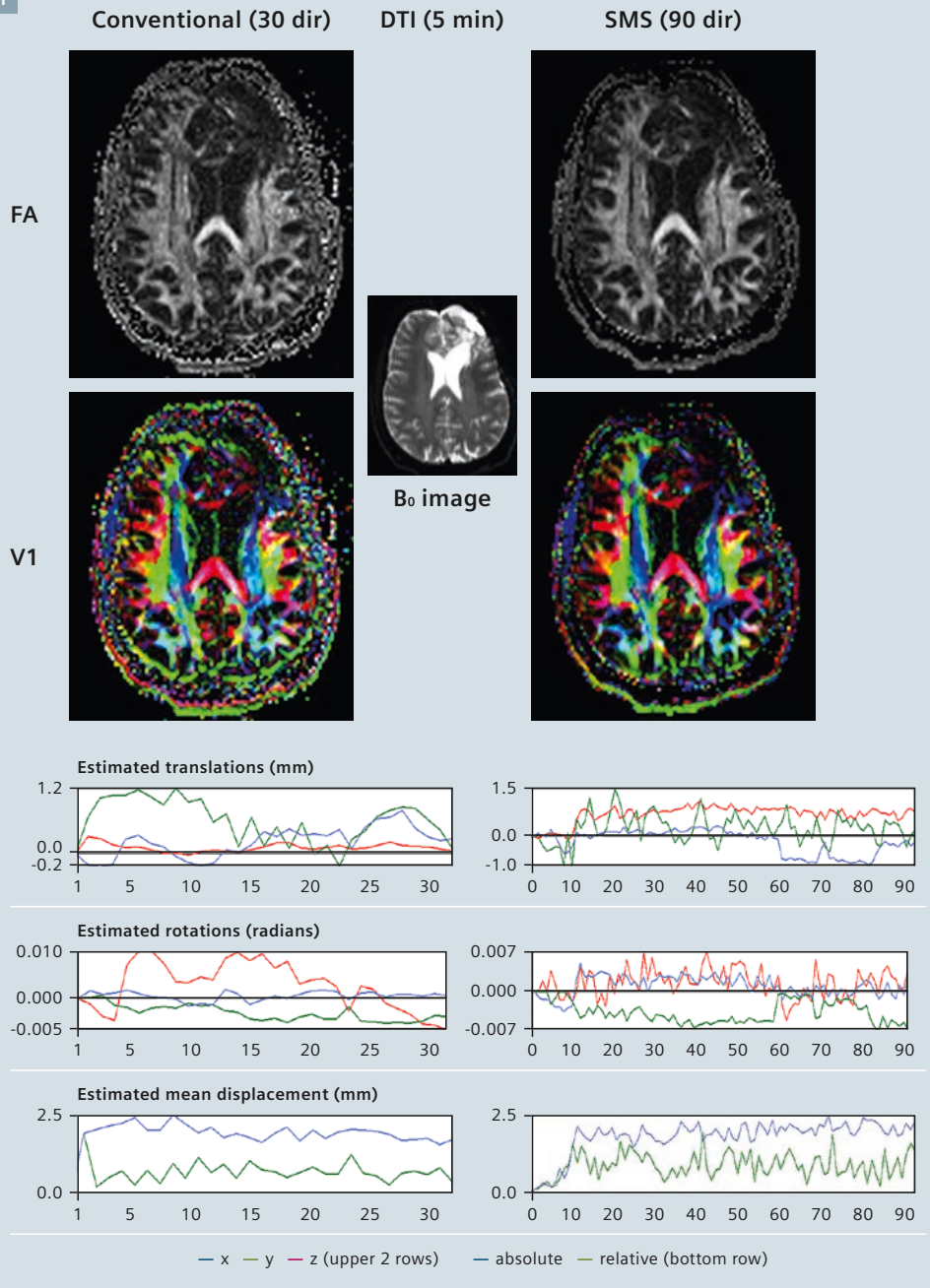

1 Comparison of conventional (30 diffusion encoding directions) vs. SMS DTI (90 directions; SMS factor 3), both recorded with whole-brain coverage at 1.8 mm isotropic in 5 min, in a patient with a partially resected, left frontal oligodendroglioma (same slice position but scans not coregistered). Online-generated FA **(top)** and color-coded V1 maps **(middle)** illustrate less noisy estimates from more sampled diffusion directions by SMS. Between-volume motion tends to be slightly lower for SMS compared to conventional DWI **(bottom)**. A subdural hygroma abutting the left frontal lobe is apparent in the middle image with no diffusion but T2-weighting.

While SMS imaging is applicable to different pulse sequences such as echo-planar imaging (EPI) and turbo spin echo (TSE), it has gained particular attention for BOLD fMRI and diffusion EPI. While SMS-accelerated EPI may be able to increase statistical confidence and / or to reduce experimental scan duration of clinical BOLD fMRI (see Fig. 2 in this article; Figs. 4, 5 of the article by Miller et al. in this issue), the benefit of fast temporal sampling becomes particularly apparent for diffusion EPI. Here, multi-directional (MDDW) and high-angular resolution diffusion-weighted imaging (HARDI), possibly across multiple b-value shells, are instrumental for diffusion-tensor (DTI; Fig. 1) or -kurtosis imaging (DKI) and tractography (Figs. 2, 3, 5, 6). For example, recording 3 times more unique diffusion directions by SMS within the same period of time compared to conventional DTI can reduce the noise in fractional anisotropy (FA) and color-coded first eigenvector (V1) maps (Fig. 1, top).

For DWI requiring just 3 diffusion-encoding directions (e.g., stroke or epidermoid imaging), there is, in terms of acquisition speed, relatively little to gain: Here, SMS reduces the default imaging time only by a fraction and in the magnitude of 15 to 20 seconds for each whole-brain average. In a busy practice scanning up to 40 neuroradiological patients in 10 hours, this may enable the examination of one additional patient per day.

For DTI or tractography studies investigating structures with rather uniformly directed diffusion and few crossing fibers, such as in the peripheral nervous system, potential gains offered by SMS are probably less related to sampling more diffusion directions and more to extend the coverage and facilitate isotropic recordings.

For structures in the central nervous system with lots of crossing fibers or tractography into low FA areas, such as perifocal tumor edema [6], sampling more diffusion directions can considerably improve the tracking of the fiber pathways of interest (Fig. 2, bottom). Diffusion tractography nowadays regularly supplements fMRI for pre-surgical planning and intra-operative neuronavigation, and here SMS allows us to record high-resolution (1.8 mm isotropic) diffusion-weighted (e.g., at $b = 1500$ s/mm^2) whole-brain data of, for example, 160 unique encoding directions in less than 10 minutes while comparable conventional recordings without SMS would normally exceed the scanning tolerance of clinical patients, especially if fMRI is conducted in the same session.

Additionally, faster scanning by SMS imaging may, at least in theory, reduce motion artifacts. Other than motion between consecutive volumes, within-volume motion is usually not correctable. In our experience, estimated motion between EPI volumes tends to be slightly lower for SMS recordings (Fig. 1, bottom). Thereby, SMS may increase the quality of the scans recorded.

For fMRI, SMS changes the auto-correlation structure and 'spin history' effects of the data. Statistical modeling and inference can account for the former, while dense temporal sampling in SMS fMRI makes the data more amenable to denoising procedures to remove effects of the latter. SMS fMRI is attractive for clinical applications considering potential gains in 'functional' signal-to-noise ratios (SNR) that can be achieved at the individual patient level. Assuming that the detected functional signal adds up linearly with each measurement and that the random noise increases with the square root of the number of measurements, the 'functional SNR' would increase by the square root of the number of samples. In other words, if we measure the same functional signal four times and sum up the measurements, we increase the SNR by a factor of two compared to a single measurement. Even though these assumptions are certainly simplistic, SMS is able to boost statistical confidence, and these gains can be invested

I) to render first-level FMRI results more robust (see Fig. 2 in this article; Figs. 4, 5 in the article by Miller et al. in this issue),

II) to increase the spatial resolution of the measurements (see Fig. 4 in the article by Miller et al. in this issue) and / or

III) to shorten the experimental acquisition time (see Fig. 5 in the article by Miller et al. in this issue).

Increasing the spatial resolution of fMRI and diffusion tractography is relevant for clinical applications to improve spatial accuracy, including registration to anatomical scans, but penalized by a loss in SNR because the measured signal decreases approximately linearly with the voxel size. Additionally, the relative contribution of thermal noise increases nonlinearly at higher spatial resolutions. This is also the reason why task-based SMS fMRI data tend to require a similar amount of smoothing like low-resolution recordings to achieve comparable results [11]. However, recent statistical advances specifically addressing pre-surgical fMRI indicate that the potentially detrimental effects of smoothing (blurring of larger or elimination of smaller activations, leading to false-positive or -negative detections in space) can be avoided [16].

Given that patients (especially children[1], elderly, neuropsychologically impaired, mentally handicapped and those suffering from intractable epilepsies) often have a limited tolerance for long scan durations, the potential benefits of SMS-accelerated scanning to obtain high-quality data are substantial. At the same time, there is no obvious drawback: Auditory noise characteristics are the same for conventional and SMS EPI (with the fundamental frequency peak being determined by the echo spacing of the read-out gradient, [5]), and the risk for peripheral nerve stimulations (due to rapid read-out gradient switches) should not be increased. In fact, we have *not* observed an increased number of such incidents with SMS over the past three years.

Therefore, pre-surgical BOLD fMRI and diffusion tractography are prime examples of where the use of SMS-

[1] MR scanning has not been established as safe for imaging fetuses and infants under two years of age. The responsible physician must evaluate the benefit of the MRI examination in comparison to other imaging procedures.

accelerated EPI is expected to translate into obvious clinical advantages, and we have decided to share our experience with this new technology in this context based on selected cases.

Case-based illustrations of SMS benefits

Head-to-head comparisons of conventional vs. SMS fMRI and diffusion-weighted EPI were performed in Figures 4 and 5 of the article by Miller et al. in this issue and in Figures 1 and 2 of this presentation. Figure 2 illustrates the core findings:

Recording more time points and more diffusion directions by SMS acceleration is able to enhance the statistical confidence of fMRI and diffusion tractography results. Such improvements may lead to increased spatial extent and maximum height probabilities to detect functional activations and structural connectivities. In other words, SMS can improve the sensitivity of functional and diffusion MRI. Sensitivity is crucial for pre-surgical fMRI and tractography applications because most of these aim to avoid infliction of new clinical deficits to the patient by minimizing false-negative detections.

For the patient shown in Figure 2, right-brain speech had already been confirmed by intra-operative electrical stimulation mapping (ESM) during the primary, partial tumor resection. However, ESM was, at the time, complicated by a series of intra-operative seizures, and the current fMRI examination prior to secondary resection was considered helpful in supporting a sufficient safety margin between the recurrent, low-grade glioma and cortical fMRI activations (Fig. 2, top). Probabilistic diffusion tractography revealed the proximity of the arcuate fasciculus (AF) to the upper medial tumor nodule, with SMS suggesting

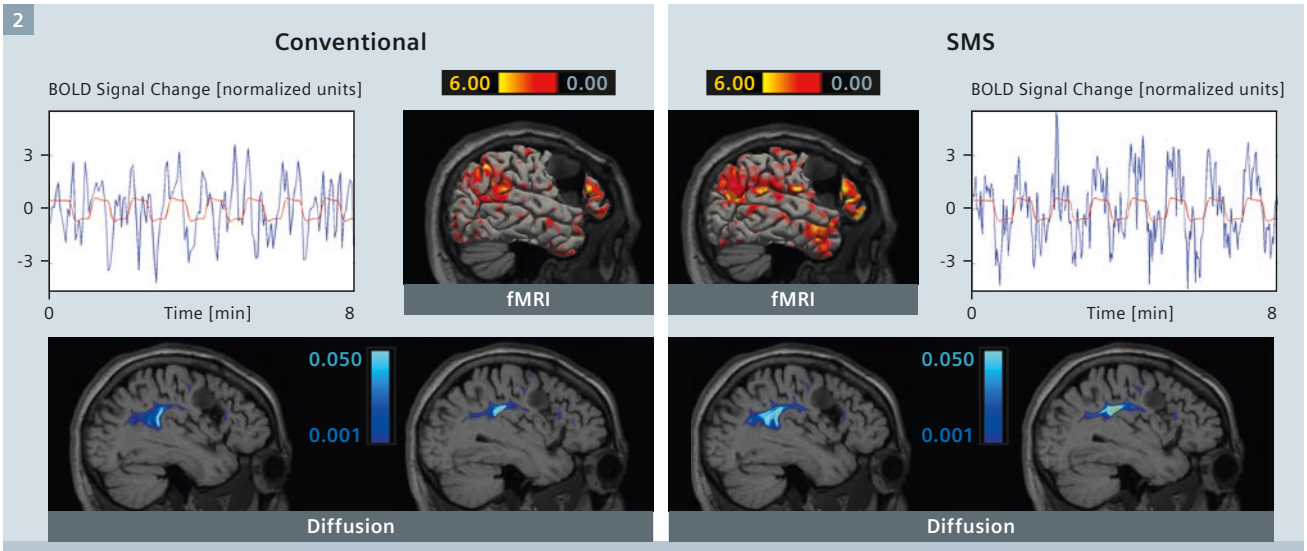

2 Comparison of conventional vs. SMS BOLD fMRI (**top**; TR 3.0 vs. 1.5 secs) and diffusion tractography (**bottom**; 60 vs. 180 directions; distortion-corrected by phase reversal – cf. Fig. 3) in a left-hander with a recurrent, right frontal low-grade glioma prior to second surgery. Doubling the temporal fMRI resolution by SMS increased the statistical confidence (red-to-yellow Z-statistics obtained by independent component analysis ICA / dual regression) of the activations correlated with the language paradigm and improved the temporal correlation of the respective time-courses (blue) with the model (red; r = 0.2 vs. 0.7; **top**). Similarly, tripling the number of diffusion directions by SMS increased conditional probabilities to reconstruct streamlines of the superior longitudinal / arcuate fascicle (blue-to-light blue, thresholded at 1 ‰ of the number of samples making it from seed to target [6]; **bottom**).

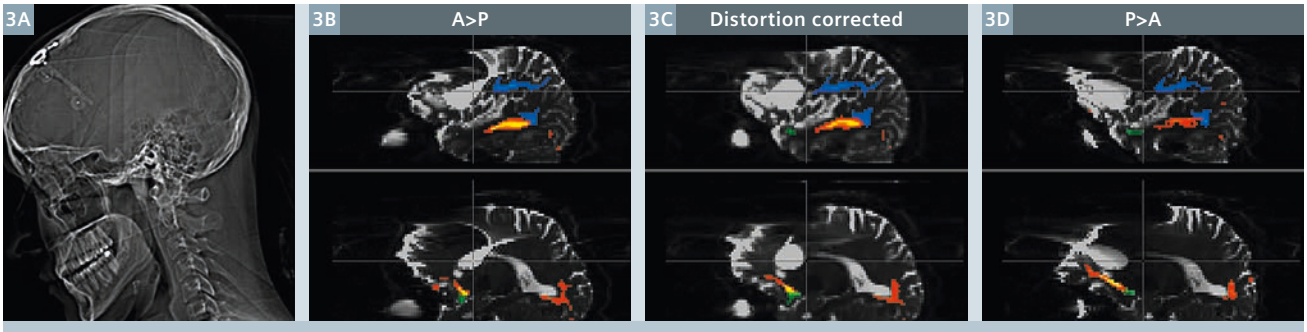

3 Distortion correction by SMS SE-EPI using alternate phase encodings (A>P **(3B)** vs. P>A **(3D)**). Patient with a left fronto-opercular cystic ganglioglioma, craniofix and Ommaya reservoir **(3A)**. Probabilistic tractography of SMS DWI with the arcuate **(blue-to-lightblue)**, inferior longitudinal **(red-to-yellow)** and uncinate **(green-to-lightgreen)** fascicle. Note distortion of the tumor cyst depending on the phase-encode direction and the resulting neuro-navigation error as indicated by the cross hairs.

a smaller safety margin than conventional diffusion tractography (Fig. 2, bottom). We regularly provide these data to the operating neurosurgeon for transfer into the neuro-navigation system. It is useful to define ESM points and to tailor the neurosurgical approach to the functionally relevant anatomy.

Figures 3 – 6 further illustrate the application of SMS to pre-surgical fMRI and tractography. Distortion correction of BOLD and diffusion-weighted EPI is essential for accurate pre-surgical planning and intra-operative neuro-navigation, particularly in patients with

I) lesions close to the skull base and

II) previous surgery, craniofix and metallic implants (Fig. 3). SMS spin-echo (SE-) EPI is currently the fastest means to acquire field map data for distortion correction by alternate phase encodings. Figure 3 illustrates the profound neuro-navigation error that may result if geometric distortions are not adequately corrected for.

Figure 4 depicts the same patient as in Figure 4 of the article by Miller et al. in this issue. Here, SMS BOLD fMRI was used for cerebrovascular reactivity mapping (CVRM) [17].

4

Cerebrovascular Reactivity Mapping (CVRM)

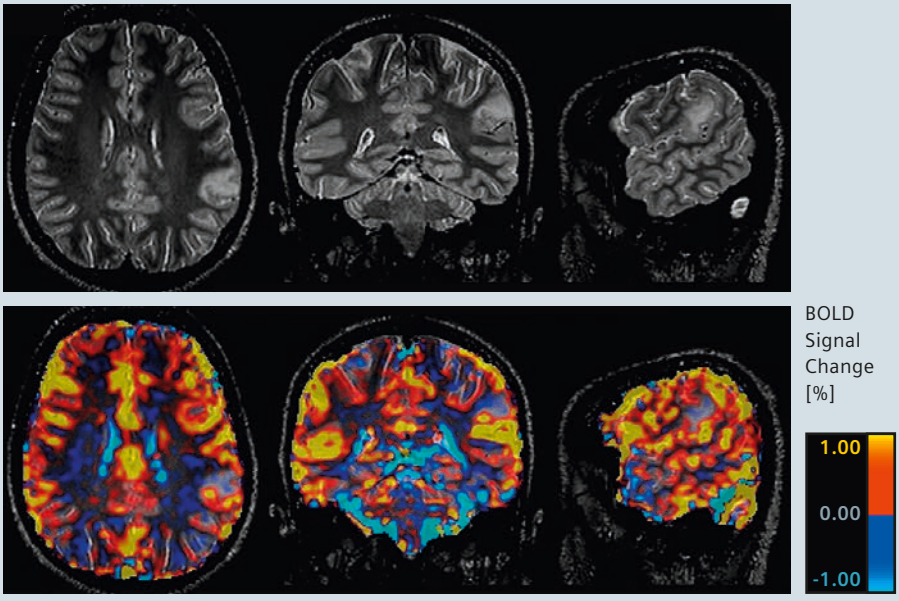

The incidentally detected, left supramarginal focal cortical dysplasia (FCD) without transmantle sign, which was initially mistaken for a low-grade glioma but then shown to lack any spectral tumor pattern, revealed reduced BOLD signal changes in response to hypercapnic fluctuations evoked by simple breath holding.

Abolished or decreased cerebrovascular reactivity may increase false-negatives of cognitive task-based and resting-state fMRI results. Based on SMS mapping of speech and language functions, however, the lesion was considered to occupy an eloquent location in the dorsal stream [12], a conclusion indeed primarily supported by SMS but not conventional BOLD fMRI (cf. Fig. 4 of the article by Miller et al. in this issue). Follow-up of the lesion with reduced mechanical compliance established by MR elastography [7, 9] over the past two years was stable and resection was therefore not recommended.

Figure 4 also illustrates the usage of advanced physiological signal monitoring: Respiration, pulse and ECG can all be recorded along with SMS, and Siemens' proprietary implementation logs these signals in precise temporal synchronization with each acquired slice and volume to (pseudo-) DICOM series. From these, the recorded signals can be read out for physiological noise modeling to 'regress out' effects of physiological noise in fMRI, for example. This feature makes physiological signal monitoring very convenient and easy to handle without the need for any third-party equipment.

4 Cerebrovascular reactivity mapping (CVRM) by SMS BOLD fMRI, same patient as in Fig. 4 of the article by Miller et al. in this issue. **Top:** SMS identified reduced cerebrovascular BOLD reactivity of the left supramarginal focal cortical dysplasia (FCD). **Bottom:** Logged respiration (blue) by Siemens' proprietary physiological monitoring confirmed patient compliance with breath-hold commands (red), motion correction estimates reveal increased head motion (green) during free breathing.

Figures 5 and 6 spotlight the application of SMS fMRI and diffusion tractography to patients with drug-resistant seizures evaluated prior to invasive electrocorticography and epilepsy surgery.

Epilepsy differs from tumor surgery in that patients with intractable seizures but with no identifiable brain lesions and no pre-surgical neurocognitive impairments (such as the case in Fig. 6) are at particular risk to develop new postsurgical deficits. In contrast, for patients who undergo surgical resections of brain tumors or other intra-axial lesions, those with no pre-surgical deficits generally fare best (such as the case in Fig. 2).

The patient shown in Figure 5 is the case of a 9-year-old, handicapped boy with classical Sturge-Weber syndrome (Figs. 5A, B) evaluated prior to left hemispherotomy considered for surgical treatment of refractory seizures. Absent visual resting-state fMRI signal fluctuations in the primarily affected left hemisphere (Fig. 5C) reflected right visual field hemianopsia of the patient. Speech mapping (passive story listening vs. scrambled sounds) with SMS BOLD fMRI detected predominantly right hemispheric activations (Fig. 5D), using both general linear modeling (GLM; model time-course in green) and independent component analysis (ICA) with spatial mixture modeling (MM) for statistical inference [20]. Right-brain speech was later confirmed by left intracarotid WADA testing and corresponded to degeneration of the left arcuate fasciculus (AF), especially in the posterior segment, detected by probabilistic SMS diffusion tractography (Fig. 5E). Similarly, the left corticospinal tract showed signs of degeneration that corresponded to the patient's right hemiparesis (and impeded unbiased handedness evaluation). Left hemispherotomy was successfully performed (Fig. 5F), effectively eliminating the previous frequent seizures, and did not result in aphasic complications but just slight worsening of the hemiparesis. Rapid temporal sampling by SMS was instrumental to minimize the acquisition time for BOLD fMRI and diffusion tractography (< 30 min) obtaining high-quality data (280 fMRI time-points, 320 diffusion directions) without exceeding the scanning tolerance of the patient.

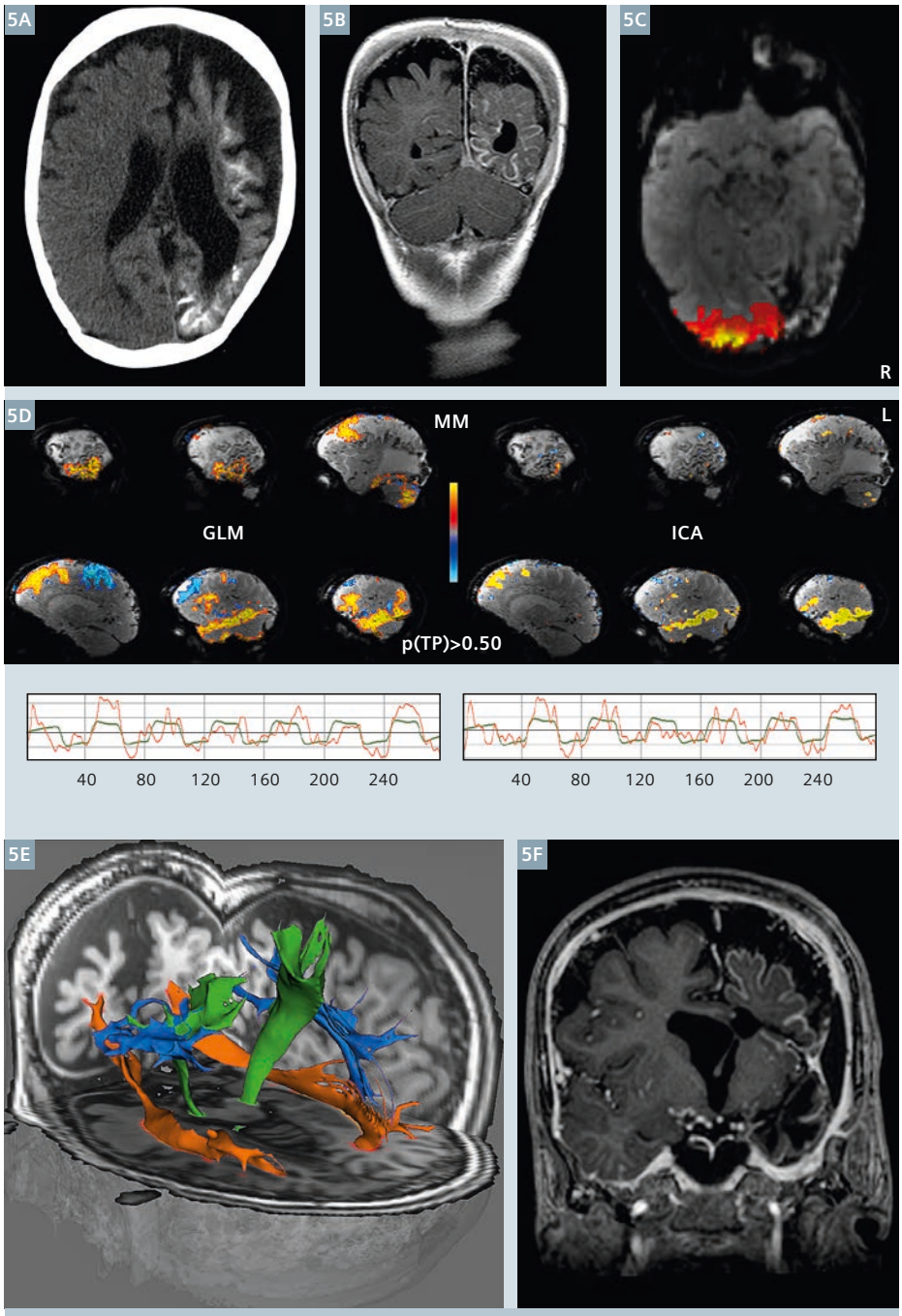

5 SMS BOLD fMRI and diffusion tractography in a boy with Sturge-Weber syndrome prior to surgical treatment of refractory seizures. Pathognomonic CAT **(5A)** and contrast-enhanced T1-weighted MRI **(5B)** scans revealing left leptomeningeal angiomatosis and intra-axial calcifications. SMS BOLD fMRI detected no signal fluctuations of visual resting-state networks in the degenerated left occipital lobe, corresponding to a right visual field hemianopsia of the patient **(5C)**. Speech mapping by SMS BOLD fMRI suggested right hemispheric language lateralization **(5D)**. SMS diffusion tractography **(5E)** indicated degeneration of the left arcuate (AF; **blue**) and pyramidal (**green**) tract, while the left inferior fronto-occipital fasciculus (IFOF; **orange**) seemed largely intact. Subsequent left hemispherotomy was successful **(5F)** without aphasic deficits.

6

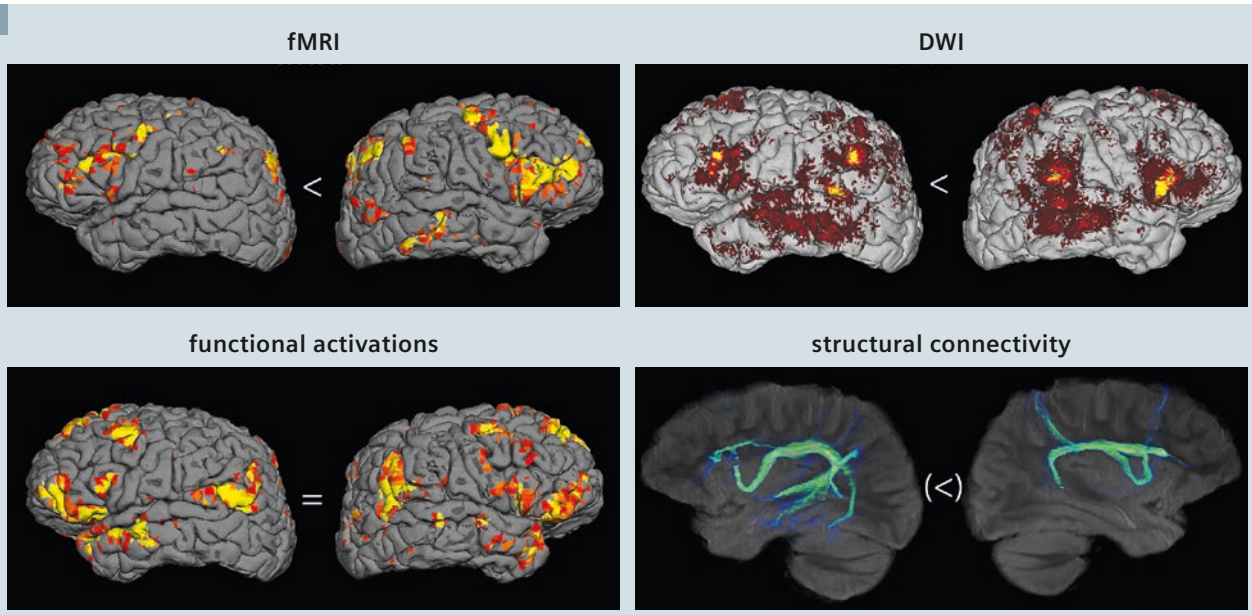

6 SMS BOLD fMRI and diffusion tractography in a left-handed boy with no apparent lesion (according to structural MRI) but drug-resistant, left frontal lobe seizures. Speech mapping by SMS BOLD fMRI **(left)** detected two paradigm-correlated components: one right-lateralized **(top left)** and another bilateral **(bottom left)**. SMS diffusion tractography **(right)** revealed spatial cross-correlation of right triangular activation probabilities with association fiber projection probabilities of the arcuate fasciculus **(top right)**. Its anterior segment was hypoplastic on the left **(bottom right)**. Right Broca's dominance was considered likely, invasive left frontal electrocorticography (ECoG) was recommended to further localize the seizure focus.

Figure 6 illustrates the case of a nonlesional, drug-resistant epilepsy patient, not eligible for WADA testing. He was transferred for best possible non-invasive assessment of language organization / lateralization prior to invasive electrocorticography (ECoG). ECoG was considered to better localize the seizure focus. The 13-year-old left-handed boy suffered from refractory seizures originating in the left frontal lobe (according to scalp EEG) during which he maintained the ability to speak. Using independent component analysis (ICA), speech mapping by SMS BOLD fMRI detected two paradigm-correlated independent components – one lateralized to the triangular part of the *right* inferior frontal gyrus and another with largely bilateral activations – presumably corresponding to the dorsal and ventral stream of speech and language processing, respectively [12]. Lateralization of the dorsal stream fMRI component suggested *right*-brain speech dominance for articulation, consistent with preservation of expressive speech during *left* frontal seizures. However, an important limitation is that fMRI cannot discriminate essential from dispensable (co-)activations by itself. Therefore, we sought to substantiate right-brain speech dominance by relating the functional to structural connectivity profiles [6, 13]. Probabilistic SMS diffusion tractography revealed a highly significant correspondence of right-lateralized fMRI activations with right triangular projections of the arcuate fasciculus (AF) which was not significant on the left. On the left, the anterior segment of the AF was hypoplastic. This case exemplifies a sophisticated clinical application of joint fMRI and diffusion analysis. SMS was essential to generate the underlying high-resolution data (1.8 mm isotropic) at a minimal scan time (25 min) adjusted to reduced scan compliance of the patient.

Conclusions

The case studies presented here make it evident that SMS is ready to be transferred into clinical practice. We have illustrated that SMS can increase the statistical confidence of fMRI and diffusion tractography results. This is in itself very valuable. These gains may also be used to increase spatial image resolution and coverage, to improve spatial coregistration to high-resolution anatomical scans for intra-operative neuro-navigation, and / or to shorten acquisition times. Eventually, SMS may allow us to better tailor pre-surgical fMRI and tractography to individual limitations of task performance and scanning tolerance of the patients we care for.

Pre-surgical fMRI and diffusion tractography will take advantage of this exciting new technology. In terms of auditory scan comfort, despite an increased specific absorption rate (SAR), or unwanted peripheral stimulations, no penalties are involved. Dense temporal sampling of SMS may also be of clinical interest for real-time fMRI applications, where the gains could be substantial, and potentially to better differentiate vegetative from minimally conscious states or locked-in patients. However, benefits for such clinical applications have yet to be evaluated.

Over the past decade, pre-surgical fMRI and diffusion tractography have hardly kept up with the rapid methodological advancements in the field. Pre-surgical tractography, for example, often continues to rely on 6 or 12 diffusion directions only – even though it has been demonstrated that at least 30 unique sampling orientations are required for a robust estimation of diffusion tensor orientations [14]. Current guidelines of the American Society for Functional Neuroradiology (ASFNR) do not specify a firm minimum of unique diffusion encoding directions for clinical DTI and tractography or provide a recommended set of pre- and post-processing algorithms to be used [2]. Similarly, Current Procedural Terminology (CPT) codes of the American Medical Association (AMA) for clinical fMRI [2] and practice guidelines for fMRI by the American College of Radiology (ACR) [1] make no reference to recommended data acquisition and analysis strategies to assure appropriate conduct for fMRI exams. Unfortunately, clinical settings tend to strongly favor speed over sensitivity and accuracy in data acquisition and analysis. SMS seems a perfect tool to overcome exactly these shortcomings.

Overall, SMS provides a showcase for capitalizing on recently developed, advanced data acquisition and analysis strategies that lead to tangible benefits in research [10, 15, 19] and clinical practice. It is able to facilitate patient-specific applications to optimize clinical decision-making [4] and to translate technological cutting-edge progress into medical practice. In this regard, SMS is a versatile 'kick' for functional and diffusion MRI to finally become much more than just fashionable merely by virtue of 'colored brain images'.

Acknowledgements

... to Siemens Healthcare GmbH, Germany (Thomas Beck, Thorsten Feiweier and Heiko Meyer, in particular), and the Center for Magnetic Resonance Research (CMRR) of the University of Minnesota, USA (Edward Auerbach, Steen Moeller and Essa Yacoub, in particular), for the opportunity to use their SMS EPI implementations and the excellent support.

... to the Oxford Centre for Functional MRI of the Brain (FMRIB) and the Laboratory for Computational Neuroimaging of the Martinos Center for Biomedical Imaging at MGH / Havard University Boston, USA, for the outstanding software (FSL & FreeSurfer) they are developing. I have used it with great clinical benefits for my patients.

... to Optoacoustics', Israel (http://www.optoacoustics.com/), supreme Active Noise Cancellation (ANC) system to cancel out EPI read-out noise making both fMRI as well as diffusion scanning much more comfortable. For fMRI it also greatly improves auditory stimulus transmission. Data shown in Figures 5, 6 were recorded using ANC (and these patients would have hardly tolerated unattenuated EPI noise).

References

1 American College of Radiology (ACR), 2007: http://www.asfnr.org/wp-content/uploads/fMRI-Clinical-Guidelines.pdf.

2 American Society for Functional Neuroradiology (ASFNR), 2012: http://www.asfnr.org/wp-content/uploads/ASFNR-Guidelines-for-DTI.pdf and http://www.asfnr.org/cpt-codes/.

3 Anderson, J. L. R. (2014). Geometric distortions in diffusion MRI. In: Diffusion MRI: from quantitative measurement to in-vivo neuroanatomy. Johansen-Berg, H. & Behrens, T. E. (Eds.), 2nd edition, Elsevier Academic Press, Amsterdam (ISBN 978-0-12-396460-1), 2014. pp. 63-85.

4 Bartsch, A. J., et al., Diagnostic functional MRI: illustrated clinical applications and decision-making. J Magn Reson Imaging, 2006. 23: 921-932.

5 Bartsch, A. J., et al., Scanning for the scanner: FMRI of audition by read-out omissions from echo-planar imaging. NeuroImage, 2007. 35: 234-243.

6 Bartsch, A. J., et al., Presurgical tractography applications. In: Diffusion MRI: from quantitative measurement to in-vivo neuroanatomy. Johansen-Berg, H. & Behrens, T. E. (Eds.), 2nd edition, Elsevier Academic Press, Amsterdam (ISBN 978-0-12-396460-1), 2014. pp. 531-568.

7 Bartsch, A.J., et al., Erratum to: State-of-the-art MRI techniques in neuroradiology: principles, pitfalls, and clinical applications. Neuroradiology, 2015. 57(10):1075.

8 Feinberg, D. A., et al., Multiplexed echo planar imaging for sub-second whole brain FMRI and fast diffusion imaging. PLoS One, 2010. 5(12): e15710.

9 Gallichan, D., et al., TREMR: Table-resonance elastography with MR. Magn Reson Med, 2009. 62(3): 815–821.

10 Glasser, M. F., et al., The minimal preprocessing pipelines for the Human Connectome Project. NeuroImage, 2013. 80:105-24.

11 Harms, M. P., et al., Impact of multiband EPI acquisition in a simple FMRI task paradigm analysis. OHBM (Human Brain Mapping Conference), 2013. 3448.

12 Hickok, G., et al., The cortical organization of speech processing. Nat Rev Neurosci, 2007. 8: 393-402.

13 Homola, G. A., et al., A brain network processing the age of faces. PLoS One, 2012. 7: e49451.

14 Jones, D. K., The effect of gradient sampling schemes on measures derived from diffusion tensor MRI: a Monte Carlo study. Magn Reson Med, 2004. 51: 807-815.

15 Kalcher, K., et al., The spectral diversity of resting-state fluctuations in the human brain. PLoS One, 2014. 9(4):e93375.

16 Liu, Z., et al., Pre-surgical fMRI Data Analysis Using a Spatially Adaptive Conditionally Autoregressive Model. Bayesian Analysis, 2015. http://projecteuclid.org/euclid.ba/1440594946.

17 Pillai, J. J., et al., Cerebrovascular reactivity mapping: an evolving standard for clinical functional imaging. AJNR Am J Neuroradiol, 2015. 36(1):7-13.

18 Setsompop, K., et al., Blipped-controlled aliasing in parallel imaging for simultaneous multislice echo planar imaging with reduced g-factor penalty. Magn Reson Med, 2012. 67: 1210-1224.

19 Smith, S. M., et al., Resting-state fMRI in the Human Connectome Project. NeuroImage, 2013. 80: 144-168.

20 Woolrich, M., et al., Mixture Models with Adaptive Spatial Regularisation for Segmentation with an Application to FMRI Data. IEEE Trans. Medical Imaging, 2005. 24(1):1-11.

Contact

Andreas Joachim Bartsch, M.D.
Radiologie Bamberg
http://www.radiologie-bamberg.de/
Heinrichsdamm 6
96047 Bamberg
Germany
bartsch@radvisory.net

Improving Sensitivity and Specificity in BOLD fMRI Using Simultaneous Multi-Slice Acquisition

Richard D. Hoge[1]; AmanPreet Badhwar[2]; Julien Doyon[2]; David Ostry[3,4]

[1] McConnell Brain Imaging Centre, Montréal Neurological Institute, Deptartment of Neurology & Neurosurgery, McGill University, Montreal, Quebec, Canada
[2] Unité de Neuroimagerie Fonctionnelle, Institut Universitaire de Gériatrie de Montréal, Université de Montréal, Montreal, Quebec, Canada
[3] Deptartment of Psychology, McGill University, Montreal, Quebec, Canada
[4] Haskins Laboratories, New Haven, CT, USA

Abstract

Functional MRI techniques, which involve rapid serial imaging of the brain to detect activation-induced changes, have always placed high demands on the speed, precision, and stability of MRI systems. This is particularly true of studies requiring high spatial resolution, due to the dramatic reduction in signal amplitude with decreasing voxel volume. Recent developments in simultaneous multi-slice (SMS) encoding promise to have a major impact on functional MRI. Current trends in MRI system hardware will help maximize this impact, and expand the range of fMRI applications that are feasible in clinical practice and basic research. In this article, the authors discuss the advantages of highly accelerated fMRI and show example images from a visual activation paradigm. The future benefits of this technology include the ability to perform pre-surgical mapping with high reliability and detail, with clinically feasible exam times.

Introduction

Conventional echo-planar imaging (EPI), which has been widely adopted for functional imaging of the brain over the last decade, has typically acquired multiple 2D slices in a rapid sequence whose minimum duration is limited by the echo-time (TE) required for sensitivity to blood oxygenation, the EPI readout length, and the number of slices required. This has generally meant that, despite advances in parallel imaging that can shorten single-slice readouts, the minimum time needed to image the entire brain with typical slice thicknesses has been on the order of two seconds or more. Simultaneous multi-slice imaging removes this limitation, reducing the number of TE delays required to image the entire brain while preserving the necessary T2*-weighting.

To understand the benefits of slice-accelerated fMRI, it is helpful to recall that sensitivity in functional MRI depends ultimately on the ratio between a given functional effect size and the degree of unrelated measurement variability. This measurement variability, or noise, arises from three main sources: 1) so-called 'thermal' noise; 2) physiological fluctuations in the subject; and 3) instrumental instability. Thermal noise is physically unavoidable in electronic measurements conducted above absolute zero, but as uncorrelated Gaussian noise its impact can be systematically reduced through signal averaging or increasing the size of image voxels. Physiological fluctuations in the subject, such as cardiac or respiratory cycles, are evidently difficult to eliminate but it is possible to control for their effects through physiological noise modelling methods [1]. Instrumental instability can contribute low level signal fluctuations that, while not necessarily dominant in standard BOLD fMRI acquisitions, can limit the

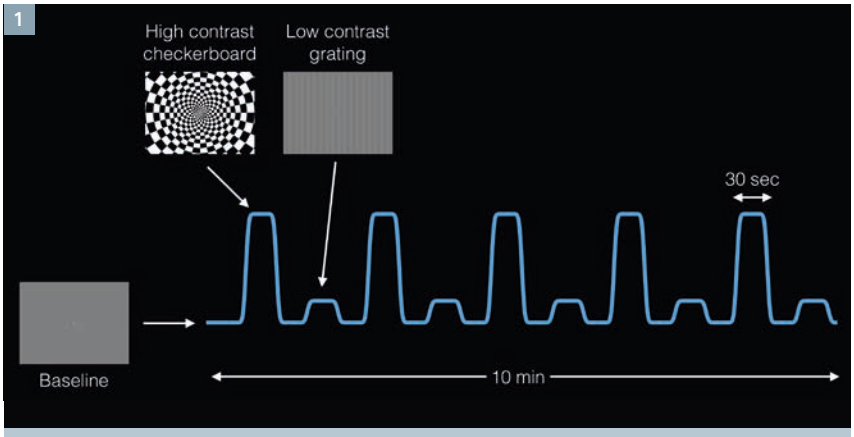

1 Stimulation paradigm with high and low-intensity visual stimulation. All condition blocks were 30 seconds long, with a total run duration of ten minutes.

SNR gains achievable by managing the other noise sources. Optimizing sensitivity in fMRI generally involves identifying the dominant noise source in a particular application and reducing it until other types of noise become significant.

Acquisition speed in fMRI

In typical BOLD fMRI experiments (3 Tesla, ~3 mm resolution, 2-3 second repetition time), physiological noise is by far the dominant noise source [2]. Because of this, it has been noted that BOLD fMRI time series commonly exhibit a high degree of temporal autocorrelation [3]. This would suggest that there is little statistical power (and hence sensitivity) to be gained through increases in imaging rate, since faster sampling of an autocorrelated signal does not necessarily increase the number of independent samples. However, this reasoning applies only in the case where autocorrelated physiological noise is dominant. Indeed, the popularity of 3T fMRI at an isotropic resolution of 3 mm is likely due to the fact that further reductions in voxel size lead to a relatively precipitous drop in SNR. This drop is due to the third power loss of signal with voxel volume, which results in a shift to thermal noise as the predominant source of signal fluctuation. Conversely, increases in voxel size above 3 mm yield little improvement in signal stability, because uncontrolled physiological fluctuations are already the dominant noise source. With this in mind, it becomes apparent that acquisitions in which uncorrelated thermal noise is dominant may still stand to benefit significantly from increases in imaging rate. At 3T, this is true for situations including high spatial-resolution BOLD fMRI (e.g. ≤2 mm) and arterial spin-labeling, in which the labeling signal is generally much smaller than typical BOLD effect sizes.

Simultaneous multi-slice acquisition

While imaging rates attainable in fMRI applications have been fairly constant for many years, a recent resurgence in simultaneous multi-slice (SMS) encoding techniques has created exciting possibilities for highly accelerated functional imaging. The general concept was proposed as early as 2001 [4] but has become practical only more recently with the emergence of techniques for managing issues such as voxel tilting and aliasing [5]. SMS encoding allows substantial increases in imaging rate compared with standard sequential multi-slice methods. It is based on the parallel imaging approach [6], in which the spatial information provided by an array of localized RF coil elements is used to reduce the number of 2D Fourier samples required to generate an unaliased image. While parallel imaging has been in use for nearly a decade to reduce the time needed for standard multi-excitation images, its impact on the single-excitation readouts used for BOLD fMRI has been limited due to the need for a relatively long post-excitation echo-time (TE) in each slice, in order to achieve the T2*-weighting required for sensitivity to blood oxygenation. The advance enabled by SMS encoding has been preservation of the long TE needed for BOLD fMRI while reducing the impact of this delay on the total time needed to cover the entire brain. The result is that whole-brain acquisitions formerly requiring up to three seconds can now be performed in less than half a second. This corresponds to a factor of six or more increase in the number of images acquired per unit time, which can have a substantial impact on statistical power particularly when thermal noise is dominant. A well-known application of this has been the use of an 8x slice acceleration factor to achieve 2 mm isotropic resolution with excellent sensitivity in the Human Connectome Project (HCP) [7].

Methods

To better understand the performance gains achievable using SMS in task activation studies, the authors have performed a systematic assessment of BOLD fMRI sensitivity using a range of acceleration factors and functional effect sizes, in both thermal and physiological noise-dominated regimes. In these tests healthy human subjects underwent a visual activation study including blocks of intense visual stimulation using a high luminance-contrast radial checkerboard modulated in a temporal squarewave, as well as much weaker stimulation using low-contrast sinusoidal gratings drifting slowly across the visual field (Fig. 1). This allowed sensitivity and specificity to be assessed under conditions of both high and low-amplitude effects. The acquisitions were repeated with larger (3 mm) and smaller (2 mm) isotropic voxels sizes, to create conditions under which physiological and thermal noise are respectively dominant.

Experiments were conducted on a 3T Siemens scanner (MAGNETOM Trio, A Tim System), running software release *syngo* MR B17, and the 32-channel head coil. For comparison against accelerated acquisitions, a standard gradient-echo EPI/BOLD sequence with TR 3 s, TE 30 ms, α 90° was used as a reference. Resolutions of 3 mm isotropic and 2 mm isotropic were acquired, with respective matrix sizes of 64 x 64 and 100 x 100. The 3 mm isotropic scans had 42 slices, while the 2 mm scans had 30 slices due to the longer readout required at the higher resolution. In addition to these standard scans, both resolutions were also repeated with a slice acceleration factor of 6x using a WIP sequence[1]. The number of time points acquired over the ten minute stimulation protocol was 200 for the non-accelerated sequence, with 1,200 time points for the 6x SMS scan. The TR values for the accelerated scan was 0.5 s, and the flip angle was adjusted to the Ernst angle assuming the T1 of grey matter, corresponding to a flip angle of 45°.

[1] The product is still under development and not commercially available yet. Its future availability cannot be ensured.

All image time-series were processed using in-house software used for quantitative image analysis. Motion correction was performed, followed by spatial smoothing with 3D Gaussian kernels with FWHM values of 6 mm for the 3 mm scan and 4 mm for the 2 mm acquisition. Smoothing was performed at these widths because they were found to provide an optimal compromise between sensitivity, specificity, and spatial resolution. Following preprocessing, the time series data were fit using a General Linear Model (GLM) including separate regressors for the high and low-amplitude stimulation. T statistics were computed by dividing estimated effect sizes by the residual standard error assuming uncorrelated residuals. The resultant T values were converted to the negative logarithm of the p value, -log(p), based on the nominal degrees of freedom in the time series. Neglecting autocorrelations in the data can result in exaggerated significance levels, but the errors are modest in the standard fMRI scans, particularly for the 2 mm acquisitions. The importance of autocorrelation may be further reduced due to the attenuation of steady-state magnetization at the shorter TR values. The maps of -log(p) are referred to as significance maps in the remainder of this article.

Results

Figure 2 shows unthresholded significance maps for 3 mm scans overlaid in false color on the grayscale EPI scans for reference. Maps are shown for standard and accelerated scans, and for high and low-intensity stimulation. The color legend has been matched in all maps to allow comparison of apparent significant levels, although autocorrelated noise might artificially boost the values in the accelerated scans. Nonetheless, the region of visual activation is extremely well delineated in the accelerated scans, for both levels of stimulus intensity. Extents of activation appeared less clearly in the maps computed from non-accelerated data, although this might simply have reflected the dynamic range chosen.

Because of the potential for exaggeration of significance levels in the accelerated scans, and the clear difference in dynamic range, we also assessed activation maps with the color legends adapted to the respective maps. These alternatively displayed maps (also for 3 mm scans) are shown in Figure 3. By 'zooming' the dynamic range for the non-accelerated maps, the location and extent of active areas is indeed more apparent. However, this also amplifies the background noise (random fluctuations in the significance level following its distribution under the null hypothesis) and it can be seen that the sensitivity and spatial specificity of the accelerated maps remains superior.

Although the spatial specificity afforded by slice acceleration in the unthresholded maps shown in Figures 2 and 3 is striking, fMRI has customarily involved thresholding of activation maps after correction of significance values for the multiple comparisons inherent in image data. To assess the performance gains of SMS acquisition in this setting, the significance maps for 3 mm scans were thresholded using the false discovery rate (FDR) approach, with a threshold of 0.001. The thresholded maps are shown in Figure 4, which reveals that the non-accelerated scan failed to detect the weak activation associated with the low-contrast grating. It should be noted that relaxing the threshold sufficiently to

2

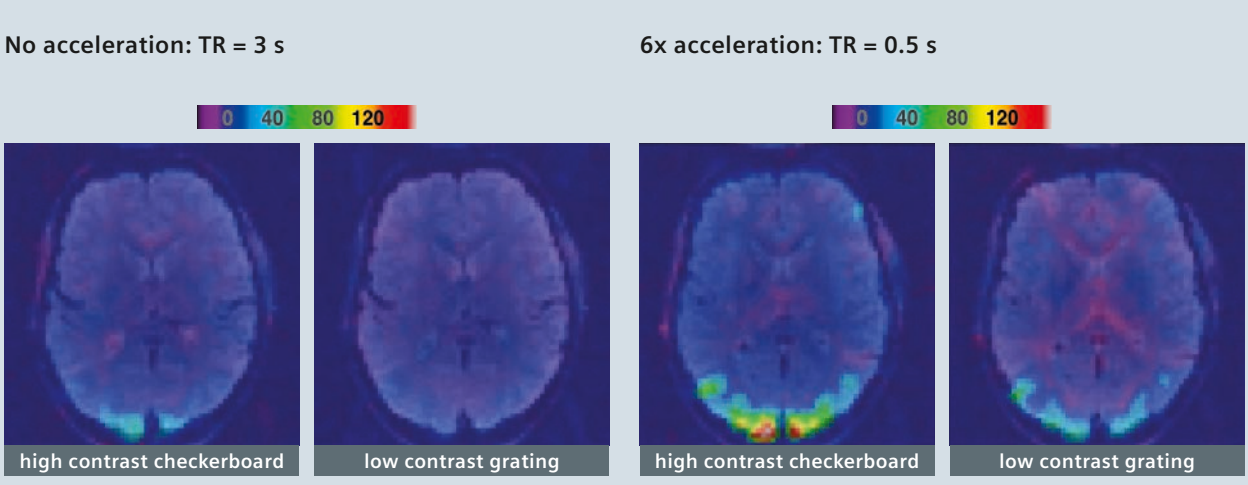

2 Significance maps for high and low-intensity stimulation, with 1x and 6x acceleration at 3 mm isotropic resolution (before smoothing). False colour significance maps are overlaid on greyscale EPI scans. Dynamic range of colour legend is equalized for both acquisitions.

reveal the patch of weak activation in the low-contrast, non-accelerated scan also resulted in the appearance of substantial swaths of non-visual artifact.

In addition to apparent improvements in the sensitivity and specificity of 3 mm scans, we also noted significant improvements in the higher resolution 2 mm scans. Figure 5 shows significance maps for the high-contrast stimulus, acquired at 2 mm resolution with and without acceleration. While the occipital visual response is readily detected in both cases, careful inspection of the maps reveals that the accelerated maps provide considerably improved delineation of cortical activation. In the maps acquired with acceleration, much of the cortical ribbon can be clearly discerned in the activation pattern, with robust specificity against background fluctuations.

Discussion and conclusions

The results shown above demonstrate that slice acceleration can substantially improve the sensitivity, specificity, and spatial detail of BOLD functional MRI. Despite concerns that gains might be limited due to autocorrelated noise, the unthresholded maps suggest that the apparent improvements reflect more than simple boosting of significance caused by inflated degrees

3

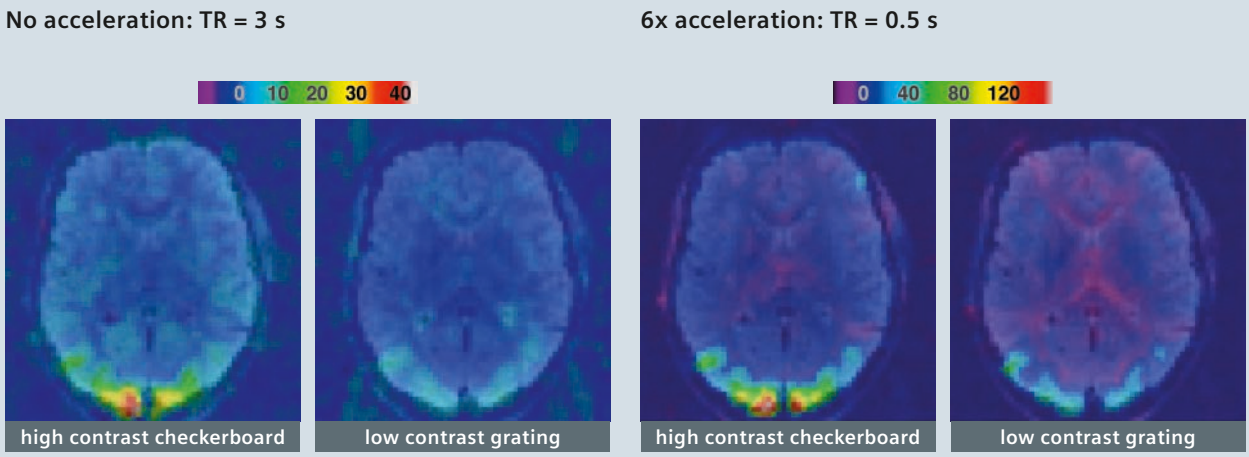

3 Significance maps for high and low-intensity stimulation from 3 mm scans, with colour legend adapted to dynamic range of respective acquisitions.

4

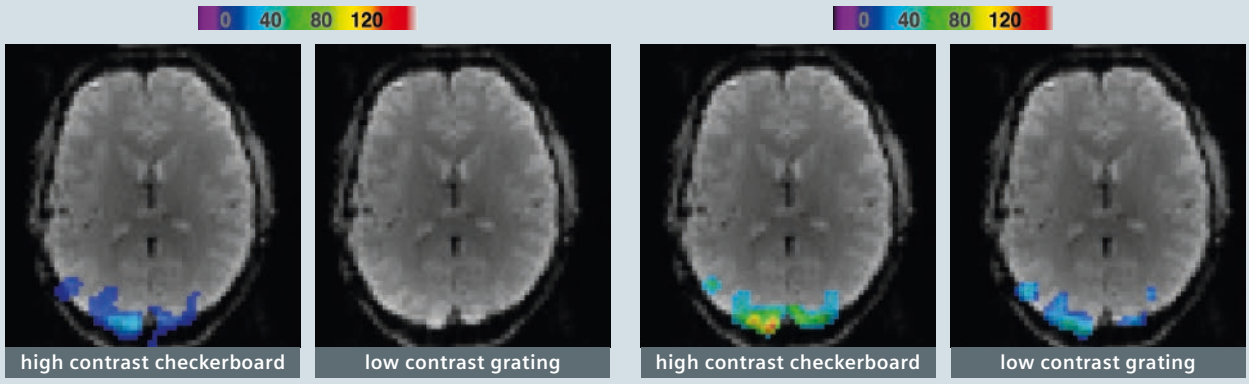

4 Significance maps for high and low-intensity stimulation during 3 mm scans, thresholded at FDR 0.001.

5

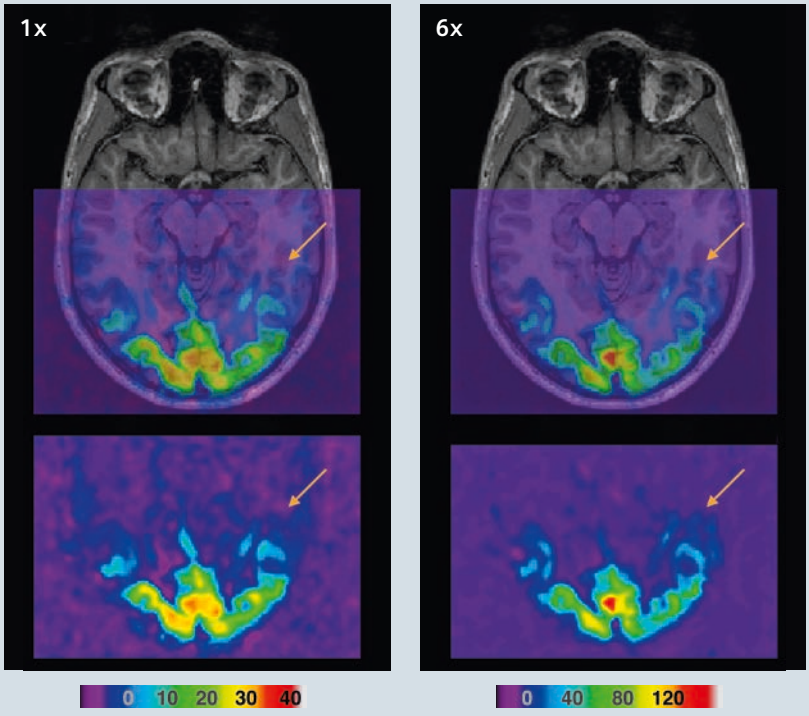

5 Significance maps high-intensity stimulation, based on 2 mm isotropic data. The orange arrows indicate a section of cortical ribbon that can be readily delineated in the 6x accelerated scan. Top row shows false color significance maps overlaid on greyscale T1-weighted scan. Bottom row shows unthresholded activation map alone.

of freedom. For clinical applications in which averaging over repeated fMRI runs is not feasible, these capabilities offer significant advantages. An obvious example is pre-surgical mapping, in which functional images of high reliability must be acquired in a relatively short time.

During the planning and optimization of protocols, considerable effort was devoted to finding suitable readout characteristics such as bandwidth, echo spacing, and matrix size. Improvements in gradient technology should increase the flexibility with which SMS techniques can be applied, while preserving and even improving image quality. A second challenge met during these experiments was related to the long reconstruction times required to generate images from the SMS raw data. Here too, improvements in scanner technology to cope with the greatly increased data throughput and complexity will play an important role.

Acknowledgements

This work was supported by the Canadian Foundation for Innovation (Leaders Opportunity Fund 17380), Canadian Institutes of Health Research (MOP-273379), Natural Sciences and Engineering Council of Canada (355583-2010) and MITACS (scholarship held by A.B.).

References

1 R. H. Tijssen, M. Jenkinson, J. C. Brooks, P. Jezzard, and K. L. Miller. Optimizing RetroICor and RetroKCor corrections for multi-shot 3D FMRI acquisitions. Neuroimage, 84:394–405, Jan 2014.

2 C. Triantafyllou, R. D. Hoge, G. Krueger, C. J. Wiggins, A. Potthast, G. C. Wiggins, and L. L. Wald. Comparison of physiological noise at 1.5 T, 3 T and 7 T and optimization of fMRI acquisition parameters. Neuroimage, 26(1):243–250, May 2005.

3 P. L. Purdon and R. M. Weisskoff. Effect of temporal autocorrelation due to physiological noise and stimulus paradigm on voxel-level false-positive rates in fMRI. Hum Brain Mapp, 6(4):239–249, 1998.

4 D. J. Larkman, J. V. Hajnal, A. H. Herlihy, G. A. Coutts, I. R. Young, and G. Ehnholm. Use of multicoil arrays for separation of signal from multiple slices simultaneously excited. J Magn Reson Imaging, 13(2):313–317, Feb 2001.

5 K. Setsompop, B. A. Gagoski, J. R. Polimeni, T. Witzel, V. J. Wedeen, and L. L. Wald. Blipped- controlled aliasing in parallel imaging for simultaneous multislice echo planar imaging with reduced g-factor penalty. Magn Reson Med, 67(5):1210–1224, May 2012.

6 K. P. Pruessmann, M. Weiger, M. B. Scheidegger, and P. Boesiger. SENSE: sensitivity encod- ing for fast MRI. Magn Reson Med, 42(5):952–962, Nov 1999.

7 S. M. Smith, C. F. Beckmann, J. Andersson, E. J. Auerbach, J. Bijsterbosch, G. Douaud, E. Duff, D. A. Feinberg, L. Griffanti, M. P. Harms, M. Kelly, T. Laumann, K. L. Miller, S. Moeller, S. Petersen, J. Power, G. Salimi-Khorshidi, A. Z. Snyder, A. T. Vu, M. W. Woolrich, J. Xu, E. Yacoub, K. U?urbil, D. C. Van Essen, and M. F. Glasser. Resting-state fMRI in the Human Connectome Project. Neuroimage, 80:144–168, Oct 2013.

Contact

Richard Hoge
Room WB316
McConnell Brain Imaging Centre
Montreal Neurological Institute
3801 University Street
Montreal, Quebec H3A 2B4, Canada
Phone: +1 (514) 398-1929
Fax: +1 (514) 398-2975
rick.hoge@mcgill.ca

Simultaneous Multi-Slice Imaging for Resting-State fMRI

Karla L. Miller[1]; Andreas J. Bartsch[1,2]; Stephen M. Smith[1]

[1] Oxford Centre for Functional MRI of the Brain (FMRIB), University of Oxford, UK
[2] Departments of Neuroradiology, Universities of Heidelberg and Würzburg, and Radiologie Bamberg, Germany

Background

Functional MRI (fMRI) is a primary tool in neuroscience that enables non-invasive detection and characterization of brain activity. fMRI is often described in terms of spatial 'mapping'; importantly, however, fMRI experiments encode information about brain activity in the temporal domain. Echo-planar imaging (EPI) has therefore been crucial to this development by enabling temporal resolution (TR) of several seconds per whole-brain image volume. Nevertheless, the encoding of activity in the temporal domain means that fMRI data quality is fundamentally tied to temporal resolution. It is therefore notable that a typical fMRI experiment with TR = 3 s may encode hundreds of thousands of voxels, but can only achieve 200 time points in 10 minutes. The advent of parallel imaging has enabled reduction of image distortions in EPI; however, unlike many structural MRI techniques, parallel imaging 'acceleration' has little effect on volume scan times in fMRI.

Temporal resolution in fMRI has until recently remained directly proportional to the number of slices (TR = 2-3 s). The explosion of simultaneous multi-slice (SMS, also known as multiband) technology in the past 5 years, described in detail elsewhere in this issue, has now removed the strict coupling between the number of slices and the temporal resolution. The dense temporal sampling enabled by SMS techniques can enormously benefit our ability to identify which voxels are activated by a task or define regions that spontaneously co-activate in resting-state fMRI, provided other aspects of data quality are not unduly compromised.

The source of these gains is somewhat complex, and we therefore go into some detail on this point below.

In this article, we will focus in particular on the benefits SMS has to offer for resting-state fMRI. In resting-state fMRI [1, 3], intrinsic signal fluctuations are used to identify connectivity patterns in the brain under the (now well-established) hypothesis that connected brain regions will co-fluctuate in activity level even in the absence of an experimentally imposed task (Fig. 1). A given neural network would thus be characterized by a common time course of activity that is shared within the network and largely independent of activity outside the network[1]. Many resting-state studies aim to capture the dynamics of a rich set of networks, placing even greater demand on the temporal domain than simple tasks with predefined timings. Moreover, dense temporal sampling has the potential

[1] This simplistic description of independent time courses would only strictly hold if the brain was composed of isolated networks. In practice, the picture is more one of networks that are more and less tightly coupled, representing a hierarchy of connectivity that is reflected in the degree to which time courses are shared.

1

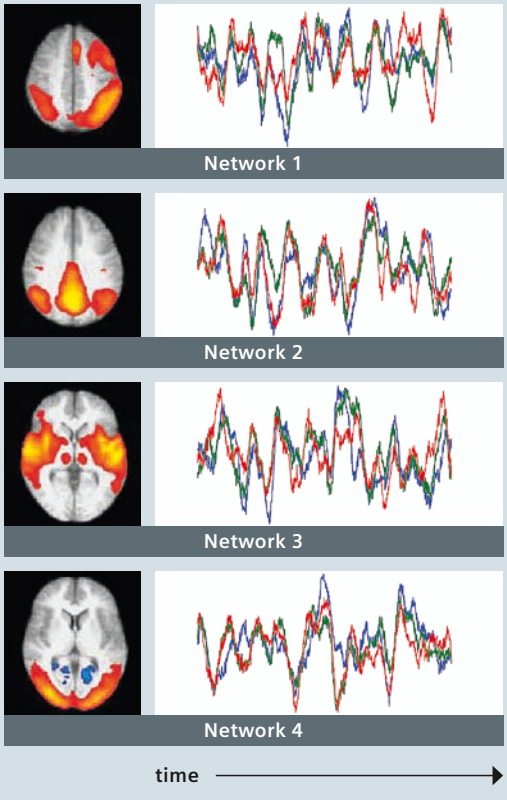

1 Resting-state fMRI identifies patterns of connectivity across the brain based on spontaneous fluctuations of the BOLD signal (in the absence of an experimentally-induced mental or cognitive state). Each map represents the spatial distribution of one brain network, with example voxel time courses depicted in the color plots to the side. Brain networks are inferred by identifying voxels that share a common time course (e.g. are temporally correlated), as simulated here. The centrality of the time domain for identifying networks makes SMS acquisition a powerful technology for resting-state fMRI.

to reveal subtle aspects of these networks, such as transient connectivity. We discuss the role that SMS has to play in achieving these goals.

Benefits of high temporal resolution for resting-state fMRI

Statistical benefits of fast sampling
One fundamental characteristic of fMRI is that the blood oxygenation level-dependent (BOLD) response to neural activity is relatively sluggish, as described by the blurred hemodynamic response function used to model the BOLD response to a task. It may seem at first as if there is little to be gained from sampling a slowly-varying signal faster than is necessary to characterize its basic temporal features. This intuition would seem to be supported if one compares the size of BOLD signal change to the standard deviation of the measurement noise (the contrast-to-noise ratio), for which the density of samples has little effect.

Critically, however, the statistical tests used to identify brain activity as 'above threshold' depend on both the noise level *and* the number of independent measurements. Increasing the number of time points reduces the influence of noise on estimates of BOLD signal change in much the same way that averaging of repeated measurements reduces noise. That is, an increased number of time points drives an improved estimate of the *noise*, even if the *signal* is much smoother than the temporal sampling rate. From this perspective, it is clear that the achievable benefits depend on the specific properties of the noise, which is inextricably linked to signal modeling.

fMRI analysis most typically decomposes the measured data into modeled 'signal' and noise 'residuals' (defined as the component of the measured data that is unexplained by the signal model). A simple regression analysis of task fMRI might fit one regressor time series matching a pre-defined task to each voxel's measured time course. More sophisticated analyses can include multiple regressors to account for independent cognitive processes, as well as artifactual fluctuations such as physiological variations or movement. In all cases, a voxel's residuals would be given by the difference between the complete model fit (including all regressors) and the measured data.

Inclusion of a larger number of regressor time courses by definition reduces the 'noise' residuals; but intuitively, there is a limit to the number of regressors that can be usefully fit. This intuition is partly quantified by the temporal 'degrees of freedom', which is essentially the number of data points available to the regression[2]. SMS can directly increase the degrees of freedom by enabling more time points in a given experimental duration, thereby boosting statistical significance.

This is a key insight into the role of SMS in fMRI: Acquiring more samples per unit time increases degrees of freedom and supports fitting of an increased number of regressors; conversely, experiments with a small number of regressors are intrinsically high degrees-of-freedom and therefore have less to gain from SMS in a statistical sense.

Resting-state fMRI analysis
In task fMRI, the timing of a given cognitive, sensory or motor process is controlled. By comparison, resting-state fMRI analyses must empirically determine the time course of any resting-state network (RSN) of interest. There are broadly two approaches to this problem: 'seed' analyses extract the desired time course based on pre-specified anatomy, whereas data-driven 'multivariate' analyses decompose the data set as a whole into network components based on certain criteria of interest.

Seed analysis is at heart similar to the regression described above for task fMRI. Investigators specify a seed voxel or region that they know to be part of a network of interest, from which a characteristic time series is extracted. This time series is then used in the same way as a task regressor to identify voxels that share this time course, representing brain areas with connectivity to the seed (i.e. RSNs) [3]. This concept can be extended to multiple networks by defining a set of seed regions and extracting the unique time series from each region using multiple regression. For example, in the 'dual regression'[3] approach [5], network maps from a population brain atlas are used to extract subject-specific time courses, which are then used in a multiple regression to define subject-specific spatial maps for each RSN (typically 10s of networks).

Multi-variate analyses, most notably independent component analyses (ICA), are fundamentally different from regression. Rather than analyzing each voxel independently with a seed-derived time series, the entire 4-dimensional data set (3D space x 1D time for one subject) is decomposed simultaneously. This analysis aims to holistically identify RSNs as 'modes' (or 'components') of variation in the 4-dimensional data that are in some sense independent. Each mode represents an RSN and is characterized by a canonical time course and its associated spatial map. Temporal ICA aims to identify components based on temporal independence, which this fits with the characterization of networks based on temporal co-fluctuation; alternatively, spatial ICA require that the modes are spatially independent, i.e. non-overlapping. In practice, the fact that most fMRI protocols achieve several orders of magnitude more samples in space than time means that spatial ICA is far more robust than temporal ICA. For ICA, the number of networks that are identified is set by the investigator, and typically in the range of 10-100.

SMS for resting-state fMRI
As in task fMRI, both seed and multivariate analyses decompose fMRI data into 'signal' (corresponding to RSNs) and noise residuals. Hence, we can apply similar arguments regarding the benefits of SMS for

[2] More precisely, degrees of freedom is the number of independent time points in the model-fitting residuals, reduced by the model complexity (i. e. the number of regressors).
[3] While dual regression is not typically described as a seed-based technique, it is useful and appropriate to characterize it as such for our purposes.

resting-state fMRI based on the degrees of freedom, considering both the complexity of the model (number of RSNs) and the number of independent noise measurements. For example, the most common seed-based analysis includes only a few regressors, and thus has intrinsically high degrees of freedom even without SMS. Seed-based analyses will therefore have little to gain from SMS in many situations, although SMS may be beneficial to seed-based analyses in clinical applications if it can confer reduced scan times.

The potential of SMS is at its greatest when a large number of RSNs are considered, for example in dual regression. As originally defined [5], the first stage of dual regression uses ICA to derive a group-wide atlas of RSN spatial maps, potentially parcellating the entire cerebral cortex. Alternatively, the dual regression approach can utilize a network atlas that is derived from another data set or resource, such as the Human Connectome Project. In either case, the limiting degrees of freedom is at the individual subject level, since it is at this stage that a multiple regression is used to refine each RSN to its subject specific spatial map. The degrees of freedom for this multiple regression is thus determined by the number of time points in each subject's scan and the number of RSNs being studied. In dual regression, the increased degrees of freedom offered by SMS acquisition directly enable consideration of a richer set of networks.

Intrinsically multi-variate analyses like ICA have the potential to decompose fMRI data into hundreds of brain parcels representing a detailed network hierarchy, although more commonly 20-50 RSNs might be identified. The loss of degrees of freedom implied by this relatively large number of components would require a proportionate increase in the number of time points to robustly identify RSNs. Previously, this increase in time points could only be achieved by combining at a group level across a large cohort of subjects (requiring the assumption that brain regions co-align across subjects) or acquiring long time series from a given subject. Increasing the density of temporal sampling using SMS within a more modest experimental duration for a single subject (5-20 minutes) can therefore directly enable a more detailed analysis of a network hierarchy, such as the temporal functional modes [6] and clinical applications described below.

Resting-state fMRI in practice

The gains described above can be leveraged in several ways to improve the quality of resting-state fMRI data. First, for a fixed duration of experiment, the increased degrees of freedom confers statistical benefit, which may be useful for detecting subtle differences between networks or for a more fine-scale differentiation of a given network. Alternatively, one can leverage this statistical advantage to combat the reduced SNR associated with smaller voxels to achieve gains in spatial resolution. Finally, one could reduce scan time in the face of limited subject compliance, with clinical applications in particular having much to gain. This final goal is directly enabled by SMS up to a point; however, resting-state fMRI acquisitions must be long enough to observe brain networks in a broad range of its repertoire of 'states'.

Large-scale population studies

Several neuroimaging initiatives have been launched in recent years that aim to distribute large-scale databases of resting-state fMRI. These resources share the hypothesis that certain insights into brain function and connectivity can only be gained from a large number of subjects. Resources like the 1000 Functional Connectomes Project [7] achieve large numbers by aggregating many smaller existing studies, with the benefit of low additional cost but requiring researchers to account for heterogeneity across study protocols. An alternate approach is to explicitly acquire large cohorts with a single protocol to maximize data homogeneity and quality. We will briefly highlight the role of SMS in two such prospective studies representing different extremes of data acquisition: the Human Connectome Project (HCP) and the UK Biobank Project.

The HCP Consortium is focused on characterizing connectivity in the brain [8], with the WashU-UMinn consortium focusing on healthy adults and acquiring a range of modalities including resting-state fMRI in 1200 subjects [9]. SMS has been a central technology to the HCP from the outset, and a number of technical developments have arisen from this project in addition to the data resource (see articles by Uğurbil and Yacoub in this issue). Within the HCP, the benefits of SMS have been intensely optimized to achieve both high spatial and temporal resolution fMRI (2 mm, TR = 0.72 s), with individual subjects undergoing four 15-minute resting-state scans. Subjects undergo a total of 4 hours of imaging, which additionally includes task fMRI, diffusion imaging and anatomical scans, as well as intense non-imaging phenotyping. Data are acquired on a single scanner (representing a pre-cursor to the MAGNETOM Prisma 3T platform) that was designed specifically for this study. The use of state-of-the-art SMS fMRI has enabled the HCP to achieve exquisite data quality for individual subjects, as well as protocol homogeneity over a relatively large, extensively phenotyped cohort.

UK Biobank is an established epidemiological cohort of 500,000 subjects aged 45-75 that has undergone (non-imaging) phenotyping, behavioral/lifestyle measures and genotyping, and will be followed for long-term health outcomes via the UK National Health Service. An Imaging Enhancement study is currently in the pilot phase, and ultimately aims to enlist 100,000 of the existing cohort for imaging, including brain, cardiac and body scans. Successfully scanning of this cohort over five years corresponds to extremely high throughput: three dedicated centers running 7 days per week, each accumulating 18 subjects per day. The resulting brain imaging protocol is limited to 35 minutes, during which several imaging modalities are acquired (task and resting-state fMRI, diffusion imaging and multiple anatomical modalities). SMS imaging techniques developed for the HCP [10]

have been critical to achieving this highly-ambitious goal without requiring significant compromise relative to conventional data quality. The resting-state fMRI protocol achieves 2.4 mm resolution with sub-second sampling (TR = 0.73 s) using an SMS acceleration of 8, enabling 500 time points per subject in just 6 minutes.

Revealing novel aspects of functional connectivity

Coincident with the development of SMS acceleration for fMRI has been an explosion of ambitious resting-state research with respect to both sophisticated data analysis techniques and attempts to probe increasingly subtle aspects of brain function. The benefit of high temporal resolution for resting-state fMRI is likely to extend beyond boosted statistics or improvements in spatial resolution. Here, we highlight one example from our research where SMS has directly enabled novel methodology and preliminary insights into functional connectivity, namely the identification of temporally independent modes of functional activity.

The goal of most resting-state studies is to derive estimates of apparent connection strength between brain regions. While many potential measures of connection strength exist, the most common are based on temporal correlation. Standard approaches parcellate the brain into regions and associated time courses, and estimate the connection strength between a pair of regions based on the correlation between regional time series. Regardless of how the regions are derived (seed- or ICA-based), this approach is underpinned by some problematic assumptions. Temporal correlation is only able to capture the time-averaged behavior of the connectivity between two regions, which would conceal neuroscientifically interesting variations in connection strength over time ('non-stationarities'). Examples include independent networks with spatial overlap (due to interdigitation of neural populations or simply limited spatial resolution), or temporal modulation of physical connections due to processes like attention. In the case of multiple networks that contain a common (overlap) region but are largely independent, the 'networks' identified by both spatial ICA and seed-based approaches are unsatisfying: spatial ICA requires components to be non-overlapping, whereas seed-based analysis identifies all correlated areas as a single network, even if the extended regions do not significantly correlate with each other. These assumptions are problematic, both with respect to basic neuroscience investigations and

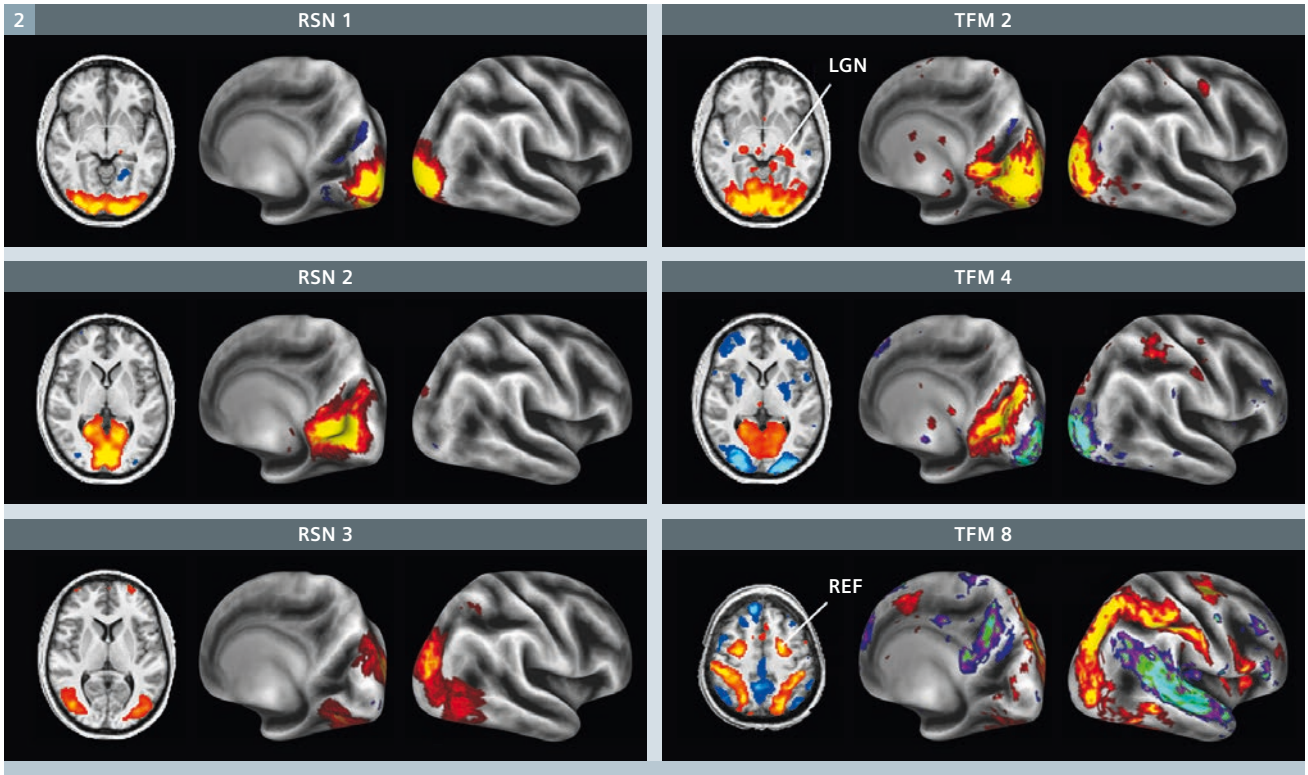

2 Components of the visual system identified from resting-state data using ICA. On the left, spatial independence breaks the occipital lobe into non-overlapping 'resting-state networks' corresponding to early stages of processing of information at the centre and periphery of vision (RSN 1 and RSN 2, respectively), and higher-level visual processing (RSN 3). On the right, temporal independence combines across these areas to identify extended visual networks that correspond to known anatomical support for processes such as low-level visual processing (TFM 2), high vs low visual eccentricity (TFM 4) and the dorsal visual stream (TFM 8). *Reproduced with permission from [2].*

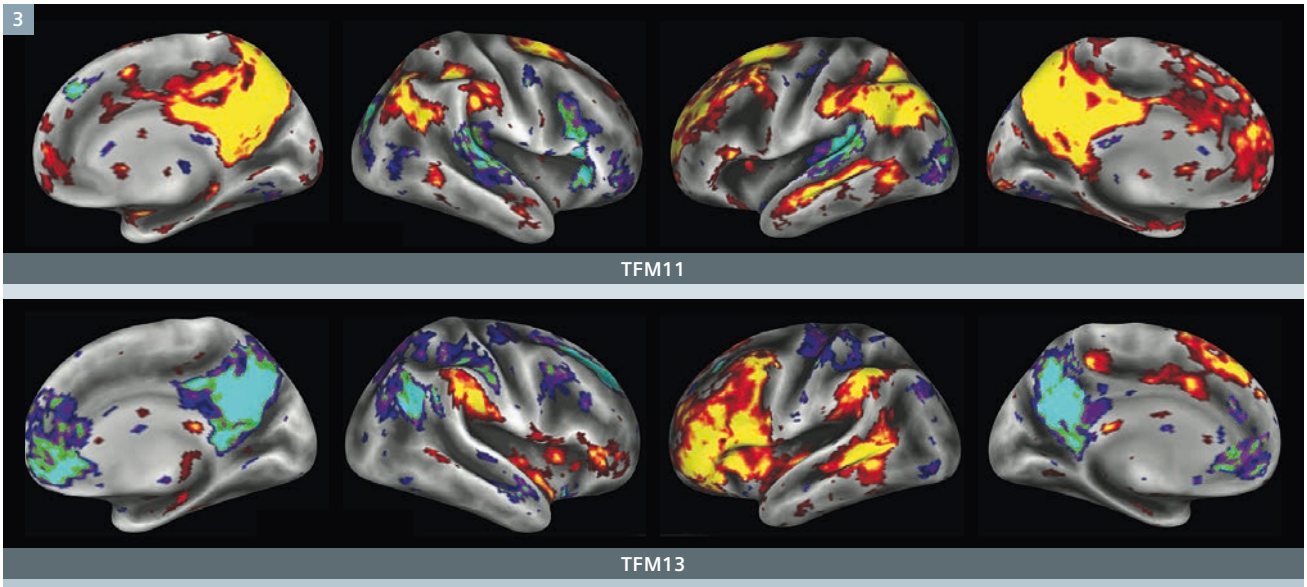

3 High-level cognitive networks identified from resting-state fMRI data on the basis of temporal independence, both including overlap with the well-established 'default mode network' [1]. The network on the top (TFM 11) is reasonably symmetric across hemispheres and involves a set of regions that are involved semantic processing. The network displayed below (TFM 13) contains significant overlap with this semantic network, but is strongly lateralized and includes language regions. *Reproduced with permission from [2].*

for clinical applications, particularly pre-surgical planning, as described below.

Identification of more subtle temporal features like the non-stationarities described above, places a strong demand on the temporal domain of the acquired data, which is typically several orders of magnitude smaller than the spatial domain of image voxels. We explored the potential to identify extended brain networks using temporal independence (temporal ICA), in which a brain network would be recognized based on having a unique temporal signature [2]. Unlike spatial ICA, this analysis does not penalize spatial overlap between networks, but it does require a large number of temporal samples to robustly identify these independent time processes. This approach was demonstrated using pilot resting-state SMS data acquired by the HCP. We combined data across five subjects with TR = 0.8 s to accumulate 24,000 time points over 360 minutes. Following careful data clean up (see below), the data was parcellated into 142 regions using spatial ICA, which were then fed into temporal ICA to identify 21 temporally independent functional modes (TFMs).

The resulting TFMs contained significant spatial overlap, with most of the spatial ICA parcels contributing significantly to multiple modes. Encouragingly, most of the TFMs also corresponded to extended networks of known functional anatomy. The visual system was decomposed into well-established streams of visual information processing (Fig. 2), while other TFMs capture high-level cognition such as semantic processing or language (Fig. 3).

Clinical fMRI at the individual patient level

The use of resting-state fMRI in the clinical domain is fairly recent, but has begun to attract attention for clinical applications in general, and for pre-surgical mapping in particular [11, 12]. Resting-state fMRI does not depend on task performance and is less contingent on patient compliance. It is also less demanding with respect to experimental setup than task-based fMRI and can be more easily acquired by MRI technicians. In some instances, such as when probing orofacial motor functions, task-based fMRI is prone to task-correlated head motion. Furthermore, there is initial evidence that resting-state fMRI data may establish intra- and perilesional BOLD reactivity and thereby serve as a less stressful substitute for cerebrovascular reactivity mapping by experimentally induced hypercapnia [13]. Clinical applications can benefit directly from the increase in statistical significance conferred by SMS, or can leverage statistical gains to increase spatial resolution or reduce scan durations – all of which are extremely desirable for clinical applications.

Increasing the spatial resolution of fMRI improves spatial accuracy, including registration to anatomical scans, but incurs a reduction in SNR proportionate to voxel volume. In some contexts, data quality can be improved through the combined use of high spatial resolution with edge-preserving smoothing to increase SNR, reducing partial volume and signal dropout compared to data acquired at the filtered resolution. However, smoothing can artificially extend or eliminate true activations, both of which are problematic for pre-surgical mapping and intra-operative neuro-navigation. Sophisticated data analysis strategies will thus be required to translate the potential improvements in spatio-temporal resolution with SMS fMRI into clinical applicability [14, 15].

4

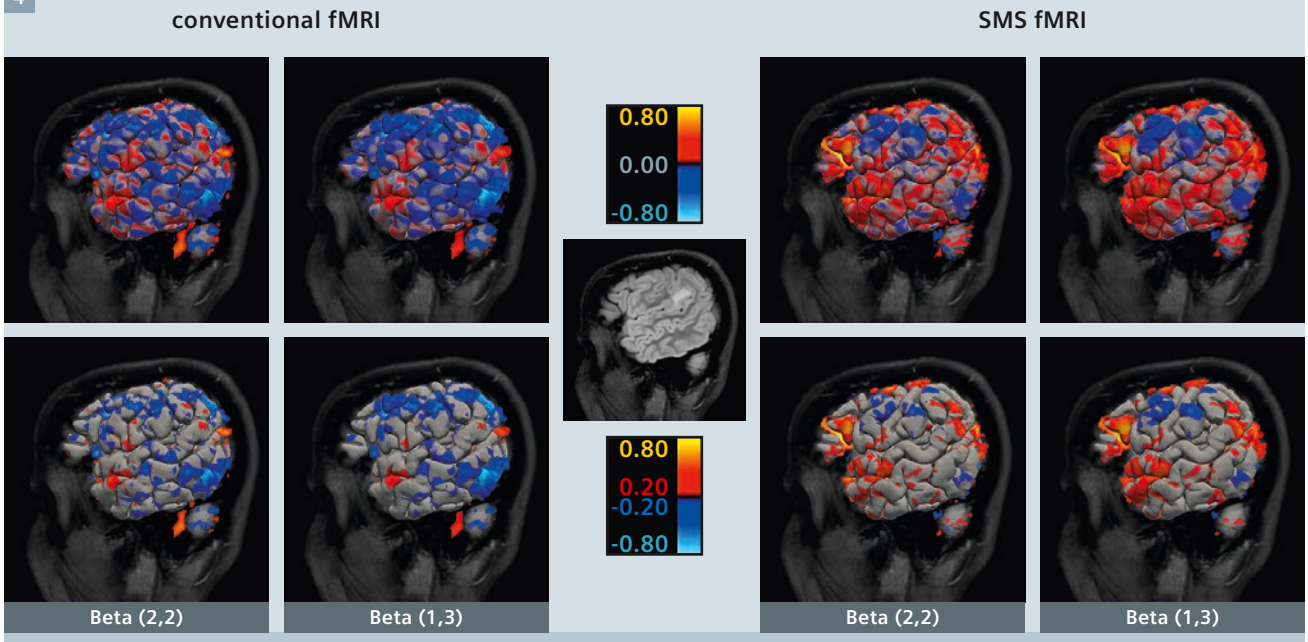

4 Improved single-subject fMRI results with SMS fMRI. Speech mapping data in the same patient, using non-SMS low spatio-temporal resolution (3 mm, TR = 3s) vs. SMS high spatio-temporal resolution (1.8 mm isotropic, TR = 1.5 s, SMS factor 3). Statistical confidence of the SMS results increases remarkably (*top*: unthresholded, *bottom*: thresholded using different Beta priors [14] instead of smoothing kernels), demonstrating that doubling the temporal resolution by SMS over-compensated the reduced SNR at higher spatial resolution. The lesion was an incidentially detected, left supramarginal focal cortical dysplasia (small center image), initially mistaken for a low-grade glioma, with reduced intra- and perilesional cerebrovascular reactivity.

5

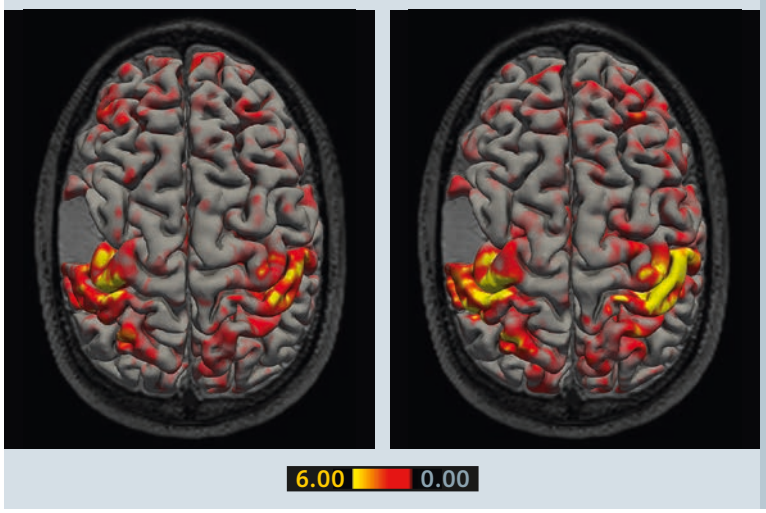

5 Improved (sensori-)motor mapping by SMS resting-state fMRI in a left precentral low-grade glioma prior to resective surgery. The patient suffered from focal motor seizures involving both eyebrows (bilateral N.VII innervation), the contralateral mouth corner (contralateral N.VII innervation), chewing, vocalizations and speech arrest (N.V, IX, X and XII innervation), corresponding to the motor humunculus representation below the handknob. Task-based fMRI would have been confounded by stimulus-correlated head motion potentially causing false-positive detections primarily at the tumor border. Resting-state fMRI reveals statistical gains (color-coded Z-statistics) of SMS high (TR = 1.56 s, SMS factor 3) over non-SMS low (TR = 3.33 s) temporal resolution fMRI, despite the shorter acquisition time (6.5 vs. 14 min).

An example of the benefits of increased spatio-temporal resolution by SMS fMRI for language mapping in a patient is given in Figure 4.

Shorter experiments are desirable not only because scan time is precious in the clinical domain, but also considering limitations in task performance and/or compliance in patients.

Figure 5 illustrates corresponding gains that can be achieved by SMS for pre-surgical fMRI, exemplified by sensorimotor mapping. These benefits have to be substantiated and systematically explored by future studies. Note that motor mapping is, even in the case of space-occupying lesions, rarely indicated because the sensori-motor strip can be identified in most patients by pure anatomic criteria. The real challenge to transfer resting-state fMRI into pre-surgical practice lies in the mapping of 'eloquent' functions with no absolute cortical representation. That is, the meaningful pre-surgical mapping of essential functions whose cortical

representations cannot be predicted by anatomic criteria alone, such as speech and language in particular. While it is intrinsically difficult to avoid a circularity of assumptions about the hemispheric representation and dominance of speech and language in this context, recent attempts to relate connectivity gradients from SMS resting-state fMRI to language lateralization in non-clinical samples of the HCP project have been promising [16]. However, task-based pre-surgical fMRI mapping can be performed in 3 to 8 minutes while the recording of these high-quality SMS resting-state data took one hour (see above), and initial efforts to translate such sophisticated analyses to real pre-surgical tumor patients using clinically acceptable scan times of 6 to 13 min have proven difficult. Generally, acquiring high-quality resting-state fMRI data that provide access to subtle information in the spatio-temporal domain (such as robust functional connectivity gradients or TFMs; see above) will continue to require longer scan times than simple task-based fMRI even if SMS acceleration is used.

Cautions, challenges and confounds

Achieving the benefits of SMS in fMRI does require some additional care to protocol design and data analysis. Here we review several common challenges and strategies to overcome them.

High temporal resolution using SMS requires careful consideration of standard analysis pipelines. Residuals are generally assumed to be 'white noise' (with each time point independent of other time points), making any source of structured noise problematic. Violation of this assumption (for example, temporally smooth noise) can cause the residuals to have lower degrees of freedom than anticipated and thereby inflate the apparent statistical significance. At high temporal resolution, it is therefore crucial to account for any structure in the residuals [4]. Most fMRI software packages enable suitable noise corrections, although this may not be a default option.

Fast temporal sampling with SMS will typically reduce the repetition time down to the second or sub-second range, such that the magnetization will not recover fully from one RF excitation to the next. This results in some loss of signal in each individual volume relative to more typical temporal sampling at a rate of 2-3 seconds. Reducing the excitation to the Ernst angle can mitigate these effects, but some signal loss is inevitable. Nevertheless, it is straightforward to demonstrate that the signal loss in a given image volume is more than compensated by the statistical gains described above [17].

Despite the benefits described above, fast sampling is not a panacea for overcoming some limitations of functional MRI based on the *BOLD response*. Neurovascular coupling, which determines BOLD signal delays, is dependent on region, physiological state and neurovascular pathology. Hence, while faster sampling enables detection of the BOLD response to *neural* activity with greater temporal precision, uncertainties in the hemodynamic response mean that it is unlikely to provide the ability to infer neural timings with greater precision [18]. It may, however, enable the detection of subtle temporal features of the hemodynamic response, such as an initial signal reduction (known as the 'initial dip') that has been long hypothesized to provide improved spatial specificity to the locus of neural activity [19].

Another challenge associated with short repetition time is signal instability from 'spin history' effects that disturb the signal steady state, such as caused by subject motion. Motivated in part by recent innovations in SMS technology, machine learning techniques have been developed to automatically 'clean' data by removing these artifacts [20]. These techniques, which have been extensively evaluated within the HCP, can remove much of the signal fluctuations due to physiological noise, hardware instabilities and motion. Indeed, the fact that methods for cleaning data often are based on the same analytical techniques (multivariate analysis [20] or regression [21]) suggests that SMS data may be more intrinsically amenable to clean-up than conventional non-SMS data.

Conclusions

Simultaneous multi-slice imaging offers enormous potential benefits to functional MRI in general, and resting-state fMRI in particular. These benefits derive primarily from the statistical advantage of increasing the experimental degrees of freedom. For simple tasks, this could enable shorter experiments, but the primary benefit is expected when estimating a number of separate time courses reflecting different aspects of brain function. In resting-state fMRI, experiments that probe a rich hierarchy of brain networks are limited by the degrees of freedom. SMS fMRI can therefore be expected to have particular impact in this area. Several examples of such benefit have been highlighted here, including deployment in large cohorts, unique insights into connectivity and clinical applications.

References

1 M.E. Raichle, et al., A default mode of brain function. Proc Natl Acad Sci 2001. 98: p. 676-682.
2 Smith, S.M., et al., Temporally-independent functional modes of spontaneous brain activity. Proceedings of the National Academy of Sciences, 2012. 109(8): p. 3131-3136.
3 Biswal, B., et al., Functional connectivity in the motor cortex of resting human brain using echo-planar MRI. Magn Reson Med, 1995. 34: p. 537-541.
4 Bullmore, E., et al., Statistical Methods of Estimation and Inference for Functional MR Image Analysis. Magn Reson Med, 1996. 35(2): p. 261-277.
5 Filippini, N., et al., Distinct patterns of brain activity in young carriers of the APOE-e4 allele. Proc National Academy of Sciences USA, 2009. 106: p. 7209-7214.
6 Smith, S., et al., Temporally-independent functional modes of spontaneous brain activity. Proceedings of the National Academy of Sciences, 2012. 109(8): p. 3131-3136.
7 Biswal, B.B., et al., Toward discovery science of human brain function. Proceedings of the National Academy of Sciences, 2010. 107(10): p. 4734-4739.
8 Van Essen, D.C., et al., The Human Connectome Project: A data acquisition perspective. NeuroImage, 2012. 62(4): p. 2222-2231.

9 Smith, S., et al., Resting-state fMRI in the Human Connectome Project. NeuroImage, 2013. 80(C): p. 144-168.
10 Ugurbil, K., et al., Pushing spatial and temporal resolution for functional and diffusion MRI in the Human Connectome Project. NeuroImage, 2013. 80(C): p. 80-104.
11 Lee, M.H., C.D. Smyser, and J.S. Shimony, Resting-state fMRI: a review of methods and clinical applications. AJNR Am J Neuroradiol, 2013. 34(10): p. 1866-72.
12 Kokkonen, S.M., et al., Preoperative localization of the sensorimotor area using independent component analysis of resting-state fMRI. Magn Reson Imaging, 2009. 27(6): p. 733-40.
13 Zaca, D., et al., Cerebrovascular reactivity mapping in patients with low grade gliomas undergoing presurgical sensorimotor mapping with BOLD fMRI. J Magn Reson Imaging, 2014. 40(2): p. 383-90.
14 Liu, Z., et al., Pre-surgical fMRI Data Analysis Using a Spatially Adaptive Conditionally Autoregressive Model. Bayesian Analysis, 2015. http://projecteuclid.org/euclid.ba/1440594946.
15 Johnson, T.D., et al., A Bayesian non-parametric Potts model with application to pre-surgical FMRI data. Stat Methods Med Res, 2013. 22(4): p. 364-81.
16 Haak, K., et al., Toward assessing language lateralization with resting-state fMRI, in Organization for Human Brain Mapping. 2015. p. 2304.
17 Feinberg, D.A., et al., Multiplexed echo planar imaging for sub-second whole brain FMRI and fast diffusion imaging. PLoS ONE, 2010. 5(12).
18 Smith, S., et al., The danger of systematic bias in group-level FMRI-lag-based causality estimation. NeuroImage, 2012. 59: p. 1228-1229.
19 Hu, X. and E. Yacoub, The story of the initial dip in fMRI. NeuroImage, 2012. 62(2): p. 1103-1108.
20 Salimi-Khorshidi, G., et al., Automatic denoising of functional MRI data: Combining independent component analysis and hierarchical fusion of classifiers. NeuroImage, 2014. 90: p. 449-468.
21 Glover, G.H., T. Li, and D. Ress, Image-based method for retrospective correction of physiological motion effects in fMRI: RETROICOR. Magn Reson Med, 2000.

Contact

Karla Miller, Ph.D.
Professor of Biomedical Engineering
Nuffield Department of Clinical Neurosciences
FMRIB Centre
John Radcliffe Hospital
Oxford OX3 9DU
UK
karla@fmrib.ox.ac.uk

Learn more!

Don't miss the talks of experienced and renowned experts on all aspects of MR imaging at:

www.siemens.com/magnetom-world

Multiband techniques for functional and structural neuroimaging: Technical challenges, applications and future prospects

Essa Yacoub, PhD
CMRR, University of Minnesota

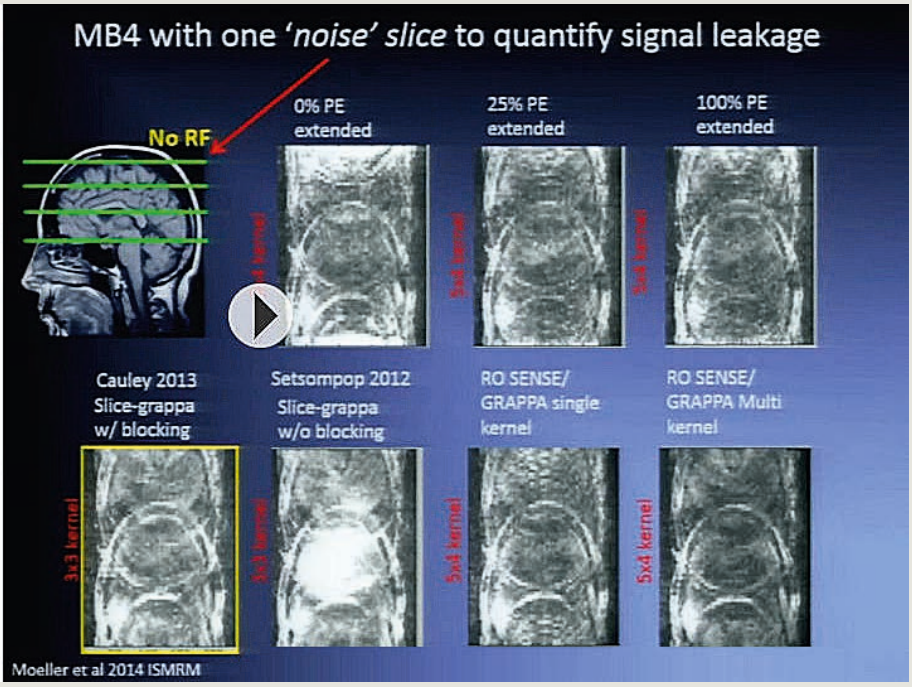

Multiband Simultaneous Multi-Slice Acquisitions in BOLD at 7T

An T. Vu; Steen Moeller; Eddie Auerbach; Sudhir Ramanna; Emily Kittelson; Keith Jamison; Kâmil Uğurbil; Essa Yacoub

Center for Magnetic Resonance Research (CMRR), University of Minnesota, Minneapolis, MN, USA

The use of 7 Tesla MRI[1] to study human brain function was motivated by the promise of higher signal-to-noise ratios (SNR), larger BOLD-based fMRI contrast, and improved functional specificity [1, 2]. Intrinsic gains in BOLD sensitivity make the acquisition of higher resolution images attractive. In addition, lower resolution studies at high fields typically become dominated by physiological noise [3-5], as increases in signal are accompanied by increases in physiological noise, albeit some of this noise may actually be signals of interest in resting-state fMRI. Consequently, high-field gains in sensitivity are often traded in for spatial resolution or other applications which may be SNR starved at low fields. Problematic to increases in spatial resolution are the subsequent increases in acquisition times during any single readout train, and the longer volume TRs, due to the many more slices needed to cover the same volume. Accordingly, the high-resolution fMRI prospects at high magnetic fields have historically been limited to small fields-of-view in isolated parts of the brain, as was the first 7T fMRI study in humans nearly fifteen years ago [6]. While this study, and several follow-up studies, capitalized on the advantages of 7T fMRI using reduced FOV approaches [7-10], many applications, such as resting-state studies of functional connectivity, which require the simultaneous monitoring of several cortical areas, were not attractive for 7T applications. For resting-state fMRI, increases in the spatial resolution could, however, allow for more clear delineations of neuronal processes from those of a vascular nature, a reduction of partial volume effects, or more accurate cortical parcellations of functional areas. For more localized higher-resolution studies, such as layer specific fMRI, increases in the volume coverage [7] would allow monitoring of feedback signals associated with neuronal processing, which can originate from very distant brain regions. In addition, increases in volume coverage of high-resolution studies would allow for improved motion correction, a bottleneck in high-resolution studies of humans.

Reasons like these inspired the use of multiband (MB) excitation, which promised to increase the temporal efficiency of high resolution 2D EPI acquisitions at 7T [11]. This initial 7T fMRI study, followed by the subsequent announcement of the NIH's Human Connectome Project (HCP), which aimed to map functional and structural connectivity at high spatial and temporal resolutions across 1200 subjects, sparked several more studies and developments in multiband technology [12-15]. One of the first studies, supported in part by the HCP, explored the possibility of acquiring high-resolution resting-state data at 7T over the whole brain. This study demonstrated robust detection of resting-state networks across the brain at varying spatial resolutions, down to 1 mm isotropic [16]. It also demonstrated the potential advantages of higher spatial resolutions for resting-state fMRI and the obvious temporal inefficiency limitations (due to the required long TRs). This study employed conventional single band single-shot EPI with acceleration along the phase-encode direction only. At the time, the MB technique was not available for mainstream use or for

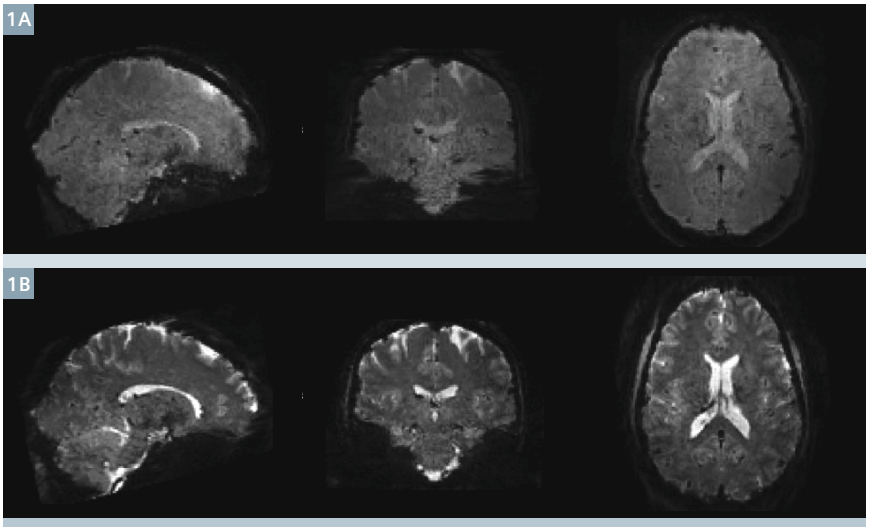

1 HCP fMRI images at 3T **(1A)** and 7T **(1B)**. EPI images acquired using the HCP protocol at 3T and 7T. (3T: 2 mm, TR 0.72 s, multiband (MB) 8. 7T: 1.6 mm, TR 1.0 s, MB 5, iPAT 2).

[1] MAGNETOM 7T is ongoing research. All data shown are acquired using a non-commercial system under institutional review board permission. MAGNETOM 7T is still under development and not commercially available yet. Its future availability cannot be ensured.

high throughput studies like the HCP, as it required saving raw data and doing offline image reconstructions. It was thus not used in this initial 7T resting-state study. Subsequently, through support from the HCP, the MB technique was fully integrated, optimized, and packaged for use on Siemens scanners and has become the default choice for functional and diffusion imaging protocols at sites across the world (http://www.cmrr.umn.edu/multiband/). While the technique, referred to as either multiband, simultaneous multi-slice (SMS), or slice acceleration, was originally proposed for 7T fMRI [11], its subsequent translation to 3T was comparatively straightforward as in-plane accelerations were not a requirement, and issues related to B_0 and B_1 were drastically reduced at 3T [17, 18]. Ironically, this resulted in unprecedented image qualities, accelerations, and SNRs at 3T and it became imperative for the ubiquitous technical challenges at high fields to be dealt with in order for the MB technique to be competitive and equally attractive at 7T. Outlined below are some of the technical issues and advances that have since made MB slice accelerations at 7T routine, and the possibility of acquiring higher spatial resolutions over the entire brain with conventional TRs or faster, a reality.

High-field, high-resolution imaging requires the use of in-plane accelerations if full field-of-view images with high in-plane resolutions are desired. As such, the use of slice accelerations directly competes with in-plane accelerations in terms of the use of the spatial encoding information available from the coil sensitivity profile. At 3T, because in-plane accelerations are not always required, much higher slice-acceleration factors can be used [15]. While the total achievable acceleration factors are higher at 7T [19], slice-acceleration factors used at 3T are typically higher than those used at 7T, as is evident by the HCP fMRI protocol (Fig. 1). In addition, the use of in-plane accelerations is accompanied by additional under-sampling SNR losses and increased sensitivity to motion. In-plane reference scans acquired with segmented EPI acquisitions, unlike reference scans for multiband images (i.e. single band reference), are highly sensitive to subject motion, including physiology, which becomes increasingly more problematic at high resolutions, and can result in additional ghosting or banding artifacts in the EPI images (Fig. 2). This can result in significantly reduced temporal SNR and compromised image quality in accelerated BOLD images at 7T. To address this, we explored using gradient recalled echo or FLASH scans for calibration, acquiring a single line of *k*-space after each RF pulse [20-22]. This approach, now standard on 7T acquisitions, does not exhibit noticeable sensitivity to subject motion (Fig. 2) and results in higher temporal SNR. Current and future efforts are still highly focused on improving image quality (i.e. ghost and artifact reduction) for EPI applications at 7T, specifically those employing high amounts of acceleration both in the slice and in plane directions [11, 23, 24].

The combined use of high fields and multiband pulses results in significant B_1 limitations. First, the conventional approach to generating a MB RF pulse simply sums the single banded waveforms, which quickly reaches the peak power limitation of the system. To deal with this, one can reduce RF bandwidth by increasing the pulse durations or use RF techniques such as VERSE [25] or PINS [26], albeit at the cost of poorer slice profiles, especially in the presence of B_0 inhomogeneities. The use of approaches, such as time and phase shifting of the RF pulses [12] or parallel transmit [14], promises to relax peak power and SAR requirements without compromising the slice profile, while also providing increased signal homogeneity and SNR across the brain. At 3T, although such B_1 limitations can also arise, they do not significantly affect gradient echo BOLD imaging and tend to be manageable in MB-accelerated diffusion protocols. However, the use of slice-accelerated diffusion imaging at 7T requires the aforementioned approaches to deal with B_1 limitations, and these are currently being developed for use in 7T applications [27]. B_1 management is one of the primary ongoing efforts aimed at improving both diffusion and BOLD MB acquisitions at 7T.

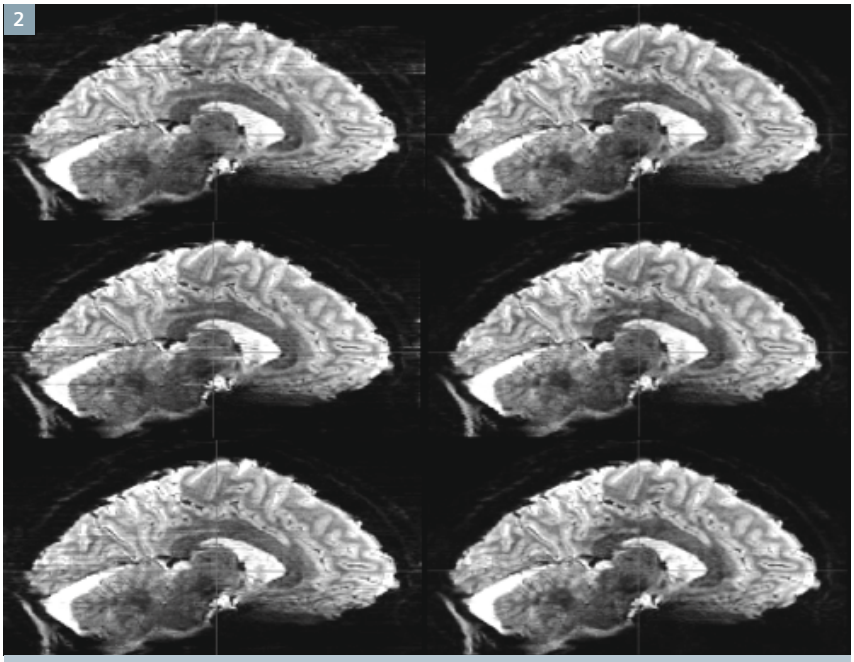

2 Reduction of motion sensitivity in auto calibration scans. Comparison of in-plane accelerated EPI images, from three different acquisitions, using standard segmented EPI as reference scans (left column) versus the same three scans reconstructed with a single GRE reference scan (right column). (7T, 1.25 mm, MB 3, iPAT 3)

Common to both high-resolution BOLD and diffusion studies at 7T, made possible by slice-acceleration approaches and the extremely high channel counts, is the unprecedented amount of data being acquired and the rate at which it is acquired. It is not uncommon for the image reconstruction time to substantially exceed the data acquisition time. Users of the multiband sequence quickly noticed that an hour of scanning time would require several hours of image reconstruction time. In addition, the hard disk space where the raw data was stored could be filled in an hour or so, meaning data needed to be transferred off the raw disk or it would be overwritten. As such, in the early days of 2D slice-accelerated BOLD imaging, specifically at 7T, scans were limited to less than an hour and real-time feedback on image quality was unavailable. A significant effort was invested in reducing the reconstruction bottleneck so that such slice-accelerated sequences could be used in more conventional studies and in high throughput studies like the HCP. One of the more significant improvements was achieved with the use of GPU enabled computers reducing the reconstruction time by a factor of 3 or 4, bringing it to near real-time levels. For a 1 mm 7T BOLD fMRI protocol that uses an MB factor of 3 with a 32-channel coil, raw data is generated at a rate of nearly 5 GB/min. For a 10 minute resting-state scan, this amounts to around 50 GB of raw data. With the use of a GPU enabled image reconstructor at the scanner, as is now standard on the MAGNETOM Prisma 3T, DICOM images can be generated in real time. In addition to offline reconstruction no longer being needed, the immediate feedback on image quality and subject performance is also invaluable. For example, if data quality has been compromised, as is often the case with clinical and other vulnerable populations, re-scans can be considered while the subject is still available. Further, applications such as real-time fMRI can now also consider using MB techniques as the data can also be analyzed in real time as well.

Conclusions

The HCP has to date collected data in nearly 150 subjects (including 40 min of diffusion, 1 hr of resting-state, and 1.5 hrs of task fMRI – per subject) on a commercial 7T system. All of these scans employ slice accelerations (combined with in-plane) and have yielded impressive data sets at high spatial and temporal resolutions (Fig. 3). This is a testament to the robustness of the technique, the scanner hardware, and the general applicability at 7T, which has allowed 7T to provide a unique contribution of very high resolution whole-brain images of structural and functional connectivity to an already impressive HCP data set from 3T. Going forward, continued technical improvements in slice accelerated technology at 7T are likely to not only enhance and enable the countless possibilities of high resolution imaging applications at 7T, including submillimeter resolutions over the entire brain (Fig. 4), but will also likely directly translate into improvements at lower fields.

3

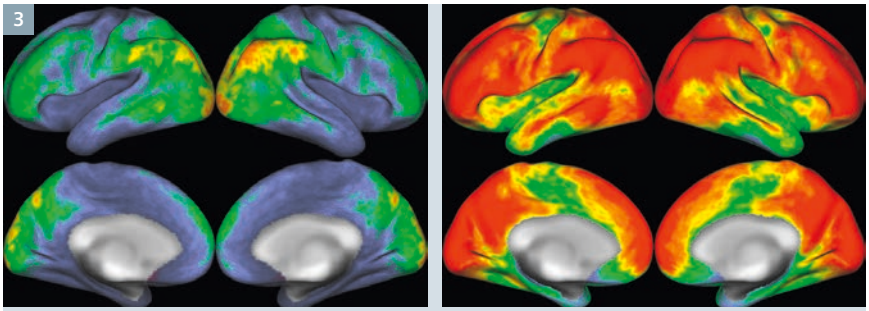

3 Functional contrast-to-noise from 3T and 7T HCP data sets. Maps were generated from 24 subjects using an hour of resting-state fMRI data acquired at 3T or 7T (3T: 2 mm, TR 0.72 s, MB 8. 7T: 1.6 mm, TR 1.0 s, MB 5/iPAT 2).
Images courtesy of Steve Smith and Matt Glasser for the HCP.

4

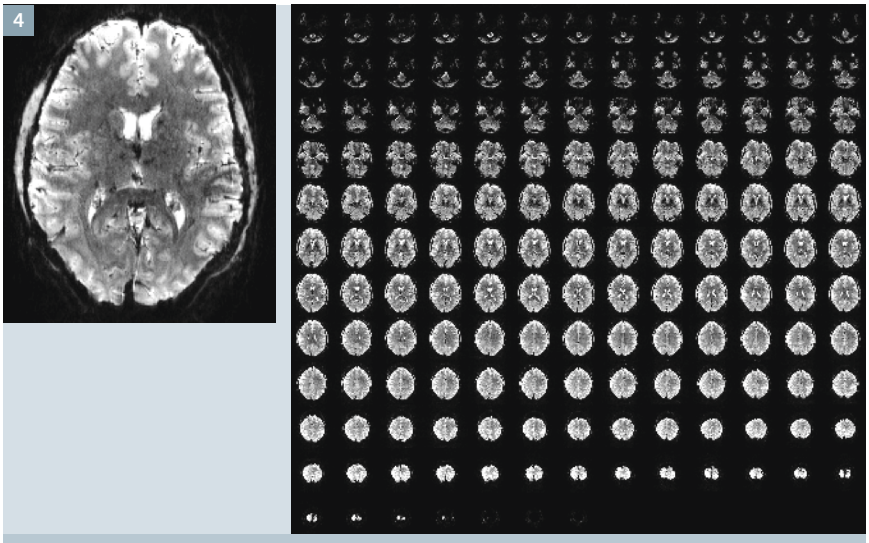

4 Sub-millimeter whole brain fMRI at 7T. A single image acquired using: 0.9 mm isotropic, iPAT 3, MB 3, TR 3.7 s and 150 slices. A zoomed view of one slice is also shown.

Acknowledgments

The work reported in this article was supported by the Human Connectome Project (1U54MH091657) from the 16 Institutes and Centers of the National Institutes of Health that support the NIH Blueprint for Neuroscience Research and by the Biotechnology Research Center (BTRC) grant P41 EB015894 from NIBIB and the NINDS Institutional Center Core Grant P30 NS076408.

References

1 Ogawa, S., et al., Functional brain mapping by blood oxygenation level-dependent contrast magnetic resonance imaging. Biophys J, 1993. 64: p. 800-812.
2 Uludag, K., B. Muller-Bierl, and K. Ugurbil, An integrative model for neuronal activity-induced signal changes for gradient and spin echo functional imaging. Neuroimage, 2009. 48(1): p. 150-65.
3 Hyde, J.S., B. Biswal, and A. Jesmanowicz, High-resolution fMRI using multislice partial k-space GR-EPI with cubic voxels. Magn. Reson. Med, 2001. 46: p. 114-125.
4 Kruger, G. and G.H. Glover, Physiological noise in oxygenation-sensitive magnetic resonance imaging. Magn Reson Med, 2001. 46(4): p. 631-7.
5 Triantafyllou, C., et al., Comparison of physiological noise at 1.5 T, 3 T and 7 T and optimization of fMRI acquisition parameters. Neuroimage, 2005. 26(1): p. 243-50.
6 Yacoub, E., et al., Imaging brain function in humans at 7 Tesla. Magn Reson Med, 2001. 45(4): p. 588-94.
7 Olman, C.A., et al., Layer-specific fMRI reflects different neuronal computations at different depths in human V1. PLoS One, 2012. 7(3): p. e32536.
8 Yacoub, E., N. Harel, and K. Ugurbil, High-field fMRI unveils orientation columns in humans. Proc Natl Acad Sci U S A, 2008. 105(30): p. 10607-12.
9 Yacoub, E., et al., Robust detection of ocular dominance columns in humans using Hahn Spin Echo BOLD functional MRI at 7 Tesla. Neuroimage, 2007. 37(4): p. 1161-77.
10 Zimmermann, J., et al., Mapping the organization of axis of motion selective features in human area MT using high-field fMRI. PLoS One, 2011. 6(12): p. e28716.
11 Moeller, S., et al., Multiband multislice GE-EPI at 7 tesla, with 16-fold acceleration using partial parallel imaging with application to high spatial and temporal whole-brain fMRI. Magn Reson Med, 2010. 63(5): p. 1144-53.
12 Auerbach, E.J., et al., Multiband accelerated spin-echo echo planar imaging with reduced peak RF power using time-shifted RF pulses. Magn Reson Med, 2013.
13 Setsompop, K., et al., Blipped-controlled aliasing in parallel imaging for simultaneous multislice echo planar imaging with reduced g-factor penalty. Magn Reson Med, 2012. 67(5): p. 1210-24.
14 Ugurbil, K., et al., Pushing spatial and temporal resolution for functional and diffusion MRI in the Human Connectome Project. Neuroimage, 2013. 80: p. 80-104.
15 Xu, J., et al., Evaluation of slice accelerations using multiband echo planar imaging at 3 T. Neuroimage, 2013. 83: p. 991-1001.
16 De Martino, F., et al., Whole brain high-resolution functional imaging at ultra high magnetic fields: an application to the analysis of resting state networks. Neuroimage, 2011. 57(3): p. 1031-44.
17 Feinberg, D.A., et al., Multiplexed Echo Planar Imaging for Sub-Second Whole Brain FMRI and Fast Diffusion Imaging. PLoS One, 2010. 5(12): p. e15710.
18 Smith, S.M., et al., Temporally-independent functional modes of spontaneous brain activity. Proc Natl Acad Sci U S A, 2012. 109(8): p. 3131-6.
19 Wiesinger, F., et al., Parallel imaging performance as a function of field strength--an experimental investigation using electrodynamic scaling. Magn Reson Med, 2004. 52(5): p. 953-64.
20 Griswold, M.A., et al., Autocalibrated coil sensitivity estimation for parallel imaging. NMR Biomed, 2006. 19(3): p. 316-24.
21 Haase, A., et al., FLASH Imaging: Rapid NMR Imaging Using Low Flip Angle Pulses. J. Magn. Reson., 1986. 67: p. 258-266.
22 Talagala, S.L., J.E. Sarlls, and S. Inati. Improved temporal SNR of accelerated EPI using a FLASH based GRAPPA reference scan in ISMRM 21st Annual Meeting. 2013. Salt Lake City.
23 Moeller, S., et al. EPI 2D ghost correction and integration with multiband : application to diffusion imaging at 7T. in Proc. Intl. Soc. Mag. Reson. Med. 23. 2015. Toronto.
24 Moeller, S., et al. Slice-specific navigator correction for multiband imaging. in ISMRM 22nd Annual Meeting. 2014. Milan.
25 Hargreaves, B.A., et al., Variable-rate selective excitation for rapid MRI sequences. Magn Reson Med, 2004. 52(3): p. 590-7.
26 Norris, D.G., et al., Power Independent of Number of Slices (PINS) radiofrequency pulses for low-power simultaneous multislice excitation. Magn Reson Med, 2011. 66(5): p. 1234-40.
27 Vu, A.T., et al., High resolution whole brain diffusion imaging at 7T for the Human Connectome Project. Neuroimage, 2015. 122: p. 318-331.


Steen Moeller


Eddie Auerbach


An T. Vu


Keith Jamison


Kâmil Uğurbil


Essa Yacoub


Emily Kittelson


Sudhir Ramanna

Contact

Essa Yacoub, Ph.D.
Center for Magnetic Resonance Research
2021 6th Street SE
Minneapolis, MN 55455
USA
Phone: +1 6126262001
yaco0006@umn.edu

High-Resolution Diffusion-Weighted Neuroimaging at 3T and 7T with Simultaneous Multi-Slice RESOLVE

Robert Frost[1]; Peter J. Koopmans[1]; George W. Harston[2]; James Kennedy[2]; Peter Jezzard[1]; Karla L. Miller[1]; David A. Porter[3]

[1] FMRIB Centre, Nuffield Department of Clinical Neurosciences, University of Oxford, Oxford, UK
[2] Radcliffe Department of Medicine, University of Oxford, Oxford, UK
[3] Fraunhofer Institute for Medical Image Computing MEVIS, Bremen, Germany

Introduction

Single-shot echo-planar imaging

Diffusion-weighted imaging is an important tool in both clinical imaging and neuroscience research. Its widespread use is due to the advent of the single-shot echo-planar imaging (ss-EPI) sequence [1], which is relatively immune to motion-related diffusion-encoding artifacts because all the required data for each image are acquired in a single 'shot' after the diffusion encoding. This insensitivity to motion, particularly cardiac-related brain pulsation, and the ability to rapidly acquire a multi-slice volume are the reasons why, 25 years after it was first introduced [2], spin echo ss-EPI remains the most commonly-used diffusion imaging sequence for the assessment of acute stroke [3] and white matter anisotropy [4]. However, ss-EPI suffers from the well-known geometric distortion artifact as well as the more subtle blurring due to T2* decay of the signal. These issues limit the achievable spatial resolution, particlularly at high field strengths where increased artifact levels directly undermine the goal of improved spatial resolution.

RESOLVE

One approach to overcoming these limitations is to use diffusion-weighted, readout-segmented EPI (RESOLVE) [5] which is becoming established as an alternative to ss-EPI that provides improved image quality in a wide range of clinical applications throughout the body [6-14].

RESOLVE belongs to a family of sequences that have addressed the ghosting and blurring artifacts that arise in multi-shot diffusion imaging due to phase inconsistencies between the shots. RESOLVE measures the motion-related phase caused by the diffusion encoding in a so-called 'navigator' echo acquired at the centre of *k*-space (see Fig. 1A). The navigator phase information is acquired after every shot of the multi-shot image and is used to correct motion-induced phase errors to generate an artifact-free image [15, 16].

A particular advantage of the readout-segmented approach to multi-shot image acquisition [17] (shown in Fig. 1B) is that an efficient 2D non-linear navigator phase correction [18]

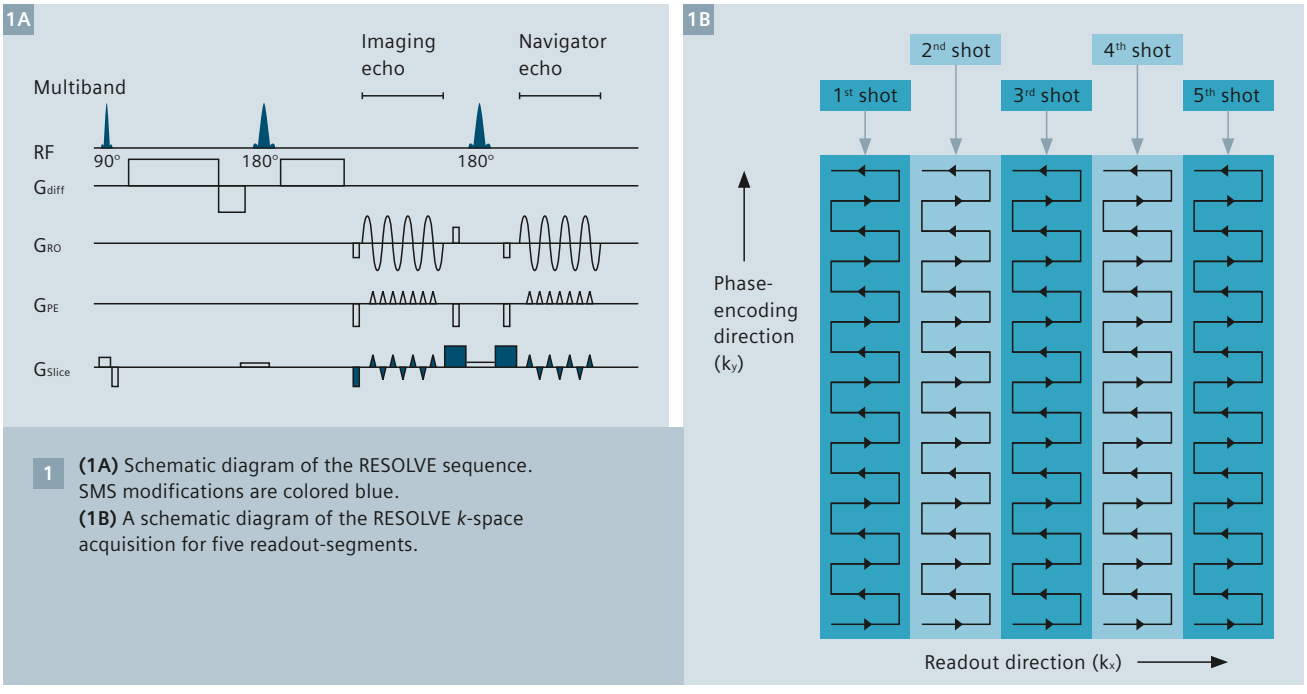

1 **(1A)** Schematic diagram of the RESOLVE sequence. SMS modifications are colored blue. **(1B)** A schematic diagram of the RESOLVE *k*-space acquisition for five readout-segments.

can be used because the *k*-space data sampling fulfils the Nyquist condition, which avoids the confounding effects of aliased signal contributions. A related feature of RESOLVE that is necessary for robust diffusion imaging, is a navigator-based selective reacquisition that identifies shots with particularly severe motion-induced phase corruption and reacquires them [19, 20].

The possibility of multi-shot acquisition with RESOLVE reduces sensitivity to distortion and T2* blurring artifacts in comparison to ss-EPI. Images are less distorted because the phase evolution time between adjacent *k*-space lines (echo-spacing) is shorter and T2* blurring is reduced because the total duration of each shot is shorter. Both features are consequences of acquiring sub-sets of *k*-space in multiple shots or repetition times (TRs) rather than encoding the whole of *k*-space in a single shot. This makes it possible to acquire high-spatial-resolution diffusion-weighted images because the sequence avoids the severe limitations seen with ss-EPI, where there is a trade-off between resolution and the level of geometric distortion and blurring.

RESOLVE can also be combined with GRAPPA [21] to further reduce the effective echo-spacing and readout duration [22]. The reduced duration of the EPI readout with RESOLVE compared to ss-EPI also results in a shorter echo time (TE), which reduces signal loss due to T2 decay; this is particularly significant at ultra-high field strengths, such as 7T, due to the shorter T2 decay times.

Simultaneous multi-slice RESOLVE

Acquiring multiple shots to form each image increases the RESOLVE scan time compared to ss-EPI. Techniques to accelerate the sequence are therefore important for routine clinical use and to increase the number of diffusion-weighted directions for diffusion tensor imaging (DTI) or tractography. Two advances that reduce RESOLVE scan times have recently been demonstrated: 1) readout partial Fourier (PF) acquisition [23] and 2) simultaneous multi-slice (SMS) acceleration [24, 25]. These two techniques are compatible and can, in combination, deliver substantial reductions in the RESOLVE scan time, thereby making whole-brain studies with multiple diffusion directions feasible.

At 7T, radiofrequency (RF) heating constraints often lead to extended scan times and this is exacerbated when acquiring multiple slices simultaneously with SMS acceleration, which, in itself, increases the specific absorption rate (SAR). These effects can be mitigated by using low-SAR 'Power Independent of Number of Slices' (PINS) RF pulses [26], which make SMS acceleration possible at 7T. The PINS technique has therefore been combined with SMS RESOLVE to enable 1 mm isotropic DTI at ultra-high field [27].

The recent work described in this article demonstrates how time-efficient, high-resolution SMS RESOLVE[1] images have important advantages over ss-EPI for clinical stroke imaging and for DTI. In addition, the article shows how the combination of PINS and SMS RESOLVE makes it possible to acquire high-resolution, whole-brain DTI at ultra-high field.

SMS RESOLVE

SMS acquires data from multiple slices together and extracts the slice-specific information using a parallel imaging reconstruction [28]. As fewer slice excitations are required to cover the volume, the TR can be reduced, thereby accelerating the scan and increasing the SNR efficiency. A crucial feature of EPI-based SMS is the blipped-CAIPIRINHA modification that improves SNR by reducing the *g*-factor [29] of the reconstruction, which is achieved by imparting differential in-plane shifts of adjacent slices using slice gradients during the EPI readout [30-33].

The SMS modifications to RESOLVE [24, 25] are shown in Figure 1A (colored blue). Data were acquired on a MAGNETOM Verio 3T and an actively-shielded MAGNETOM 7T[2]. Figure 2 shows examples of SMS RESOLVE images with 26 slices acquired at 3T in 2:14 min with a nominal pixel size of 1 × 1 × 5 mm, an SMS acceleration factor (R_{slice}) of 2 and an in-plane GRAPPA acceleration factor (R_{PE}) of 2; single-shot EPI images acquired in 55 s are provided for comparison.

[1] The product is still under development and not commercially available yet. Its future availability cannot be ensured.

[2] MAGNETOM 7T is ongoing research. All data shown are acquired using a non-commercial system under institutional review board permission. MAGNETOM 7T is still under development and not commercially available yet. Its future availability cannot be ensured.

2

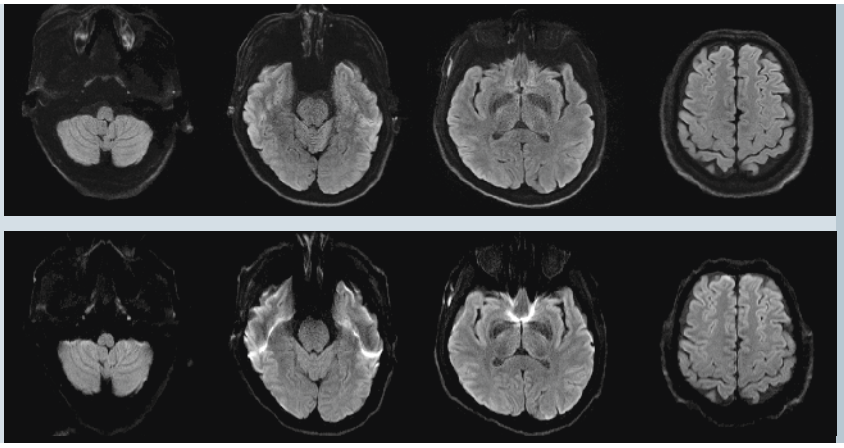

2 Comparison of nominal 1 × 1 × 5 mm resolution trace-weighted images between SMS RESOLVE (top row) and ss-EPI (bottom row) acquired at 3T with 26 slices.

The SMS RESOLVE images show a significant reduction in distortions and T2* blurring compared to the ss-EPI images.

The single-shot EPI images acquired in this study used a routine clinical protocol with a partial Fourier (PF) factor of 6/8 in the phase-encode direction to reduce the echo time (TE) and thereby boost SNR. The images were reconstructed in the standard way using zero-filling (ZF) which creates additional blurring in the phase-encode direction. Despite this blurring, it is standard practice to use ZF with diffusion-weighted ss-EPI because it is more robust than other PF reconstruction algorithms in the presence of motion-induced phase imparted during the diffusion preparation [34].

Comparisons with standard ss-EPI in this study did not use SMS to accelerate the ss-EPI scans. SMS would reduce the scan times and increase the SNR efficiency of the ss-EPI acquisitions, but the image quality, which is the focus of the comparisons, would not be affected.

Clinical stroke imaging with SMS RESOLVE

SMS RESOLVE scans can be a viable clinical alternative to standard ss-EPI DWI for stroke diagnosis, which is typically acquired using an isotropic resolution of around 2 mm. SMS RESOLVE with $R_{slice} = 2$ and $R_{PE} = 2$ can reliably acquire high-quality data at higher resolution with reduced distortion and blurring artifacts. Figure 3 demonstrates the improved image quality provided by SMS RESOLVE with a 1.5 mm isotropic resolution (78 slices) compared to typically-acquired lower-resolution ss-EPI images with $R_{PE} = 2$ and a nominal pixel size of 1.8 × 1.8 × 2 mm with 0.6 mm slice gap (50 slices). The following comparisons (Figs. 4-6) show matched 3:20 min scan times and 1.5 mm isotropic resolution (78 slices) for SMS RESOLVE versus ss-EPI (3 averages) and indicate further potential advantages of using SMS RESOLVE.

3

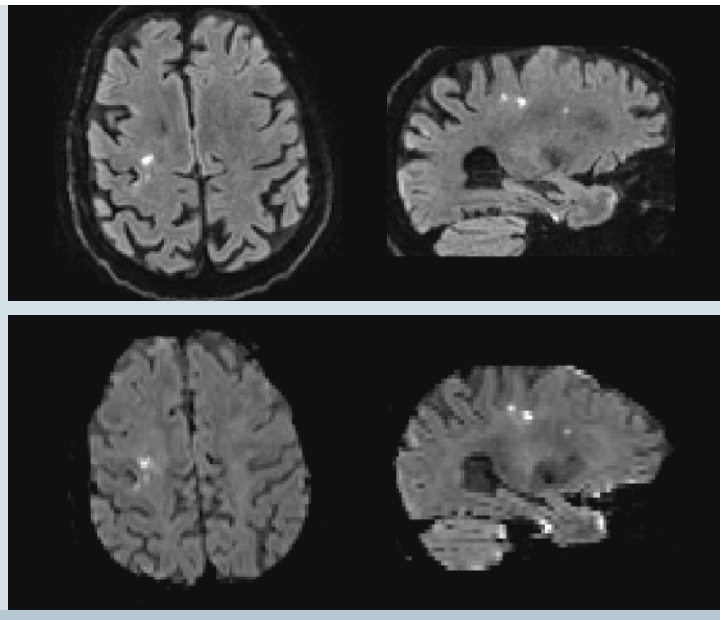

3 Comparison of 1.5 mm isotropic SMS RESOLVE (top row) and 1.8 × 1.8 × 2 mm with 0.6 mm slice gap ss-EPI images (bottom row) acquired at 3T. The images show a right subcortical infarct. The SMS RESOLVE and ss-EPI scans acquired 78 and 50 slices, respectively.

Reduced distortion artifact confounds

SMS RESOLVE has fewer confounding 'signal pile-up' artifacts caused by distortion, in the posterior fossa, brainstem and in proximity to the sinuses, especially the frontal sinus. The improvements are especially apparent in Figures 4 and 5, which show the similarity in appearance of infarcts and signal pile-up artifact in the ss-EPI images. Suppressing these artifacts in the SMS RESOLVE images improves the recognition of regions of true restricted diffusion.

Improved quantification of infarct volume

Previous clinical imaging studies in stroke [10] and of pelvic tumors in radiotherapy planning applications [12] have confirmed that RESOLVE provides an improved geometric distortion performance when compared to ss-EPI; similar benefits are to be expected when SMS RESOLVE images are used to estimate infarct volume in acute stroke. The importance of accurately tracking infarct volume in acute stroke imaging has recently been identified in the Acute Stroke Imaging Research Roadmap II [35]. However, the accuracy of quantifying infarct volume from standard ss-EPI images is limited by the substantial distortion and blurring artifacts. In particular, subtle injuries depicted in Figure 6 are better defined in the SMS RESOLVE images.

7T DTI with PINS SMS RESOLVE

RESOLVE DWI becomes more advantageous at higher resolution because the corresponding ss-EPI acquisitions require an increase in both the echo-spacing and the number of echoes to increase resolution along the readout and phase-encoding axes respectively; this results in a substantial increase in the level of distortion and T2* blurring. These effects become particularly significant at 7T due to amplification of susceptibility and reduced relaxation times. In the case of RESOLVE, the higher resolution in the readout direction is achieved by increasing the number of readout segments, or shots, without a change in echo spacing and only the number of echoes is increased; in this case, there is no increase in distortion at higher resolution and T2* blurring is substantially less than in the ss-EPI case.

However, the technical capability to perform DWI with small voxel sizes and

4A

SMS RESOLVE

ss-EPI

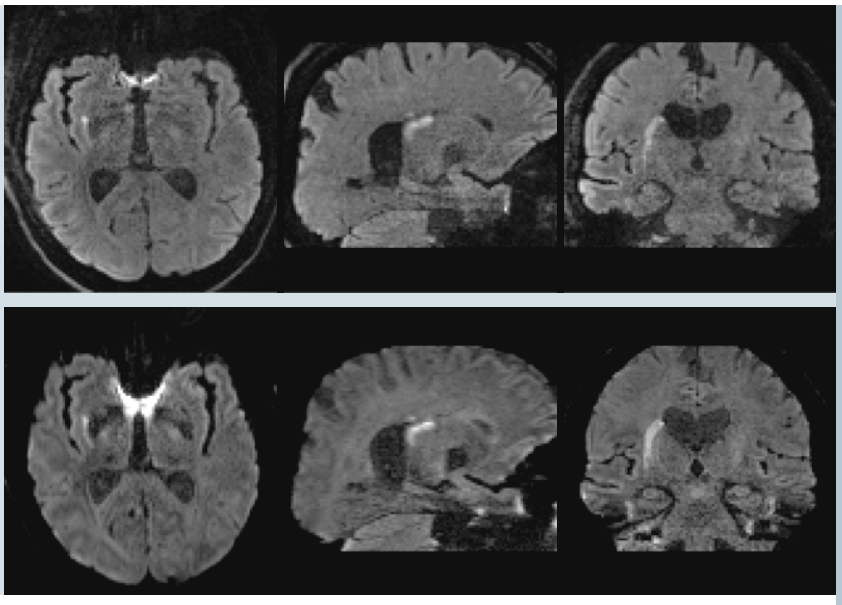

4B

SMS RESOLVE

ss-EPI

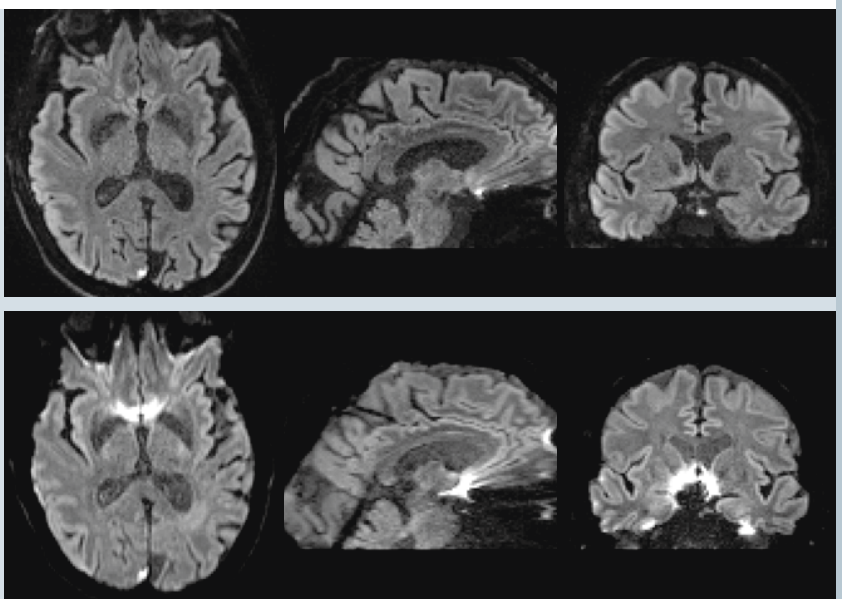

4 Comparison of 1.5 mm isotropic SMS RESOLVE (top row) and ss-EPI images (bottom row) acquired at 3T highlighting the reduction of signal pile up artifact caused by geometric distortions. Panel **(4A)** shows a right lenticulostriate artery infarct and panel **(4B)** shows a right occipital infarct. 78 slices were acquired in both scans.

5

SMS RESOLVE

ss-EPI

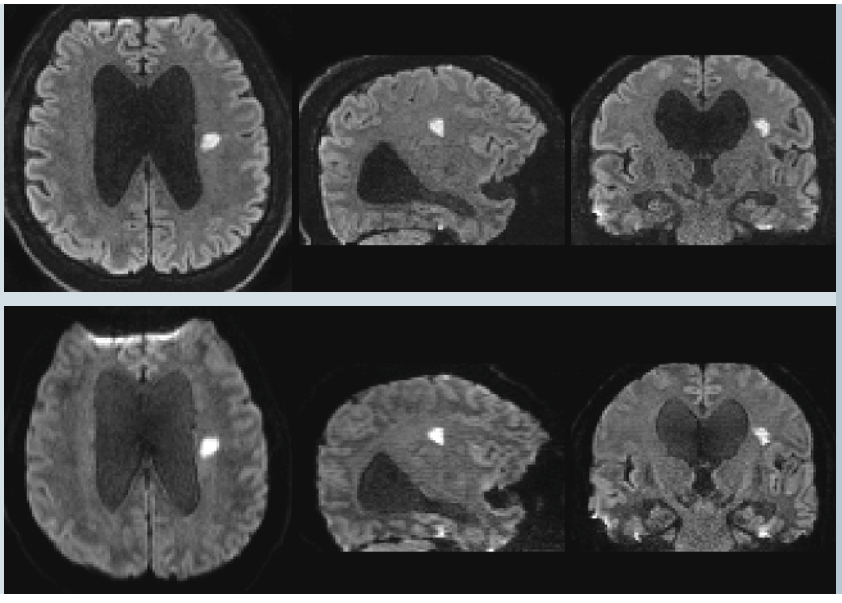

5 Comparison of 1.5 mm isotropic SMS RESOLVE (top row) and ss-EPI images (bottom row) acquired at 3T highlighting the reduction of geometric distortion in proximity to the frontal sinuses. The images show a left lacunar infarct. 78 slices were acquired in both scans.

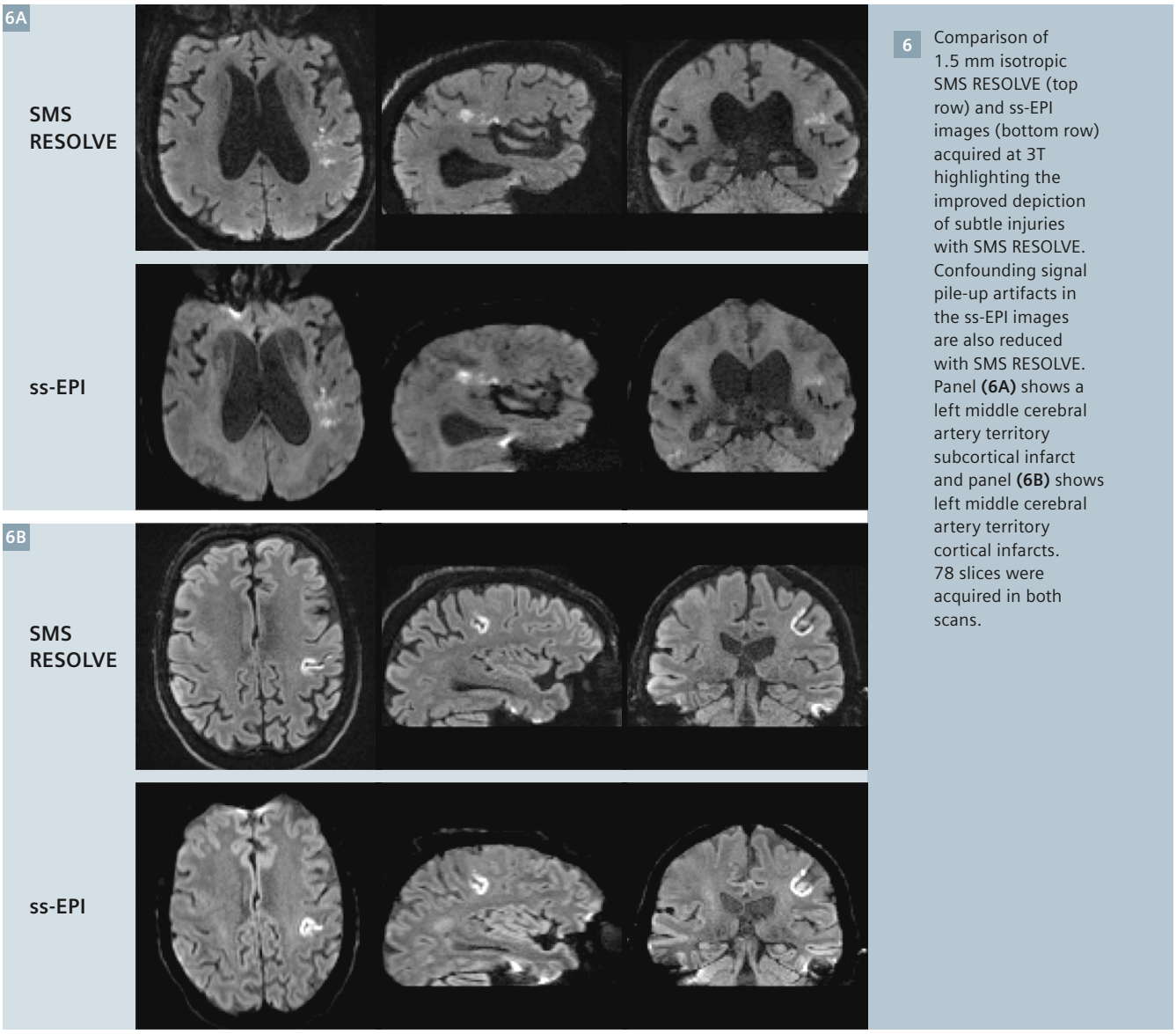

6 Comparison of 1.5 mm isotropic SMS RESOLVE (top row) and ss-EPI images (bottom row) acquired at 3T highlighting the improved depiction of subtle injuries with SMS RESOLVE. Confounding signal pile-up artifacts in the ss-EPI images are also reduced with SMS RESOLVE. Panel **(6A)** shows a left middle cerebral artery territory subcortical infarct and panel **(6B)** shows left middle cerebral artery territory cortical infarcts. 78 slices were acquired in both scans.

a low level of T2* blurring is compromised by the corresponding reduction in SNR, which is already inherently low in DWI due to signal attenuation at high b-value. For isotropic resolution with a small slice thickness, SNR efficiency is further reduced by the requirement to use long TR times to accommodate the increased number of slices. Strategies for increasing SNR and maximising acceleration therefore have an important role to play when using RESOLVE to perform high-resolution DTI.

One way to meet these goals is to perform imaging studies at higher B_0 field strength, where there is increased SNR and improved performance of parallel imaging because the coil sensitivities are more distinct [36]. There are however a number of additional challenges at 7T, including B_0 and RF inhomogeneity, SAR constraints and shorter T2 values than at lower field strengths. The combination of PINS and SMS RESOLVE has the potential to meet these challenges and provide a technique that can exploit the potential benefits of diffusion-weighted imaging at 7T. In particular, the shortened readout time reduces distortion, T2* blurring and the effects of signal loss due to T2 decay, and the low-SAR PINS RF pulses allow high slice-acceleration factors to be used with low TR, resulting in high SNR efficiency.

SMS RESOLVE at 7T

As shown previously in studies without SMS, the RESOLVE acquisition scheme is inherently less sensitive to the very high level of B_0 distortion and T2* blurring that affects ss-EPI at 7T [37]. Figure 7 demonstrates how these benefits can also be seen when the technique is combined with slice acceleration to reduce scan time; the figure compares 1.2 mm isotropic SMS RESOLVE images using $R_{slice} = 3$ and $R_{PE} = 2$ with standard ss-EPI images (also with $R_{PE} = 2$). The SMS RESOLVE scan with 99 slices was acquired with 6 segments (6/7 readout PF), 0.32 ms echo-spacing, 32 b = 1000 s/mm² diffusion directions, and with 4 interspersed low-b-value images in 35 min. A consequence of the

7

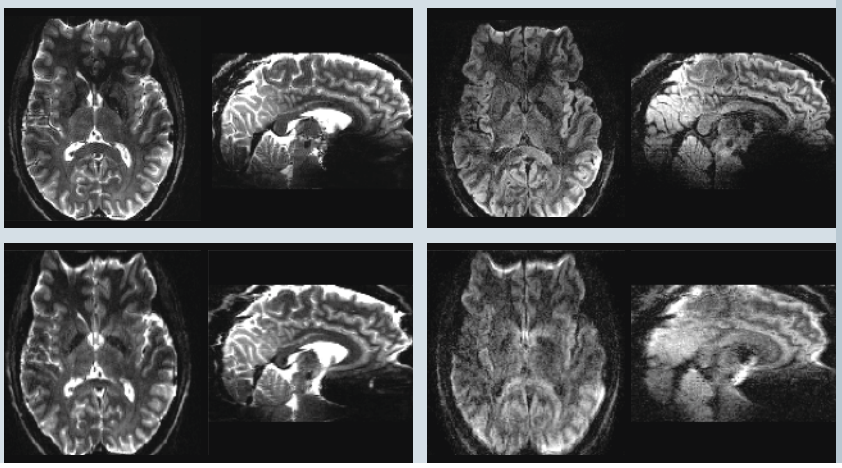

7 Comparison of 1.2 mm isotropic SMS RESOLVE (top row) and ss-EPI images (bottom row) acquired at 7T (99 slices) highlighting the reduction of geometric distortion and blurring with SMS RESOLVE.

8

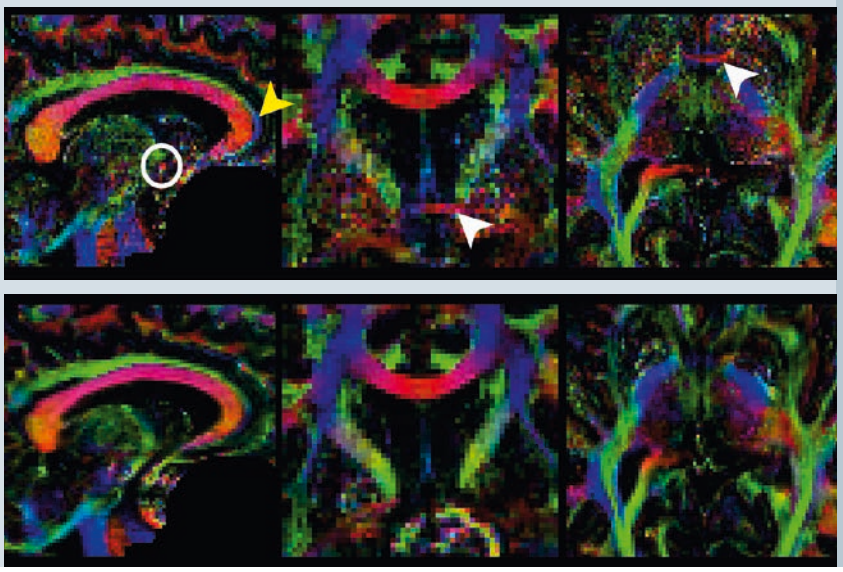

8 7T DTI results comparing blurring and distortion in 1.2 mm isotropic SMS RESOLVE and ss-EPI acquisitions with 99 slices. Color-coded maps of the principal diffusion direction weighted by the fractional anisotropy are shown. The SMS RESOLVE data show the anterior commissure (white circle and arrows), which is not present in the ss-EPI data. SMS RESOLVE also exhibits reduced blurring and distortion in the cingulum (yellow arrow). Color code: green, anterior–posterior; blue, superior–inferior; red, left–right.

artifact reduction is highlighted in the color-coded principal diffusion direction (PDD) maps weighted by the fractional anisotropy (FA) of Figure 8. The thin anterior commissure tract is missing in the ss-EPI data (in both the matched slice and the surrounding slices) because it is in a region of high distortion but it is clearly visualised in the SMS RESOLVE images. However, in this first proof of principle, the SMS RESOLVE data utilized standard (non-PINS) RF pulses, which resulted in SAR limitations that necessitated an increased TR, and, as such, the ideal 3-fold scan time reduction could not be achieved.

PINS SMS RESOLVE at 7T

PINS RF pulses directly address the SAR restriction that otherwise limits the SMS

9

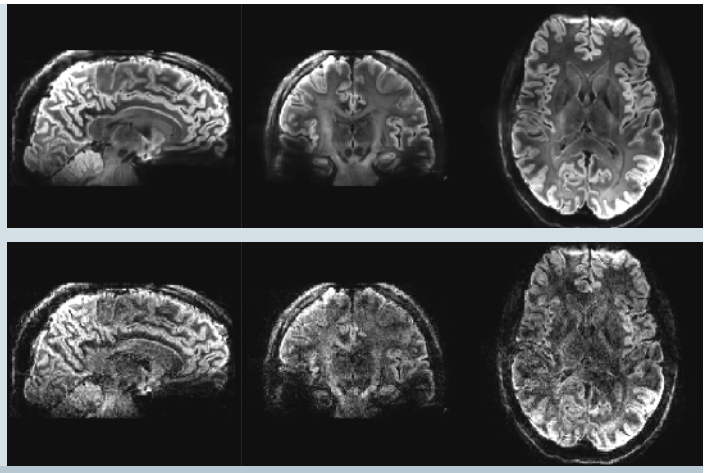

9 1.2 mm isotropic PINS SMS RESOLVE images (99 slices) acquired at 7T with b = 800 s/mm². The mean of 80 diffusion directions (top row) and a single diffusion direction are shown (bottom row).

scan-time reduction that can be realized at 7T. Figure 9 shows 1.2 mm isotropic images with 99 slices acquired using PINS SMS RESOLVE [27] with 80 diffusion-gradient directions and 12 averages with low b-value in a scan time of 38 minutes; the data were acquired without readout partial Fourier using $R_{slice} = 3$, $R_{PE} = 2$, five readout segments, an echo-spacing of 0.38 ms and b = 800 s/mm^2; the figure shows the mean of all the diffusion-weighted images and data from a single diffusion direction. The color-coded PDD FA map in Figure 10 highlights the fine tract resolution and good contrast of these data.

Figure 11 shows data from a PINS SMS RESOLVE scan with 1 mm isotro-

10

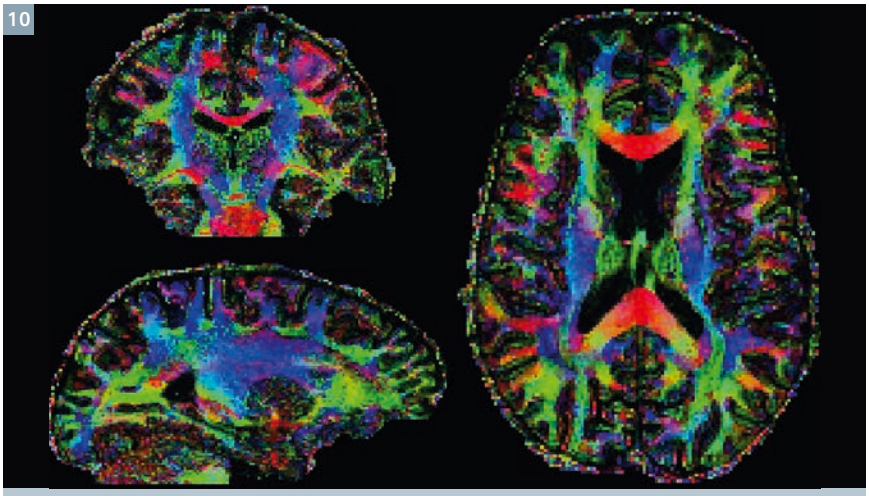

10 7T DTI results of a 1.2 mm isotropic PINS SMS RESOLVE acquisition (99 slices) demonstrating fine resolution and good contrast of the anisotropy. Color-coded maps of the principal diffusion direction weighted by the fractional anisotropy are shown. Color code: green, anterior–posterior; blue, superior–inferior; red, left–right.

11

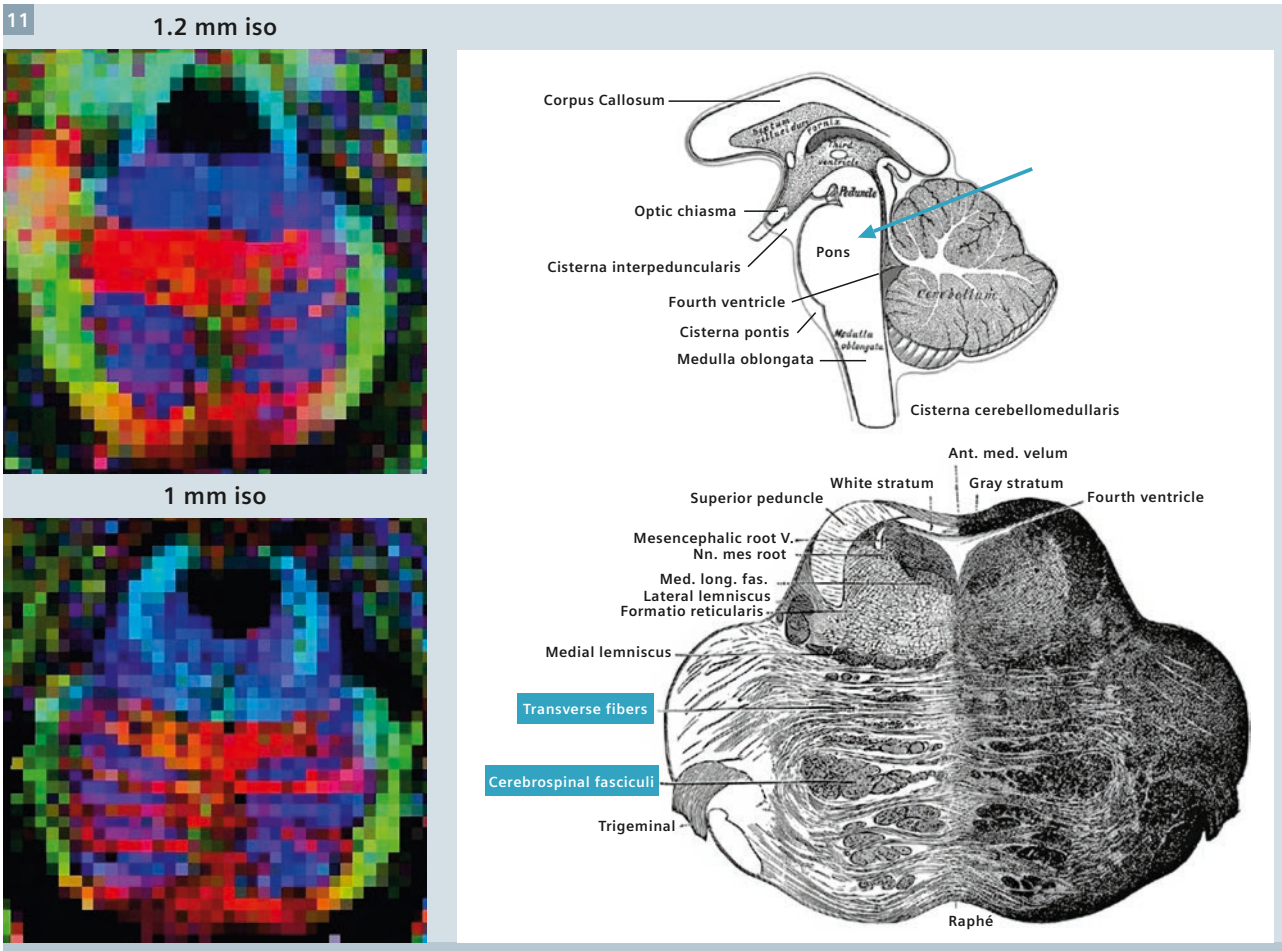

11 7T DTI results comparing 1.2 mm and 1 mm isotropic PINS SMS RESOLVE acquisitions. The thin transverse pontocerebellar fibers are more clearly resolved in the 1 mm isotropic images (in a different healthy volunteer). The transverse pontocerebellar fibers (running right-left, colored red) interdigitate with the cerebrospinal fasciculi (running superior-inferior, colored blue). The 1.2 mm and 1 mm acquisitions acquired 99 and 117 slices, respectively. Color-coded maps of the principal diffusion direction weighted by the fractional anisotropy are shown. Color code: green, anterior–posterior; blue, superior–inferior; red, left–right. *The anatomical drawings are adaped from Gray's Anatomy (1918).*

12

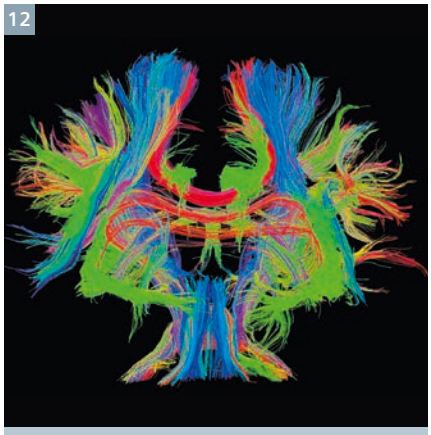

12 7T tractography generated from 1 mm isotropic PINS SMS RESOLVE data with 117 slices. Color code: green, anterior–posterior; blue, superior–inferior; red, left–right.

pic resolution and 117 slices in a scan time of 45 minutes; the images were acquired with $R_{slice} = 3$, $R_{PE} = 2$ using 3 readout segments (3/5 readout PF), an echo spacing of 0.40 ms, 60 scans at b = 580 s/mm², 60 scans at b = 1160 s/mm² and 13 scans with low b-value. This, in comparison with the 1.2 mm isotropic data suggests potential advantages of high-resolution DTI by showing improved depiction (in a different subject) of the transverse pontocerebellar fibers (running right-left) that interdigitate with the cerebrospinal fasciculi (running superior-inferior). An example of whole-brain tractography with the 1 mm isotropic data is shown in Figure 12. This image was generated using the Diffusion Toolkit and TrackVis [38].

In summary, PINS RF pulses make it possible to acquire high-resolution RESOLVE at 7T with a slice-acceleration factor of three; this enables acquisition protocols with a large number of diffusion directions and multiple b-value shells with acquisition times that are acceptable for neuroscientific applications. Data sets of this type provide valuable input for advanced tractography analyses that probe secondary fiber populations. The preliminary results acquired with the technique suggest that the SMS RESOLVE sequence could become a powerful tool for *in vivo* tractography of fine structure.

Other applications of SMS RESOLVE

In addition to the brain imaging applications reported in this paper, preliminary work reported elsewhere has shown that SMS RESOLVE can provide data for combined tractography studies of the brain and cervical spine [39]. Studies of this type are not possible with ss-EPI due to the high level of susceptibility-based distortion around the spinal cord. The SMS RESOLVE technique has also been applied to diffusion-weighted breast imaging of healthy volunteers, demonstrating acquisitions with reduced acquisition times with potential application in clinical studies of breast tumors [40], where the standard RESOLVE technique has been shown to provide a clinical benefit [8].

As an alternative to the SMS RESOLVE technique described in this paper, a simultaneous, multi-slab acquisition method has also been proposed, in which a 3D-encoded version of the RESOLVE sequence [41] is used to simultaneously encode data in multiple slabs [42].

Conclusion

The results shown in this paper demonstrate that SMS RESOLVE makes it possible to perform diffusion-weighted imaging of the whole brain with isotropic resolution and shortened scan times that are suitable for clinical stroke protocols. The improved image quality compared to ss-EPI provides a clearer depiction of infarcts with fewer confounding susceptibility artifacts and the reduction in geometrical distortion is expected to provide a more accurate quantification of lesion volume.

This paper has also shown how the SMS RESOLVE technique can be combined with PINS RF pulses to exploit slice-acceleration at 7T without the constraints of high SAR, making it possible to acquire high-quality data sets for advanced tractography studies which require a large number of diffusion-gradient directions. The technique also promises to enhance clinical diffusion-weighted imaging at 7T, for which preliminary studies with the standard RESOLVE technique are producing promising results [43].

SMS RESOLVE is an appealing alternative to standard ss-EPI DWI with potential benefits for clinical and scientific applications in the brain and other organs. The clinical benefit of the standard RESOLVE technique has been established in a large number of studies, but there is typically an acquisition-time penalty relative to lower-quality image acquisitions with ss-EPI. This limitation is much less prohibitive when RESOLVE is combined with SMS and readout PF to accelerate the scans and this combination increases the potential of the technique to substantially improve the quality of diffusion-weighted imaging in a wide variety of applications.

Acknowledgements

We thank the NIHR Oxford Biomedical Research Centre and the Medical Research Council for funding. PK acknowledges funding by the Wellcome Trust [WT100092MA]. We are also grateful for funding to the NIHR Clinical Research Network, the Dunhill Medical Trust [grant number: OSRP1/1006] and the Centre of Excellence for Personalized Healthcare funded by the Wellcome Trust and Engineering and Physical Sciences Research Council [grant number: WT088877/Z/09/Z]. We thank Thorsten Feiweier of Siemens Healthcare for the diffusion preparation module used in this work. We also thank Juliet Semple and Peter Manley for assistance with data acquisition and are grateful for the facilities provided by the Oxford Acute Vascular Imaging Centre (AVIC).

References

1 Mansfield P, Pykett IL. Biological and medical imaging by NMR Journal of Magnetic Resonance (1969) 1978;29:355–373.
2 Turner R, Le Bihan D, Maier J, Vavrek R, Hedges LK, Pekar J. Echo-planar imaging of intravoxel incoherent motion. Radiology 1990;177:407–414.
3 Warach S, Gaa J, Siewert B, Wielopolski P, Edelman RR. Acute human stroke studied by whole brain echo planar diffusion-weighted magnetic resonance imaging. Ann Neurol 1995;37:231–241.
4 Basser PJ, Mattiello J, LeBihan D.

Estimation of the effective self-diffusion tensor from the NMR spin echo. J Magn Reson B 1994;103:247–254.
5 Porter DA, Heidemann RM. High resolution diffusion-weighted imaging using readout-segmented echo-planar imaging, parallel imaging and a two-dimensional navigator-based reacquisition. Magn Reson Med 2009;62:468–475.
6 Hayes LL, Jones RA, Palasis S, Aguilera D, Porter DA. Drop metastases to the pediatric spine revealed with diffusion-weighted MR imaging. Pediatr Radiol 2012;42:1009–1013.
7 Rumpel H, Chong Y, Porter DA, Chan LL. Benign versus metastatic vertebral compression fractures: combined diffusion-weighted MRI and MR spectroscopy aids differentiation. Eur Radiol 2013;23:541–550.
8 Bogner W, Pinker-Domenig K, Bickel H, Chmelik M, Weber M, Helbich TH, Trattnig S, Gruber S. Readout-segmented Echo-planar Imaging Improves the Diagnostic Performance of Diffusion-weighted MR Breast Examinations at 3.0 T Radiology 2012;263:64–76.
9 Wisner DJ, Rogers N, Deshpande VS, Newitt DN, Laub GA, Porter DA, Kornak J, Joe BN, Hylton NM. High-resolution diffusion-weighted imaging for the separation of benign from malignant BI-RADS 4/5 lesions found on breast MRI at 3T Journal of Magnetic Resonance Imaging 2014;40:674–681.
10 Morelli J, Porter D, Ai F, Gerdes C, Saettele M, Feiweier T, Padua A, Dix J, Marra M, Rangaswamy R, Runge V. Clinical evaluation of single-shot and readout-segmented diffusion-weighted imaging in stroke patients at 3 T. Acta Radiol 2013;54:299–306.
11 Thian YL, Xie W, Porter DA, Weileng Ang B. Readout-segmented echo-planar imaging for diffusion-weighted imaging in the pelvis at 3T-A feasibility study. Acad Radiol 2014;21:531–537.
12 Foltz WD, Porter DA, Simeonov A, Aleong A, Jaffray D, Chung P, Han K, Ménard C. Readout-segmented echo-planar diffusion-weighted imaging improves geometric performance for image-guided radiation therapy of pelvic tumors Radiotherapy and Oncology.
13 Tokoro H, Fujinaga Y, Ohya A, Ueda K, Shiobara A, Kitou Y, Ueda H, Kadoya M. Usefulness of free-breathing readout-segmented echo-planar imaging (RESOLVE) for detection of malignant liver tumors: comparison with single-shot echo-planar imaging (SS-EPI). Eur J Radiol 2014;83:1728–1733.
14 Friedli I, Crowe LA, Viallon M, Porter DA, Martin P, de Seigneux S, Vallee J. Improvement of renal diffusion-weighted magnetic resonance imaging with readout-segmented echo-planar imaging at 3T. Magn Reson Imaging 2015;33:701–708.
15 Ordidge RJ, Helpern JA, Qing ZX, Knight RA, Nagesh V. Correction of motional artifacts in diffusion-weighted MR images using navigator echoes. Magn Reson Imaging 1994;12:455–460.
16 Anderson AW, Gore JC. Analysis and correction of motion artifacts in diffusion weighted imaging. Magn Reson Med 1994;32:379–387.
17 Robson MD, Anderson AW, Gore JC. Diffusion-weighted multiple shot echo planar imaging of humans without navigation. Magn Reson Med 1997;38:82–88.
18 Miller KL, Pauly JM. Nonlinear phase correction for navigated diffusion imaging. Magn Reson Med 2003;50:343–353.
19 Nguyen Q, Clemence M, Ordidge RJ. The use of intelligent re-acquisition to reduce scan time in MRI degraded by motion. In: Proceedings of the 6th Annual Meeting of ISMRM, 1998 (abstract 134).
20 Porter DA. 2D-navigator-based re-acquisition for motion artefact suppression in multi-shot, diffusion-weighted imaging. In: Proceedings of the 14th Annual Meeting of ISMRM, 2006 (abstract 1047).
21 Griswold MA, Jakob PM, Heidemann RM, Nittka M, Jellus V, Wang J, Kiefer B, Haase A. Generalized autocalibrating partially parallel acquisitions (GRAPPA). Magn Reson Med 2002;47:1202–1210.
22 Porter DA, Heidemann RM. Multi-shot, diffusion-weighted imaging at 3T using readout-segmented EPI and GRAPPA In: Proceedings of the 14th Annual Meeting of ISMRM, Seattle, Washington, USA, 2006 (abstract 1046).
23 Frost R, Porter DA, Miller KL, Jezzard P. Implementation and assessment of diffusion-weighted partial Fourier readout-segmented echo-planar imaging. Magn Reson Med 2012;68:441–451.
24 Frost R, Porter DA, Douaud G, Jezzard P, Miller KL. Reduction of diffusion-weighted readout-segmented EPI scan time using a blipped-CAIPI modification. In: Proceedings of the 20th Annual Meeting of ISMRM, 2012 (abstract 116).
25 Frost R, Jezzard P, Douaud G, Clare S, Porter DA, Miller KL. Scan time reduction for readout-segmented EPI using simultaneous multislice acceleration: Diffusion-weighted imaging at 3 and 7 tesla. Magn Reson Med 2015;74:136–149.
26 Norris DG, Koopmans PJ, Boyacioglu R, Barth M. Power Independent of Number of Slices (PINS) radiofrequency pulses for low-power simultaneous multislice excitation. Magn Reson Med 2011;66:1234–1240.
27 Koopmans PJ, Frost R, Porter DA, Wu W, Jezzard P, Miller KL, Barth M. Diffusion-weighted readout-segmented EPI using PINS simultaneous multislice imaging. In: Proceedings of the 23rd Annual Meeting of ISMRM, 2015 (abstract 959).
28 Larkman DJ, Hajnal JV, Herlihy AH, Coutts GA, Young IR, Ehnholm G. Use of multicoil arrays for separation of signal from multiple slices simultaneously excited. J Magn Reson Imaging 2001;13:313–317.
29 Pruessmann KP, Weiger M, Scheidegger MB, Boesiger P. SENSE: sensitivity encoding for fast MRI. Magn Reson Med 1999;42:952–962.
30 Breuer FA, Blaimer M, Heidemann RM, Mueller MF, Griswold MA, Jakob PM. Controlled aliasing in parallel imaging results in higher acceleration (CAIPIRINHA) for multi-slice imaging. Magn Reson Med 2005;53:684–691.
31 Nunes RG, Hajnal JV, Golay X, Larkman DJ. Simultaneous slice excitation and reconstruction for single shot EPI. In: Proceedings of the 14th Annual Meeting of ISMRM, 2006 (abstract 293).
32 Setsompop K, Cohen-Adad JA, McNab JA, Gagoski B, Wedeen VJ, Wald LL. Improving SNR per unit time in diffusion Imaging using a blipped-CAIPIRINHA simultaneous multi-slice EPI acquisition. In: Proceedings of the 18th Annual Meeting of ISMRM, 2010 (abstract 187).
33 Setsompop K, Gagoski BA, Polimeni JR, Witzel T, Wedeen VJ, Wald LL. Blipped-controlled aliasing in parallel imaging for simultaneous multislice echo planar imaging with reduced g-factor penalty. Magn Reson Med 2012;67:1210–1224.
34 Robson MD, Porter DA. Reconstruction as a source of artifact in non-gated single-shot diffusion-weighted EPI. Magn Reson Imaging 2005;23:899–905.
35 Wintermark M, Albers GW, Broderick JP, Demchuk AM, Fiebach JB, Fiehler J, Grotta JC, Houser G, Jovin TG, Lees KR, Lev MH, Liebeskind DS, Luby M, Muir KW, Parsons MW, von Kummer R, Wardlaw JM, Wu O, Yoo AJ, Alexandrov AV, Alger JR, Aviv RI, Bammer R, Baron J, Calamante F, Campbell BCV, Carpenter TC, Christensen S, Copen WA, Derdeyn CP, Haley ECJ, Khatri P, Kudo K, Lansberg MG, Latour LL, Lee T, Leigh R, Lin W, Lyden P, Mair G, Menon BK, Michel P, Mikulik R, Nogueira RG, Ostergaard L, Pedraza S, Riedel CH, Rowley HA, Sanelli PC, Sasaki M, Saver JL, Schaefer PW, Schellinger PD, Tsivgoulis G, Wechsler LR, White PM, Zaharchuk G, Zaidat OO, Davis SM, Donnan GA, Furlan AJ, Hacke W, Kang D, Kidwell C, Thijs VN, Thomalla G, Warach SJ. Acute Stroke Imaging Research Roadmap II. Stroke 2013;44:2628–2639.
36 Wiesinger F, Van de Moortele P, Adriany G, De Zanche N, Ugurbil K, Pruessmann KP. Potential and feasibility of parallel MRI at high field NMR in Biomedicine 2006;19:368–378.
37 Heidemann RM, Porter DA, Anwander A, Feiweier T, Heberlein K, Knosche TR, Turner R. Diffusion imaging in humans at 7T using readout-segmented EPI and

GRAPPA. Magn Reson Med 2010;64:9–14.
38 Wang R, Benner T, Sorensen AG, Wedeen VJ. Diffusion Toolkit: a software package for diffusion imaging data processing and tractography. In: Proceedings of the 15th Annual Meeting of ISMRM, 2007 (abstract 3720).
39 Liu W, Bhat H, Cohen-Adad J, Setsompop K, Wang D, Beck T, Cauley SF, Zhou K, Porter DA. Large-FOV tractography of the brain and spinal cord with reduced scan time: a study using diffusion-weighted readout-segmented EPI and simultaneous multi-slice acceleration In: Proceedings of the 23rd Annual Meeting of ISMRM, 2015 (abstract 4434).
40 Liu W, Bhat H, Weiland E, Wang D, Beck T, Cauley SF, Porter DA. Readout-segmented EPI with simultaneous, multi-slice acceleration for the rapid acquisition of high-resolution, diffusion-weighted images of the breast In: Proceedings of the 23rd Annual Meeting of ISMRM, 2015 (abstract 1605).
41 Frost R, Miller KL, Tijssen RHN, Porter DA, Jezzard P. 3D Multi-slab diffusion-weighted readout-segmented EPI with real-time cardiac-reordered k-space acquisition. Magn Reson Med 2014;72:1565–1579.
42 Frost R, Jezzard P, Porter DA, Tijssen RHN, Miller KL. Simultaneous multi-slab acquisition in 3D multi-slab diffusion-weighted readout-segmented echo-planar imaging. In: Proceedings of the 21st Annual Meeting of ISMRM, 2013 (abstract 3176).
43 Bogner W, Pinker K, Zaric O, Baltzer P, Minarikova L, Porter D, Bago-Horvath Z, Dubsky P, Helbich TH, Trattnig S, Gruber S. Bilateral diffusion-weighted MR imaging of breast tumors with submillimeter resolution using readout-segmented echo-planar imaging at 7 T. Radiology 2015;274:74–84.

Contact

Dr. Robert Frost
FMRIB Centre
John Radcliffe Hospital
Oxford OX3 9DU
UK
robert.frost@ndcn.ox.ac.uk

Learn more!

Don't miss the talks of experienced and renowned experts on all aspects of MR imaging at:

www.siemens.com/magnetom-world

Multislice accelerated RESOLVE for time-efficient, high-resolution diffusion imging

Robert Frost, PhD
FMRIB Centre, University of Oxford

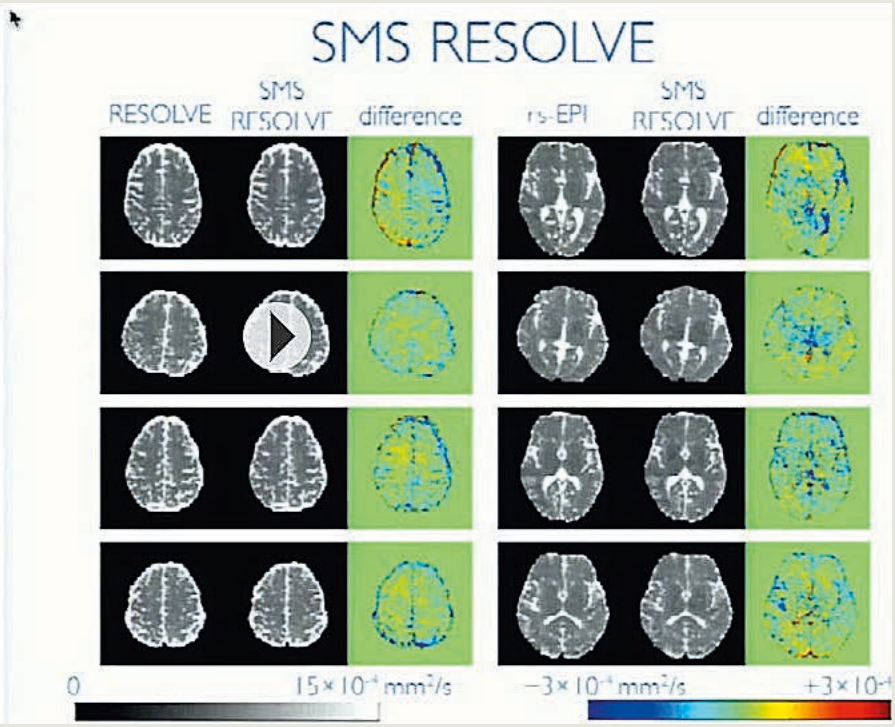

Simultaneous Multi-Slice (Slice Accelerated) Diffusion EPI: Early Experience for Brain Ischemia and Cervical Lymphadenopathy

Val M. Runge, M.D.[1]; Johannes K. Richter, M.D.[2]; Markus Klarhöfer, Ph.D.[3]; Thomas Beck, Ph.D.[4]; Johannes T. Heverhagen, M.D.[1]

[1] Department of Diagnostic, Interventional and Pediatric Radiology, University Hospital of Bern, Inselspital, Bern, Switzerland
[2] Clinics for Neuroradiology, University Hospital Zurich, Switzerland
[3] Siemens Healthcare, Zurich, Switzerland
[4] Siemens Healthcare, Erlangen, Germany

Introduction

In single shot EPI, the entirety of *k*-space is traversed after one shot (excitation). Readout-segmentation acquires *k*-space in multiple shots for reduced TE and encoding time. Real-time reacquisition of unusable shots is also supported. The result is markedly improved image quality, with reduced susceptibility artifact and image blur. The challenge with this approach, termed RESOLVE, is the longer scan time, which scales with the number of readout segments. Here slice acceleration (simultaneous multi-slice) can play a very important role, to reduce scan time, when applied in combination with RESOLVE.

Simultaneous multi-slice (SMS) accelerated diffusion-weighted echo planar imaging employs an innovative acquisition and reconstruction scheme that allows multiple slices to be acquired simultaneously [1-4]. The approach offers a substantial decrease in image acquisition time, or alternatively improved spatial / diffusion resolution. The advent of this technique is analogous to that years ago of 2D multi-slice, and as such may represent one of the major innovations in this decade for MRI with widespread clinical utility. This short article covers briefly the theory behind the approach, advantages and limitations, and applications in the brain and the soft tissues of the neck using clinical cases.

Method

The breadth of capabilities and current limitations with SMS diffusion EPI in brain imaging are illustrated at 3T. In this approach (provided as a works-in-progress software package[1]), multiple slices are acquired simultaneously using blipped-CAIPIRINHA technique with the individual slices then reconstructed using a slice-GRAPPA method. Slice acceleration with axial imaging, as applied, requires a phased array coil with sufficient elements in the z-direction, which in this instance was accomplished by use of a 32-channel head coil.

For slice acceleration, the RF excitation is modified, to excite multiple slices simultaneously, and during readout, phase-blips are applied to shift / alias simultaneously excited slices. Aliased slices are separated during reconstruction using a slice-GRAPPA approach, with a high-quality slice separation requiring an appropriate multi-element coil. SMS acceleration allows more slices per TR or TR to be reduced with the same slice coverage. Potentially there is no SNR loss due to undersampling, and the *g*-factor penalty is reduced by employing gradient-based CAIPIRINHA.

[1] The product is still under development and not commercially available yet. Its future availability cannot be ensured.

Case 1

Slice acceleration with RESOLVE for decreased scan time. The patient presented with both Broca's (motor) and Wernicke's (sensory) aphasia, together with transient weakness of the right hand. A large early subacute infarct is seen in the left middle cerebral artery and watershed territories. With an acceleration factor of 2, the scan time is reduced by 1 minute (from 3:08 to 2:06 min:sec), with no loss in image quality. Indeed, the resultant image has less blur.

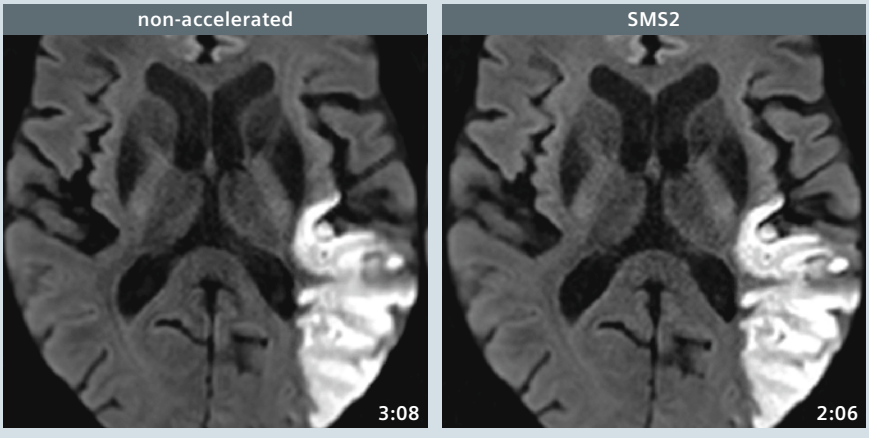

Case 2

Slice acceleration with RESOLVE to achieve a thinner axial section. This is the same patient as illustrated in case 1, but at a higher level showing scattered punctate early subacute infarcts in the cortex and deep white matter of the parietal lobe. By moving to a 2 mm slice (not possible without slice acceleration due to the long scan time), the small pinpoint infarcts that are present are better seen (black arrows), and some revealed for the first time (white arrow). Scan times are given in the lower right hand corner of each image, with complete coverage of the brain in each instance (30 slices with a 4 mm thickness vs. 60 slices with a 2 mm thickness).

For 2D diffusion-weighted imaging (DWI) of the brain, TR is typically ≈ 6000 msec. However a reduction to 3500 does not impact substantially image quality or signal-to-noise ratio (SNR). Making use of the possibility to shorten TR expands the potential of SMS accelerated imaging, whether slice thickness is maintained or reduced. Specifically, SMS acceleration can be used in clinical brain DWI in this manner to either shorten scan time or to allow thinner sections covering the entire brain within a reasonable acquisition time.

Depending upon level of the brain, likely coil dependent, SNR results vary. Near the vertex, SNR was essentially equivalent for all scans. At the level of the lateral ventricles, mild decreases in SNR were seen that could be attributable not only to the decrease in TR and slice thickness, but also to the number of simultaneously excited slices (*g*-factor of the coil). When comparing the standard 4 mm single shot scan, to the SMS acceleration 3, 2 mm, short TR scan, the decrease in SNR was 27%, likely primarily due to the thinner slice.

The combination of the readout segmented approach (RESOLVE) with slice acceleration (SMS RESOLVE) provides images with markedly reduced bulk susceptibility effect as well as image blur, with 2 mm slices through the entire brain, in a relatively short scan time. Alternatively, if the slice thickness is kept at 4 mm – the standard for clinical imaging of the brain at 3T, scan time is reduced by a third, in the approach implemented. Not evaluated, but extremely simple and of substantial clinical value, would be the use of slice acceleration to acquire a higher number of b-values in the same scan time.

Similarly, SMS RESOLVE can be applied in the neck, provided a sufficient number of coil elements are present in the slice direction. Here, with a 3 mm slice thickness, the primary application would be for a reduction in scan time.

Conclusion

The utility of SMS in combination with RESOLVE is demonstrated in cerebral ischemia, by allowing – with equivalent image quality – scan acquisition time to be shortened or slice thickness to be reduced [5]. A reduction in scan time was also demonstrated for imaging of the soft tissues of the neck. SMS RESOLVE with slice acceleration 2 led to a scan time reduction from 3:08 (min:sec) to 2:06, with the reference scan acquisition implemented (in the current works-in-progress package) preventing a true factor of 2 reduction in scan time. Combining an SMS acceleration of 3 with a reduction in slice thickness, 2 mm sections through the entire brain were also demonstrated, with scan time and image quality comparable to the 4 mm single slice RESOLVE diffusion EPI acquisition.

SMS accelerated imaging offers a marked reduction in the time required for data acquisition (scan time). Using this approach, thin section (2 mm) DWI of the entire brain can also be acquired in a scan time and with image quality equivalent to 4 mm imaging with conventional DWI. Thin section imaging brings a marked further improvement in diagnostic image quality to 3T of the brain. This holds true especially for exams in patients with suspected brainstem pathology (a region in which every voxel contains eloquent tracts or nuclei). This new sequence approach is also easily applied in other anatomic areas, with many potential applications [6]. Looking further to the future, SMS accelerated imaging can be extended to additional pulse sequences, specifically TSE T2-weighted imaging.

Case 3

Slice acceleration with RESOLVE – the advantages of a thinner section. Bulk susceptibility artifacts on DWI are further reduced, and small pinpoint lesions with restricted diffusion are better seen. And, as shown, in certain instances small pinpoint lesions can be visualized only on the thinner sections, such as this small cortical infarct (arrow) in the left middle frontal gyrus.

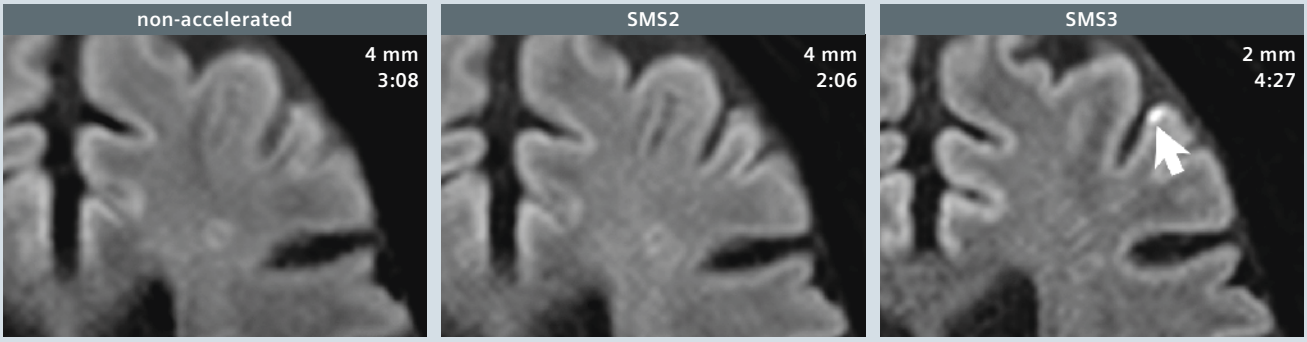

Case 4

Do we have good depiction of this lateral medullary infarct, with single shot imaging (upper row)? The conventional answer would be that the infarct is well delineated, with 4 mm slices acquired at 3T. But no, this is just a misconception, due to limited experience with thinner sections! This small infarct is not nearly as well seen as with 2 mm sections – acquired using slice acceleration (lower row), where the infarct is more sharply defined on each section and we have an additional slice (in between). The patient, an 87-year-old woman, presented one day prior to the MR with dizziness, nausea and vomiting, and left facial paralysis.

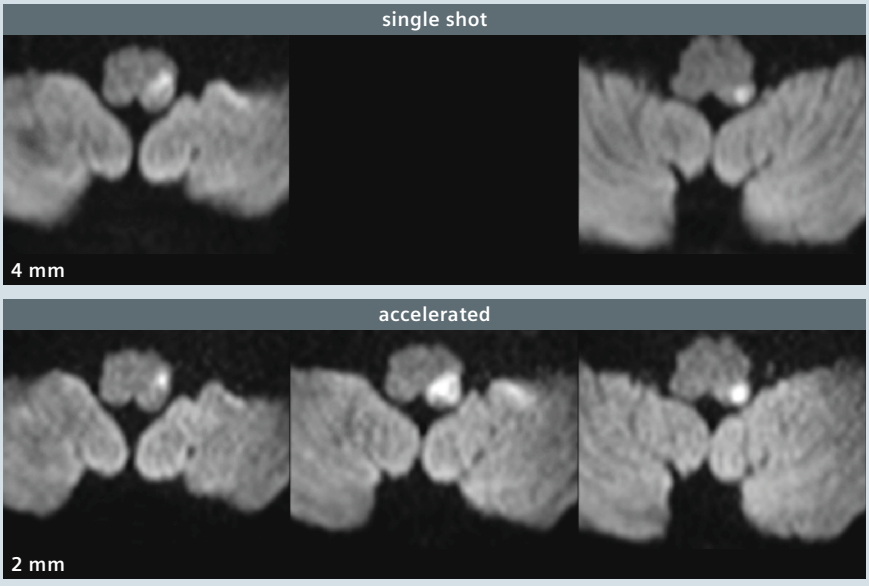

Case 5

In this example, the patient (with multiple punctate, acute, left middle cerebral artery distribution infarcts) was combative and moved throughout the exam despite sedation, degrading image quality. Motion artifact is greatest on the readout segmented DWI exam, due both to the long scan duration (3:26 min:sec) and the acquisition scheme, and least on the 2 mm slice accelerated scan. This 67-year-old patient presented one day prior to the MR with global aphasia, a right facial palsy and – on other imaging studies – a distal M1 segment occlusion.

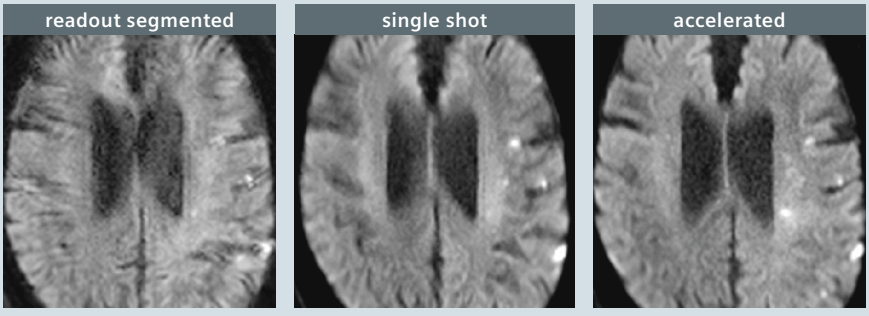

Case 6

Axial (part 1, 6A-C) and sagittal (part 2, 6D, E) soft tissue neck images from a normal volunteer are presented, without and with slice acceleration. In part 1, a single-shot (ss) DWI exam is compared to RESOLVE acquired without and with slice acceleration. Note the artifactual foreshortening in the AP dimension on the ss exam, which leads to a lymph node (arrow) that is anterior to the submandibular gland on the left being projected over the gland. On the RESOLVE images, there is no anatomic distortion, with the effective spatial resolution also improved due to the absence of the artifactual blurring present in the ss exam (and inherent to this technique). The use of slice acceleration allowed the RESOLVE sequence to be obtained in a very similar scan time as with the ss DWI, 2:07 vs 1:50 min:sec. In part 2, off-midline sagittal RESOLVE diffusion-weighted images are presented. Of intermediate signal intensity is a very small part of the submandibular gland with a high signal intensity small lymph node immediately anteriorly (in the middle of image), with a portion of the parotid gland seen in the more superior portion of the image. Depiction of the multiple scattered, high signal intensity, normal lymph nodes and SNR are equivalent for the two scans, with slice acceleration reducing scan time by nearly a factor of 2 (from 3:44 to 2:07 min:sec). Images were acquired with the Head/Neck 64-channel coil.

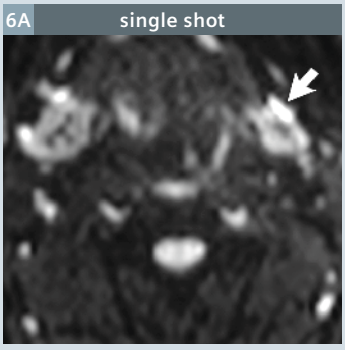

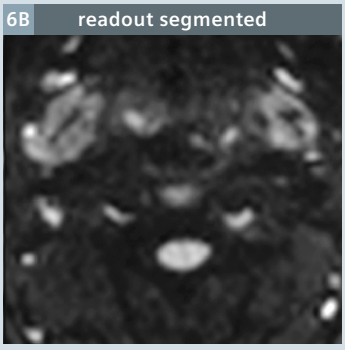

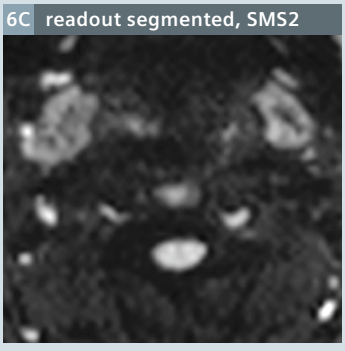

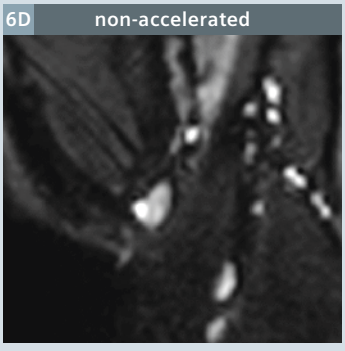

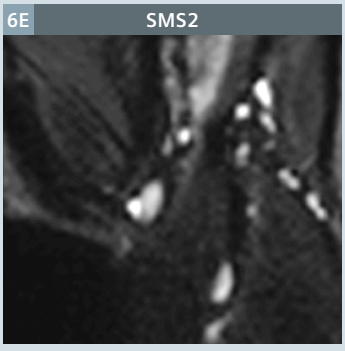

Acknowledgement

All images were acquired at 3T on a MAGNETOM Skyra MR system.

References

1 Larkman DJ, Hajnal JV, Herlihy AH, et al. Use of multicoil arrays for separation of signal from multiple slices simultaneously excited. J Magn Reson Imaging. 2001;13(2):313-7.

2 Setsompop K, Gagoski BA, Polimeni JR, et al. Blipped-controlled aliasing in parallel imaging for simultaneous multislice echo planar imaging with reduced g-factor penalty. Magn Reson Med. 2012;67(5):1210-24.

3 Frost R, Jezzard P, Douaud G, et al. Scan time reduction for readout-segmented EPI using simultaneous multislice acceleration: Diffusion-weighted imaging at 3 and 7 Tesla. Magn Reson Med. 2015;74:136-49.

4 Poser BA, Anderson RJ, Guerin B, et al. Simultaneous multislice excitation by parallel transmission. Magn Reson Med. 2014;71(4):1416-27.

5 Runge VM, Aoki S, Bradley WG, Jr., et al. Magnetic Resonance Imaging and Computed Tomography of the Brain-50 Years of Innovation, With a Focus on the Future. Invest Radiol. 2015;50(9):551-6.

6 Filli L, Piccirelli M, Kenkel D, et al. Simultaneous Multislice Echo Planar Imaging With Blipped Controlled Aliasing in Parallel Imaging Results in Higher Acceleration: A Promising Technique for Accelerated Diffusion Tensor Imaging of Skeletal Muscle. Invest Radiol. 2015;50(7):456-63.

Contact

Val M. Runge, M.D.
Editor-in-Chief, Investigative Radiology
Department of Diagnostic,
Interventional and Pediatric Radiology
University Hospital of Bern, Inselspital
Bern, Switzerland
ValMurray.Runge@insel.ch

Epilepsy Imaging with Simultaneous Multi-Slice Turbo Spin Echo

Michael Kean, FSMRT[1,2]; Dr Lee Coleman, BSc MB ChB FRANZCR[1,2]; Sonal Josan, Ph.D.[3]; Benjamin Schmitt, Ph.D.[3]

[1] Royal Children's Hospital, Melbourne, Australia
[2] Murdoch Children's Research Institute Parkville, Melbourne, Australia
[3] Siemens Healthcare, Melbourne, Australia

Background

In today's modern pediatric epilepsy protocols, high-resolution, T2-weighted (T2w) imaging plays a very important role in evaluating patients who present with epilepsy. At our institution, the use of 3T combined with high-density receive arrays has improved our diagnostic sensitivity and specificity for the detection of small cortically-based lesions.

Historically, 3D T1-weighted volume acquisitions such as MPRAGE have been integral in identifying small areas of cortical dysplasia. In previous iterations of epilepsy protocols, the T2-weighted imaging has been the Achilles heel of the examination due to inefficient use of the available TR and long scan times but with the increased signal-to-noise (SNR) ratios attributed to modern scanners, T2-weighted acquisitions are improving the diagnostic accuracy of scans.

The ability to reduce the sequence acquisition time has been the ultimate goal for pulse sequence developers since Hennig et al. [1] published their work on RARE imaging. As with most advances in pulse sequence development, clinicians are usually quite reserved in transitioning the current gold standard protocols due to the potential differences in signal intensity and tissue contrasts demonstrated by these acquisitions [2, 3].

The next advancement to significantly reduce T2w acquisition times were techniques proposed by Pruessmann [4, 5] and Griswold [6] using reconstruction algorithms that used the unique properties coil array geometry to undersample data resulting in reduced scan times at the cost of a reduction in SNR.

Several authors have proposed modifications to these techniques to reduce the amount of noise encoded into the images and further reduce scan times, one of the most significant was Breuer [7] with the development of phase and slice-based acceleration – CAIPIRINHA.

Recently several authors [9-12] have proposed the implementation of

Case 1

Figure 1 demonstrates a coronal T2w slice orientated perpendicular to the hippocampus. This slice was chosen to demonstrate the capabilities of the sequence because of the complex anatomy and potential for artifacts originating from physiological sources. It demonstrates the image quality achievable using SMS TSE with a significant reduction in scan time. Importantly, when the images were de-identified, the only reliable factor used by the radiologist in identifying the gold standard TSE was the higher signal intensity of CSF. The reduction of CSF signal was attributed to saturation effects associated with the application of the SMS RF pulse. The overall impression was that the accelerated acquisition appeared slightly sharper and this was probably due to slightly altered noise level associated with parallel imaging reconstruction.

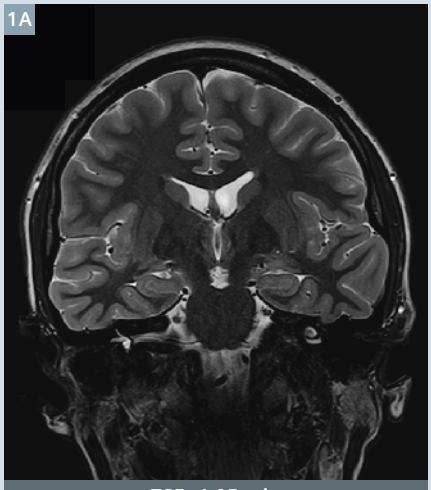

TSE, 4:05 min

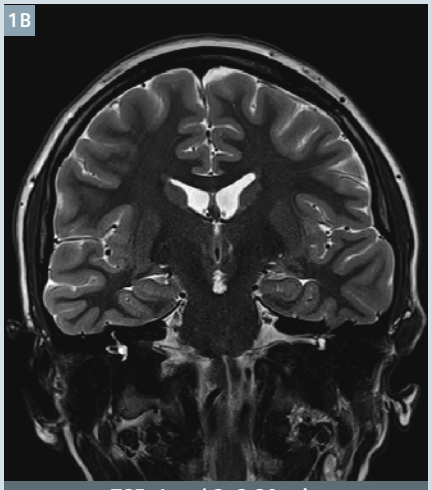

TSE_Accel 2, 2:30 min

CAIPIRINHA based reconstruction methods into conventional turbo spin echo to accelerate T2w acquisitions without the SNR penalties associated with data undersampling reconstruction methods. The implementation of simultaneous multi-slice (SMS) sequences into routine imaging will enable a more efficient TR-to-slice ratio, the potential to use higher echo train lengths while staying within current SAR restrictions, and reduced scan times. More importantly, these techniques can help overcome some of the limitations of conventional parallel imaging techniques such as *g*-factor penalties and SNR loss with undersampling.

The cases presented here are our initial experience with SMS TSE[1] in clinical epilepsy cases. All acquisitions were anatomically matched to an equivalent standard T2w TSE acquired on a MAGNETOM Trio or MAGNETOM Verio 3T (with software verison *syngo* MR B17) using the product 32-channel head coil. A whole-brain high-resolution T2 coronal with non-interpolated resolution of 0.5 x 0.6 x 2.5 mm^3 was achieved in all acquisitions. All images were evaluated for signal-to-noise, contrast-to-noise, image sharpness, artifacts, reconstruction faults, diagnostic confidence and lesion detectability.

Conclusion

Our initial experience with SMS TSE with a slice acceleration factor of 2 in conjunction with in-plane parallel imaging acceleration factor of 2 is very encouraging, producing scans of a similarly high diagnostic quality when compared to our gold standard TSE (with in-plane parallel imaging acceleration factor of 2) in much shorter scan times. Modifications to the protocol have enabled our team to incorporate slice accelerated TSE into protocols developed for our pediatric[2] epilepsy program.

As with many variations to pulse sequences, our team had concerns

[1] The product is still under development and not commercially available yet. Its future availability cannot be ensured.

Case 2

10-year-old patient presented with seizures. Preliminary imaging demonstrated a dysembryoplastic neuroepithelial tumour (DNET) in the right anterior temporal lobe.

The images demonstrate a complex lesion involving the anterior component of the right temporal lobe.

Both sequences equally demonstrate the complex nature of the lesion including small cysts, calcification including blurring and loss of grey and white matter.

There is slight anatomical disparity with the comparative images as there was patient movement between the acquisitions.

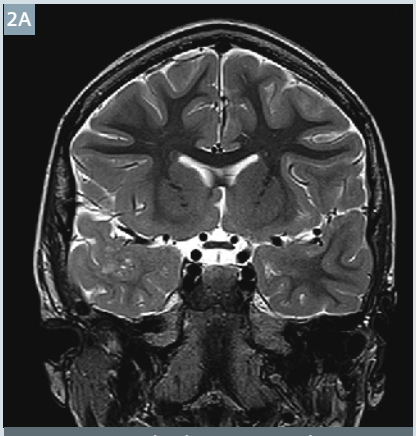

Standard T2w coronal

TSE Accel 2, 2:39 min

Case 3

5-year-old patient presented to our Epilepsy unit with aphasia and seizures originating from left anterior temporal lobe. A comprehensive epilepsy protocol was undertaken including comparative TSE and SMS TSE high-resolution T2-weighted coronal images aligned perpendicular to the hippocampus.

The images demonstrate a complex lesion adjacent to the left MCA involving the left anterior temporal lobe and amygdala. Based on the imaging characteristics, the lesion probably represents a dysembryoblastic neuroepithelial tumor (DNET).

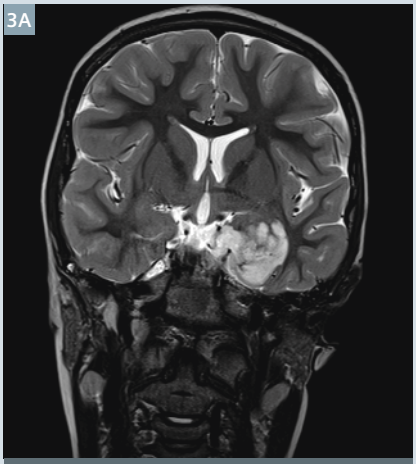

Standard T2w coronal

TSE Accel 2, 2:39 min

Case 4

11-year-old with periventricular nodular heterotopia (PVNH) for further evaluation of the PVNH and to demonstrate any right occipital focal cortical dysplasia.

The images demonstrate a complex malformation of cortical development with clear delineation of multiple areas of PVNH and occipital polymicrogyria.

T2w TSE, 4:05 min

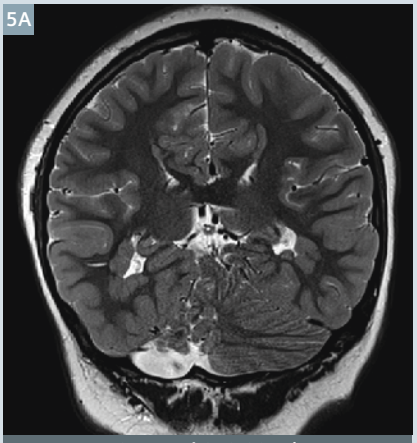

TSE Accel 2, 2:20 min

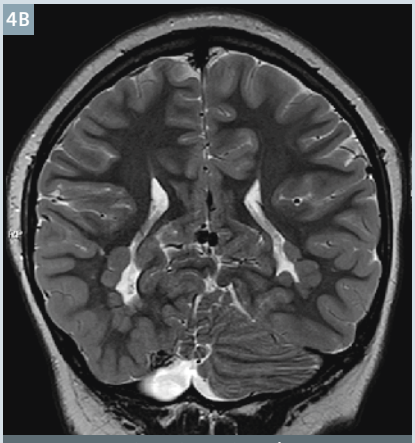

T2w TSE, 4:05 min

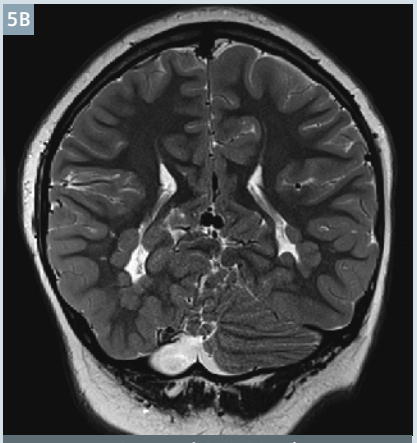

TSE Accel 2, 2:20 min

T2w TSE, 4:05 min

TSE Accel 2, 2:20 min

over a number of factors that would potentially impact on the diagnostic quality of the scans:

1. Sequence RF pulse techniques to reduce the SAR of the acquisition would influence image sharpness. The concern related to the implementation of low SAR VERSE pulses would increase echo-spacing has been unfounded and the general impression is that the accelerated T2 acquisitions appear sharper.
2. The reduction of CSF signal, potential loss of grey matter / white matter ratio and general SNR were highlighted as potential areas that would limit clinical integration. A number of scans on complex cerebral infections were undertaken to evaluate the diagnostic accuracy of the sequence and this comparison demonstrated equal diagnostic quality between the two sequences, with no significant difference in contrast to noise ratios in grey matter and white matter or CSF pulsation artifacts. The initial comments were that these concerns were similar to the transition from spin echo to TSE and then TSE with hyper-echo.
3. The acquisition and reconstruction strategy could invoke inter-slice leakage that could influence image quality. This has not been demonstrated to affect image quality as we expect a maximum leakage factor of less than 5%.
4. SMS TSE would have limited clinical utility due to SAR limitations. As with all MR sequences, there are numerous options to facilitate SAR management and we have obtained scans using low-SAR and normal RF pulses. The goal is to operate the system in normal operating mode and as such we tend to use low SAR RF pulses in the majority of cases.

[2] MR scanning has not been established as safe for imaging fetuses and infants under two years of age. The responsible physician must evaluate the benefit of the MRI examination in comparison to other imaging procedures.

The team has also started using the sequence in brain tumor imaging with very encouraging results. We have developed acquisition strategies to obtain high-resolution thin slice whole-brain coverage using acceleration factors of 3 in under 24 seconds for a limited clinical indication.

Acknowledgements

The authors wish to acknowledge the expertise of the Children's MRI Centre Staff, the assistance of Dr Simone Mandelstam for reviewing images, Dr Dingxin Wang and Siemens Healthcare for access to VB17_sliceaccel_WIP1003.

References

1 Hennig, J., Nauerth, A. & Friedburg, H., 1986. RARE imaging: a fast imaging method for clinical MR. Magnetic Resonance in Medicine : 3(6), pp.823–833.
2 Prenger, E.C. et al., 1994. Comparison of T2 weighted spin echo and fast spin echo techniques in the evaluation of myelination. : JMRI, 4(2), pp.179–184.
3 Patola, W.B. et al., 2001. A comparison of conventional spin-echo and fast spin-echo in the detection of multiple sclerosis.: JMRI, 13(5), pp.657–667.
4 Pruessmann, K.P. et al., 1999. SENSE: sensitivity encoding for fast MRI. Magnetic Resonance in Medicine : 42(5), pp.952–962.
5 Pruessmann, K.P. et al., 2001. Advances in sensitivity encoding with arbitrary k-space trajectories. Magn Reson in Med : 46(4), pp.638–651.
6 Griswold MA, Jakob PM, Heidemann RM, et al. Generalized autocali-brating partially parallel acquisitions (GRAPPA). Magn Reson Med. 2002;47:1202–1210
7 Breuer, F.A. et al., 2005. Controlled aliasing in parallel imaging results in higher acceleration (CAIPIRINHA) for multi-slice imaging. Magnetic Resonance in Medicine : 53(3), pp.684–691.
8 Eichner, C. et al., 2013. Slice accelerated gradient-echo spin-echo dynamic susceptibility contrast imaging with blipped CAIPI for increased slice coverage. Magnetic Resonance in Medicine 72(3), pp.770–778.
10 Gagoski, B.A. et al., 2015. RARE/turbo spin echo imaging with simultaneous multislice Wave-CAIPI. Magnetic resonance in medicine : 73(3), pp.929–938.
11 Bilgic, B. et al., 2014. Wave-CAIPI for highly accelerated 3D imaging. Magnetic Resonance in Medicine : 73(6), pp.2152–2162.
12 Wang, D 2014 Multiband Slice Accelerated TSE: Application in Brain Imaging. Proc Int Soc Mag Reson Med 22 , 4317

Contact

Michael Kean, FSMRT
Chief MRI Technologist
The Royal Children's Hospital
Flemington Road
Parkville Victoria 3052
Australia
michael.kean@rch.org.au

Learn more!

Don't miss the talks of experienced and renowned experts on all aspects of pediatric MR imaging at:

www.siemens.com/magnetom-world

Body MRI and Whole-Body Staging in Pediatric Patients

Günther Schneider

Saarland University Hospital
(Homburg, Germany)

Urogenitary Malformations and Their Imaging Features

J. Damian Grattan-Smith

Children's Healthcare of Atlanta
(Atlanta, GA, USA)

Running Pediatric MRI as an Effective Clinical and Cost Centre

Thomas Vogl

Frankfurt University Hospital
(Frankfurt/Main, Germany)

Case Study: Simultaneous Multi-Slice Accelerated Turbo Spin-Echo Magnetic Resonance Imaging of the Spine

Stephen F. Kralik, M.D.[1]; Dingxin Wang, Ph.D.[2]; Bruce Spottiswoode, Ph.D.[3]; Mary McCrate, M.D.[1]; Chen Lin, Ph.D.[1]

[1] Indiana University Department of Radiology and Imaging Sciences, Indianapolis, IN, USA
[2] Siemens Medical Solutions USA, Inc., Minneapolis, MN, USA
[3] Siemens Medical Solutions USA, Inc., Chicago, IL, USA

Introduction

Magnetic Resonance Imaging (MRI) of the spine may be performed for a wide range of clinical symptoms and indications including evaluation of back pain, radiculopathy, spondylosis, infection, and neoplasms. Standard MRI spine protocols include multiplanar T1-weighted (T1w), T2-weighted (T2w), and short tau inversion recovery (STIR) or a T2w fat-saturated sequence most commonly in the sagittal and axial planes. Post-contrast imaging is indicated for evaluation of infection, neoplasm, and in the post-operative setting. Because imaging of the spine in the axial plane requires a large number of slices to adequately detect pathology, the simultaneous multi-slice (SMS) imaging technique using multiband (MB) pulses may be valuable for imaging the spine as it reduces imaging time while providing similar detection of pathology and similar image quality. In this case study we describe the use of SMS turbo spin echo (SMS TSE)[1] for evaluation of the lumbar spine among patients who have been given intravenous contrast for various clinical indications including neoplasms and post-operative scenarios.

Sequence details

MRI of the lumbar spine was performed at a 1.5T MR scanner (MAGNETOM Symphony, A Tim System, Siemens Healthcare, Erlangen, Germany). Post-contrast axial T1 TSE sequences (conventional and SMS) with fat saturation (T1w contrast-enhanced (CE) TSE FS) were performed following administration of 0.1 mmol/kg intravenous gadolinium dimeglumine (Multihance; Bracco Diagnostics, Princeton, NJ, USA) contrast. Parameters for the conventional TSE sequence were TR 637-684 ms, TE 12-13 ms, 4 mm slice thickness, and 192 x 256 matrix. The SMS T1w CE TSE fat saturation sequence consisted of TR 632 ms, TE 14 ms, 4 mm slice thickness, and 192 x 256 matrix. Average acquisition times for conventional axial T1w CE FS TSE and SMS T1w CE TSE FS were 5:33 min (range 5:24 to 5:48 min) and 4:00 min respectively.

[1] The product is still under development and not commercially available yet. Its future availability cannot be ensured.

Case 1

A 60-year-old female with a previous history of an intradural schwannoma resection in 2013 who reported continued low back pain and left lower extremity radiculopathy. Representative images from the conventional axial T1w CE TSE FS **(1A, C)** and SMS axial T1w CE TSE FS **(1B, D)** demonstrate a laminectomy site at L2-3 with small amount of enhancing scar tissue at the laminectomy site but no evidence of recurrent schwannoma in the thecal sac.

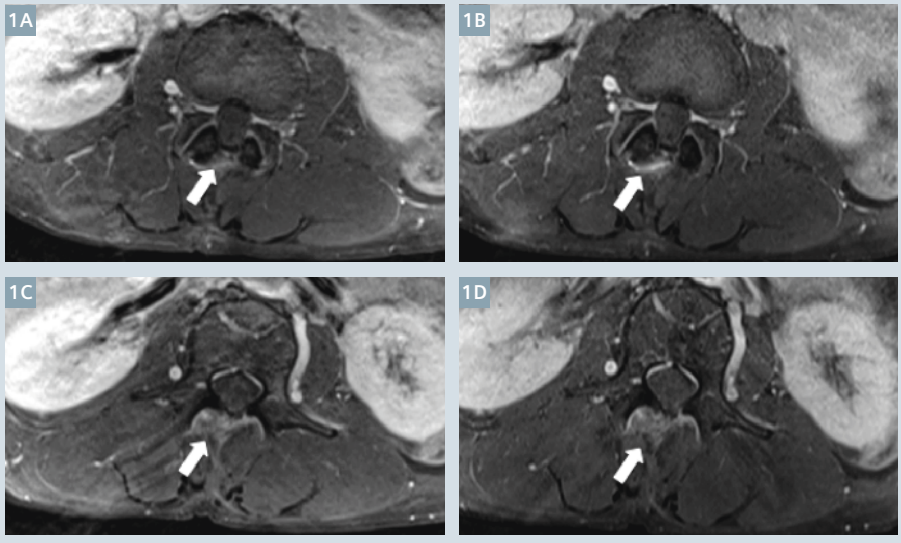

Case 2

An 80-year-old male presented with a history of metastatic cholangiocarcinoma and left leg weakness. Both, the conventional axial T1w CE TSE FS **(2A)** and SMS axial T1w CE TSE FS **(2B)** demonstrated no evidence of metastatic disease. Representative images of the lumbar spine demonstrate similar differentiation of the bones, muscles, spinal canal, and remainder of the extraspinal soft tissues.

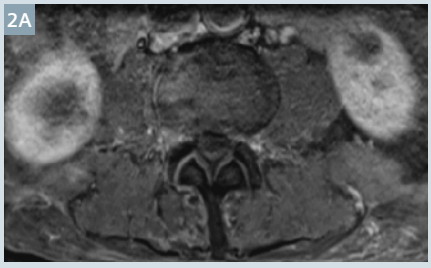

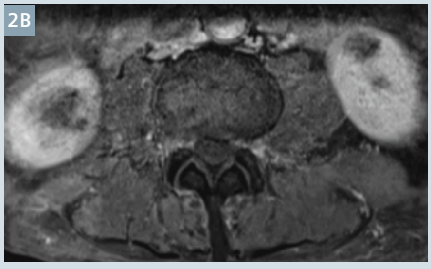

Case 3

A 58-year-old patient with metastatic breast cancer and low back pain. Representative images from both the conventional axial T1w CE TSE FS **(3A, C, E)** and SMS axial T1w CE TSE FS **(3B, D, F)** demonstrate multifocal enhancing lesions in the bones consistent with osseous metastases. There is similar conspicuity of the bone lesions with the SMS TSE compared to the conventional TSE.

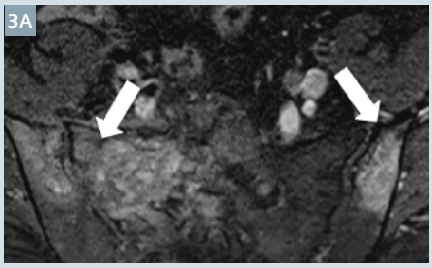

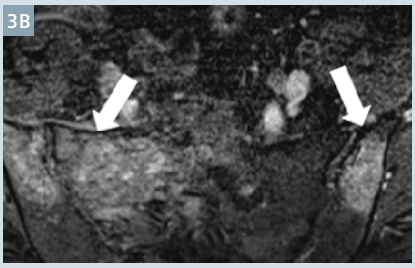

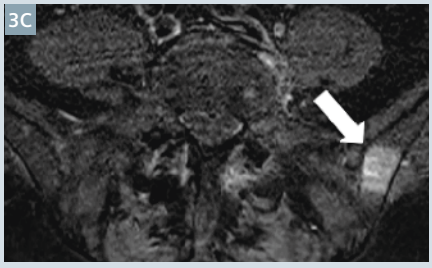

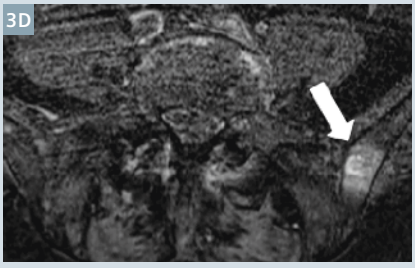

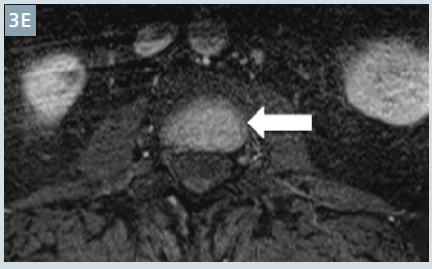

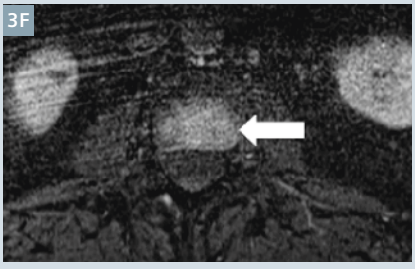

Conclusion

We performed SMS TSE of the lumbar spine in this small clinical case series and determined that SMS TSE can be reliably performed in the clinical setting. Compared to the conventional T1w CE TSE, the T1w CE SMS TSE demonstrates similar detection of pathology while reducing imaging time compared to conventional TSE which is considered a clinical advantage of the SMS TSE. No qualitative differences in image quality, such as anatomic detail or imaging artifacts, were encountered with SMS TSE which would preclude its use in the clinical setting. Further quantitative investigation of image quality and pathology detection in the clinical setting using SMS TSE will be undertaken to evaluate if this technique can replace conventional TSE imaging of the spine in the near future.

References

1 Wang D, Kollasch P, Auerbach EJ et al. T1-weighted Imaging of Lumbar Spine using Multiband Slice Accelerated Spin Echo Proceedings of the International Society for Magnetic Resonance in Medicine (21) 2013, 244.

2 Wang D, Kollasch P, Li X et al., "Multiband Slice Accelerated TSE: Clinical Applications in Brain imaging", Proceedings of the International Society for Magnetic Resonance in Medicine (22) 2014, 4317.

3 Wang D, Padua A, Ellermann J et al., "Multiband Slice Accelerated TSE for High Resolution Knee Imaging", Proceedings of the International Society for Magnetic Resonance in Medicine (22) 2014, 1216.

Contact

Stephen F. Kralik, M.D.
Assistant Professor of Radiology
Indiana University
Department of Radiology and Imaging Sciences
714 N Senate Ave #100
Indianapolis, IN 46202, USA
Phone: +1 317-274-5555
skralik@iupui.edu

Case Report: Evaluation of Simultaneous Multi-Slice Accelerated TSE for Knee Joint MR Imaging

Xiaona Li[1]; Zhigang Peng[1]; Panli Zuo[2]; Dingxin Wang[3]; Jianling Cui[1]

[1] Department of Radiology, Hebei 3rd Hospital, Province Biomechanical Key Laboratory of Orthopedics, Shijiazhuang, China
[2] Siemens Healthcare, MR Collaborations NE Asia, Beijing, China
[3] Siemens Medical Solutions USA, Inc., Minneapolis, MN, USA

Introduction

The turbo spin echo (TSE) sequence is one of the most utilized sequences in clinical routine MRI, providing high image quality, strong lesion conspicuity and multiple tissue contrasts (T1w, T2w, FLAIR and proton density-weighted (PD)). In musculoskeletal (MSK) imaging, TSE is widely used as it offers excellent depiction of cartilage, ligaments, menisci, and periarticular soft tissues. However, high spatial resolution with a large number of slices is rarely used clinically because of the prolonged acquisition time for complete coverage when using a conventional 2D-TSE sequence.

Simultaneous multi-slice (SMS) is a promising parallel imaging method to increase the acquisition speed without a significant decrease to the signal-to-noise ratio (SNR). SMS has been proved to work well with echo-planar imaging (EPI) readout for both diffusion-weighted and BOLD functional magnetic resonance imaging (fMRI). The SMS method excites multiple spatially distributed slices simultaneously using a multi-band (MB) radiofrequency (RF) pulse and separates the simultaneously acquired slices by parallel imaging reconstruction technique utilizing the multiple receiver coils sensitivities [1-4]. With integration of the 'controlled aliasing in parallel imaging result in higher acceleration' (CAIPIRINHA) method the *g*-factor related SNR penalty is significantly reduced [3, 7; also see articles by the same authors in this issue]. SMS allows an increase in the imaging coverage with higher spatial resolution and shorter acquisition time [2, 3, 5-7].

Several recent studies have addressed the possibility of applying the SMS method to TSE acquisition schemes [8-10]. In this study, we applied the SMS 2D-TSE sequences[1] with gradient-based CAIPIRINHA in MSK examination to assess its value for MSK related diseases.

Method

All MR scans were performed on a 3T MAGNETOM Verio system (Siemens Healthcare, Erlangen, Germany) with an 8-channel knee coil or a 4-channel flex coil. Sagittal T1-weighted TSE, sagittal, coronal and transverse PD-weighted TSE with fat suppression imaging were performed for the whole knee joint to compare the image quality of conventional TSE and SMS TSE sequences.

[1] The product is still under development and not commercially available yet. Its future availability cannot be ensured.

Imaging parameters include field-of-view (FOV) of 160 × 160 mm², matrix of 320 × 256, slice thickness of 3 mm with a gap of 10%, 36 slices, excitation/refocusing flip angle of 90/150°. Slice acceleration factor is 2 and FOV shift factor is 2 for all SMS TSE sequences. Matching imaging parameters including TR/TE and turbo factor were used for conventional and SMS TSE. For covering the 36 slices, SMS TSE used only half number of concatenations as conventional TSE. Sagittal T1w imaging was performed using TR 499 ms, TE of 13 ms and turbo factor of 3. Sagittal T1w imaging with fat saturation was performed using TR 573 ms, TE 13 ms and turbo factor of 3. All T1w imaging acquisitions used 4 concatenations for conventional TSE and 2 concatenations for SMS TSE. Sagittal PD-weighted imaging with fat saturation was performed using TR 3200 ms, TE 40 ms and turbo factor of 8. Coronal PD-weighted imaging with fat saturation was performed using TR 3200 ms, TE 40 ms and a turbo factor of 9. Axial PD-weighted imaging with fat saturation

Parameter	sag-T1	sag-T1+fs	sag-PD+fs	cor-PD+fs	tra-PD+fs
TR/TE (ms)	499/13	573/13	3200/40	3200/40	3200/41
ETL	3	3	8	9	10
Concatenation	4 (Conv.) 2 (SMS)	4 (Conv.) 2 (SMS)	2 (Conv.) 1 (SMS)	2 (Conv.) 1 (SMS)	2 (Conv.) 1 (SMS)

Table 1: Other imaging parameters.

Sequences	sag-T1	sag-T1+fs	sag-PD+fs	cor-PD+fs	tra-PD+fs
conventional TSE	5:11	5:57	5:41	5:32	4:24
SMS TSE	2:36	2:58	2:48	2:47	2:38

Table 2: Acquisition time for conventional TSE and SMS TSE (in minutes).

Case 1

40-year-old female with a painless slow-growing swelling for 10 years in the right distal femur. CT sagittal image demonstrated an irregular bone protuberance with a wide base in the posterior of right distal femur. Calcification shadow and continuity of the lesion with the cortical bone were seen in the lesion (Fig. 1A). MRI with both SMS TSE and conventional TSE demonstrated a local thickened cartilaginous cover in the rim of the bone protuberance (Figs. 1B-G). The cortical and medullary continuity between the osteochondroma and host bone can be observed. Calcified areas of the cover presented low signal intensity in T1 and PD-weighted images with fat saturation. Water in the non-calcified portion showed a low signal to the surrounding bone on T1w images and a high signal on PD-weighted images with fat saturation.

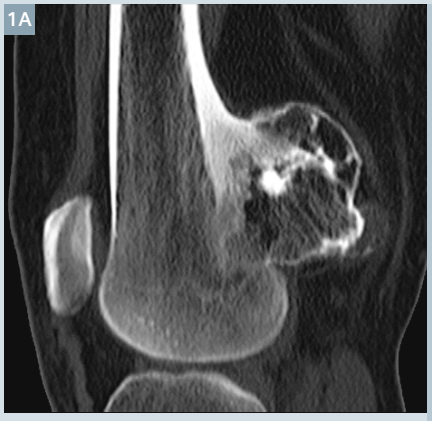

1 A patient (40-year-old, female) with osteochondroma in the bone of the distal femoral. **(1A)** is the CT sagittal image. **(1B-D)** are SMS TSE and **E**, **F**, and **G** are conventional TSE images for sagittal T1-weighted imaging **(1B, E)**, sagittal PD-weighted imaging with fat saturation **(1C, F)** and axial PD-weighted imaging with fat saturation **(1D, G)**.

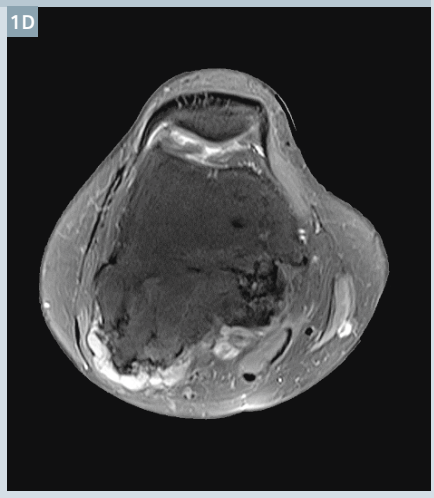

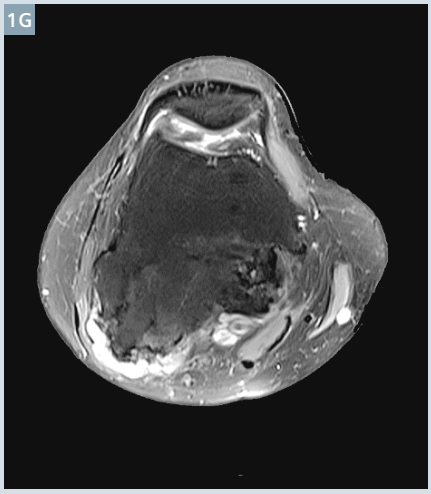

Case 2

68-year-old male with pain in the right leg for half a year without an adequate history of corresponding trauma. CT coronal image demonstrated a round-shaped lesion with a sclerosis rim (Fig. 2A). The size of the lesion was 3 × 4 × 7 cm^3. A calcification shadow was seen in the lesion with a sharp rim. MRI with both SMS TSE and conventional TSE demonstrated the lesion of inhomogeneous isointense to surrounding muscles on T1w images (Figs. 2B (SMS) and E (conventional)). Foliated hyperintensity signals were also seen in the lower lesion. On PD-weighted images with fat saturation (Figs. 2C (SMS) and F (conventional)), the lesion predominantly presented high signal intensity, within punctiform hypo- and isointensity. Post-Gadoteridol T1w images with fat saturation showed partly slightly enhancement intensity (Figs. 2D (SMS) and G (conventional)). The diagnosis was fibrous dysplasia in the bone of proximal tibia.

2 A patient (68-year-old, male) with fibrous dysplasia of proximal tibia. **(2A)** is the coronal CT image. **(2B-D)** are SMS TSE and **(2E-G)** are conventional TSE images for sagittal T1w imaging **(2B, E)**, sagittal T1w imaging with fat saturation after contrast agent injection **(2C, F)**, and PDw imaging with fat saturation **(2D, G)**.

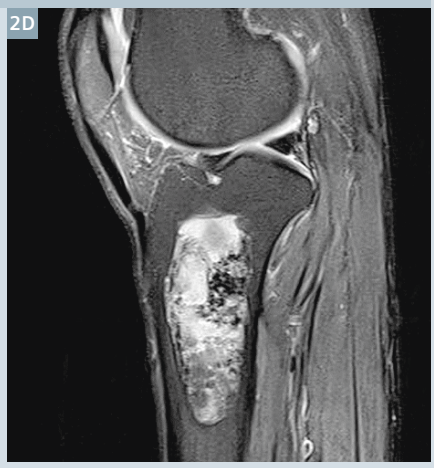

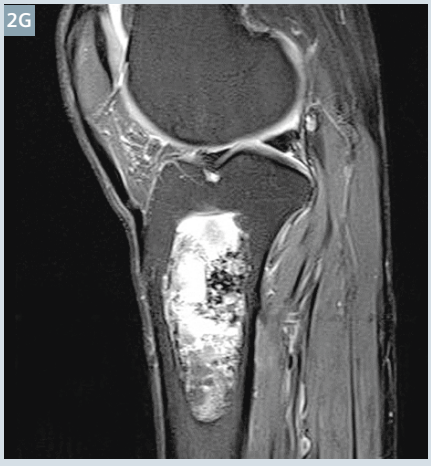

Case 3

31-year-old female with pain in the left knee since 2 months. Both SMS TSE and conventional TSE MR sagittal images demonstrate a geographic lesion in the distal femur and proximal tibia with slight hypointensity of the skeletal muscle on T1w images (Figs. 3B (SMS) and D (conventional)) and hyperintensity in PDw fat saturation images (Figs. 3A (SMS) and C (conventional)). The diagnosis was bone infarction.

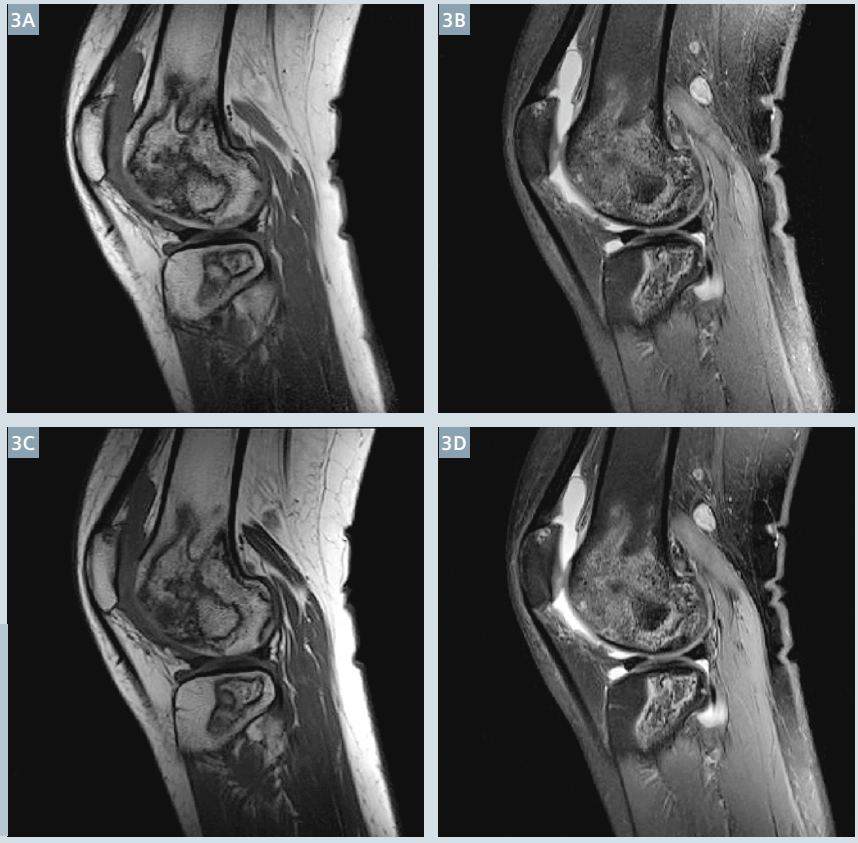

3 A patient (31-year-old, female) with fibrous bone infarction. **(3A, B)** are SMS TSE, **(3C, D)** are conventional TSE images for sagittal T1w imaging **(3A, C)**, and sagittal PDw imaging with fat saturation **(3B, D)**.

Case 4

71-year-old male with pain in the right knee since 10 years after sprain. Both SMS TSE and conventional TSE MR sagittal images demonstrate an anterior cruciate ligament tear and multiple bone proliferation which supports the diagnosis of osteoarthritis. There was a slight hypointensity to skeletal muscle on T1w images (Figs. 4A (SMS) and C (conventional)) and hyperintensity with slightly low intense clumps on PDw images (Figs. 4B (SMS) and D (conventional)).

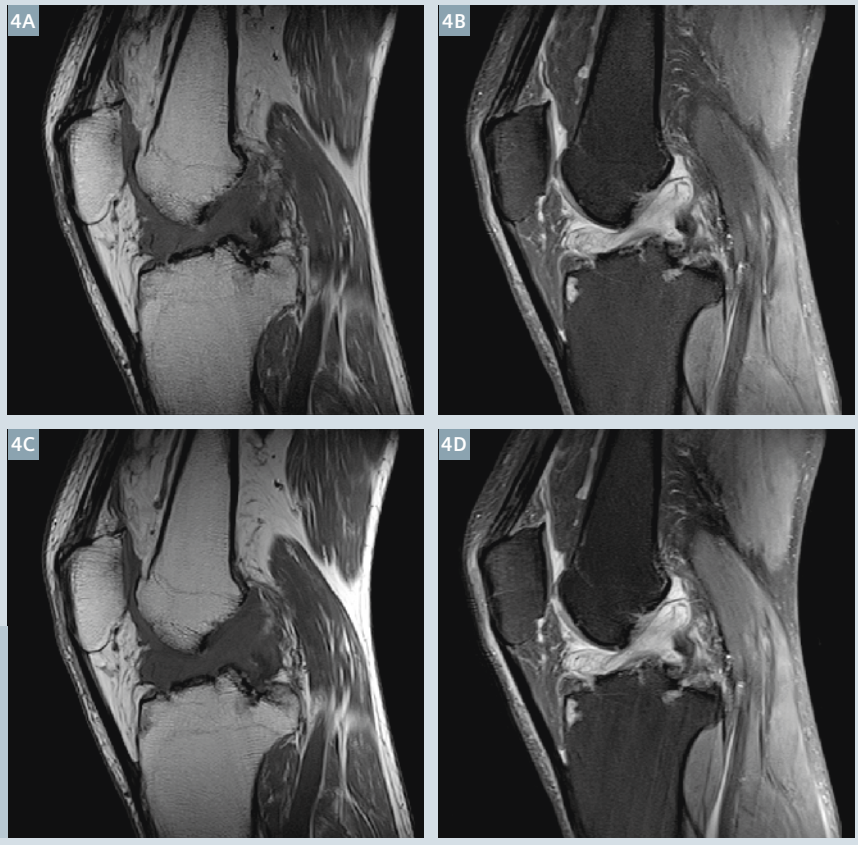

4 A patient (71-year-old, male) with osteoarthritis. **(4A, B)** are SMS TSE, and **(4C, D)** are conventional TSE images for sagittal T1w imaging **(4A, C)**, and sagittal PDw imaging with fat saturation **(4B, D)**.

was performed using TR 3200 ms, TE 41 ms, and turbo factor of 10. All PD-weighted imaging acquisitions used 2 concatenations for conventional TSE and 1 concatenation for SMS TSE. Other imaging parameters are shown in Table 1 and 2.

Conclusion

SMS TSE reduced the scanning time for TSE imaging significantly without compromise to diagnostic image quality, bringing strong value to routine musculoskeletal examinations. This especially benefits patients with larger tumors where full coverage may be difficult to achieve using conventional TSE sequence and also for patients with small injuries to ligaments and cartilage who will require higher spatial resolution imaging for an accurate diagnosis.

References

1 Xu J, Moeller S, Auerbach EJ et al (2013) Evaluation of slice accelerations using multiband echo planar imaging at 3 T. Neuroimage 83:991-1001.

2 Moeller S, Yacoub E, Olman CA et al (2010) Multiband multislice GE-EPI at 7 tesla, with 16-fold acceleration using partial parallel imaging with application to high spatial and temporal whole-brain fMRI. Magn Reson Med 63:1144-1153.

3 Setsompop K, Gagoski BA, Polimeni JR, Witzel T, Wedeen VJ, Wald LL (2012) Blipped-controlled aliasing in parallel imaging for simultaneous multislice echo planar imaging with reduced g-factor penalty. Magn Reson Med 67:1210-1224.

4 Sotiropoulos SN, Moeller S, Jbabdi S et al (2013) Effects of image reconstruction on fiber orientation mapping from multi-channel diffusion MRI: reducing the noise floor using SENSE. Magn Reson Med 70:1682-1689.

5 Feinberg DA, Moeller S, Smith SM et al (2010) Multiplexed echo planar imaging for sub-second whole brain FMRI and fast diffusion imaging. PLoS One 5:e15710.

6 Smith SM, Miller KL, Moeller S et al (2012) Temporally-independent functional modes of spontaneous brain activity. Proc Natl Acad Sci U S A 109:3131-3136.

7 Breuer, FA, Blaimer M, Heidemann RM et al., (2005) Controlled aliasing in parallel imaging results in higher acceleration (CAIPIRINHA) for multi-slice imaging. Magnetic Resonance in Medicine 53(3): 684–691.

8 Norris DG, Boyacioglu R, Schulz J, Barth M, Koopmans PJ (2014) Application of PINS radiofrequency pulses to reduce power deposition in RARE/turbo spin echo imaging of the human head. Magn Reson Med 71:44-49.

9 Wang D, Kollasch P, Li X et al., "Multiband Slice Accelerated TSE: Clinical Applications in Brain imaging", Proceedings of the International Society for Magnetic Resonance in Medicine (22) 2014, 4317.

10 Wang D, Padua A, Ellermann J et al., "Multiband Slice Accelerated TSE for High Resolution Knee Imaging", Proceedings of the International Society for Magnetic Resonance in Medicine (22) 2014, 1216.

Contact

Jianling Cui
Department of Radiology
The Third Hospital of Hebei Medical University
Hebei Province Biomechanical Key Laboratory of Orthopedics
Ziqiang Road 139
Shijiazhuang, Hebei 050051
China

Improved Visualization of Femoroacetabular Impingement Cartilage Damage with Multi-band Simultaneous Multi-Slice Acceleration

Casey P. Johnson[1]; Luning Wang[1]; Shelly Marette[1]; Takashi Takahashi[1]; Patrick Morgan[2]; Kâmil Uğurbil[1]; Dingxin Wang[1,3]; Jutta Ellermann[1]

[1] Department of Radiology (CMRR), University of Minnesota, Minneapolis, MN, USA
[2] Department of Orthopaedic Surgery, University of Minnesota, Minneapolis, MN, USA
[3] Siemens Medical Solutions USA Inc., Minneapolis, MN, USA

Introduction

Femoroacetabular impingement (FAI) is a common source of hip pain in adults caused by a pathological abutment of the head-neck junction of the femur and the acetabular rim of the hip [6]. This abutment leads to mechanical friction, which can in turn cause labral and chondral lesions and lead to osteoarthritis (OA) [1, 2, 4, 5, 8]. The recommended treatment for FAI is joint preservation surgery if a labral tear has occurred, cartilage damage is not severe, and patient symptoms cannot be managed conservatively with physical therapy [3, 10, 11]. In FAI, cartilage damage is typically limited to the acetabulum and occurs deep within the tissue as a debonding of articular cartilage from underlying bone [2]. This so-called 'cartilage delamination' is the hallmark of the disease. If cartilage damage is severe, as would be the case if there was prevalent cartilage delamination, then joint preservation surgery will fail and total hip replacement will be necessary. Therefore, in order to appropriately recommend treatment for FAI, imaging is needed to evaluate the hip joint for both labral tears and cartilage delamination.

However, cartilage delamination is not seen using current clinical imaging protocols because spatial resolution is insufficient. The necessary resolution cannot be achieved due to prohibitively long acquisition times. Additionally, labral tears can be difficult to diagnose, also due to limited spatial resolution. Specifically, slices of 3 to 4 mm are too thick, leading to problematic volumetric averaging within voxels along the curved surface of the acetabulum that obscures the cartilage and labral pathology. Multiband Simultaneous Multi-Slice (SMS) acceleration technology [7, 9] can be used to improve the spatial resolution while not increasing the acquisition time (or, equivalently, reducing the acquisition time for a given spatial resolution). Multiband allows multiple imaging slices to be excited simultaneously, thereby enabling more slices (and thus higher spatial resolution) to be acquired within a given acquisition time. In this study, we evaluated the potential clinical benefits of utilizing a multiband SMS accelerated turbo spin echo (TSE) sequence[1] to either improve diagnostic accuracy of cartilage delamination and labral tears or save scan time while maintaining diagnostic image quality.

[1] The product is still under development and not commercially available yet. Its future availability cannot be ensured.

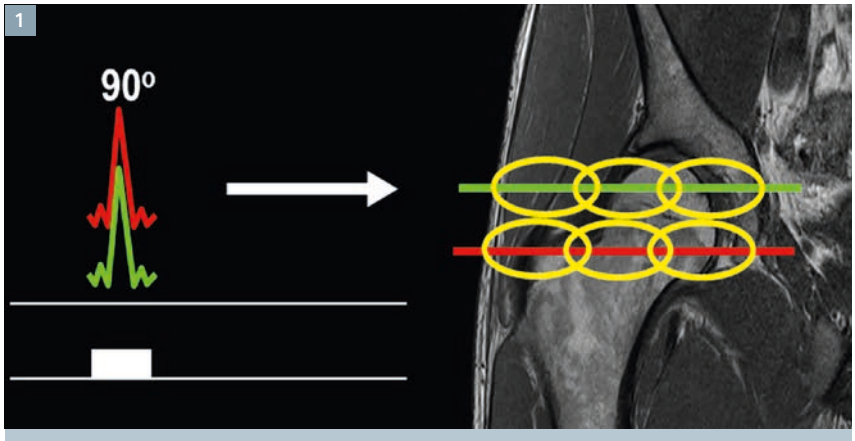

1 Multiband excitation allows multiple slices to be acquired during one acquisition. In this diagram, a multiband simultaneous multi-slice acceleration factor of two is illustrated. The red and green slices passing through the femoral head are excited and refocused simultaneously using two selective RF pulses. The acquired signal is then received by a multi-channel receive coil array placed about the hip (yellow circles), which have sensitivity profiles that are unique at each slice position. Using the spatial dependence of the array sensitivity profile, aliasing artifacts caused by the simultaneous slice excitation are corrected during image reconstruction.

Case 1

A 58-year-old patient suffered left hip pain for 5 years and pain got exacerbated with prolonged periods of running. A labral tear was clearly identified using the SMS-accelerated T1-weighted TSE sequence with fat saturation (slice acceleration factor 2) following the administration of intra-articular gadolinium contrast agent (MR arthrogram), which provided high spatial resolution (2.0 mm slice thickness) in a clinically feasible acquisition time (Fig. 2). Bright contrast-enhanced signal is seen within the chondrolabral junction. However, the standard resolution acquired for the clinical exam (3.0 mm slice thickness) was insufficient and the labral tear could only be vaguely seen due to partial volume averaging.

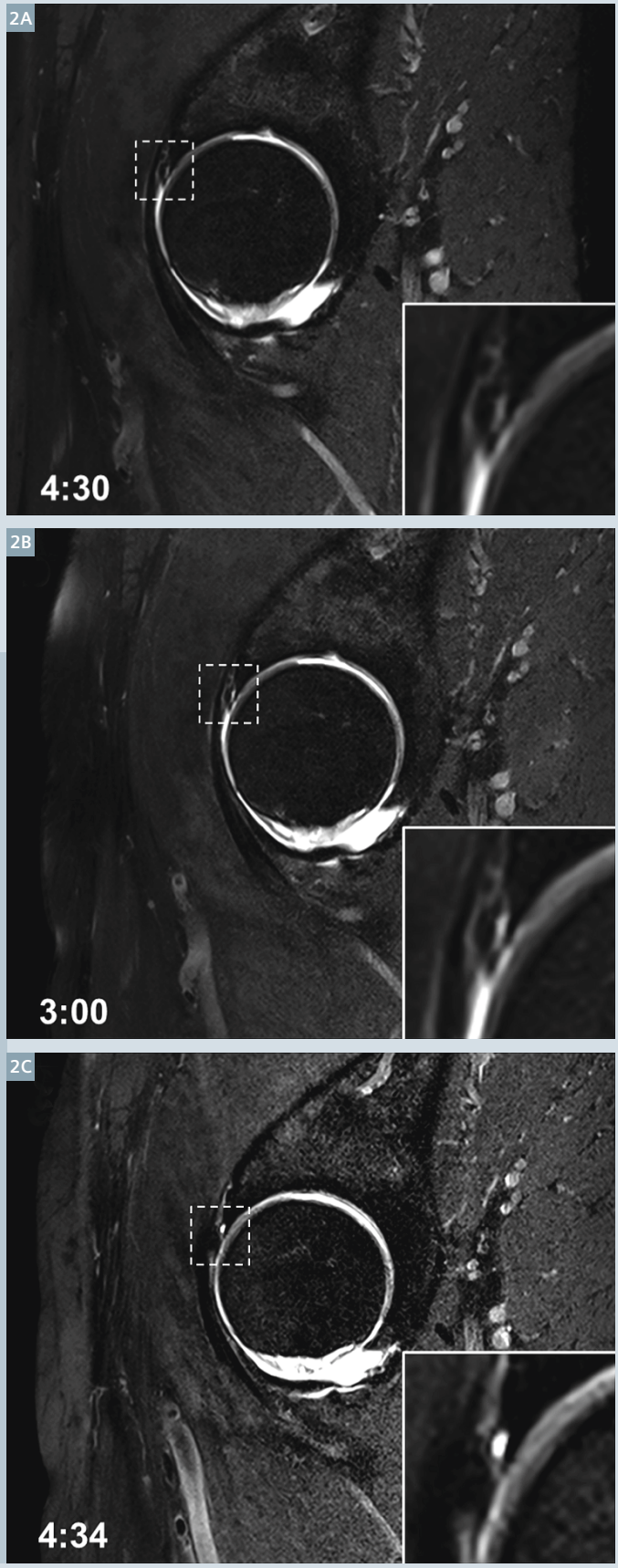

2 Multiband SMS acceleration provides sharper visualization of a labral tear using 3T MR arthrography. **(2A)** Standard clinical MR arthrogram utilizing a T1-weighted TSE sequence with fat saturation. The region with the labral tear (dashed box) is zoomed-in and shown in the lower-right corner. The labral tear, identified by contrast-enhanced fluid infiltration into the chondrolabral junction, cannot be confidently diagnosed at the acquired spatial resolution. **(2B)** Applying multiband SMS acceleration enables the same image quality in (2A) to be obtained in a reduced acquisition time (3:00 min vs. 4:30 min), but this does not solve the spatial resolution deficit. **(2C)** Utilizing the time-savings provided by multiband SMS acceleration to increase spatial resolution for the same acquisition time as in (2A) provides a much sharper depiction of the labral tear, allowing clear clinical diagnosis.

Imaging parameters of the MR arthrogram: FOV 180 ×180 mm^2, matrix size 384 × 384, in-plane resolution 0.47 × 0.47 mm^2, 20% slice spacing, excitation/refocusing flip angle 90°/120°, readout bandwidth 195-215 Hz/pixel, in-plane GRAPPA acceleration factor 2, T1-weighted with spectral fat saturation, ETL 4;

Standard TSE: 3 mm thickness, 30 slices, TR 656 ms, TE 13 ms, 100% phase oversampling, 4 concatenations, TA 4:30 min; 2 mm thickness, 46 slices, TR 631 ms, TE 12 ms, 100% phase oversampling, 6 concatenations, TA 6:30 min;

Multiband SMS Accelerated TSE: slice acceleration factor 2, 3 mm thickness, 30 slices, TR 656 ms, TE 13 ms, 160% phase oversampling, 2 concatenations, TA 3:00 min; 2 mm thickness, 46 slices, TR 631 ms, TE 12 ms, 100% phase oversampling, 4 concatenations, TA 4:34 min.

Images acquired with MAGNETOM Skyra 3T MR scanner (Siemens Healthcare, Erlangen, Germany)

Case 2

A 25-year-old male, who played hockey in high school, presented with left hip pain. Cartilage delamination was identified in a clinically feasible acquisition time using multiband SMS accelerated T2-weighted TSE with fat saturation and a slice acceleration factor of two (Fig. 3). The higher spatial resolution provided by multiband SMS acceleration (2.0 vs. 3.0 mm slice thickness) depicted debonding of articular cartilage from the underlying bone in the acetabulum as revealed by slightly higher signal interposed between the underlying bone and the dark line of the superficial layer of the cartilage. While the subjacent normal cartilage has a smooth thin surface and a homogeneous intermediate intensity signal, the area of delamination has a slightly higher intensity signal with a surface that appears darker, thicker, and slightly wavy. The border between the normal cartilage and the abnormal debonded cartilage has a vertical gray line. However, without slice acceleration and the resultant increase in spatial resolution, the cartilage delamination could not be identified. The acquisition time would be prohibitively long if the desired spatial resolution was acquired without multiband SMS (6:30 min vs. 4:34 min).

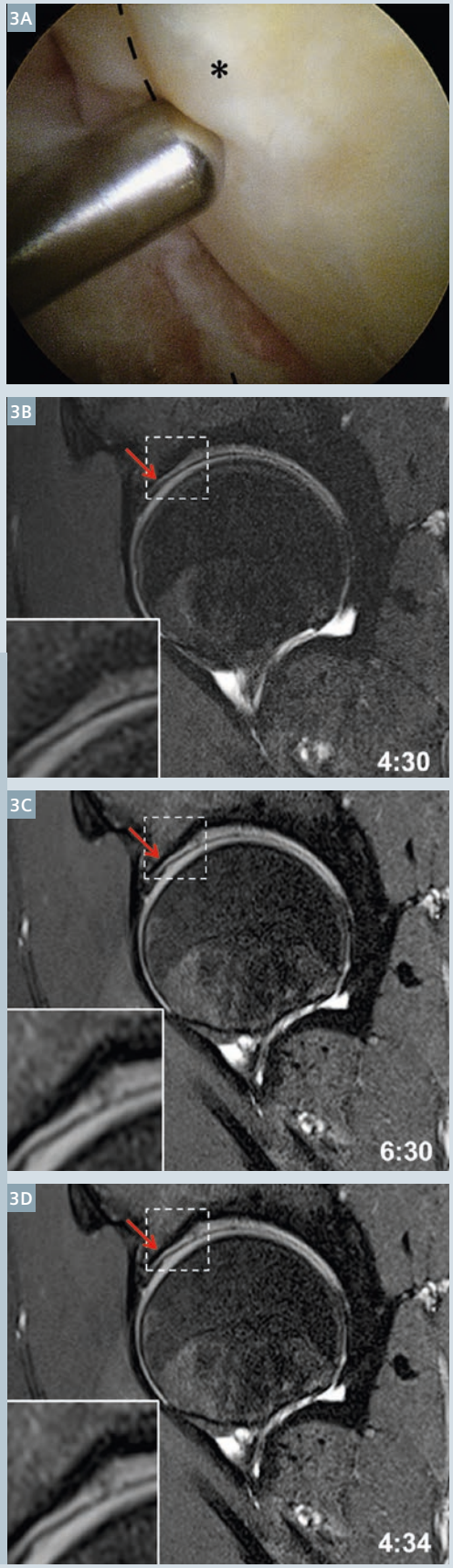

3 Multiband SMS acceleration enables identification of cartilage delamination in a clinically feasible acquisition time. **(3A)** Representative image taken during arthroscopic surgery probing of the articular cartilage of the acetabulum in another patient [12]. As the probe pushes against the cartilage, a bulge is seen (*), which indicates that the cartilage has debonded from the bone. The dashed line reveals the chondrolabral junction, with the acetabular labrum identified to the left of the dashed line. The cartilage can be seen to be attached to the bone to the right of the asterisk (*). **(3B)** In the pre-operative standard clinical T2-weighted MRI protocol with fat saturation (3.0 mm slice thickness), the cartilage delamination is not well visualized and cannot be confidently diagnosed. The red arrow points to the location probed in (3A), and the region of delamination is outlined by the dashed box (zoomed-in at the lower left corner). **(3C)** If the slice thickness is reduced from 3.0 to 2.0 mm, the cartilage delamination can be clearly seen. However, this increase in spatial resolution comes at the cost of increased acquisition time (6:30 vs. 4:30 min). **(3D)** Multiband SMS enables slice thickness to be reduced to 2.0 mm while maintaining a reasonable acquisition time (4:34 min). Note that the image quality is comparable to the result in (3C) despite being >30% faster.

Imaging parameters: FOV 160 × 160 mm², matrix size 320 × 288, in-plane resolution 0.50 × 0.56 mm², 20% slice spacing, excitation/refocusing flip angle 90°/140°, readout bandwidth 180-260 Hz/pixel, echo spacing 12 ms, T2w with spectral fat saturation, ETL 12, hyper-echo;

Standard TSE: 3 mm thickness, 26 slices, TR 4580 ms, TE 52 ms, 100% phase oversampling, TA 4:30 min; 2 mm thickness, 38 slices, TR 6680 ms, TE 52 ms, 100% phase oversampling, TA 6:30 min;

Multiband SMS Accelerated TSE: slice acceleration factor 2, 2 mm thickness, 38 slices, TR 4200 ms, TE 52 ms, 120% phase oversampling, TA 4:34 min.

Images acquired with MAGNETOM Prisma 3T MR scanner (Siemens Healthcare, Erlangen, Germany)

Methods

Patients with hip pain undergoing a clinical MR evaluation (current standard of care) for FAI were imaged using both a clinical and a multiband SMS accelerated sagittal multi-slice 2D TSE sequence with fat saturation under an Institutional Review Board approved protocol for which informed consent was obtained. Imaging was done using Siemens 3T MRI systems (MAGNETOM Skyra and MAGNETOM Prisma, Siemens Healthcare, Erlangen, Germany) with an 18-channel flex body coil wrapped about either the right or left hip in combination with an integrated 32-channel spine coil array. This enabled unilateral imaging of the hip joint for higher spatial resolution by limiting the receive coil sensitivity to one side of the body to avoid signal wrap.

Multiband technology was used to simultaneously excite and acquire more than one imaging slice simultaneously (Fig. 1). Multiband RF pulses were generated for simultaneous multi-slice excitation and echo refocusing, and the VERSE technique was applied to the RF pulses to reduce peak power and SAR. A low-resolution multi-slice 2D GRE scan integrated into the SMS TSE sequence was used as the reference scan to obtain the coil sensitivities. Image reconstruction techniques based on parallel imaging methodology were then used to unalias the signal acquired for the multiple slices.

Discussion

Accurate assessment of the acetabular cartilage is fundamental to the evaluation of and the clinical decision-making for patients with symptomatic FAI. Patients with moderate to advanced cartilage degeneration will fail arthroscopic repair, leading to total hip arthroplasty. Multiband SMS acceleration technology enables higher spatial resolution to be acquired with minimal impact on image quality and no increase in acquisition time. As shown in the two clinical cases, this technique provides improved diagnostic information that can better inform treatment decisions. In our initial clinical experience, we found that the multiband SMS accelerated TSE sequence can provide 30% higher spatial resolution within a given acquisition time to improve diagnostic accuracy of cartilage delamination and labral tears, or alternatively over 30% time savings for a given spatial resolution while maintaining diagnostic image quality. In general, multiband SMS acceleration will enable higher-quality imaging protocols for clinical 3T applications by targeting higher resolution to allow for more diagnostic accuracy in a standard clinical setting.

Contact

Jutta M. Ellermann, M.D.
Associate Professor
Department of Radiology (CMRR)
University of Minnesota
420 Delaware St., S.E. MMC 292
Minneapolis, MN 55455
USA
Phone: +1 612-626-3342
eller001@umn.edu

References

1 Allen D, Beaule PE, Ramadan O, Doucette S. Prevalence of associated deformities and hip pain in patients with cam-type femoroacetabular impingement. J Bone Joint Surg Br. 2009;91(5):589-594.

2 Beck M, Kalhor M, Leunig M, Ganz R. Hip morphology influences the pattern of damage to the acetabular cartilage: femoroacetabular impingement as a cause of early osteoarthritis of the hip. J Bone Joint Surg Br. 2005;87(7):1012-1018.

3 Beck M, Leunig M, Parvizi J, Boutier V, Wyss D, Ganz R. Anterior femoroacetabular impingement: part II. Midterm results of surgical treatment. Clin Orthop Relat Res. 2004(418):67-73.

4 Dudda M, Albers C, Mamisch TC, Werlen S, Beck M. Do normal radiographs exclude asphericity of the femoral head-neck junction? Clin Orthop Relat Res. 2009;467(3):651-659.

5 Ganz R, Leunig M, Leunig-Ganz K, Harris WH. The etiology of osteoarthritis of the hip: an integrated mechanical concept. Clin Orthop Relat Res. 2008;466(2):264-272.

6 Ganz R, Parvizi J, Beck M, Leunig M, Notzli H, Siebenrock KA. Femoroacetabular impingement: a cause for osteoarthritis of the hip. Clin Orthop Relat Res. 2003(417):112-120.

7 Larkman DJ, Hajnal JV, Herlihy AH, Coutts GA, Young IR, Ehnholm G. Use of multicoil arrays for separation of signal from multiple slices simultaneously excited. J Magn Reson Imaging. 2001;13(2):313-317.

8 Leunig M, Beaule PE, Ganz R. The concept of femoroacetabular impingement: current status and future perspectives. Clin Orthop Relat Res. 2009;467(3):616-622.

9 Moeller S, Yacoub E, Olman CA, et al. Multiband multislice GE-EPI at 7 tesla, with 16-fold acceleration using partial parallel imaging with application to high spatial and temporal whole-brain fMRI. Magn Reson Med. 2010;63(5):1144-1153.

10 Philippon M, Schenker M, Briggs K, Kuppersmith D. Femoroacetabular impingement in 45 professional athletes: associated pathologies and return to sport following arthroscopic decompression. Knee Surg Sports Traumatol Arthrosc. 2007;15(7):908-914.

11 Philippon MJ, Briggs KK, Yen YM, Kuppersmith DA. Outcomes following hip arthroscopy for femoroacetabular impingement with associated chondrolabral dysfunction: minimum two-year follow-up. J Bone Joint Surg Br. 2009;91(1):16-23.

12 Ellermann J, Ziegler C, Nissi MJ, Goebel R, Hughes J, Benson M, Holmberg P, Morgan P. Acetabular cartilage assessment in patients with femoroacetabular impingement by using T2* mapping with arthroscopic verification. Radiology 2014;271(2):512-23.

The entire editorial staff at Oxford University and at Siemens Healthcare extends their appreciation to all the radiologists, technologists, physicists, experts and scholars who donate their time and energy – without payment – in order to share their expertise with the readers of MAGNETOM Flash.

MAGNETOM Flash – Imprint

Publisher:
Siemens Healthcare GmbH
Magnetic Resonance,
Karl-Schall-Straße 6, D-91052 Erlangen, Germany

Guest Editor:
Professor Peter Jezzard, Oxford Centre for Functional Magnetic Resonance Imaging of the Brain (FMRIB), University of Oxford, John Radcliffe Hospital, Headington, Oxford, UK

Editor-in-chief: Antje Hellwich (antje.hellwich@siemens.com)

Editorial Board: Reto Merges; Wellesley Were; Sunil Kumar S.L., Ph.D.; Gary R. McNeal, MS (BME); Peter Kreisler, Ph.D.

Production: Norbert Moser, Siemens Healthcare GmbH

Layout:
Agentur Baumgärtner, Friedrichstraße 4, D-90762 Fürth, Germany

Printer:
G. Peschke Druckerei GmbH, Taxetstrasse 4, D-85599 Parsdorf b. Munich, Germany

MAGNETOM Flash is sent free of charge to Siemens MR customers, qualified physicians, technologists, physicists and radiology departments throughout the world. It includes reports in the English language on magnetic resonance: diagnostic and therapeutic methods and their application as well as results and experience gained with corresponding systems and solutions. It introduces from case to case new principles and procedures and discusses their clinical potential. The statements and views of the authors in the individual contributions do not necessarily reflect the opinion of the publisher.

We welcome your questions and comments about the editorial content of MAGNETOM Flash. Please contact us at magnetomworld.med@siemens.com.

Manuscripts as well as suggestions, proposals and information are always welcome; they are carefully examined and submitted to the editorial board for attention. MAGNETOM Flash is not responsible for loss, damage, or any other injury to unsolicited manuscripts or other materials. We reserve the right to edit for clarity, accuracy, and space. Include your name, address, and phone number and send to the editors, address above.

MAGNETOM Flash is also available online:

www.siemens.com/magnetom-world

On account of certain regional limitations of sales rights and service availability, we cannot guarantee that all products included in this brochure are available through the Siemens sales organization worldwide. Availability and packaging may vary by country and is subject to change without prior notice. Some/All of the features and products described herein may not be available in the United States.

The information in this document contains general technical descriptions of specifications and options as well as standard and optional features which do not always have to be present in individual cases, and which may not be commercially available in all countries. Due to regulatory reasons their future availability cannot be guaranteed. Please contact your local Siemens organization for further details.

Siemens reserves the right to modify the design, packaging, specifications, and options described herein without prior notice. Please contact your local Siemens sales representative for the most current information.

Note: Any technical data contained in this document may vary within defined tolerances. Original images always lose a certain amount of detail when reproduced.

Not for distribution in the US

Siemens Healthcare Headquarters
Siemens Healthcare GmbH
Henkestraße 127
91052 Erlangen
Germany
Phone: +49 9131 84-0
siemens.com/healthcare

Order No. A91MR-1000-117M-7600 | Printed in Germany | CC MR 3113 111510. |

siemens.com/magnetom-world